OPTIMAL CONTROL AND FRACTIONAL ORDER MODELING OF THE WITHIN-HOST DYNAMICS OF MALARIA PARASITE INFECTION

Jemal Muhammed Ahmed

A Ph.D. Dissertation Submitted to Department of Applied Mathematics School of Applied Natural Science

Presented in Fulfillment of the Requirement for the Degree of Doctor of Philosophy in Applied Mathematics

Office of Graduate Studies
Adama Science and Technology University

June, 2024
Adama, Ethiopia

OPTIMAL CONTROL AND FRACTIONAL ORDER MODELING OF THE WITHIN-HOST DYNAMICS OF MALARIA PARASITE INFECTION

Jemal Muhammed Ahmed

Major Supervisor
Dr. Getachew Tashome

Co-Supervisor
Dr. Shambel Tadesse.

A Ph.D. Dissertation Submitted to Department of Applied Mathematics, School of Applied Natural Science

Presented in Fulfillment of the Requirement for the Degree of Doctor of Philosophy in Applied Mathematics

Office of Graduate Studies, Adama Science and Technology University

June, 2024
Adama, Ethiopia

DECLARATION

I declare that this dissertation entitled " **OPTIMAL CONTROL AND FRACTIONAL ORDER MODELING OF THE WITHIN-HOST DYNAMICS OF MALARIA PARASITE INFECTION** " is my own work and has not been submitted to any university for a similar purpose. The references used in this dissertation are duly recognized by proper citations.

_____	_____	_____
Name of Student	Signature	Date

RECOMMENDATION

I, the major supervisor/co-supervisor of this dissertation, hereby, certify that I have closely supervised the student while developing this dissertation and read the draft entitled " **OPTIMAL CONTROL AND FRACTIONAL ORDER MODELING OF THE WITHIN-HOST DYNAMICS OF MALARIA PARASITE INFECTION** " prepared under my guidance by **Jemal Muhammed Ahmed**. Therefore, I recommend the submission of the dissertation to the department for further review and evaluation.

_____	_____	_____
Major supervisor	Signature	Date
_____	_____	_____
Co-supervisor	Signature	Date

APPROVAL

I hereby, certify that the recommendations and suggestions made by the board of examiners are appropriately incorporated into the final version of the dissertation entitled " **OPTIMAL CONTROL AND FRACTIONAL ORDER MODELING OF THE WITHIN-HOST DYNAMICS OF MALARIA PARASITE INFECTION** "

Major supervisor	Signature	Date
Minor supervisor	Signature	Date

We, the undersigned, members of the Board of Reviewers of the dissertation open defense by **Jemal Muhammed Ahmed** have read and evaluated the dissertation entitled " **OPTIMAL CONTROL AND FRACTIONAL ORDER MODELING OF THE WITHIN-HOST DYNAMICS OF MALARIA PARASITE INFECTION** " and examined the candidate during open defense. This is, therefore, to certify that the dissertation is accepted for partial fulfillment of the requirement of the degree of Doctor of Philosophy in **Applied Mathematics**.

Chairperson	Signature	Date
Internal Examiner 1	Signature	Date
Internal Examiner 2	Signature	Date
External Examiner 1	Signature	Date
External Examiner 2	Signature	Date

Finally, approval and acceptance of the dissertation is contingent upon submission of its final copy to the Office of Postgraduate Studies (OPGS) through the candidate's Department Graduate Council (DGC) and School Graduate Committee (SGC).

Department Head	Signature	Date
School Dean	Signature	Date
Office of Postgraduate Studies, Dean	Signature	Date

ACKNOWLEDGMENT

First of all, I would like to thank the Almighty Allah, who gave me the courage to get through all sorts of difficulties until this dissertation work was accomplished. All praise is for Allah Lord of all worlds. I am especially grateful to my main supervisor, Dr Getachaw Tashome, for his constant support and guidance. I am also indebted to my co-supervisor Dr. Shambel Tedesse, for his support constructive discussions, and wonderful relationships along the way. It would have not been possible without their unconditional support. It is also my pleasure to thank my friends Mekasha Ali and Girma Tafessew for their technical assistance throughout the process of publication and dissertation write-up. My special thanks should go to my beloved wife Meriam Lolo and my children Mahadi Jemal and Mekfira Jemal. I am deeply grateful for her kindness, support, and honesty. I thank Allah for his abundance of blessings and for keeping my family safe and happy regardless of all the challenges we have passed through during my studies. I would like to Adama Science and Technology University and Oda Bultum University for all the support and commitment in realizing the Ph.D. program. Finally, I would like to express my deepest gratitude to my father and mother. May god bless them and give them a long life.

TABLE OF CONTENTS

LIST OF TABLES

LIST OF FIGURES

ABBREVIATIONS AND ACRONYMS

ACT	Artemisinin-based combination therapy
CTLs	Cytotoxic T lymphocytes
EEF	Exoerythrocytic Forms
FODE	Fractional Ordinary Differential Equations
FC	Fractional calculus
GDP	Global distribution of per-capita gross domestic product
HBV	Hepatitis B virus
HCV	Hepatitis C virus
IPTp	Intermittent preventive treatment
iRBCs	Infected Red Blood Cells
IRS	Indoor residual spraying
ITNs	Insecticide-treated bed nets
ODE	Ordinary differential equation
PFE	Parasite free equilibrium
PPE	Parasite persistence equilibrium
RBCs	Red Blood Cells
SSA	Sub-Saharan Africa
UNCEF	United Nations Children and Emergency Fund

ABSTRACT

Malaria is a major global health challenge, with nearly half of the world's population at risk of infection. It is caused by parasites of the genus Plasmodium and transmitted through the vectors. Malaria remains a significant global health concern with substantial socioeconomic implications. Understanding the within-host dynamics of the malaria parasite infection is crucial for designing effective intervention strategies. In this dissertation, we developed and analyzed mathematical models to investigate within-host dynamics and optimal control strategies for malaria infection. First, we presented the blood stage dynamical model that captures the interactions between infected cells, malaria parasites, and the host immune response using the nonlinear Michaelis-Menten-Monod function. We analyzed the stability of the parasite-free and parasite persistence equilibrium and determined the basic reproduction number as a key epidemiological threshold. Next, we extend the model to incorporate antimalarial drug treatment, analyzing the effect of stage-specific interventions. We then proposed a within-host model that incorporates the adaptive immune responses, characterizing the stability of the equilibria using Routh-Hurwitz criteria. Moreover, we developed an optimal control framework to investigate the most effective intervention strategies. We considered four control variables targeting the elimination of infected hepatocytes, infected red blood cells, merozoites, and gametocytes. Applying Pontryagin's Minimum Principles, we derived an optimality system that characterizes the optimal control interventions. The result suggested that simultaneous application of all control measures could effectively eliminate malaria infection within the host cell. Finally, we formulated a fractional order derivative model of within-host malaria infection to investigate the impact of memory effects on parasite dynamics. We established the existence, uniqueness, boundedness, and positivity of solutions, qualitative analysis, and presented numerical simulations using the generalized predictor-corrector method. Our findings provide valuable insights into the complex within-host dynamics of malaria and offer a framework for developing optimal control strategies to combat this global health threat. In future work, to understand more about the complexity of malaria infection, the researcher will be extend the models by considering different strains of malaria parasite, time delay model, and reaction-diffusion model.

Keywords:- Mathematical model; Malaria parasite; Erythrocytes; Hepatocyte cells; Optimal control; Fractional order derivative; Cell-mediated immune system; Cytotoxic T-cell; Parasite-free equilibrium.

LIST OF PUBLICATIONS

1. Jemal Muhammed Ahmed, Getachew Teshome Tilahun, and Shambel Tadesse Degefa. Within-host mathematical model of malaria parasite with cell-mediated and antibody-mediated immune systems. International Journal of Modelling and Simulation, pages 1–18, 2023. https://doi.org/10.1080/02286203.2023.2288771

2. Jemal Muhammed Ahmed, Getachew Tashome Tilahun, and Shambel Tadesse Degefa. A cell-level dynamical model for malaria parasite infection with antimalarial drug treatment. Frontiers in Applied Mathematics and Statistics, 9:1282544. https://doi.org/10.3389/fams.2023.1282544

3. Jemal Muhammed Ahmed, Getachew Tashome Tilahun, and Shambel Tadesse Degefa. In-host fractional order model for malaria parasite dynamics with immune system. Modeling Earth Systems and Environment, pages 1–21, 2024. https://doi.org/10.1007/s40808-024-02004-4

4. Mathematical model and analysis for within-host dynamics of the malaria parasite infection with optimal control strategies (***Under review***)

5. A mathematical model for the within-host dynamics of malaria parasite with adaptive immune responses (***Under review***)

CHAPTER 1

INTRODUCTION

1.1 Background of the study

Malaria is an acute febrile illness caused by *Plasmodium* parasites, which is transmitted to people via the bites of infected female Anopheles mosquitoes (WHO, 2016). The four Plasmodium species that infect humans *Plasmodium falciparum, P.vivax, P. ovale, and P.malariae* are usually transmitted by anopheline mosquitoes. Malaria has become a global concern because it is the fifth cause of death from infectious diseases worldwide (after respiratory infections, HIV/AIDS, diarrheal diseases, and tuberculosis) (Baihaqi and Adi-Kusumo, 2020). According to the WHO World Malaria 2020 report, there were 241 million cases worldwide and more than 627000 people died of the disease. Malaria is widely spread in tropical and subtropical regions, including Africa, Asia, Latin America, the Middle East, and some parts of Europe (Sabatinelli, 2000). Most cases and deaths occur in Sub-Saharan Africa (Olaniyi and Obabiyi, 2013).

In particular, about 95% of malaria cases and 96% of all malaria deaths in the world today occur in Sub-Saharan Africa (SSA). This is because the majority of infections are caused by *Plasmodium falciparum*, the most dangerous of the four human malaria parasites and the most effective malaria vector, the mosquito *Anopheles gambiae* is the most widespread (Mbacham et al., 2019) and the most difficult to control (Samba, 1997). An estimated one million people in Africa die from malaria each year and most of these are children (Fischer and Bialek, 2002; Stauffer and Fischer, 2003). In areas of stable malaria transmission, very young children and pregnant women are the population groups at the highest risk for malaria morbidity and mortality (Samba, 1997). According to the United Nations Children and Emergency Fund, a child under age of five dies of malaria every two minutes, and over 12 million women's pregnancies in the WHO African region were exposed to malaria, resulting in fetal loss, low birth weights, and other morbidities (Badmos et al., 2021).

Ethiopia is one of the countries in Sub-Sahara Africa. An epidemic of malaria, covering about 100,000 square miles in four central provinces in the highlands of Ethiopia and portions of the highlands of five other provinces, was observed between June and December of 1958. *Anopheles gambiae* was the only vector involved. In Ethiopia the four species of malaria are cause of infection. Of the four *Plasmodium* species, *P. falciparum* was the predominant malaria parasite. It is responsible for more severe morbidity and mortality followed by *P. vivax* with proportions of 60% and 40%, respectively (Kendie et al., 2021; Adugna, 2011; Bugssa and Tedla, 2020). It accounted for the severe acute illness that characterized the clinical syndrome of most cases and the high mortality observed in many districts (Fontaine et al., 1961). In

Ethiopia, three-quarters of its territory is considered endemic for malaria, putting more than 60 million (60% of the total population) people at risk for malaria infection. Approximately, 4–5 million cases of malaria and 70,000 related deaths have been reported annually (Girum et al., 2019).

Malaria adversely affects the health of the people as well as the economic development of many developing countries including Ethiopia. The WHO reported that the total funding for malaria control and elimination reached 3 billion dollars by 2019 with an excess of 900 million dollars from governments of endemic countries. Despite this, malaria remains largely uncontrolled in the Sub-Saharan Africa region (Badmos et al., 2021). Malaria spending is estimated to cost Ethiopia about $200 million annually or 10% of its total health expenditure (Assebe et al., 2020; Bugssa and Tedla, 2020).

1.2 The malaria parasite life cycle

The malaria parasite has a complex life cycle characterized by cyclical sexual and asexual stages between the human hosts and female Anopheles mosquitoes. Both sexual and asexual stages occur within the human host. This is preceded by another sexual phase within the mosquito vectors. Malaria begins when *Plasmodium* sporozoites are deposited in the host skin by a female *Anopheles* mosquito (Figure 1.1). Sporozoites then enter blood vessels and move to the liver through blood vessels, infect hepatocytes, and remain in a clinically silent stage between 5 to 16 days depending on the *Plasmodium* species (Su et al., 2020a). Inside the hepatocyte, a parasite divides into thousands of merozoites through a process called schizogony (Dhangadamajhi et al., 2010), where they differentiate into exoerythrocytic forms (EEFs) (Risco-Castillo et al., 2015). Mature merozoites enter the bloodstream after the rupture of the infected hepatocyte (liver-schizont) and invade erythrocytes, starting a new cycle of schizogony within red blood cells (RBCs) which includes asexual replication of their haploid genome. Within RBCs, parasites develop through immature trophozoite, mature trophozoite, and schizont stages (Su et al., 2020a).

The parasite remains in the immature trophozoite form, which displays low metabolic activity and changes little morphologically. The parasite then progresses to the mature trophozoite (feeding) stage, in which it becomes more metabolically active and grows rapidly. DNA synthesis and nuclear division take place until the parasite becomes a schizont with the onset of nuclear division, but not cytokinesis (Sherling and van Ooij, 2016). The resulting mature schizont is segmented in appearance and contains 16–32 daughter merozoites. The infected red blood cells (iRBCs) ruptures, releasing the daughter merozoites and invading new RBCs. This cycle of erythrocytic development takes approximately 24 hr for *P. knowlesi*, 48 hr for *P. falciparum, P. vivax, and P. ovale*, and 72 hr for *P. malariae* (Su et al., 2020a; Sherling and van Ooij, 2016).

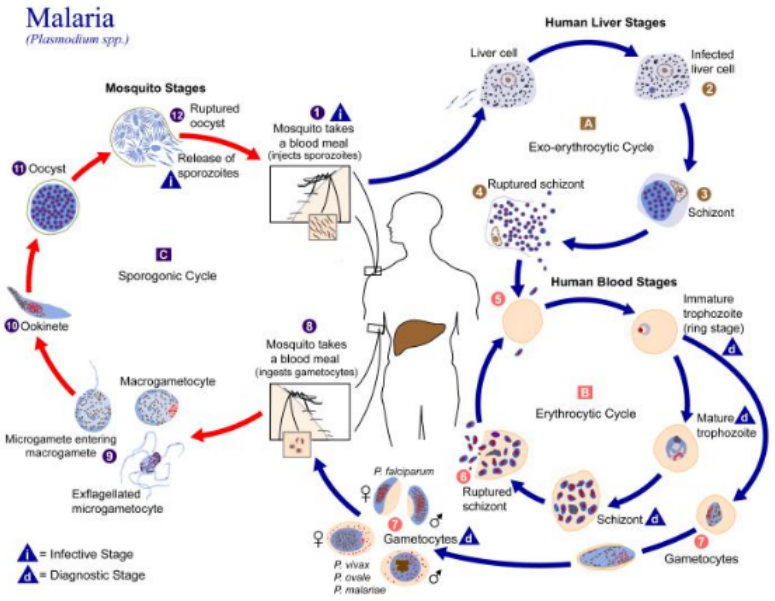

Figure 1.1: Life cycle of malaria parasites. Source: CDC: https://www.cdc.gov/malaria/about/biology/index.html

After invading RBCs, some merozoites are sexually differentiated into male (microgametes) and female (macrogametes) gametocytes (Acharya et al., 2017). If a mosquito takes a blood meal from an infected host, the gametocytes undergo sexual development in the mosquito's midgut. Within a few minutes of moving to the mosquito midgut, male and female gametocytes differentiate into male and female gametes that fertilize to form zygotes and then into motile ookinetes. Ookinetes penetrate the mosquito's midgut wall to grow into oocysts, which include thousands of sporozoites (Su et al., 2020a; Mandala et al., 2021). The mature sporozoites travel to the salivary glands, which can be introduced into the bloodstream of a susceptible human host if bitten by the mosquito (McQueen et al., 2013; Sreenivasamurthy et al., 2013; Ullman, 2006). These processes are repeated and recycle the malaria parasites between human populations and malaria mosquitos if no any control is applicable.

1.3 The role of immune response in mitigating malaria parasite infection

The immune system is a complex network of biological systems that works to protect a human from various diseases. It has the ability to detect and respond to a wide range of pathogens, including viruses, bacteria, and parasites, as well as abnormal cells such as cancer cells. The immune system also distinguishes these harmful objects from the human healthy tissues and works to eliminate them. In particular, the immune cells respond when malaria parasites are present in the human body. As parasites enter the host cell, the immune system can be stimulated, producing immune responses to fight the interactions (De Boer and Perelson, 1995;

Malaguarnera and Musumeci, 2002). It can prevent either malaria parasites or clear the infected cells from the host cell.

There are two types of immune responses: innate (non-specific) and adaptive (antigen-specific) immune responses (Pilyugin and Antia, 2000; Gowda and Wu, 2018). Both innate and adaptive immune responses are induced by the malaria parasite. An innate immune response is triggered during malaria infection as the first line of defense, while the adaptive immune response acts as the second line of defense. This protects the host cells against interacting with the same parasite perennially (Coban et al., 2007; Augustine et al., 2009; Stevenson and Riley, 2004). The host immune system fights against parasites via two mechanisms, viz., humoral (antibody-mediated) and cellular (cell-mediated) immune responses. These two play a role at different specific stages of the parasite onslaught.

Antibody-mediated immune system refers to immune defense by *B lymphocytes* which is activated by the presence of merozoites in the blood, including secreted antibodies, and proteins. In turn, the *B-cells* release antibodies into the bloodstream. The antibodies neutralize merozoites by attaching to their surface binding sites, blocking them from attaching to target cell receptors and inhibiting red blood cell invasion (Vande Waa et al., 1984). Moreover, antibodies play a role in instructing immune system macrophage cells to engulf the attached merozoites and remove them from the host cell. Cell-mediated immune cells act as *T lymphocytes* secrete proteins called cytokines (Kamangira et al., 2014) to act directly or indirectly against the merozoites and also stimulate *cytotoxic T-cells* (Long and Zavala, 2017). The *cytotoxic T-cells* and natural killer (NK) cells play an important role in the protection of the host cells by killing iRBCs and thus reducing the production of merozoites and gametocytes (Long and Zavala, 2017; Belachew, 2018; Osii et al., 2020; Burrack et al., 2019).

1.4 Malaria vaccination and treatment

The WHO recommends indoor residual spraying (IRS) and long-lasting insecticidal nets (ITNs) as the primary methods for preventing and reducing malaria transmission in areas with a high prevalence of the disease (Oxborough, 2016). In addition, different regions of the world today use the malaria vaccine, chemoprophylaxis, and antimalarial treatments to prevent and cure clinical malaria infection (Cibulskis et al., 2016; Bhatt et al., 2015). A malaria vaccination strategy is used to either enhance immune system responses that are protective before becoming infected with malaria or to give protection in the case of a disease outbreak.

The malaria vaccines can be categorized into three types: Pre-erythrocytic vaccine (PEV), blood-stage vaccine (BSV), and transmission-blocking vaccines (TBVs) (Zheng et al., 2019) that target the parasite at different stages of its life cycle. *Pre-erythrocytic malaria vaccines*, also known as anti-infective vaccines, mainly target the *Plasmodium* during its sporozoite and liver stages (inducing antibodies that block the invasion of hepatocytes by sporozoites and/or

cell-mediated immune responses that target infected hepatocytes) (Duffy et al., 2012). They trigger certain antibodies that destroy infected liver cells or hinder the malaria parasite during liver cell proliferation, preventing the generation of contagious merozoites and having an anti-infection effect, and can reduce progression to blood-stage infection (Zheng et al., 2019; Duffy et al., 2012). The RTS, S/AS01 is the most sophisticated pry-erythrocyte malaria vaccine to date (RTS, 2011,0).

Blood-stage vaccine (BV), also known as elicits anti-invasion and anti-disease responses at blood stage (Moorthy et al., 2004). It can be classified into those that attempt to target the infected red blood cells (iRBCs) and those that target the merozoite. Most anti-merozoite vaccines seek to produce antibodies that bind to proteins involved in the process of red blood cell (RBC) entry, which leads to a barrier in RBC invasion (Illingworth et al., 2019). The merozoite surface protein 1 (MSP1) vaccines that are placed on the merozoite surface where it plays a vital role in erythrocyte invasion (Zheng et al., 2019; Ogutu et al., 2009) and merozoite surface protein 3 (MSP3) (Pattaradilokrat et al., 2016; Audran et al., 2005) are the leading blood stage vaccine candidates for *plasmodium* parasite (Plowe et al., 2009).

Transmission-blocking vaccines (TBV) against malaria are intended to prevent mosquitoes from transmitting malaria parasites. Transmission-blocking vaccines can break the life cycle of the parasite by preventing mosquitoes from becoming infected by malaria-causing parasites when they feed on infected host (Carter, 2001). TBV increases the amount of antibodies against antigens in gametes, zygotes, and ookinetes. This prevents the transition of the ookinete to the oocyst, and that in turn stops the development of parasites inside the midgut of the mosquito (Carter et al., 2000). As a result, there are significantly reduced malaria sporozoites in mosquito salivary glands. There are different potential antigenic targets of transmission-blocking vaccines in malaria have been investigated (Zheng et al., 2019; Wu et al., 2015). The leading malaria transmission-blocking vaccine candidates antigens are surface proteins expressed on the zygotes and mature ookinetes of the malaria parasites, which are Ps25 and Ps28. (Carter, 2001). In this study, we have provided important insights into the impacts of improved vaccine efficacy on the dynamics of clinical malaria infection. We have also analyzed a combination of different vaccine antigens to improve their overall efficacies. Figure 1.2 is reveals the stage specific malaria vaccines.

Antimalarials mostly act by mechanisms that seek to block two or more stages of the parasite life cycle (Pinheiro et al., 2018). Several anti-malarial drugs have been developed and categorized as: *Primary tissue schizontocides* act on the pre-erythrocytic forms (primary tissue phase) of the malaria parasite. Complete prevention of erythrocytic infection by the administration of drugs to eliminate either sporozoites or primary tissue forms. Primaquine, pamaquine, as well as potential quinocide are active against primary tissue schizonts. *Blood schizontocides* act on the asexual erythrocytic forms of all malaria parasites. These drugs prevent malarial symptomatic assaults in the earliest stages and are the primary medications that

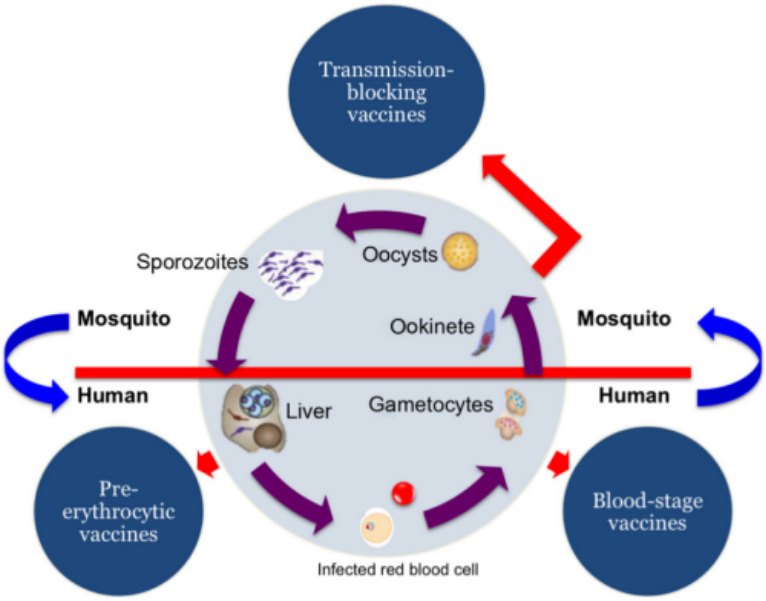

Figure 1.2: Malaria vaccines: Arama and Troye-Blomberg (2014).

are used in treatment for the cure of malaria. Quinine, mepacrine, 4-aminoquinolines, chloroquine, or amodiaquine have a powerful and immediate effect and are used for treatment as well as for temporary prevention (suppression) of blood schizontocides (Bruce-Chwatt, 1962). *Gametocytocidal drugs (gametocytocidal)* prevent the transmission of parasites into mosquitoes and diminish the human reservoir of the disease. The 8-aminoquinolines, pamaquine, plasmoid, primaquine, and quinocide are among the medications that are most effective against the sexual (male and female gametocytes) forms of all species of malaria parasites (Munro and McMorran, 2022).

1.5 Mathematical model of infectious diseases

There is a long and distinguished history of mathematical models in epidemiology, going back to the eighteenth century (Bernoulli, 1760). Since that time, theoretical epidemiology has observed numerous developments. Some of these studies can be found in Anderson and May (1991a), and Hethcote (2000). A massive number of models have been formulated, analyzed, and applied to a variety of infectious diseases qualitatively and quantitatively. The mathematical models have become important tools in analyzing the spread and control of infectious diseases. Furthermore, mathematical models now play a key role in policy-making, including health-economic aspects, emergency planning, risk assessment, control-program evaluation, and optimizing various detections.

For example control the outbreak of vector-borne disease (Okosun et al., 2013,0), the human immunodeficiency virus (HIV) and sexually transmitted infections (Omondi et al., 2018; Ayele et al., 2021), hepatitis B and hepatitis C virus (Adu et al., 2014; Rihan et al., 2017),

severe acute respiratory syndrome (SARS) (Donnelly et al., 2004) and Middle East respiratory syndrome coronavirus (MERS-CoV) (Cauchemez et al., 2014). Moreover, the mathematical model has a role in the study within-host level of infectious diseases like HIV (Perelson and Ribeiro, 2013), COVID-19 (Nath et al., 2021), and malaria infection (Kamangira et al., 2014).

1.6 Applications of optimal control

Mathematical models provide a rational basis to inform how to control disease. Optimal control for infectious diseases has garnered more attention in recent decades. It has proven to be a successful tool in understanding ways to curtail the spread of infectious diseases by devising optimal disease intervention strategies (Bussell et al., 2019). Mathematical models with optimal control analysis have become an important tool for understanding the dynamics of disease transmission and decision-making processes regarding intervention programs for disease control (Nepomuceno et al., 2021). Strategies such as vaccination and treatment are essential in controlling the spread of various infectious diseases. The application of optimal control is very important as it is a necessary tool for making decisions on workable control strategies to eradicate diseases (Keno et al., 2022).

The optimal control is applied in the study, HIV disease (Ayele et al., 2021), hepatitis B virus (HBV) (Khan et al., 2023), malaria (Okosun et al., 2013) and tuberculosis (Ullah et al., 2020b) at population level. Moreover, an optimal control has been applied in the study within the human host dynamics of Tuberculosis Adi (2021), HIV Ngina et al. (2018), and malaria Orwa et al. (2022). However, the study of the dynamics of malaria parasite infection within-host and the effort of the adaptive immune system and antimalarial treatment using mathematical models has not paid attention. Understanding the within-host dynamics of the malaria parasite infection is crucial for designing effective intervention strategies, this study seeks to investigate optimal control strategies for the within-host dynamics of malaria parasite infection.

1.7 Fractional order mathematical model

In recent years, fractional differential equation models have become widely used in biological science. Researchers found that biological cell membranes have electron conductivity, which could be classified as a fractional-order model (Zhang et al., 2015; Arafa et al., 2014; Miao et al., 2017; Dehingia et al., 2022; Ullah et al., 2020a). Furthermore, some biological models developed using fractional differential equations have tested out to be more helpful than classical-order models (Su et al., 2020b; Arafa et al., 2012; Chatterjee and Ahmad, 2021). This is because of fractional-order ordinary differential equations are naturally related to systems with memory, which exist in most biological systems. In addition, fractional-order ordinary

differential equations are closely related to fractals, which are common in biological systems (Boukhouima et al., 2018).

Moreover, fractional order derivative helps in order to observe the memory effect and gain more insights about infectious diseases. The fractional order derivative study transmission dynamics of HIV (Nazir et al., 2020), HBV, malaria and COVID-19 co-infection dynamics (Abioye et al., 2023) at population level as well as HIV (Zhang et al., 2015; Arafa et al., 2014; Miao et al., 2017; Ullah et al., 2020a), HBV (Dehingia et al., 2022), and COVID-19 (Chatterjee and Ahmad, 2021) at cell level. However, the study of the within-host dynamics of malaria parasite infection dynamics using fractional order models has not received enough attention. Therefore, this study also investigates the fractional order model of in-host malaria infection to obtain the memory effect and get more insight into the infection.

1.8 Statement of the problem

Malaria is a serious parasitic disease in the developing world, causing high morbidity and mortality (Laishram et al., 2012). It is thought that approximately half of the world's population is currently at risk from malaria. In 2022, there were an estimated 249 million malaria cases and 608,000 malaria deaths globally across 85 countries. The WHO African Region bears a disproportionately high share of the global malaria burden, accounting for 94% of malaria cases and 95% of malaria deaths. About 80% of all malaria deaths in the Region were among children under the age of five (WHO et al., 2023). Every year, nearly one million deaths result either directly or indirectly from malaria infection from Africa Region. The four countries in the Region Nigeria (26.8%), the Democratic Republic of the Congo (12.3%), Uganda (5.1%) and Mozambique (4.2%) accounted for nearly half of all malaria cases globally. Between 2019 and 2022, there was a significant increase in the total estimated number of malaria cases in the African Region. Notable case increases were observed in Nigeria (5.3 million), Ethiopia (2.4 million), Madagascar (1.5 million), Uganda (1.3 million), the United Republic of Tanzania (1.3 million), Mali (1.1 million), and Mozambique (1 million) (Venkatesan, 2024).

In Ethiopia, malaria remains one of the major public health and socioeconomic problems. According to the Ethiopian National Malaria Strategic Plan (NMSP), the population of Ethiopia was 126.5 million in 2023. Of this population, about 52 percent live in areas at risk of malaria. The highest malaria burden regions are usually areas of intense malaria transmission with altitudes below 1,000 meters located mainly in areas of Gambela, Benishangul-Gumuz, Western Oromia, Amhara, some parts of South Nations, Nationalities and Peoples' (SNNP), and Tigray regions (Olani et al., 2023).

Malaria affects the health and wealth of nations and individuals alike. In Africa today, malaria is understood to be both a disease of poverty and a cause of poverty. Malaria has significant measurable direct and indirect costs and is a major constraint to economic develop-

ment. For developing countries, this has meant the gap in prosperity between countries with malaria and countries without malaria has become wider every single year. Annual economic growth in countries with high malaria transmission has historically been lower than in countries without malaria (Malaria, 2011). The loss of growth in countries with endemic malaria is estimated to be as high as 1.3% per year up to US$12 billion in lost productivity due to malaria occurring in Africa annually (Barnes et al., 2009; Malaria, 2011). When compounded over the years, this penalty leads to substantial differences in the global distribution of per-capita gross domestic product(GDP) between countries with and without malaria and severely restrains the economic growth of the entire region (Malaria, 2011).

To date, the WHO considers effective malaria control strategies such as long-lasting insecticidal nets (ITNs) and IRS as the main ways to prevent and reduce malaria transmission in communities with high malaria prevalence. Chemoprophylaxis and antimalarial drugs such as chloroquine and artemisinin-based combination therapy (ACT) are currently used to prevent and treat clinical malaria, respectively, in different parts of the world. These strategies have contributed to the substantial global reduction in malaria mortality and morbidity (Heller and Roepe, 2019; Orwa, 2020). Despite the global success in malaria control, global malaria cases and mortality are still quite high and malaria remains a global health problem. The WHO-African region still bears the highest burden of malaria infection.

The study of the disease using mathematical models with optimal control strategy plays an important role in the modeling of real-life phenomena in various fields of application. Several researchers are studying the dynamical behavior of malaria disease both the transmission from vector to human (population or community-level) and within-host cell (cell-level) using the mathematical model. The non-linear dynamical phenomena in host-parasite interactions to a series of different problems ranging from the impact on transmission of control measures based on vaccination and chemotherapy and the effects of immunological responses targeted at different stages in a parasite's life-cycle were studied by Anderson et al. (1989). However, the authors consider only asexual blood-stage malaria parasite infection.

In Hetzel and Anderson (1996) a mathematical model of blood-stage infection with a single strain of malaria was investigated. Analyzing the cell population dynamics in the absence of a host immune response, they demonstrate a relationship between host and parasite parameters that defines a criterion for the successful invasion and persistence of the parasite. The blood-stage dynamics of malaria in an infected host is studied by incorporating red blood cells, malaria parasite, and immune effectors into a mathematical model with nonlinear bounded Michaelis-Menten-Monod functions describing how immune cells interact with infected red blood cells and merozoites Li et al. (2011). The study not consider the pre-erythrocyte stage of malaria infection. In (Song et al., 2019) the authors develop mathematical models to understand the evolution of drug resistance within an infected host by considering competition (which is between drug-sensitive parasites and drug-resistant parasites), drug treatment, and

immune response. To explicit the effect of immunity, they construct two models with and without considering the immune response.

In Chiyaka et al. (2008) the in-host model of malaria infection with the immune system and drug therapy is developed. The authors extend Anderson et al. (1989) by incorporating immune response, antibodies, and the effects of antimalarial drugs. However, the authors do not consider the sexual replication of malaria parasites and stage specific immune responses. The work by Tumwiine et al. (2008b) developed a blood-stage malaria parasite model with stage-specific immune responses, but the scholars do not advise stage-specificity of humoral and cellular immune responses explicitly, the sexual productions of the merozoites and they use the bilinear function to show the interaction between parasites and immune responses.

In previous findings, mathematical studies did not take into account the impact of anti-malarial treatment and the adaptive immune response on the within-host dynamics of malaria infection. Additionally, the within-host dynamics of malaria parasite infection with optimal control and memory effect were not considered. Therefore, this study aims to develop and analyze a mathematical model of the malaria parasite within the host cell, taking into consideration the effect of antimalarial treatment and the adaptive immune system, as well as the within-host dynamics of malaria infection with optimal control and memory effect.

1.9 Objectives of the study

1.9.1 General Objective

The general objective of this study is to develop and analyze a mathematical models that capture the within-host dynamics of malaria parasite infection by incorporating optimal strategies and fractional order derivative approach.

1.9.2 Specific Objectives

The specific objectives of this study are to:

1. develop and analyze a within-host mathematical model that captures the dynamics of malaria parasite infection with cell-mediated and antibody-mediated immune systems
2. construct a cell-level dynamical model for malaria parasite infection by integrating the effects of antimalarial drug treatment.
3. formulate a within-host mathematical model that describes the dynamics of malaria parasite in the presence of an adaptive immune response.
4. analyze a within-host mathematical model of malaria parasite infection with optimal control strategies.
5. develop a fractional order model characterize the within-host dynamics malaria parasite infection with immune system.

1.10 Significance of the study

The development and analysis of the within-host mathematical models will provide deeper insights into parasites, host cells, and the immune system. This enhanced understanding of the underlying mechanisms driving malaria infection and progression can inform the design of more effective treatment and prevention strategies. The incorporation of optimal control strategies into the within-host models will help identify the most effective combinations of interventions (e.g. vaccine, antimalarial drugs treatment, immune modulators) to minimize the parasite load and mitigate the adverse health impacts. Optimal control analysis can guide policymakers and healthcare providers in allocating resources and implementing targeted interventions for improving malaria management. The development of a fractional order within-host model for malaria infection can provide new insights into the memory effects and nonlinear dynamics inherent in the parasite-host interventions.

The fractional order modeling can capture the complex long-range temporal dependencies in the disease prorogation's, which may not adequately capture traditional integer-order models. The findings from the fractional-order analysis can inform the design of more accurate and predictive models for malaria dynamics, with potential applications in personalized medicine and precision public health. The findings of the study can provide valuable information to the scientific community working on malaria research and control. The investigation of optimal control strategies and fractional-order modeling approaches can open new dimensions for exploring innovative treatment and prevention methods, potentially leading to improved clinical outcomes and reduced malaria burden. The incorporation of fractional-order modeling techniques adds a new dimension to the study allowing for the exploration of the memory effects in the immune response and providing a more comprehensive understanding of the long-term dynamics of infection. This contributes to the advancement of mathematical modeling methods in infectious disease research.

1.11 Organization of the dissertation

The dissertation is subdivided into nine Chapters. Chapter one is an introduction. Chapter 2 gives a review of mathematical models that have been formulated and analyzed previously to provide insights on malaria disease transmission and control. Particular reviews concentrate on in-host malaria models and significant findings from such chosen models. The optimal control theory and its application to disease interventions and fractional order derivative models especially malaria infection are also reviewed. The methodology used in conducting this dissertation is presented in Chapter 3. Chapter 4 covers the overall dynamics of malaria infection at the blood stage of the parasite life cycle, in the presence of cell-mediated and antibody-meditated immunological responses. In Chapter 5, the model formulated in Chapter 4 is mod-

ified to incorporate liver stage dynamics of the infection with antimalarial drug treatments. In Chapter 6, the model formulated in Chapter 4 is modified by taking into account the effect of adaptive immune responses (cytotoxic T-cells, and antibody immune responses). In Chapter 7, the optimal control theory is applied to the within-host malaria infection model. Control strategies in the form of antimalarial drug treatment and malaria vaccine antigens are applied both at the pre-erythrocytic and the blood stages. In Chapter 8 a fractional order derivative is presented using Caputo fractional order derivative. Finally, a summary, conclusions, and recommendations of the study are provided in Chapter 9.

CHAPTER 2

LITERATURE REVIEW

The biology and life cycle of the malaria parasites is exceedingly complicated, with many unidentified dynamics and behavioral disorders. The parasite carries out its intricate infectious life cycles by shifting between the female *Anopheles mosquito* carrier and the human host. The transmission of the parasite from human host to mosquito and vice versa has been studied for many years. Understanding such complex dynamics has been significantly straightforward with the use of mathematical modeling. This chapter provides an overview of mathematical models that have been created and studied previously to provide insights into the transmission and control of malaria parasite disease. Reviews are concentrated more on within-host malaria parasite infection models. It also reviews the optimal control theory and fractional order model along with the way it applies to interventions for disease, particularly malaria infection.

2.1 Role of mathematical modeling in the infectious disease

Mathematical modeling has an important role in the study of dynamic infectious diseases both at the host level and within the host. Describing the transmission processes of infectious diseases using mathematical language is not new. As early as 1766, Daniel Bernoulli used mathematical life table analysis to describe the effect of smallpox variolation (a precursor of vaccination) on life expectancy (Abramson, 2001; Helmersson, 2012), however only in the twentieth century, the nonlinear dynamics of infectious disease transmission was better understood. Hamer (1906) was one of the first to recognize that the decreasing density of susceptible persons alone could stop the epidemic. The Chernin (1988) developed mathematical models to investigate the effectiveness of various intervention strategies for malaria. In 1927, Kermack and McKendrick derived the celebrated threshold theorem. They found that a threshold quantity is needed for an infectious disease to spread in a susceptible population. Mathematical modeling became more widespread toward the end of the 20^{th} century (Helmersson, 2012).

The Kermack and McKendrick SIR deterministic model was first developed to describe the transmission mechanisms of bubonic plague given as

$$\begin{aligned} \frac{dS}{dt} &= -\beta SI, \\ \frac{dI}{dt} &= \beta SI - \alpha R, \\ \frac{R}{dt} &= \alpha R, \end{aligned} \tag{2.1}$$

where the total population is classified into three mutually exclusive disease states, with $S(t)$ representing the susceptible population, $I(t)$ the infected, and $R(t$ the recovered or removed

population. The parameter β is the infection (contact) rate and α is the rate of recovery (or removal) for infected individuals. Individuals infected are removed from the infectious state at recovery rate α. The previous *SIR* model (2.1) can be expanded to different models taking into account significant and realistic epidemiological and biological features.

2.2 Within-host mathematical model of malaria infection

The first in-host malaria parasite mathematical model was developed by Anderson et al. (1989). The model describes the within-host dynamics of malaria infection in the absence immune response against the parasite infection. The authors consider the interactions between the healthy erythrocytes $X(t)$, infected erythrocytes $Y(t)$, and free merozoites $M(t)$ at a time t. Their model is given as follows:

$$\begin{aligned} \frac{dX}{dt} &= \lambda - \mu x - \beta XM, \\ \frac{dY}{dt} &= \beta XM - \alpha Y, \\ \frac{dM}{dt} &= \alpha rY - dM - \beta XY, \end{aligned} \tag{2.2}$$

where $X(t)$, $Y(t)$, and $M(t)$ are the density of healthy/uninfected erythrocytes, infected erythrocytes, and merozoites, respectively. λ is the recruitment of the RBCs, β is the infection rate of RBCs by merozoites, α is the rupture and death rate of infected red blood cells, and d is the natural death rate of merozoites.

Assume that healthy red blood cells are generated from bone marrow at a rate λ, die naturally at a rate μ, and get infected by merozoites by the law of mass action to produce the infected/parasite red blood cells at a rate of β. The iRBCs rupture and die at a rate α. The merozoites are produced if the infected red blood cells rupture and release r merozoites per iRBCs. The merozoites die naturally at a rate d or observed by uninfected red blood cells at a rate β. The study considered only the blood stage dynamics of malaria parasite with asexual form of malaria meroziotes. The mathematical model (2.2) was later expanded by taking into account immunological response against merozoites (Anderson et al., 1989). The researcher considers the effect of immune response on malaria merozoite and iRBCs. The model is defined as

$$\begin{aligned} \frac{dX}{dt} &= \lambda - \mu X - \beta XM, \\ \frac{dY}{dt} &= \beta XM - \alpha Y - \omega_y YW, \\ \frac{dM}{dt} &= \alpha rY - dM - \beta xm - \omega_m MW, \\ \frac{dW}{dt} &= \eta_y YM + \eta_m MW - \mu_w W, \end{aligned} \tag{2.3}$$

where W represents the immunological response against malaria infection. The infected red blood cell and malaria merozoite are killed (removed) by the immune response, expressed by

the mass-action terms $\omega_y YW$ and $\omega_m MW$, respectively. The immune system growth is affected by infected red blood cells and merozoites. The immune system population of activated when they contact free merozoites and infected red blood cells at net rates $\eta_y YW$ and $\eta_m MW$, respectively. The activation is proportional to the density of free merozoites and infected red blood cells multiplied by the immune cell population.

Furthermore, the model is refined by incorporating the effect of the immunological responses targeted at stage-specific malaria parasite life cycle in Anderson et al. (1989). The target is cell-mediated and antibody mediated immune response in the reduction of parasite abundance and development within the human host. The antibody-mediated one targets free merozoites whereas the cell-mediated is targets iRBCs. The life expectancy of the infected red blood cells and free merozoites are inversely proportional to their removal rate due to immunological response. From the model findings, they conclude that the immune response against merozoites is less effective than the immune response against infected erythrocyte cells and that therefore vaccines based on infected red blood cell antigens are likely to be more effective than vaccines based on merozoite antigens. This is an important intervention because the rupture of red blood cells releases daughter parasites that quickly invade fresh red blood cells to renew the cycle.

Hellriegel (1992) extended the model formulated in Anderson et al. (1989) which describes the immunological response against the asexual form of malaria parasites by incorporating the sexual form (gametocytes) of malaria parasite $g_i(t)$. Furthermore, the author assumed the existence of two parasite genotypes (genotype-specific and non-specific) that differ in immunogenicity, immunopositivity, gametocytogenesis, and rate of invasion of the erythrocytes. The findings demonstrated that there is no coexistence of the parasites when the two parasite genotypes for the erythrocytes are computed. Also, in the presence of immunological response uninfected erythrocytes significantly higher as well as the coexistence of both parasite genotypes appears.

Hetzel and Anderson (1996) extend the work by Anderson et al. (1989) with and without immunological response against parasite infection by introducing superinfecting merozoites to invade red blood cells that were already infected. Also, the authors neglect the effects of gametocytogenesis which are considered secondary to other processes in the initial dynamics of infection. The effects of cell density, inhibitory cytokines, or natural death are illustrations of the regulatory negative feedback mechanism that can reduce immune population growth at a net rate proportional to the square of its density bT^2. In Austin et al. (1998) the in-host parasite model is developed. This model is similar to that discussed in Hetzel and Anderson (1996).

The work in Anderson et al. (1989) was reformulated by Tumwiine et al. (2008b) by taking into account the stage-specific cell-mediated and antibody-mediated immune response against the malaria parasite. The authors also incorporate the natural death rate of iRBCs in addition

to the rupture rate of iRBCs, as well as the observation of merozoites into healthy red blood cells. The model contains the interaction of red blood cells, free merozoites, and the immune system with the consecration of red blood cells X, infected red blood cells Y, free merozoites, M, and immune response, I to investigate in-host malaria infection and memory effect. Their dynamical system is presented as

$$\begin{aligned}
\frac{dX}{dt} &= \Lambda - \mu_x X - k_s MX, \\
\frac{dY}{dt} &= k_s MX - (\mu_1 + \mu_y)Y - \mu_c YI, \\
\frac{dM}{dt} &= \gamma\mu_y Y - k_s MX - \mu_h MI, \\
\frac{dI}{dt} &= (\lambda_y Y + \lambda_m M)I - \mu_i I.
\end{aligned} \tag{2.4}$$

Li et al. (2011) examined the blood-stage dynamics of malaria parasite infection by incorporating healthy erythrocyte cells, parasitized/infected erythrocyte cells, malaria parasitemia, and immunological response against parasite infection into a mathematical model. The model is an extension of the basic models (Anderson et al., 1989) and (Anderson, 1998), which uses nonlinear Michaelis-Menten-Monod functions to describe how the immune system interacts with infected red blood cells and merozoites. Moreover, the biological feasibility of the model, the existence and stability of parasite-free, parasite persistence without specific immunological response, and with specific immunological response equilibria are presented. The model exhibits periodic oscillations due to Hopf bifurcation at the positive equilibrium (parasite persistence equilibrium point with specific immune response) by using the proliferation rate of the immune system induced by infected erythrocyte cells as the bifurcation parameter, which illustrates that synchronicity is a normal characteristic of malaria infection with immunological response.

Song et al. (2019) studied two models with and without host immunity against malaria parasite infection by considering the competition between two strains of malaria parasites (drug sensitivity and drug resistance malaria parasites). The mathematical model is incorporated to describe the dynamics of within-host infection, including three cell populations: healthy red blood cells, $S(t)$; drug-sensitive malaria parasites, $I_s(t)$; drug-resistant malaria parasites, $I_r(t)$. The dynamical system for the within-host model is as follows:

$$\begin{aligned}
S'(t) &= \Lambda - \beta_1 SI_s - \beta_2 SI_r - d_1 S, \\
I_s'(t) &= \alpha\beta_1 SI_s + p\alpha\beta_2 SI_r - \gamma_1 I_s I_r - (d_2 + \mu)I_s, \\
I_r'(t) &= (1-p)\alpha\beta_2 SI_r - \gamma_2 I_s I_r - d_3 I_r.
\end{aligned} \tag{2.5}$$

The healthy red blood cell is generated at a rate of Λ from bone marrow and dies naturally at a rate d_1. The healthy RBCs get infected by drug-sensitive parasites and drug-resistant parasites with rates of β_1 and β_2 respectively. The infected RBCs eventually develop into a mature

schizont to rupture and release several merozoites by a single infected red blood cell at a rate α. The drug sensitivity and drug resistance malaria parasites compute for the vulnerable red blood cells at a rate γ_1 and γ_2. The drug-resistant parasites and sensitive parasites die at a rate of d_2 and d_3, respectively. The parameter p is the proportion of drug-sensitive parasites released from the red blood cell infected by drug-resistant parasites. Furthermore, the within-host model with immune response and its qualitative analysis like existence and stability analysis of the equilibrium points are presented. The model exhibits the Hopf bifurcation due to periodic oscillation in the presence of host immunity against parasite infection.

A mathematical model of malaria within-host was developed in Iggidr et al. (2006), that incorporated k stages for the infected red blood cells and generation of sexual parasites (gametocytes) as well as n strains (genotypes) in the parasite population. They investigated the model equilibrium points and their stability in terms of basic reproduction number, R_0. The disease-free equilibrium point is globally asymptotically stable if the basic reproduction number is less than unit whereas, the endemic equilibrium point is globally asymptotically stable if the basic reproduction number is greater than unit.

Kamangira et al. (2014) investigated a blood-stage mathematical model of malaria parasite infection with stage-specific immune responses and a combination of antimalarial drug therapies. Initially, the model was developed by considering the stage-specific immune systems without antimalarial drug treatments. To investigate more the effect of stage-specific immunological response, the researchers consider independently the effect of $CD8^+$ cell, antibodies (A), gamma interferon IFN_γ, Tumor necrosis factor alpha TNF_α, interleukin-12 IL_{12}, and other immune on healthy red blood cells, infected red blood cells and merozoites. Next, the model is extended by incorporating the effect of antimalarial drug treatments. The combination therapy coartem, Sulfadoxine-pyrimethamine (SP), and Atovaquone-proguanil (AP) are administered. The important drug efficacies required for the clearance of parasites based on the critical point for the reproductive number in the presence of medications are computed.

The basic reproductive number in the presence of drugs is always less than R_0 for all values of the drug efficacy in the range of zero to one and equal to R_0 only when the drug efficacy is zero. This indicated that the drug was completely ineffective. The R_0 in the presence of drug therapy is less than one whenever the drug efficacy is greater than the critical drug efficacy. This implies that if the drug efficacy is greater than the critical drug efficacy, malaria parasites can be eliminated from an infected host cell. The study compared the effect of Coartem, sulfadoxine-pyrimethamine (SP), and atovaquone-proguanil (AP) on parasite clearance. With the probability of 0.965 and 0.978, the coartem is, therefore, more effective than SP at curing parasitemia, indicating that a person taking coartem will have fewer intracellular and extracellular merozoites. However, in the comparison of Coartem with AP, it is not specified.

The work by Chiyaka et al. (2008) developed a blood-stage mathematical model for malaria infection with the immune system and antimalarial drug therapy. The model is the extension

of the basic model investigated by (Anderson, 1998). The qualitative model analysis like equilibria and their stability is performed, where the infection-free equilibrium point is locally and globally asymptotically stable if the within-host basic reproduction number when there is an immune response only, $R_0 < 1$ and unstable if $R_0 > 1$. Bifurcation analysis is performed by differing the average number of merozoites per bursting iRBCs, r. If r is less than r^c (critical value) uninfected steady state is stable and if $r > r^c$ endemic equilibrium point is stable. Moreover, (Chiyaka et al., 2008) extends to incorporate the effect of drug treatment. Antimalarial drugs implemented during infection (blood schizonticides) concentrate in parasitized red blood cells. When the medication is taken, the burst size of infected erythrocytes, r becomes $(1-\gamma)r$, where γ is drug efficacy and is assumed to lie between zero, which denotes complete ineffectiveness, and one, which denotes 100% effectiveness. Critical drugs efficacy γ^c is examined and given as $\gamma^c = 1 - 1/R_0$, where R_0 is the basic reproductive number when there is an immunological response only. If human immunity against malaria infection fails to clear the parasites $(R_0 > 1)$, the drug is then administered, to lower R_0. Within-host reproduction where the antimalarial drug is administrated, R_γ is always less than R_0 for all γ between zero and one. The $R_\gamma = R_0$ only if $\gamma = 0$. This implies that the drug is completely ineffective. The $R_\gamma < 1$ whenever $\gamma^c < \gamma$, hence malaria parasites can be eliminated from infected individuals.

A mathematical model of blood-stage infection of malaria parasites with and without immune response is presented in Tewa et al. (2012). The model is almost similar to the works (Anderson, 1998; Hetzel and Anderson, 1996), and (Anderson et al., 1989). The model equilibrium points and their stability are computed in the study. The immunological response to the parasite infection is examined and it is shown that immunity against merozoites is more difficult to observe than immunity against infected red blood cells. A mathematical model has been developed in Chen et al. (2015) to describe the dynamics of two strains of malaria parasite infection within a host at the blood stage, the responses of humoral immunity, and cellular immunity. The saturated infection incidences and immunological responses are incorporated into a mathematical model of malaria infection with two competitive strains. The introduction of saturated infection rates induces the coexistence of two strains of parasites. Furthermore, conditions for the existence of equilibria and their stability are presented in Chen et al. (2015).

The study by Tumwiine et al. (2008a) looks into a continuous model with age structure in the human host malaria infection. The model is an expansion of the Anderson et al. (1989) model, incorporating an internal time delay within the red blood cell providing a more realistic biological change. Initially, they develop a system of partial differential equations with four cell populations: the uninfected erythrocytes, infected erythrocytes, free merozoites, and the immune cells for the blood stage dynamics of a single species malaria infection. Subsequently, the model reduces to a system of coupled delay differential equations with a single time delay, which denotes the amount of time between the infection of uninfected erythrocytes and the

cellular release of free merozoites into the bloodstream. The numerical simulation is analyzed, and the results show that the model behaves oscillatorily. As the infected red blood cells discharge merozoites and gametocytes, their density rises and gradually decreases via damped oscillations to a stable steady state.

Elaiw and Al Agha (2020) formulated and analyzed a reaction-diffusion model for the within-host dynamics of malaria infection with CTL and antibody immunological responses. The authors also incorporated the effects of blood-stage antimalarial drug treatment and isoleucine starvation on parasite dynamics. Additionally, the model portrays the progression of infected red blood cells through the three developmental stages: ring stage, trophozoite stage, and schizont stage. Orwa et al. (2018) developed a mathematical model for the dynamics of the *Plasmodium falciparum* parasite during the hepatocytic and erythrocytic stages. The scholars extend the model in Tumwiine et al. (2008b) by taking into account the liver stage development of the parasite. The modified in-host malaria model explains the dynamics of interactions between the malaria parasites, liver hepatocytes, red blood cells, and macrophages (immune system cells). Furthermore, the authors examined the biologically and mathematically meaningfulness of the model as well as the equilibrium points and their stability analysis. The disease-free equilibrium is locally and globally stable if, the within-host basic reproduction number, R_0 is less than unity. The existence of endemic equilibrium is presented in the study. To investigate the most influential parameters of the model they performed sensitivity analysis and global sensitivity analysis.

In Orwa et al. (2019) a blood stage mathematical model that depicts the dynamics of transmission and competition between two *P. falciparum* parasite strains within human hosts during malaria infection is formulated. They take into account the co-infection and competition between the drug-sensitive and the drug-resistant *P. falciparum* strains in the presence of antimalarial medication. Furthermore, the qualitative analysis of the model is investigated. The within-host basic reproduction number R_0 as a maximum of R_s is obtained. The drug-sensitive parasite strains will dominate the drug-resistant strains and become the infection's main cause if $R_s > R_r$. Antimalarial drugs that can kill drug-sensitive parasites should be administered to the patient in this situation to eradicate the infection. On the other hand, if $R_r > R_s$, drug-resistant parasite strains are the main cause of infection. The antimalarial drugs utilized in this situation ought to be potent enough to eradicate both drug-sensitive and drug-resistant parasite strains in the human host's blood. The authors also discussed the existence of the model equilibria and their stability analysis as well as the effect of antimalarial drugs treatment on the within-host malaria parasite infection.

The within the human host malaria infection mathematical model that describes parasite cell interactions at the liver and blood stages with the effect of malaria vaccines is explored in Orwa et al. (2018). The model is an extension of the hepatocytic–erythrocytic in-host malaria model Orwa et al. (2018) by incorporating the two compartments of gametocytes and $CD8^+T$

cells, to investigate the effects of the transmission-blocking vaccines and the general effects of $CD8^{+}T$ cells on the concentrations of the infected red blood cells. The malaria vaccine efficacy is investigated analytically and numerically in this study. In Tabo et al. (2017) a within-host mathematical model of *P. falciparum* malaria infection is proposed and analyzed by considering the combination of the liver, blood, and mosquito stages of malaria infection dynamics with blood stage antimalarial drug therapy as a control strategy on the most influential parameters.

Selemani et al. (2016) developed a deterministic mathematical model to describe the dynamics of malaria parasites both within humans and mosquitos. They investigated the existence and stability equilibria of the developed model. The local stability of the malaria-free equilibrium point is examined using the linearization technique and the global stability of the malaria-free equilibrium point is investigated using Metzler theory. Global stability of malaria infection equilibrium is established using the Lyapunov function in combination with LaSalle's invariance principle. That is the malaria-free equilibrium point is locally and globally stable if $R_0 < 1$ and the malaria-free equilibrium point is violated if $R_0 > 1$ and malaria infection equilibrium is locally and globally stable. Furthermore, the existence and stability of the equilibrium points of the model are supplemented by numerical simulations. In the work by Selemani et al. (2017a) a mathematical model for the in-human host and in-mosquito dynamics of malaria parasite with immune responses was formulated and analyzed. The researchers investigated the existence and stability analysis of the two positive equilibrium points: the parasite-free equilibrium point and the parasite persistence equilibrium point. The parasite-free equilibrium is locally asymptotically stable if $R_0 < 1$ and globally asymptotically stable if $R_0 \leq 1$. The existence and stability analysis of the parasite persistence equilibrium is investigated via numerical simulations. The effect of immune system cells to suppress the production of merozoites is noted to be higher than that of antibodies to block the invasion of human host cells by sporozoites and merozoites. The study by Selemani et al. (2017b) is almost the same as Selemani et al. (2017a).

2.3 Optimal control strategies for malaria models

In developing response strategies for epidemic diseases, policymakers, such as government and public health authorities, frequently have to make trade-offs in selecting among several treatment alternatives (Zhang et al., 2023). Finding the information needed to determine the most effective approaches to intervention before an infection that may already be present or before an unavoidable disease arises is not an easy task. There are several recognized medical treatments and vaccines available for diseases such as measles, influenza, pneumonia, and the human papillomavirus. Currently, vaccinations against high-burden diseases such as malaria and HIV/AIDS are under development, typically, the challenge is in figuring out the

best control to take that balances treatment and immunization to reduce the incidence and disease-related death at an affordable cost (Omondi et al., 2018).

An optimal control is a set of differential equations describing the paths of the control variables that minimize the cost function. The optimal control theory has been widely utilized in the finding of disease control strategies (Lenhart and Workman, 2007), particularly in the control of HIV disease (Cheneke et al., 2023; Ayele et al., 2021; Alsahafi and Woodcock, 2022; Kotola et al., 2023; Sule and Abdullah, 2015; Abiodun et al., 2023), hepatitis B virus (HBV) (Alrabaiah et al., 2020; Ullah et al., 2019; Gahamanyi et al., 2021; Khan et al., 2023; Zada et al., 2021), and tuberculosis (Moualeu et al., 2015; Gao and Huang, 2018; Ullah et al., 2020b). The optimal control utilized in these works is derived from Pontryagin's maximum principle (a necessary condition also known as Pontryagin's minimum principle or simply Pontryagin's principle) (Lenhart and Workman, 2007). The application of optimal control theory in malaria disease and control has for a long time been limited at population level models only (Mwanga et al., 2014; Okosun et al., 2013; Okosun and Makinde, 2011). These models, focus on the application of optimal control theory to minimize the number of humans infected with malaria and to minimize costs of control, such as ITNs, IRS, antimalarial treatment, and vaccine (Olaniyi et al., 2020; Al Basir and Abraha, 2023; Tchoumi et al., 2022).

In the work by Oke et al. (2020) a deterministic compartmental model for the transmission dynamics of malaria with optimal control strategies in a population is investigated. The optimal control problem was formulated using Pontryagin's maximum principle, and three control strategies for disease prevention through bed nets, treatment, and insecticides were incorporated. A nonlinear deterministic mathematical model for malaria transmission dynamics that takes into account climatic variability as a factor was developed in Keno et al. (2022). The authors also applied optimal control theory to describe the optimal control model, which includes three controls: treated bed net, antimalarial drug treatment, and indoor residual spraying strategy. The necessary condition for the optimal control problem is obtained using Pontryagin's maximum principle. The numerical simulation of the optimality system and cost-effectiveness analysis reveals that the combination of treated bed net and treatment is the most optimal and least-cost strategy to minimize malaria. Moreover, the use of mosquito-reduction strategies is more effective than personal protection.

The current research study on the application of optimal control theory to the within-host dynamics of malaria parasite infection is rare. This indicated the complex dynamics of cell-parasite interactions within the human host. In Anderson (1998) examined the impact of a control strategy based on antimalarial drug treatment, vaccine, and host immunity defense against the malaria parasite. As per analysis, there is a non-linear relationship between the amount of control effort and the impact of a given control measure on the frequency or severity of infection. Extremely high cohort immunization is necessary to stop transmission for a defined level of coverage. Gametocyte vaccine is also shown to be better with respect to

eliminating transmission of a certain degree of coverage, however, sporozoite vaccines are revealed to be very effective in reducing disease infection. The first within-host mathematical model of malaria parasites with optimal control strategies was developed by Orwa et al. (2022). Pontryagin's Maximum Principle is applied to establish optimal control strategies against infected cells and malaria parasites. The study considered pre-erythrocytic vaccine, blood-stage vaccine, blood schizontocide, and gametocytocide antimalarial drugs as control measurements. The blood-stage vaccine and blood schizontocide are highly effective in the control of clinical (blood-stage) malaria infection.

2.4 Fractional order model

In recent years, fractional differential equation models have become widely used in biology due to the researchers found that the biological cell membranes have electron conductivity, which could be classified as a fractional-order model (Zhang et al., 2015; Arafa et al., 2014; Miao et al., 2017; Dehingia et al., 2022; Ullah et al., 2020a). Some biological models developed using fractional differential equations have tested out to be more useful than integer-order models. The major distinction between the fractional-order model and the integer-order model is that the fractional-order model has the memory, while the characteristic of the immune response contains the memory (Su et al., 2020b; Arafa et al., 2012; Chatterjee and Ahmad, 2021). Also, they are closely related to fractals, which are common in biological systems (Ding and Ye, 2009; Boukhouima et al., 2018).

A fractional order HIV model considering both virus-to-cell and cell-to-cell transmissions and treatment effect is investigated in Miao et al. (2017). The model that was developed incorporates the premise that memory exists in fractional order systems in the sense of Caputo fractional order derivative, while memory is necessary for the primary immunological response. The model contains the uninfected cells, infected cells, and free virus. The authors additionally addressed conditions for the existence of the equilibria and their stability analysis. The study in Arafa et al. (2012) was conducted on the within-host fractional order derivative for HIV infection. Chatterjee and Ahmad (2021) proposed a fractional-order differential equation model of COVID-19 infection of epithelial cells with adaptive immune responses to the viral mutation to control disease transmission. The model considers three populations, viz, the uninfected epithelial cells, infected cells, and the SARS-CoV-2 virus. Also, the combination of drug therapy on the dynamics of COVID-19 and its effect is investigated in this study. The fractional order model is also used in understanding more insight into the within-host dynamics of malaria parasite infection and memory effect.

In general, the existing research on the dynamics of malaria parasite infection within the host provides valuable insights and lays the groundwork for further exploration. The studies reviewed highlight the key factors influencing the within-host dynamics of parasite infection,

the various theoretical frameworks applied, and the gaps that still need to be addressed. The literature demonstrates the complexity of the within-host dynamics of malarial parasites and the multifaceted nature of the issue. Researchers have examined the within-host dynamics of malarial parasites from diverse perspectives, offering a rich understanding of the phenomenon. However, there are still areas that require additional investigation, such as the effect of antimalarial drug treatment and adaptive immune response on the within-host dynamics of the malaria parasite, within-host dynamical models of malaria parasite infection with optimal control, and memory effect.

In the future, research should aim to expand on the groundwork laid in this study. Potential areas for further exploration include reaction-diffusion and delay differential models. The study did not account for the impact of drug-resistant malaria parasite infection on the dynamics of the parasite infection within the host. Scholars can contribute to a more comprehensive understanding of the within-host dynamics of malaria parasite infection and its drug-resistant strains.

CHAPTER 3

RESEARCH METHODOLOGY

In this chapter, we present the research methodologies that are used to attain the stated general and specific objectives. For this, we briefly discuss the method of data analysis, the source of data, the approach of study, and mathematical procedures.

3.1 Model formulation

We formulated the within-host mathematical model for the dynamics of malaria parasite infection. The system non-leaner ordinary differential equation (deterministic mathematical model) is used via realistic acquisition for the within-host malaria infection parasite. The study considered both the blood and liver-blood stage dynamics of the infection with immunological responses. The dynamics of red blood cells (uninfected red blood cells, and infected red blood cells), liver hepatocyte cells (uninfected liver hepatocyte cells, and infected liver hepatocyte cells), malaria parasites (sporozoites, merozoites, and gametocytes), and immune cells population are considered. Furthermore, we have used the nonlinear bounded Michaelis-Menten-Monod function to show the interaction between red blood cells, malaria parasites, and the immune system. Next, we extend the developed model into optimal control to invest in the effective measurement to eliminate within-host malaria parasite infection with a minimum cost of controls. Finally, we extended to the fractional order derivative in the sense of Caputo derivative to observe the memory effects and gain more insights about the in-host dynamics of malaria infection.

3.2 Model Analysis

The formulated models are analyzed both qualitatively and quantitatively using appropriate methods.

3.2.1 Qualitative analysis

The model proposed within-host mathematical models are analyzed using different mathematical tools, theories, and theorems which are suitable for the system of ordinary differential equations. The basic properties of the model such as biological feasibility and mathematical well-possedness are evaluated by showing non-negativity and boundedness of the solutions. The Ruoth-Hurwitiz stability criterion, Lyapunov global stability theorem, Castillo-Chavez and Song theorem, and bifurcation analysis are used to display the stability analysis of the steady states of the models and Descartes' Rule of signs used to show the existence of the parasite persistence steady state. Furthermore, the fixed point theorem, Laplace transform and

inverse Laplace transform are being used to provide the qualitative analysis of the fractional order derivative model. The Pontragen Maximum Principal is applied to the optimal control problem to investigate the necessary condition of optimal control.

3.2.2 Numerical analysis

To validate and supplement the analytical results, we present different numerical simulations for the models using different numerical methods (schemes). We used the fourth-order Rung-Kutta for the integer-order models, while the generalized predictor-corrector of the Adams-Bashforth-Moulton method is used for the fractional-order derivative model.

3.3 Source of data

The data required for the analysis of this study is obtained from secondary data and all sources are cited.

3.3.1 Method of data analysis

The time series analysis method is used to analyze the data. The study involved both qualitative and quantitative analysis. Thus, the study was analyzed using the software MATLAB and PYTHON and the results are displayed in the form of figures. Both programs give the same numerical simulations with the same input, and it is a matter of accessibility.

CHAPTER 4

WITHIN-HOST MATHEMATICAL MODEL OF MALARIA PARASITE WITH CELL-MEDIATED AND ANTIBODY-MEDIATED IMMUNE SYSTEMS

In this chapter, we develop a mathematical model that describes the dynamics and interactions between the malaria parasites and red blood cells in the presence of stage-specific immune effectors (cell-mediated and antibody-mediated immune systems). The basic properties of the in-host model such as biological meaningfulness and mathematically well-possedness as well as qualitative analysis including within-host reproduction number, equilibrium points and their stability analysis, bifurcation analysis, and the forward sensitivity analysis of in-host reproduction numbers are presented. Finally, numerical simulations of the in-host model are performed using Matlab.

4.1 Model formulation

We extended the within-host malaria model (Anderson et al., 1989), by incorporating the sexual parasite development (gametocytes) and stage-specific cell-mediated and antibody-mediated immunological response. The developed within-host malaria model focuses on the blood stage and describes the dynamics of the interaction between the parasite and red blood cells, as well as the responses of the immune system, including both antibody-mediated and cell-mediated responses. We consider six compartments in the model; healthy/uninfected (RBCs) $X(t)$, infected/parasitezed (iRBCs) $Y(t)$, merozoites $M(t)$, gametocytes $G(t)$, antibody-mediated immune system $H(t)$ and cell-mediated immune system $C(t)$ at a time t. Considering the fact that cell proliferation can saturate and that there is a handling time for immune responses, the more commonsensible nonlinear bounded Michaelis-Menten-Monod function (De Boer and Perelson, 1995) is used to show the interaction between RBCs, malaria parasites, and immune system.

The developed within-host model is governed by the following assumptions:

(i). The red blood cells are recruited at a constant rate from the bone marrow.

(ii). The nonlinear bounded Michaelis-Menten-Monod function (Li et al., 2011) is used to show the interaction between red blood cells, malaria parasites, and the immune system.

(iii). The infected red blood cells are removed by a cell-mediated immune system.

(iv). The malaria parasites (merozoite and gametocytes) are removed by an antibody-mediated immune system.

(v). The immune systems are recruited at a constant rate from the bone arrow.

(vi). The cell-mediated immune response is stimulated due to the presence of infected red blood cells.

(vii). The antibody-mediated immune response is stimulated due to the presence of malaria parasites such as merozoite and gametocytes.

(viii). The infection/invasion rate of uninfected red blood cells is inhibited owing to the presence of antibody-mediated immune response.

(xv). Merozoites are generated during the rupture of blood schizonts.

(x). All the biological model parameters and variables are assumed non-negative.

The dynamics of red blood cells, malaria parasites and immune system cell populations in each compartment are described as follows:

Healthy red blood cells (RBCs) X(t): Healthy RBCs are produced from bone marrow at a constant rate π_x, the RBCs are invaded by merozoite when the matured infected hepatocyte (liver schizont) burst open and release thousands of merozoites into the bloodstream at a rate β, the invasions of RBCs are inhibited by the antibody-mediated immune response at a rate $1/(1+b_0H)$, where b_0 is the efficacy of antibody-mediated immune response on erythrocytic invasion. The RBCs are removed by natural death at a rate μ_x and have a life expectancy $1/\mu_x$ of approximately 120 days.

Infected red blood cells (iRBCs) Y(t): The red blood cells get infected and progress the infected RBCs at a rate $\beta/(1+b_0H)$. The infected RBCs are removed due to cell-mediated immune response at a rate γ and die during rupturing at a rate μ_y.

Merozoites M(t): The merozoite populations produced during iRBCs rupture and release 8-36 merozoites (Su et al., 2020a) into the RBCs at a rate $N\mu_y$, where N is the average number of the merozoites that released per rupturing iRBCs, the production of merozoite inhibited by the cell-mediated immune response at a rate $1/(1+b_1C)$, where b_1 is the efficacy of the cell-mediated immune response on rupturing of infected erythrocyte (production rate of merozoites). The merozoites suffer natural death at a rate μ_m and are cleared by the antibody-mediated immune response at a rate θ.

Gametocytes G(t): The gametocyte is produced because of a small number of merozoites developing into sexual forms in the blood stage (Sreenivasamurthy et al., 2013) at a rate c. Also, production is inhibited by the antibody-mediated immune response at a rate of $1/(1+b_2H)$, where b_2 is the efficacy of antibody-mediated immune response in the development of gametocytes. The gametocyte populations die naturally at a rate μ_g and are removed by antibody-mediated immune response at a rate η.

Antibody-mediated immune system H(t): Assume that the antibody-mediated immune responses are recruited at a constant rate π_h from human bone marrow and it is activated (stimulated) during the malaria infection at a rate α and δ. The activation is inhibited owing to malaria parasites (merozoites and gametocytes) at the rate of $1/(1+c_0M)$ and $1/(1+c_1G)$, where c_0 and c_1 are the efficacy of merozoites and gametocytes on the activation of antibody-mediated immune response, respectively. Also, the antibody-mediated immune response suffers natural death at a rate μ_h.

Cell-mediated immune system C(t): We assume the cell-mediated immune responses are recruited from human bone marrow at a constant rate π_c. The cell-mediated immune response is activated (stimulated) during malaria infection at a rate ξ, and the activation is inhibited due to infected erythrocytes at a rate of $1/(1+b_3Y)$, where b_3 is the efficacy of infected erythrocyte on activation of cell-mediated immune response and the cell-mediated immune response suffer natural death at a rate μ_c. In this case, we assume that uninfected RBC observations of merozoites are to be neglected. The state variables and biological parameters that we used within the host dynamical system (4.1) and their description are given in Table 4.1 and Table 4.2, respectively.

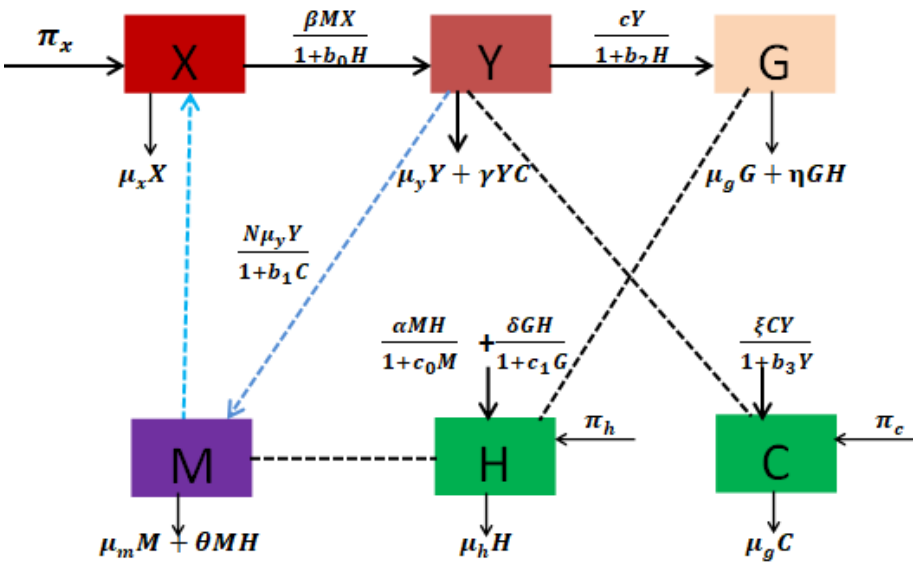

Figure 4.1: Schematic diagram of the dynamical system of blood-stage malaria parasite with immune responses, the black dotted lines indicate the interactions between iRBCs (Y), merozoites (M), and gametocytes (G) with immune responses (H and C) and the blue dotted arrows indicate the interaction between RBCs (X) and iRBCs with malaria parasites in the form of merozoites.

Based on the descriptions, assumptions, and schematic diagram (Fig.4.1) a mathematical model of the in-host dynamics of the malaria infection with cell-mediated and antibody-

Table 4.1: Model variables and their descriptions

State variables	Description
$X(t)$	Concentration of uninfected red blood cell cells at time t
$Y(t)$	Concentration infected red blood cells at time t
$M(t)$	Concentration malaria parasite in the form of merozoites at time t
$C(t)$	Concentration cellular immune response at time t
$H(t)$	Concentration antibody-mediated (humoral) immune response at time t
$G(t)$	Concentration malaria gametocytes at time t

mediated immune responses is given as

$$\begin{aligned}
\frac{dX}{dt} &= \pi_x - \frac{\beta XM}{1+b_0H} - \mu_x X, \\
\frac{dY}{dt} &= \frac{\beta XM}{1+b_0H} - \frac{cY}{1+b_2H} - \gamma YC - \mu_y Y, \\
\frac{dM}{dt} &= \frac{\mu_y NY}{1+b_1C} - \theta MH - \mu_m M, \\
\frac{dG}{dt} &= \frac{cY}{1+b_2H} - \eta GH - \mu_g G, \\
\frac{dC}{dt} &= \pi_c + \frac{\xi CY}{1+b_3Y} - \mu_c C, \\
\frac{dH}{dt} &= \pi_h + \frac{\alpha MH}{1+c_0M} + \frac{\delta GH}{1+c_1G} - \mu_h H,
\end{aligned} \tag{4.1}$$

with initial conditions

$$X(0) > 0,\ Y(0) \geq 0,\ M(0) \geq 0,\ G(0) \geq 0,\ C(0) > 0,\ H(0) > 0. \tag{4.2}$$

4.2 Model Analysis

In this section, we present the qualitative analysis of the dynamical system (4.1), including boundedness and non-negativity of solutions, equilibrium points, the basic reproduction number, local and global stability of disease-free (parasite-free) equilibrium point, bifurcation analysis, and sensitivity analysis of basic reproduction number.

4.2.1 Positivity and boundedness

The formulated model is biologically meaningful and mathematically well-posed if all the state variables and their solutions are positive and bounded in the given region. The biologically meaninfulness and mathematically well-posedness is shown by proving the boundedness and non-negativity of the solutions.

Table 4.2: Model parameters and their descriptions

Parameters	Description
π_x	The recruitment rate of uninfected RBCs from bone marrow
π_c	Production rate of cell-mediated immune response
π_h	Production rate of antibody-mediated immune response
β	Infection rate of the red blood cell by merozoites
μ_x	Natural death rate for uninfected red blood cells
μ_y	Death rate of infected red blood cells
N	Average number of merozoites per ruptured infected red blood cells
μ_m	Natural death rate of merozoites
μ_h	Natural death rate antibody-mediated immune response
μ_c	Natural death rate cell-mediated immune response
μ_g	Natural death rate of gametocyte
θ	Removal rate of merozoites due to antibody-mediated immune response
b_0	Efficacy of antibody-mediated immune response on erythrocytic invasion
b_1	Efficacy of the cell-mediated immune response on rupturing of iRBCs
c	Rate of sexual replication of merozoites in bloodstream
b_2	Efficacy of the antibody-mediated immune response on gametocytes
c_0	Efficacy of the merozoites on the activation of antibody-mediated immune system
c_1	Efficacy of the gametocytes on the activation of the antibody-mediated immune system
η	Removal rate of gametocytes due to antibody-mediated immune responses
γ	Removal rate of infected red blood cells due to cell-mediated immune response
ξ	Activation rate cell-mediated immune response owing to iRBCs
δ	Activation rate antibody-mediated immune response due to the presence of gametocytes
α	Activation rate antibody-mediated immune response due to the presence of merozoites

Theorem 4.1. *Every solution of the model system* (4.1) *is bounded in the region*

$$\Omega = \left\{ \begin{array}{l} \Omega_1 \times \Omega_2 \times \Omega_3 \in R_+^6 : \Omega_1 = \{(X,Y) \in R_+^2 : 0 < X+Y \leq \frac{\pi_x}{\mu_x}\}, \\ \Omega_2 = \{(M,G) \in R_+^2 : 0 \leq M+G \leq (N\mu_y + c)\frac{\pi_x}{a_2\mu_r}\}, \Omega_3 = \{(C,H) \in R_+^2 : 0 \leq C+H \leq \frac{\pi}{q}\} \end{array} \right\},$$

for any time $t \geq 0$.

Proof. Let $N_R(t) = X(t)+Y(t)$, $N_P(t) = M(t)+G(t)$ and $N_I(t) = C(t)+H(t)$ be the total size of RBCs, malaria parasites and immune response, respectively. □

To show that the solutions of model system (4.1) are bounded we proceed as follows:

$$\frac{dN_R}{dt} = \frac{dX}{dt} + \frac{dY}{dt} = \pi_x - \mu_x X - \mu_y Y - \frac{cY}{1+b_2 H} - \gamma YC \leq \pi_x - \mu_r N_R,$$

where $\mu_r = min\{\mu_x, \mu_y\}$. For $N_r(0) \leq \frac{\pi_x}{\mu_r}$, we found that

$$N_R(t) \leq \frac{\pi_x}{\mu_r} - \left(\frac{\pi_x}{\mu_r} - N_r(0)\right) exp\{-\mu_r t\} \leq \frac{\pi_x}{\mu_r}.$$

This implies that at any time t, $N_R(t) \leq \frac{\pi_x}{\mu_r}$. Also, this procedure can similarly be applied to the population of malaria parasites $N_P(t) = M(t) + G(t)$. Thus, we get

$$\frac{dN_P}{dt} = \left(\frac{\mu_y N}{1+b_1 C} + \frac{c}{1+b_2 H}\right) Y - a_1 H N_P - a_2 N_P = Q_1(C,H)Y - (a_1 H + a_2)N_P,$$

where $a_1 = min\{\theta, \eta\}$, $a_2 = min\{\mu_m, \mu_g\}$ and $Q_1(C,H) = \frac{\mu_y N}{1+b_1 C} + \frac{c}{1+b_2 H} \leq \mu_y N + c$.

Since $Y(t) \leq \frac{\pi_x}{\mu_r}$, we have

$$\frac{dN_P}{dt} \leq Q_1(C,H)\frac{\pi_x}{\mu_r} - a_2 N_P \leq (\mu_y N + c)\frac{\pi_x}{\mu_r} - a_2 N_P,$$
$$N_P(t) \leq (\mu_y N + c)\frac{\pi_x}{a_2 \mu_r} - \left((\mu_y N + c)\frac{\pi_x}{a_2 \mu_r} - N_P(0)\right) exp\{-a_2 t\} \leq (\mu_y N + c)\frac{\pi_x}{a_2 \mu_r}.$$

The term $(\mu_y N + c)$ is the maximum production rate of malaria parasites and $1/a_2$ is the lifespan of malaria parasites.

Finally, for immune system $N_I(t) = C(t) + H(t)$, from the last two equations of (4.1) we have

$$\begin{aligned}
\frac{dN_I}{dt} &= \pi_c + \pi_h + \frac{\xi Y}{1+b_3 Y} C + \left(\frac{\alpha M}{1+c_0 M} + \frac{\delta G}{1+c_1 G}\right) H - \mu_c C - \mu_h H \\
&\leq \pi + \xi C + (\alpha + \delta) H - a_3 N_I \\
&\leq \pi + w N_I - a_3 N_I,
\end{aligned}$$

where $\pi = max\{\pi_h, \pi_c\}$, $a_3 = min\{\mu_c, \mu_h\}$ and $w = max\{\xi, \alpha + \delta\}$.

Let $q = a_3 - w > 0$, then the above inequality holds that for $N_I(0) < \frac{\pi}{q}$.

$$\frac{dN_I}{dt} \leq \pi - q N_I, \quad N_I(t) \leq \frac{\pi}{q} - \left(\frac{\pi}{q} - N_I(0)\right) exp\{-qt\} \leq \frac{\pi}{q}.$$

Therefore, every solution of the dynamical system (4.1) is bounded by the region Ω.

Now, we show that Ω is a positively invariant and attracting region for the system (4.1). The following theorem assures that the model system is mathematically well-posed and biologically feasible in the region Ω.

Theorem 4.2. *The region Ω is positively invariant for model (4.1). That is every solution $X(t), Y(t), M(t), G(t), C(t)$, and $H(t)$ with a non-negative initial state $X(0), Y(0), M(0), G(0), C(0)$ and $H(0)$ in Ω is non-negative and will remain in Ω for all $t \geq 0$.*

Proof. Consider the first equation of the model (4.1)

$$\frac{dX}{dt} = \pi_x - \frac{\beta X M}{1+b_0 H} - \mu_x X \geq -\left(\frac{\beta M}{1+b_0 H} + \mu_x\right) X, \quad \frac{dX}{X} \geq -\left(\frac{\beta M}{1+b_0 H} + \mu_x\right) dt.$$

Integrating the above differential inequality from 0 to t, we obtained

$$X(t) \geq X_0 exp\left\{-\int_0^t \left(\frac{\beta M}{1+b_0 H}+\mu_x\right) dt\right\} > 0 \ \ for \ \ all \ \ t \geq 0.$$

Consider the second equation of the model (4.1)

$$\frac{dY}{dt} = \frac{\beta XM}{1+b_0 H} - \frac{cY}{1+b_2 H} - \gamma YC - \mu_y Y, \quad \frac{dY}{Y} \geq -(c+\gamma C+\mu_y)dt$$
$$Y(t) = Y_0 exp\left\{-\int_0^t (c+\gamma C+\mu_y)dt\right\} \geq 0 \ \ for \ \ all \ \ t \geq 0.$$

Similarly, one can show the non-negativity of solutions $M(t), G(t), C(t)$, and $H(t)$ for all $t \geq 0$. Therefore, the solutions of system equation (4.1) are non-negative for all $t \geq 0$. □

4.2.2 Parasite-free equilibrium point

The parasite-free equilibrium (PFE), E^0, is the steady state solution where there is no malaria parasite infection in the human host cell. That is, $Y = 0$, $M = 0$ and $G = 0$. Substituting this value in the system equation (4.1) and setting the right-hand side of the system equation (4.1) to zero, we obtained

$$E^0 = (X^0, Y^0, M^0, G^0, C^0, H^0) = \left(\frac{\pi_x}{\mu_x}, 0, 0, 0, \frac{\pi_c}{\mu_c}, \frac{\pi_h}{\mu_h}\right). \tag{4.3}$$

4.2.3 The basic reproduction number

From the perspective of epidemiology, a basic reproduction number is a threshold quantity which represents on average, the number of secondary infections that a single infectious case would generate in a completely susceptible populations over its entire infectious period (Dietz, 1993). The within-host basic reproduction number, $\Re_0$ is the average number of secondary cases that produced infected erythrocytes as a result of the infective agent malaria parasites of merozoites introduced in a population of purely susceptible red blood cells (erythrocyte cells). To compute the basic reproduction number $\Re_0$, we use the next-generation matrix approach (Van den Driessche and Watmough, 2002). Let

$$\frac{d\mathbf{X}}{dt} = \mathscr{F}_i - \mathscr{V}_i,$$

where $\mathbf{X}$ is the infected compartments, $\mathscr{F}_i$ is the rate of new appearance, and $\mathscr{V}_i$ is the rate of transfer of individuals from one compartment to another compartment via any other means are

given as

$$\mathscr{F}_i = \begin{pmatrix} \frac{\beta XM}{1+b_0H} \\ 0 \\ 0 \end{pmatrix}, \ \mathscr{V}_i = \begin{pmatrix} \frac{cY}{1+b_2H} + \gamma YC + \mu_y Y \\ -\frac{N\mu_y Y}{1+b_1C} + \mu_M M + \theta MH \\ -\frac{cY}{1+b_2H} + \mu_G G + \eta GH \end{pmatrix}. \tag{4.4}$$

The Jacobian matrices of the vectors $\mathscr{F}$ and $\mathscr{V}$ are investigated by differentiating $\mathscr{F}_i$ and $\mathscr{V}_i$ with respect to infected compartments at a parasite-free equilibrium point $E^0 = (\frac{\pi_x}{\mu_x}, 0, 0, 0, \frac{\pi_c}{\mu_c}, \frac{\pi_h}{\mu_h})$. Thus,

$$\mathscr{F} = \begin{pmatrix} 0 & \frac{\beta\pi_x\mu_h}{\mu_x(\mu_h+b_0\pi_h)} & 0 \\ 0 & 0 & 0 \\ 0 & 0 & 0 \end{pmatrix}, \ \mathscr{V} = \begin{pmatrix} \mu_y + \frac{c\mu_h}{\mu_h+b_2\pi_h} + \frac{\gamma\pi_c}{\mu_c} & 0 & 0 \\ -\frac{N\mu_y\mu_c}{\mu_c+b_1\pi_c} & \mu_m + \frac{\theta\pi_h}{\mu_h} & 0 \\ -\frac{c\mu_c}{\mu_h+b_2\pi_h} & 0 & \mu_g + \frac{\eta\pi_h}{\mu_h} \end{pmatrix}. \tag{4.5}$$

The inverse of matrix V is hence given by

$$\mathscr{V}^{-1} = \begin{pmatrix} \frac{1}{\left(\mu_y + \frac{c\mu_h}{\mu_h+b_2\pi_h} + \frac{\gamma\pi_c}{\mu_c}\right)} & 0 & 0 \\ \frac{N\mu_y\mu_c}{(\mu_c+b_1\pi_c)\left(\mu_y + \frac{c\mu_h}{\mu_y+b_2\pi_h} + \frac{\gamma\pi_c}{\mu_c}\right)\left(\mu_m + \frac{\theta}{\mu_h}\right)} & \frac{1}{\mu_m + \frac{\theta\pi_h}{\mu_h}} & 0 \\ \frac{c\mu_c}{(\mu_h+b_2\pi_h)\left(\mu_y + \frac{c\mu_h}{\mu_h+b_2\pi_h} + \frac{\gamma\pi_c}{\mu_c}\right)(\mu_g + \frac{\eta\pi_h}{\mu_h})} & 0 & \frac{1}{\mu_g + \frac{\eta\pi_h}{\mu_h}} \end{pmatrix}. \tag{4.6}$$

Hence, the next generation matrix is

$$\mathscr{F}\mathscr{V}^{-1} = \begin{pmatrix} \frac{\beta\pi_x\mu_h N\mu_y\mu_c}{\mu_x(\mu_h+b_0\pi_h)(\mu_c+b_1\pi_c)\left(\mu_y + \frac{c\mu_h}{\mu_y+b_2\pi_h} + \frac{\gamma\pi_c}{\mu_c}\right)\left(\mu_m + \frac{\theta}{\mu_h}\right)} & \frac{\beta\pi_x\mu_h}{\mu_x(\mu_h+b_0\pi_h)\left(\mu_m + \frac{\theta\pi_h}{\mu_h}\right)} & 0 \\ 0 & 0 & 0 \\ 0 & 0 & 0 \end{pmatrix}. \tag{4.7}$$

According to the next-generation technique given in (Van den Driessche and Watmough, 2002), the basic reproduction number of the system (4.1) is the spectral radius of $\rho(\mathscr{F}\mathscr{V}^{-1})$. It can clearly be seen that two of the three eigenvalues of matrix $\mathscr{F}\mathscr{V}^{-1}$ in equation (4.7) have zero values; that is $\lambda_2 = \lambda_3 = 0$. The first and dominant nonnegative eigenvalue λ_1 becomes the within-host basic reproduction number and given as

$$\mathfrak{R}_0 = \frac{N\mu_y\beta\pi_x}{\mu_x\left(1 + \frac{b_0\pi_h}{\mu_h}\right)\left(1 + \frac{b_1\pi_c}{\mu_c}\right)\left(\mu_y + \frac{c\mu_h}{\mu_h+b_2\pi_h} + \frac{\gamma\pi_c}{\mu_c}\right)\left(\mu_m + \frac{\theta\pi_h}{\mu_h}\right)}. \tag{4.8}$$

The expression $\mathfrak{R}_0$ is the number of secondary infections within completely susceptible RBCs due to the malaria merozoites in a healthy individual.

Note: The term $\frac{\beta\pi_x}{\mu_x\left(1+\frac{b_0\pi_h}{\mu_h}\right)}$ is the expected number of infected red blood cells by free mero-

zoites in the presence of immunity against parasite infection. The term $\frac{N\mu_y}{\left(1+\frac{b_1\pi_c}{\mu_c}\right)\left(\mu_y+\frac{c\mu_h}{\mu_h+b_2\pi_h}+\frac{\gamma\pi_c}{\mu_c}\right)\left(\mu_m+\frac{\theta\pi_h}{\mu_h}\right)}$ is the expected number of merozoites produced during parasite infection in the presence of cell-mediated and antibody-mediated immune responses. Furthermore, $\frac{1}{\left(\mu_y+\frac{c\mu_h}{\mu_h+b_2\pi_h}+\frac{\gamma\pi_c}{\mu_c}\right)}$ is the life span of infected red blood cells and $\frac{1}{\left(\mu_m+\frac{\theta\pi_h}{\mu_h}\right)}$ is the life span of the malaria merozoites with the existence of immune responses.

4.2.4 Local stability analysis of parasite-free equilibrium point

In this section, the local stability analysis of the parasite-free equilibrium point (PFE) of the model (4.1) is discussed by determining the Jacobian matrix with its eigenvalues. Now the general Jacobian matrix of model (4.1) can be written:

$$J(E)=\begin{pmatrix} -A_{11} & 0 & -\frac{\beta X}{1+b_0H} & 0 & 0 & \frac{b_0\beta XM}{(1+b_0H)^2} \\ \frac{\beta M}{1+b_0H} & -A_{22} & \frac{\beta X}{1+b_0H} & 0 & -\gamma Y & \frac{cb_2Y}{(1+b_2H)^2}-\frac{b_0\beta XM}{(1+b_0H)^2} \\ 0 & \frac{N\mu_y}{1+b_1C} & -A_{33} & 0 & 0 & -\theta M \\ 0 & \frac{c}{1+b_2H} & 0 & -A_{44} & 0 & -\eta G-\frac{cb_2Y}{(1+b_2H)^2} \\ 0 & \frac{\xi C}{(1+b_3Y)^2} & 0 & 0 & -A_{55} & 0 \\ 0 & 0 & \frac{\alpha H}{(1+c_0M)^2} & \frac{\delta H}{(1+c_1G)^2} & 0 & -A_{66} \end{pmatrix}, \tag{4.9}$$

where

$$A_{11}=\frac{\beta M}{1+b_0H}+\mu_x,\ A_{22}=\mu_y+\frac{c}{1+b_2H}+\gamma C,\ A_{33}=\mu_m+\theta H,\ A_{44}=\mu_g+\gamma H,$$
$$A_{55}=\mu_c-\frac{\xi Y}{1+b_3Y},\ A_{66}=\mu_h+\frac{\alpha M}{1+c_0M}+\frac{\delta G}{1+c_1G}.$$

Theorem 4.3. *The parasite-free equilibrium point E^0 is locally asymptotically stable if $\Re_0<1$ and unstable if $\Re_0>1$.*

Proof. The Jacobian matrix at the parasite-free equilibrium point is given as

$$J(E^0)=\begin{pmatrix} -\mu_x & 0 & \frac{-\beta\pi_x\mu_h}{\mu_x(\mu_h+b_0\pi_h)} & 0 & 0 & 0 \\ 0 & -\mu_y-\frac{c\mu_h}{\mu_h+b_2\pi_h}-\frac{\gamma\pi_c}{\mu_c} & \frac{\beta\pi_x\mu_h}{\mu_x(\mu_h+b_0\pi_h)} & 0 & 0 & 0 \\ 0 & \frac{N\mu_y\mu_c}{\mu_c+b_1\pi_c} & -\mu_m-\frac{\theta\pi_h}{\mu_h} & 0 & 0 & 0 \\ 0 & \frac{c\mu_c}{\mu_c+b_2\pi_c} & 0 & -\mu_g-\frac{\eta\pi_h}{\mu_h} & 0 & 0 \\ 0 & \frac{\xi\pi_c}{\mu_c} & 0 & 0 & -\mu_c & 0 \\ 0 & 0 & \frac{\alpha\pi_h}{\mu_h} & \frac{\delta\pi_h}{\mu_h} & 0 & -\mu_h \end{pmatrix}. \tag{4.10}$$

Applying the Routh–Hurwitz stability criteria, the parasite-free equilibrium point is locally asymptotically stable, if all the eigenvalues of the Jacobian matrix (4.10) have negative real parts. Clearly, the first, fifth, and sixth columns of the Jacobian matrix (4.10) have only diagonal entries. Thus, the eigenvalues $\lambda_1=-\mu_x$, $\lambda_5=-\mu_c$, and $\lambda_6=-\mu_h$. The remaining

eigenvalues are investigated from the sub-matrix

$$J_1(E^0) = \begin{pmatrix} -\mu_y - \frac{c\mu_h}{\mu_h+b_2\pi_h} - \frac{\gamma\pi_c}{\mu_c} & \frac{\beta\pi_x\mu_h}{\mu_x(\mu_h+b_0\pi_h)} & 0 \\ \frac{N\mu_y\mu_c}{\mu_c+b_1\pi_c} & -\mu_m - \frac{\theta\pi_h}{\mu_h} & 0 \\ \frac{c\mu_c}{\mu_c+b_2\pi_c} & 0 & -\mu_g - \frac{\eta\pi_h}{\mu_h} \end{pmatrix}. \tag{4.11}$$

The last column of the sub matrix $J_1(E^0)$ is has only diagonal entry. Hence, $\lambda_4 = -\mu_g - \theta\pi_h/\mu_h$. Again the remaining eigenvalues are investigated from the sub-matrix

$$J_2(E^0) = \begin{pmatrix} -\left(\mu_y + \frac{c\mu_h}{\mu_h+b_2\pi_h} + \frac{\gamma\pi_c}{\mu_c}\right) & \frac{\beta\pi_x\mu_h}{\mu_x(\mu_h+b_0\pi_h)} \\ \frac{N\mu_y\mu_c}{\mu_c+b_1\pi_c} & -\left(\mu_m + \frac{\theta\pi_h}{\mu_h}\right) \end{pmatrix}. \tag{4.12}$$

The associated characteristic equation is given by

$$\lambda^2 + D_1\lambda + D_0 = 0, \tag{4.13}$$

where

$$D_1 = \mu_y + \frac{c\mu_h}{\mu_h+b_2\pi_h} + \frac{\gamma\pi_c}{\mu_c} + \mu_m + \frac{\theta\pi_h}{\mu_h},$$
$$D_0 = \left(\mu_y + \frac{c\mu_h}{\mu_h+b_2\pi_h} + \frac{\gamma\pi_c}{\mu_c}\right)\left(\mu_m + \frac{\theta\pi_h}{\mu_h}\right)(1-\mathscr{R}_0).$$

Clearly $D_1 > 0$, we need to show $D_0 > 0$. Thus, $D_0 > 0$ if $\Re_0 < 1$ the characteristic equation (4.13) has negative eigenvalues. Therefore, the parasite-free equilibrium point is locally asymptotically stable if $\Re_0 < 1$ and unstable if $\Re_0 > 1$. □

4.2.5 Global stability of the parasite-free equilibrium point

Here, we investigate the global stability analysis of the parasite-free equilibrium point using the method which is discussed in (Castillo-Chavez and Song, 2004).

Theorem 4.4. *The parasite-free equilibrium E^0 is globally asymptotically stable if $\Re_0 < 1$.*

Proof. First, we divide the system equation (4.1) into uninfected and infected compartments as follows:

$$\frac{d\mathscr{U}}{dt} = \mathscr{F}(\mathscr{U},\mathscr{V}), \tag{4.14}$$
$$\frac{d\mathscr{V}}{dt} = \mathscr{G}(\mathscr{U},\mathscr{V}),\ \ \mathscr{G}(\mathscr{U},0) = 0, \tag{4.15}$$

where $\mathscr{U} = (X,C,H) \in R^3$ is represent uninfected compartments and $\mathscr{V} = (Y,M,G) \in R^3$ is infected compartments.

The parasite-free equilibrium point E^0 is globally asymptotically stable if the following conditions hold:

$\mathscr{A}_1$. For $\frac{d\mathscr{U}}{dt} = \mathscr{F}(\mathscr{U},0)$ is globally asymptotically stable, where $\mathscr{F}(\mathscr{U}^0,0) = 0$,

$\mathscr{A}_2$. $\mathscr{G}(\mathscr{U},\mathscr{V}) = \mathscr{D}\mathscr{V} - \widehat{\mathscr{G}}(\mathscr{U},\mathscr{V}), \widehat{\mathscr{G}}(\mathscr{U},\mathscr{V}) > 0$, for $(\mathscr{U},\mathscr{V}) \in \Omega$, where $\mathscr{D} = D_{\mathscr{V}}\mathscr{G}(\mathscr{U}^0,0)$ is an **M** matrix, i.e, the off diagonal elements of matrix $\mathscr{D}$ is non-negative.

Now, from system equation (4.1), we have

$$\mathscr{F}(\mathscr{U},\mathscr{V}) = \begin{pmatrix} \pi_x - \frac{\beta XM}{1+b_0H} - \mu_X X \\ \pi_C + \frac{\xi CY}{1+b_3Y} - \mu_C C \\ \pi_H + \frac{\alpha MH}{1+c_0M} + \frac{\delta GH}{1+c_1G} - \mu_H H \end{pmatrix} \text{ and } \mathscr{F}(\mathscr{U},0) = \begin{pmatrix} \pi_x - \mu_X X \\ \pi_C - \mu_C C \\ \pi_H - \mu_H H \end{pmatrix}, \tag{4.16}$$

$$\mathscr{F}(\mathscr{U}^0,0) = 0, \quad \text{where } \mathscr{U}^0 = \left(\frac{\pi_x}{\mu_x}, \frac{\pi_c}{\mu_c}, \frac{\pi_h}{\mu_h}\right).$$

Equation (4.16) has a unique equilibrium point $\mathscr{U}^0 = (\frac{\pi_x}{\mu_x}, \frac{\pi_c}{\mu_c}, \frac{\pi_h}{\mu_h})$, which is globally asymptotically stable, i.e, all the solution of equation (4.16) converge to the parasite-free equilibrium point. Thus, condition $(\mathscr{A}_1)$ is satisfied .
Next, we perform the condition $(\mathscr{A}_2)$. From system equation (4.1), we have

$$\mathscr{G}(\mathscr{U},\mathscr{V}) = \begin{pmatrix} \frac{\beta XM}{1+b_0H} - \mu_y Y - \frac{cY}{1+b_2H} - \gamma YC \\ \frac{N\mu_y Y}{1+b_1C} - \mu_M M - \theta MH \\ \frac{cY}{1+b_2H} - \mu_G G - \eta GH \end{pmatrix}. \tag{4.17}$$

And we found

$$\mathscr{D} = D_{\mathscr{V}}\mathscr{G}(\mathscr{U}^0,0) = \begin{pmatrix} -\mu_y - \frac{c}{1+b_2H^0} - \gamma C^0 & \frac{\beta X^0}{1+b_0H^0} & 0 \\ \frac{N\mu_y}{1+b_1C^0} & -\mu_M - \theta H^0 & 0 \\ \frac{c}{1+b_2H^0} & 0 & -\mu_G - \eta H^0 \end{pmatrix}, \tag{4.18}$$

which is an $\mathbf{M}-$ matrix, which means all the off-diagonal elements of the $\mathscr{D}$ are non-negative. Finally,

$$\widehat{\mathscr{G}}(\mathscr{U},\mathscr{V}) = \mathscr{D}\mathscr{V} - G(U,V) = \begin{pmatrix} \frac{\beta MX^0}{1+b_0H^0}\left(1 - \frac{(1+b_0H^0)X}{(1+b_0H)X^0}\right) + \left(\frac{c}{1+b_2H}\left(1 - \frac{1+b_2H}{1+b_2H^0}\right) + \gamma CY\left(1 - \frac{C^0}{C}\right)\right) \\ \frac{N\mu_y Y}{1+b_2C^0}\left(1 - \frac{1+b_2C^0}{1+b_2C}\right) + \theta MH\left(1 - \frac{H^0}{H}\right) \\ \frac{1}{1+b_2H^0}\left(1 - \frac{1+b_2H^0}{1+b_2H}\right)cY + \eta GH\left(1 - \frac{H^0}{H}\right) \end{pmatrix}, \tag{4.19}$$

which implies that $\widehat{\mathscr{G}}(\mathscr{U},\mathscr{V}) \geq 0$, for all $(\mathscr{U},\mathscr{V}) \in \Omega$ the conditions $(\mathscr{A}_1)$ and $(\mathscr{A}_2)$ are satisfied. Therefore, PFE is globally asymptotically stable if $\mathfrak{R}_0 < 1$. □

4.2.6 Bifurcation analysis

In this section, we investigate the bifurcation analysis of the dynamical system (4.1) using the central manifold theorem (Castillo-Chavez and Song, 2004). The system equation (4.1) is rewritten as

$$\frac{dx}{dt} = f(x),$$

where $f = (f_1, f_2, f_3, f_4, f_5, f_6)^T$ represents the right-hand side of the system equation (4.1) and $x = (x_1, x_2, x_3, x_4, x_5, x_6) = (X, Y, M, G, C, H)$. Choosing the average number of merozoites per ruptured infected red blood cells N as bifurcation parameter and N^c is its critical value. Now, by solving for N from $\Re_0 = 1$, we have

$$N = N^c = \frac{\mu_x(\mu_h + b_0\pi_h)(\mu_c + b_1\pi_c)\left(\mu_y + \frac{c\mu_h}{\mu_h + b_2\pi_h} + \frac{\gamma\pi_c}{\mu_c}\right)\left(\mu_m + \frac{\theta\pi_h}{\mu_h}\right)}{N\beta\pi_x\mu_h\mu_y\mu_c}.$$

The Jacobian matrix at parasite-free equilibrium point E^0 and N^c is given as

$$J(E^0, N^c) = \begin{pmatrix} -\mu_x & 0 & \frac{-\beta\pi_x\mu_h}{\mu_x(\mu_h+b_0\pi_h)} & 0 & 0 & 0 \\ 0 & -\mu_y - \frac{c\mu_h}{\mu_h+b_2\pi_h} - \frac{\gamma\pi_c}{\mu_c} & \frac{\beta\pi_x\mu_h}{\mu_x(\mu_h+b_0\pi_h)} & 0 & 0 & 0 \\ 0 & \frac{N^c\mu_y\mu_c}{\mu_c+b_1\pi_c} & -\mu_m - \frac{\theta\pi_h}{\mu_h} & 0 & 0 & 0 \\ 0 & \frac{c\mu_c}{\mu_c+b_2\pi_c} & 0 & -\mu_g - \frac{\eta\pi_h}{\mu_h} & 0 & 0 \\ 0 & \frac{\xi\pi_c}{\mu_c} & 0 & 0 & -\mu_c & 0 \\ 0 & 0 & \frac{\alpha\pi_h}{\mu_h} & \frac{\delta\pi_h}{\mu_h} & 0 & -\mu_h \end{pmatrix}. \tag{4.20}$$

We can easily obtain the eigenvalues $\lambda_1 = -\mu_x, \lambda_4 = -\mu_g - \theta\pi_h/\mu_h, \lambda_5 = -\mu_c, \lambda_6 = -\mu_h$ and the remaining eigenvalues are obtained from the sub-matrix

$$J_1(E^0, N^c) = \begin{pmatrix} -\left(\mu_y + \frac{c\mu_h}{\mu_h+b_2\pi_h} + \frac{\gamma\pi_c}{\mu_c}\right) & \frac{\beta\pi_x\mu_h}{\mu_x(\mu_h+b_0\pi_h)} \\ \frac{N^*\mu_y\mu_c}{\mu_c+b_1\pi_c} & -\left(\mu_m + \frac{\theta\pi_h}{\mu_h}\right) \end{pmatrix}. \tag{4.21}$$

The associated characteristic equation to (4.21) is given as

$$\lambda^2 + (\mu_y + \frac{c\mu_h}{\mu_h + b_2\pi_h} + \frac{\gamma\pi_c}{\mu_c} + \mu_m + \frac{\theta\pi_h}{\mu_h})\lambda = 0. \tag{4.22}$$

We conclude that one of the eigenvalues of the equation (4.22) is zero. So, the parasite-free equilibrium point is a non-hyperbolic equilibrium point. Let $\mathbf{v} = (v_1, v_2, v_3, v_4, v_5, v_6)$ and $\mathbf{w} = (w_1, w_2, w_3, w_4, w_5, w_6)$ be the left and right eigenvectors corresponding to the zero eigenvalue of the Jacobian matrix(4.20) at (E^0, N^c), respectively. The values of components $v_i,\ i = 1, \cdots, 6$ and $w_i, i = 1, \cdots, 6$ can be obtained by solving the matrix equation $\mathbf{v} \cdot J(E^0, N^c) = 0$

and $J(E^0,N^c)\cdot \mathbf{w}^T = 0$, respectively, where $\mathbf{w}^T$ denotes the transpose of a matrix $\mathbf{w}$ and it satisfies $v.w = 1$. After some algebraic manipulation, we obtain

$$v_1 = 0,\ v_2 = 1,\ v_3 = \frac{\beta\pi_x\mu_h^2}{\mu_x(\mu_h+b_0\pi_h)(\mu_m\mu_h+\theta\pi_h)},\ v_4 = v_5 = v_6 = 0. \tag{4.23}$$

and

$$\begin{aligned}
w_1 &= \frac{\beta\pi_x\mu_h}{\mu_x^2(\mu_h+b_0\pi_h)}w_3,\ w_2 = \frac{\beta\pi_x\mu_h}{\mu_x(\mu_h+b_0\pi_h)(\mu_y+\frac{c\mu_c}{\mu_h+b_2\pi_h}+\frac{\gamma\pi_c}{\mu_c})},\\
w_3 &= \frac{\mu_h^2(\mu_h+b_2\pi_h)(\mu_y+\frac{c\mu_c}{\mu_h+b_2\pi_h}+\frac{\gamma\pi_c}{\mu_c})(\mu_h+b_2\pi_h)(\mu_m\mu_h+\theta\pi_h)}{\beta\pi_x\pi_h\mu_x(\mu_h+b_2\pi_h)(\mu_m\mu_h+\theta\pi_h)+\beta\pi_x\mu_h^2\mu_x(\mu_h+b_2\pi_h)(\mu_y+\frac{c\mu_c}{\mu_h+b_2\pi_h}+\frac{\gamma\pi_c}{\mu_c})},\\
w_4 &= \frac{c\mu_c}{(\mu_c+b_2\pi_c)(\mu_g+\eta\pi_h/\mu_h)}w_2,\ w_5 = \frac{\xi\pi_c}{\mu_c^2}w_2,\ w_6 = \frac{\alpha\pi_h}{\mu_h^2}w_3+\frac{\delta\pi_h}{\mu_h^2}w_4.
\end{aligned} \tag{4.24}$$

Let

$$a = \sum_{k,i,j=1}^{6} v_k w_i w_j \frac{\partial^2 f_k}{\partial x_i\partial x_j}(E^0,N^c),\quad b = \sum_{k,i=1}^{6} v_k w_i \frac{\partial^2 f_k}{\partial x_i\partial N^c}(E^0,N^c).$$

Next, we can explicitly compute the coefficients a and b by taking only non-zero components of eigenvectors and computing the second derivative of f. To investigate a, we have to compute $\frac{\partial^2 f_k}{\partial x_i\partial x_j}(E^0,N^c)$, for $i,j,k = 1,\cdots,6$.
Now,

$$\begin{aligned}
&\frac{\partial^2 f_2}{\partial x_2\partial x_3}(E^0,\ N^c) = \frac{\beta\mu_h}{\mu_h+b_0\pi_h},\ \frac{\partial^2 f_2}{\partial x_6\partial x_3}(E^0,\ N^c) = \frac{cb_2}{(1+\frac{b_2\pi_h}{\mu_h})^2},\quad \frac{\partial^2 f_2}{\partial x_5\partial x_6}(E^0,\ N^c) = -\gamma,\\
&\frac{\partial^2 f_3}{\partial x_2\partial x_5}(E^0,N^c) = \frac{N\mu_y b_1}{(1+\frac{b_1\pi_c}{\mu_c})^2},\ \frac{\partial^2 f_3}{\partial x_3\partial x_4}(E^0,N^c) = -\theta,\ \frac{\partial^2 f_3}{\partial x_2\partial N^c}(E^0,N^c) = \frac{\mu_y}{1+\frac{b_1\pi_c}{\mu_c}}.
\end{aligned}$$

All the other second partial derivatives of $\frac{\partial^2 f_k}{\partial x_i\partial x_j}(E^0,N^c)$, for $i,j,k = 1,\cdots,6$ are zero.

$$\begin{aligned}
a =& \frac{\partial^2 f_2}{\partial x_2\partial x_3}v_2w_2w_3+\frac{\partial^2 f_2}{\partial x_2\partial x_6}v_2w_2w_6+\frac{\partial^2 f_2}{\partial x_5\partial x_6}v_2w_5w_6+\frac{\partial^2 f_3}{\partial x_2\partial x_5}v_3w_2w_5\\
&+\frac{\partial^2 f_3}{\partial x_5\partial x_6}v_3w_5w_6 = w_2D_1 - w_5D_2,\\
b =& v_3w_2\frac{\mu_y}{1+\frac{b_1\pi_c}{\mu_c}} > 0,
\end{aligned}$$

where $D_1 = \frac{\beta\mu_h}{\mu_h+b_0\pi_h}+\frac{w_6cb_2}{(1+\frac{b_2\pi_h}{\mu_h})^2}$, $D_2 = \frac{w_2N\mu_y b_1}{(1+\frac{b_1\pi_c}{\mu_c})^2}+(\gamma+\theta)w_6$.

If $w_2D_1 < w_5D_2$, then the model (4.1) exhibits a forward bifurcation at $\mathscr{R}_0 = 1$. If $w_2D_1 >$

w_5D_2, then the model (4.1) exhibits a backward bifurcation at $\Re_0 = 1$. These results are summarized in the following theorem.

Theorem 4.5. *The parasite-persistence equilibrium (PPE) E^* of the dynamical system (4.1) is locally asymptotically stable if $\Re_0 > 1$ and the system exhibits forward bifurcation at $\Re_0 = 1$ if $w_2D_1 < w_5D_2$. The parasite-persistence equilibrium (PPE), E^* of the dynamical system (4.1) is unstable if $\Re_0 < 1$ and the system exhibits backward bifurcation at $\Re_0 = 1$ if $w_2D_1 > w_5D_2$.*

When the basic reproduction number $\Re_0 > 1$, the criterion for the stability of the parasite-free equilibrium is violated, and the system of equations (4.1) has *PPE* in addition to the parasite-free equilibrium. Although it would be challenging to establish the explicit form of the *PPE* in this context, we shall merely demonstrate its existence numerically for a certain range of parameter values and carry out an investigation of its stability.

4.2.7 Sensitivity analysis

In this section, we investigate the sensitivity of model parameters with respect to the basic reproduction number $\Re_0$. This will also enable us to determine which of the (constant) controls leads to the greatest reduction in within-host reproduction number $\Re_0$, allowing us to identify the control strategy that is most effective at preventing within-the-host malaria infection. We use the normalized forward sensitivity index approach (Powell et al., 2005).

The normalized forward sensitivity index of basic reproduction numbers, $\Re_0$, which is differentiable with respect to the given parameters, θ is defined as

$$\Gamma_\theta^{\Re_0} = \frac{\partial \Re_0}{\partial \theta} \times \frac{\theta}{\Re_0},$$

where θ is an arbitrary parameter in the expression of $\Re_0$. Accordingly, we obtained

$$\Gamma_N^{\Re_0} = \frac{\partial \Re_0}{\partial N}\frac{N}{\Re_0} = +1,\ \Gamma_\beta^{\Re_0} = \frac{\partial \Re_0}{\partial \beta}\frac{\beta}{\Re_0} = +1,\ \Gamma_{\pi_x}^{\Re_0} = \frac{\partial \Re_0}{\partial \pi_x}\frac{\pi_x}{\Re_0} = +1,$$

$$\Gamma_{\mu_y}^{\Re_0} = \frac{\partial \Re_0}{\partial \mu_y}\frac{\mu_y}{\Re_0} = \frac{c\mu_h/(\mu_h + b_2\pi_h) + \gamma\pi_c/\mu_c}{\mu_y + c\mu_c + \gamma\pi_c/\mu_c},$$

$$\Gamma_{b_2}^{\Re_0} = \frac{\partial \Re_0}{\partial b_2}\frac{b_2}{\Re_0} = \frac{c\mu_h\pi_h/(\mu_h + b_2\pi_h)^2 b_2}{\left(\mu_y + \frac{c\mu_h}{\mu_h + b_2\pi_h} + \frac{\gamma\pi_c}{\mu_c}\right)},$$

$$\Gamma_{\mu_c}^{\Re_0} = \frac{\partial R\Re_0}{\partial \mu_c}\frac{\mu_c}{\Re_0} = \frac{((\mu_c + b_1\pi_c)(1 + \gamma\pi_c/\mu_c - \mu_c))}{(\mu_c + b_1\pi_c)}$$

$$\Gamma_{b_1}^{\Re_0} = \frac{\partial \Re_0}{\partial b_1}\frac{b_1}{\Re_0} = -\frac{b_1\pi_c}{(\mu_c + b_1\pi_c)},\ \Gamma_\theta^{\mathscr{R}_0} = \frac{\partial \Re_0}{\partial \theta}\frac{\theta}{\Re_0} = -\frac{\pi_h/\mu_h\theta}{\left(\mu_m + \frac{\theta\pi_h}{\mu_h}\right)},$$

$$\Gamma_\gamma^{\Re_0} = \frac{\partial \Re_0}{\partial \gamma}\frac{\gamma}{\Re_0} = -\frac{\pi_c/\mu_c\gamma}{\left(\mu_y + \frac{c\mu_h}{\mu_h + b_2\pi_h} + \frac{\gamma\pi_c}{\mu_c}\right)},\ \Gamma_{b_0}^{\Re_0} = \frac{\partial \Re_0}{\partial b_0}\frac{b_0}{\Re_0} = -\frac{b_0}{(\mu_h + b_0\pi_h)},$$

Table 4.3: Elasticity indices of within-host basic reproduction number, $\Re_0$ with respect to parameters in within-host model (4.1) using parameter values in Table 4.4.

Parameters	Elasticity index	Value	Parameters	Elasticity index	Value
π_x	$\Gamma_{\pi_x}^{\Re_0}$	$+1$	$b0$	$\Gamma_{b0}^{\Re_0}$	-0.033229
β	$\Gamma_{\beta}^{\Re_0}$	$+1$	π_h	$\Gamma_{\pi_h}^{\Re_0}$	-0.1739
N	$\Gamma_{N}^{\Re_0}$	$+1$	$b1$	$\Gamma_{b1}^{\Re_0}$	-0.00099
μ_h	$\Gamma_{\mu_h}^{\Re_0}$	$+0.6414$	γ	$\Gamma_{\gamma}^{\Re_0^c}$	-1
μ_y	$\Gamma_{\mu_y}^{\Re_0}$	$+0.9946$	θ	$\Gamma_{\theta}^{\Re_0}$	-0.0361
μ_c	$\Gamma_{\mu_c^{\Re_0}}$	$+0.95135$	π_c	$\Gamma_{\pi_c}^{\Re_0}$	-1.001

$$\Gamma_{\pi_h}^{\Re_0} = \frac{\partial \mathscr{R}_0}{\partial \pi_h}\frac{\pi_h}{\Re_0} = -\frac{\pi_c b_1(\mu_y + c\mu_c/(\mu_h + b_2\pi_h) + \gamma\pi_c/\mu_c) + \pi_c\gamma(\mu_c + b_1\pi_c)/\mu_c}{(\mu_c + b_1\pi_c)\left(\mu_y + \frac{c\mu_h}{\mu_h + b_2\pi_h} + \frac{\gamma\pi_c}{\mu_c}\right)},$$

$$\Gamma_{\pi_h}^{\Re_0} = \frac{\partial \Re_0}{\partial \pi_h}\frac{\pi_h}{\Re_0} = -\frac{W_1 - (\mu_y + c\mu_c/(\mu_h + b_2\pi_h) + \gamma\pi_c/\mu_c)(b_0\pi_h(\mu_m + \theta\pi_h/\mu_h) - W_2)}{(\mu_h + b_0\pi_h)\left(\mu_y + \frac{c\mu_h}{\mu_h + b_2\pi_h} + \frac{\gamma\pi_c}{\mu_c}\right)},$$

$$\Gamma_{\mu_h}^{\Re_0} = \frac{\partial \Re_0}{\partial \mu_h}\frac{\mu_h}{\Re_0} = \frac{\mu_y + c\mu_c/(\mu_h + b_2\pi_h) + \gamma\pi_c/\mu_c - c\mu_h b_2\pi_c}{\left(\mu_y + \frac{c\mu_h}{\mu_h + b_2\pi_h} + \frac{\gamma\pi_c}{\mu_c}\right)(\mu_h + b_2\pi_h)^2},$$

where $W_1 = \pi_h(\mu_h + b_0\pi_h)(\mu_m + \theta\pi_h/\mu_h)c\mu_h b_2/(\mu_h + b_2\pi_h), W_2 = \pi_h\theta(\mu_h + b_0\pi_h)$.

Sensitivity indices of basic reproduction number, $\Re_0$ with respect to parameters using parameter values in Table 4.4 is summarised in Table 4.3. A positive value on the elasticity index means that an increase (or reduction) in the value of the relevant parameter increases (or reduces) the value of $\Re_0$ and, consequently, the expansion of malaria infection. On the other hand, a parameter with a negative sign impact $\Re_0$ negatively. The rate of recruitment of uninfected red blood cells from bone marrow π_x, the infection rate of the red blood cells by merozoites β, and the average number of merozoites per ruptured infected red blood cell N, are the most sensitive metrics for predicting the diseases progression. They have the highest sensitivity indices of $+1.0000$. A 10% increase (or reduction) of π_x, β, and N produces a 10% rise (reduction) in $\Re_0$, as well as the duration of the in-host malaria parasite. The parameters μ_c, μ_y, and μ_h are the second rank in influencing the results of the model. An increase in the parameters μ_c, μ_y, and μ_h is likely to increase the in-host model $\Re_0$. On the other hand, the clearance rate of infected red blood cells as a result of cell-mediated immune response γ has a direct negative influence on $\Re_0$. A 10% increase(or decrease) in γ is a 10% decrease(or increase) in $\Re_0$.

4.3 Numerical simulation

Here, we present the numerical simulations of the within-host dynamical system (4.1) in order to supplement our analytical and theoretical results. For the simulations, we used MATLAB's

built-in ode45 function with the initial values $X_0 = 500000 cells/ml/day, Y_0 = 300 cells/ml/day$, $M_0 = 40000 cells/ml/day, G_0 = 50 cells/ml/day$, $C_0 = 0.001 cells/ml/day$,$H_0 = 0.001 cells/ml/day$. The model parameter values utilized during the simulation are listed in Table 4.4. We inves-

Table 4.4: The values for model parameters utilized in the simulation, where *mero* represents merozoites.

Parameters	Value	Source
π_x	$2.5 \times 10^8 cells/\mu l/day$	Hetzel and Anderson (1996)
μ_x	$8.3 \times 10^{-3}/day$	Anderson et al. (1989)
π_c	$30/day/\mu l^{-1}$	Chiyaka et al. (2008); Orwa et al. (2018)
μ_c	0.05/day	Anderson et al. (1989)
π_h	$30/day/\mu l^{-1}$	Orwa et al. (2019)
μ_h	0.05/day	Anderson et al. (1989)
μ_y	0.03 /day	Kamangira et al. (2014)
μ_m	48/day	Hetzel and Anderson (1996)
β	0.08 $mero/day\mu l$	Chiyaka et al. (2008)
μ_g	0.0000625/day	Selemani et al. (2016)
N	16 mero/μ l	Chiyaka et al. (2008)
θ	0.3 mero $\mu l/day$	Chiyaka et al. (2008)
b_0	0.5 immune cell/μl	Orwa et al. (2019)
b_1	0.000005 $\mu l/cell$	Chiyaka et al. (2008)
b_2	0.0004 $\mu l/cell$	Chiyaka et al. (2008)
c	0.02 /day	Hellriegel (1992)
b_3	$5 \times 10^{-4} \mu l/cell$	Chiyaka et al. (2008)
η	0.03 mero μl/day	Chiyaka et al. (2008)
γ	0.0009 cell μ l/day	Li et al. (2011); Elaiw and Al Agha (2020)
ξ	0.0005/day	Li et al. (2011)
δ	0.005/day	Li et al. (2011)
α	0.00005/day	Elaiw and Al Agha (2020)
c_0	$6.67 \times 10^{-4} \mu l/cell$	Chiyaka et al. (2008)
c_1	$6.67 \times 10^{-4} \mu l/cell$	Chiyaka et al. (2008)

tigate the dynamical behavior of the state variables numerically. After we use the parameter value, it is simple to confirm that the in-host basic reproduction number $\Re_0 = 0.5091$, which is less than unity. This implies that the parasite will eventually die out.

Figure 4.2 demonstrates the global stability of the parasite-free equilibrium point. The healthy RBCs, cell-mediated, and antibody-mediated immune system converge to $\pi_x/\mu_x, \pi_c/\mu_c$, and π_h/μ_h respectively, whereas the other compartments converge to zero. This indicates that the solutions of state variables converge to the parasite-free steady-state $E^0 = (3.012 \times 10^{+06}, 0, 0, 0, 200, 600)$. Figure 4.3 depicts the existence of a parasite-persistence equilibrium

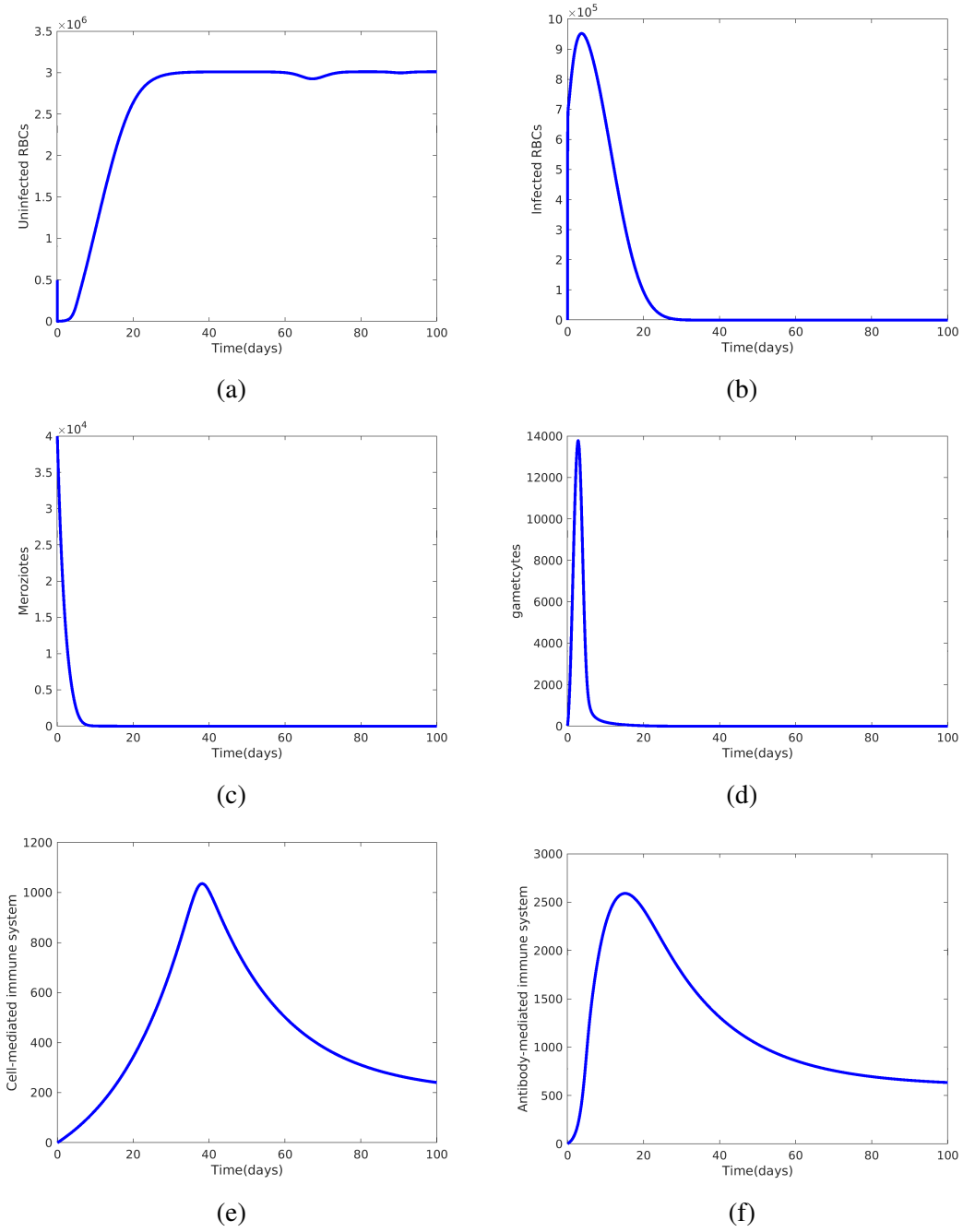

Figure 4.2: The time evolution of the state variables when $\Re_0 = 0.5091 < 1$ shows the global stability of the parasite-free steady-state E^0 of the dynamical system (4.1). The parameter values used for the simulation are given in Table 4.4

.

point. Figure 4.3(a) shows the dynamical behavior of the density of healthy RBCs. The healthy RBCs decrease at a given time interval. This is due to the invasion of healthy RBCs by merozoites. An invasion of healthy RBCs generates a responding steady growth in the concentration of iRBCs (see Figure 4.3(b)). Due to natural intervention by the immune system cells, the respective declines and rising levels of healthy RBCs and iRBCs level off and remain roughly consistent. Figure 4.3(c) exhibits an initial significant increase in merozoite concentration over

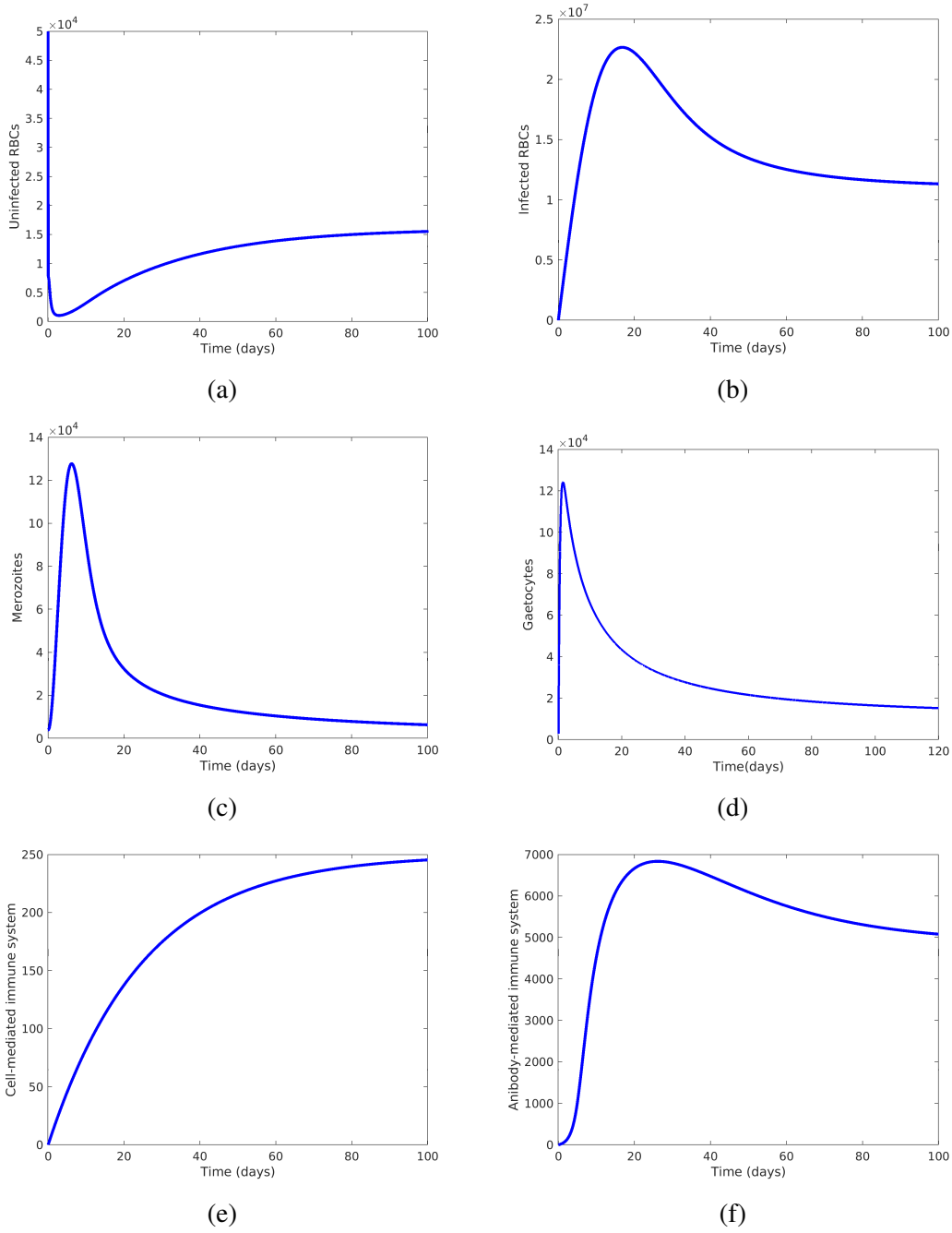

Figure 4.3: The time evolution of the state variables when $\Re_0 = 3.3031 > 1$ shows the persistence of the disease. This indicated that the parasite-persistence steady-state E^* exists and is locally asymptotically stable, for $\Re_0$ greater than unity. The parameter values used for the simulation are given in Table 4.4.

the first few days of the blood stage. The density remains high for several days, then declines and stays constant for the entire infection period of approximately two months. Similarly, the density of gametocytes significantly increases within approximately the first five days, then drop-off and stays constant for the entire infection period of two months (see Figure 4.3(d)). The dynamical behavior of the cell-mediated system is shown in Figure 4.3(e). As we see, the concentration of the cell-mediated immune system increases due to the stimulation of immu-

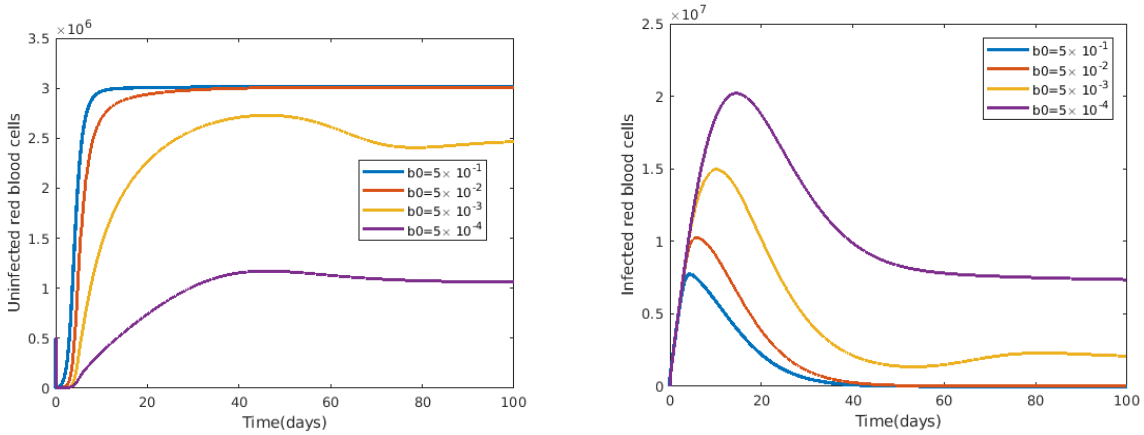

(a) (b)

Figure 4.4: The impact of antibody-mediated immune response efficacy on erythrocytic invasion b_0 for (a) healthy RBCs and (b) iRBCs, all other parameter values remaining constant.

nity caused by the presence of iRBCs. Figure 4.3(f) shows that the antibody-mediated immune cells increase in the presence of malaria parasites (merozoites and gametocytes) in host cells.

The effectiveness of the immune system antibody-mediated defenses against erythrocytic (or RBC) invasion on healthy RBCs is shown in Figure 4.4(a). The healthy RBCs decrease as the effectiveness of the immunological response mediated by antibodies to erythrocytic invasion declines. The iRBCs grow as the effectiveness of the immune response mediated by antibodies to erythrocytic invasion declines(see Figure 4.4(b)). As a result, the immune response mediated by antibodies prevents erythrocytic invasion and minimizes the density of merozoites and gametocytes in the host cell.

Figure 4.5 reveals the effect of an antibody-mediated immune response on the generation of

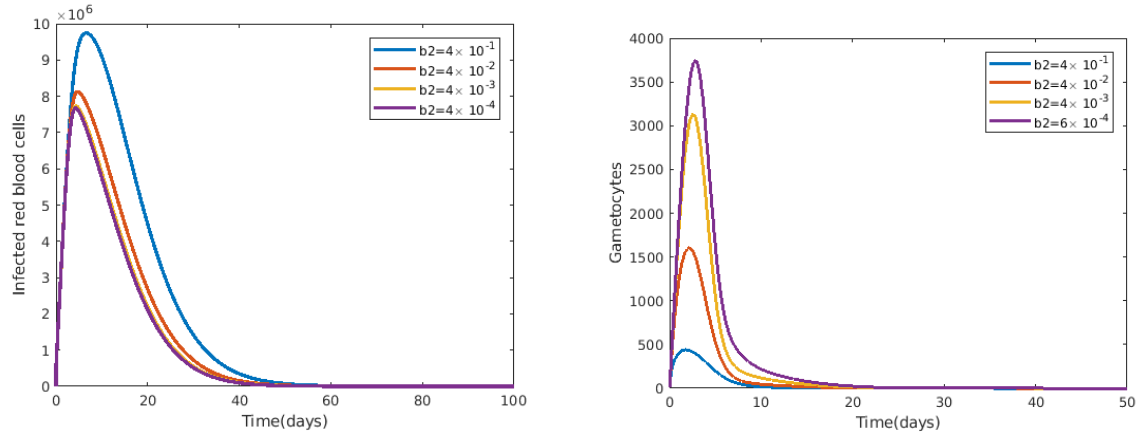

(a) (b)

Figure 4.5: The impact of antibody-mediated immune response efficacy on gametocytes production b_2 on (a) iRBCs and (b) gametocytes, all the values of other parameters are constant.

gametocyte for infected erythrocytes and gametocytes. The infected erythrocyte population declines as the effectiveness of antibody-mediated immune response on gametocyte genera-

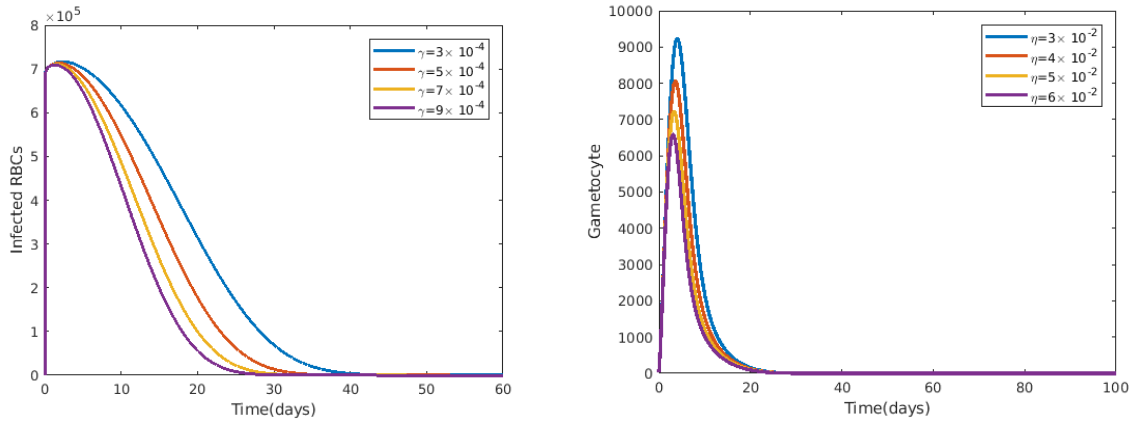

(a) (b)

Figure 4.6: (a) The impact of the removal rate of the iRBCs due to cell-mediated immune response γ on the iRBCs; (b) the impact of the removal rate of the gametocyte due to antibody-mediated immune response η; all the other values of parameters are fixed as in Table 4.4.

tion declines (see Figure 4.5(a)). The gametocyte populations rise as the effectiveness of the antibody-mediated immune response on gametocyte generation declines (see Figure 4.5(b)). The impact of the cell-mediated immune response on iRBC is depicted in Figure 4.6 (a). The immunological response, which is cell-mediated, causes a drop-off in the number of iRBCs. The gametocyte clearance rates due to the immune system antibody-mediated responses are demonstrated in 4.6(b). The gametocyte population decreases as the clearance rate of gametocytes by the antibody-mediated immune system is increases.

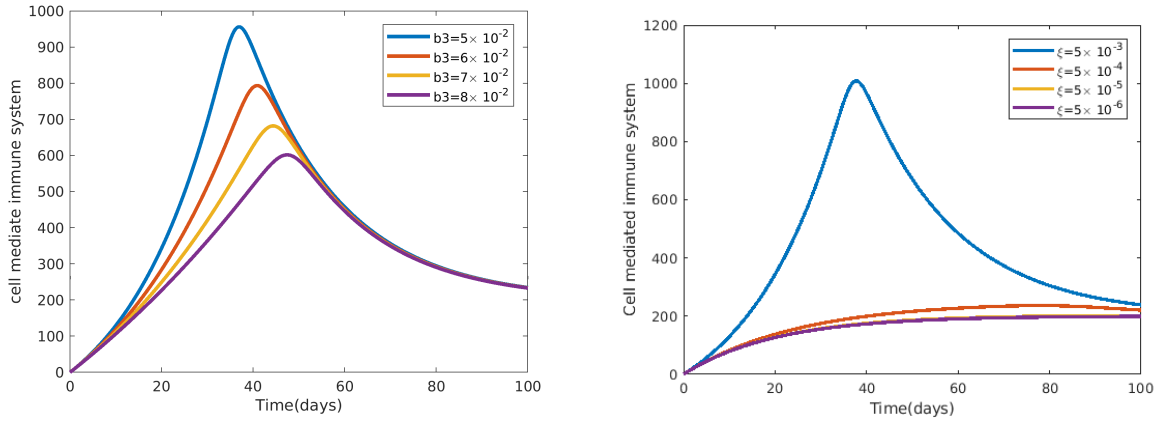

(a) (b)

Figure 4.7: (a) The impact of the efficacy of the iRBCs b_3 on the production of cell-mediated immune response, (b) impact of the activation rate of cell-mediated immunity ξ, due to the presence of iRBCs; all the other values of parameters are rigid.

Figure 4.7(a) displays the efficacy of iRBCs in stimulating the cell-mediated immune system. The cell-mediated immune system rises, as the efficacy of iRBCs in stimulating the cell-mediated immune system declines over time. The effect of the cell-mediated immune

response proliferation rate is shown in Figure 4.7(b). The cell-mediated immune response grows as the proliferation rate (activation rate of cell-mediated immune response owing to iRBCs) increases. The effect of activation rate on antibody-mediated immune response as a

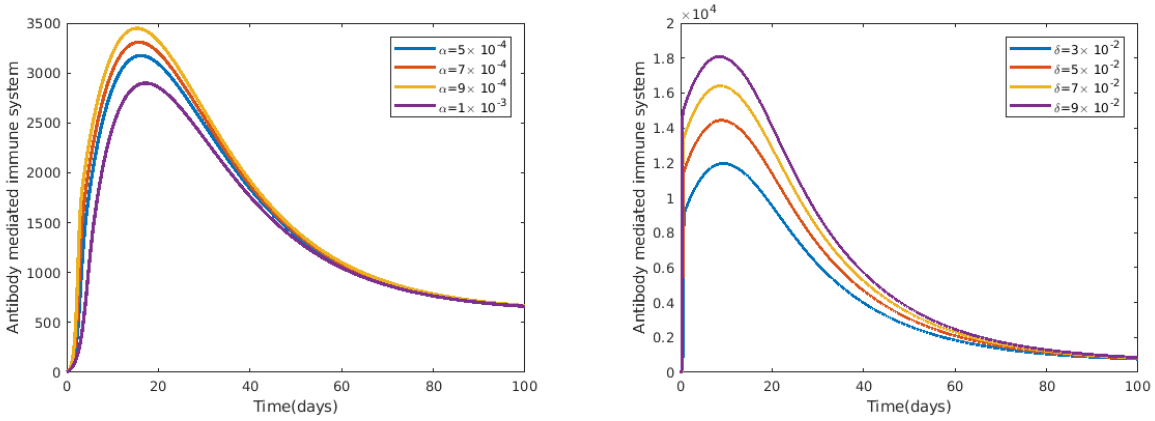

(a) (b)

Figure 4.8: (a) The impact of activation rate α on antibody-mediated immune responses caused by merozoites, (b) impact of the activation rate δ on antibody-mediated immune responses caused by gametocytes, and all other parameter values are known, as shown in Table 4.4.

.

result of interaction with merozoites is verified in 4.8(a). As the frequency of activation of the antibody-mediated immune response rises, the antibody-mediated immune system increases. We can also see from Figure 4.8(b) that the antibody-mediated immune system increases as the activation rate of antibody-mediated immune response rises owing to interaction with gametocytes.

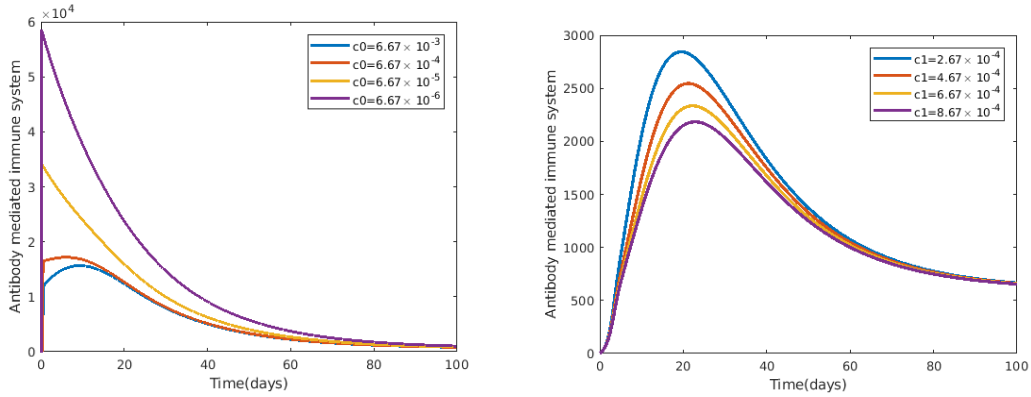

(a) (b)

Figure 4.9: (a) The impact of merozoites efficacy c_0, (b) the impact of gametocytes efficacy c_1 on the activation of the antibody-mediated immune system; all other parameter values are set according to Table 4.4.

The efficacy of merozoites in stimulating the growth of an antibody-mediated immune system is depicted in Figure 4.9(a). The proliferation of the antibody-mediated immune system increases as the merozoites' ability to promote it decreases. The efficacy of gametocytes in

stimulating the growth of the antibody-mediated immune system is portrayed in Figure 4.9(b). The proliferation of the antibody-mediated immune system rises as the efficacy of gametocytes in stimulating the growth of the antibody-mediated immune system decreases. Figure 4.10(a)

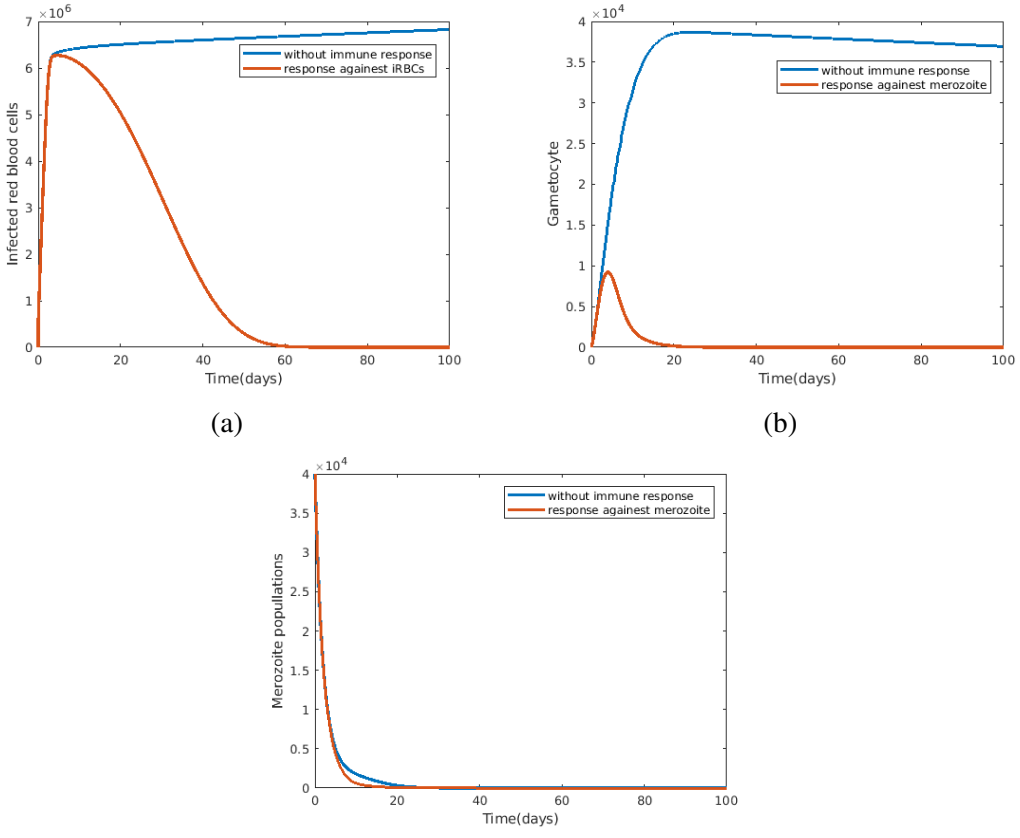

Figure 4.10: (a) The dynamical behavior of iRBCs with cell-mediated immune response ($\gamma = 0.009$) and without cell-mediated immune response ($\gamma = 0$), (b) the dynamical behavior of gametocytes with antibody-mediated immune response ($\eta = 0.003$) and without antibody-mediated immune response ($\eta = 0$), (c) the dynamical behavior of merozoites with antibody-mediated immune response ($\theta = 0.3$) and without antibody-mediated immune response ($\theta = 0$).

provides an illustration of the dynamic behavior of iRBCs with and without a cell-mediated immune system . When cell-mediated immunity is present, iRBCs rise within about 5 days and converge to zero, whereas when there is no cell-mediated immune response they rise and remain constant. In general, the removal of iRBCs through the cell-mediated immune response has a high potential to eliminate malaria parasites within the host cell. The dynamical behavior of gametocytes with and without antibody-mediated immune responses is examined in Figure 4.10(b). In the presence of antibody-mediated immune responses, the gametocyte populations increase and peak at around 8×10^3, while in the absence of such immune responses, the populations peak at about 3.8×10^4. The antibody-mediated immune response mitigate the sexual reproduction of merozoites in RBCs, which has an effect on malaria parasites. The

impact of antibody-mediated immune response on merozoites is illustrated in Figure 4.10(c). The antibody-mediated immunity against malaria infection is less effect on the free merozoites when we compere with the effect of antibody-mediated immune system on sexual replication of the parasite (gametaocytes).

4.4 Summary

In this Chapter, a nonlinear deterministic mathematical model for the within-host malaria parasite with cell-mediated and antibody-mediated responses was developed. The research explores how the stage-specific antibody-mediated and cell-mediated immune responses interact with the iRBCs, merozoites, and gametocytes using a nonlinear bounded Michaelis-Menten-Monod function to depict their dynamic behavior in the context of malaria parasites. The biological visibility and well-posedness of the proposed model are proved by revealing the non-negativity and boundedness of solutions in the feasible regions. Then, the parasite-free equilibrium point of the model is computed. The stability analysis of the parasite-free equilibrium point is investigated, revealing that the parasite-free equilibrium point is locally and globally stable if the basic reproduction number $\Re_0 < 1$. The existence and stability of the parasite-persistence equilibrium point is investigated using numerical simulation. The within-host basic reproduction number is obtained through the next-generation matrix approach and using the value of the parameter given in Table 4.4, we found $\Re_0 = 0.5091$, which is less than unity. This implies that the parasite does not invade the host RBCs and the parasite will eventually die out. Furthermore, bifurcation analysis is discussed, whereas the conditions for backward and forward bifurcation are examined.

Sensitivity analysis of the within-host basic reproduction number is provided using a normalized forward sensitivity index approach. The results indicated that the infection rate of RBCs by merozoites β, average number of merozoites per ruptured iRBCs N, removal rate of iRBCs due to cell-mediated immune response γ, and production rate of uninfected RBCs π_x are the most sensitive parameters in infection. To support our theoretical and analytical results, different numerical simulations of the model (4.1) are performed. The simulations are performed using MATLAB's built-in ode45 function. The numerical simulation shows that the cell-mediated and antibody-mediated immune responses have played a crucial role in the reduction of malaria parasites within host cells by blocking the invasion of RBCs, removing the iRBCs, merozoites, and gametocytes from host cells. The finding of this study is very important to understand the dynamical behavior of malaria parasites in host cells and the role of immune response in the elimination of parasites in the human hosts mathematically.

CHAPTER 5

A CELL-LEVEL DYNAMICAL MODEL FOR MALARIA PARASITE INFECTION WITH ANTIMALARIAL DRUG TREATMENT

In this chapter, we develop a within-host mathematical model of malaria parasite infection considering the liver-blood stage dynamics of parasite infection and antimalarial drug treatment. The model includes the interactions of malaria parasite, the host's liver hepatocyte cell and red blood cell populations.

5.1 Model formulation

A mathematical model of within-host malaria parasite infection dynamics with the effect of antimalarial treatment is presented. The compartmental model is an extension of the within-host malaria model in Chapter 4 of this dissertation. The liver and blood stages of the malaria infection are investigated. The uninfected hepatocyte $H(t)$, infected hepatocyte $H_I(t)$, and sporozoites $S(t)$ are incorporated into the model. We used the mass action to express the interaction between hepatocyte cells, erythrocyte cells, and malaria parasites. Therefore, the rest of the populations include uninfected RBCs $R(t)$, infected red-blood-cell(iRBCs) $R_I(t)$, malaria parasite in the form of merozoite $M(t)$ and gametocyte $G(t)$ at time t.

The formulated in-host model is led by the following assumptions:

(i). The liver hepatocyte cells are recruited at a constant rate from the bone marrow.

(ii). The instruction of erythrocyte and hepatocyte cells with malaria parasites is directly proportional to the density of the two cell populations.

(iii). The sporozoite is recruited into the human host during the blood feeding of infected female Anopheles mosquito.

(iv). The merozoites population is produced through rupturing of infected liver hepatocyte cells (liver-schizont) and infected red blood cells (blood-schizont).

(v). The liver-stage antimalarial drug treatment (primary tissue schizontocides) is reduce the invasion of liver hepatocytes by malaria sporozoites and average number of morozoites per ruptured liver schizonts.

(vi). Blood-stage antimalarial drug treatment (blood-schizontocides) is reduce the reduce the invasion of erythrocytes by malaria merozoites and average number of morozoites per ruptured blood schizonts.

(vii). The gametocytocidal antimalarial treatment is reduce the sexual replications of malaria parasite.

The malaria parasite in the form of sporozoites is recruited from the salivary gland of the female Anopheles mosquito while the blood meals at a constant rate π_S and die naturally at a rate μ_S. The hepatocyte cells are supplied from the bone marrow at a rate π_H. The hepatocytes are invaded by sporozoites that are injected into the human body during mosquito blood feeding at a constant rate β_1. This invasion is reduced due to tissue schizontocides (liver-stage antimalarial drug treatment) which is administrated pre-erythrocytic stage of malaria infection at a rate $(1-\xi_1)\beta_1$, where ξ_1 $(0<\xi_1\leq 1)$ is the efficacy of antimalarial drug on pre-erythrocytic malaria stage. The hepatocytes suffered natural death at a constant rate μ_H. The population of infected hepatocytes will increase as the healthy hepatocytes get infected at a rate $(1-\xi_1)\beta_1$ and decrease owing to rupture and die at a rate δ.

The healthy erythrocytes (RBCs) are recruited from the bone marrow at a constant rate π_R. They acquire infection due to the invasion of merozoites that are released from the liver schizont at a rate β_2. The invasion rate is attenuated when blood-stage antimalarial drug treatment (blood-schizontocides) is administrated at the rate $(1-\xi_2)\beta_2$, where ξ_2 $(0<\xi_2\leq 1)$ is the efficacy of antimalarial treatment on erythrocytic invasion and the RBCs die naturally at a constant rate μ_R. The iRBCs burst and die at a constant rate σ. The merozoite population is produced when the infected hepatocyte rupture and releases thousands of merozoites into the blood system at a rate δN, where N is the average number of merozoite released per ruptured infected hepatocytic cells and during the iRBCs rupture and release 16–32 merozoites per ruptured iRBC into the bloodstream at a constant rate σQ to invade fresh erythrocytes (RBCs), where Q is the average number of merozoites per ruptured iRBCs.

The production of the merozoite is reduced when antimalarial drug treatments; primary tissue(pre-erythrocytic) schizontocides and blood schizontocides are administrated at the rate of $(1-\xi_3)N$ and $(1-\xi_3)Q$, respectively, where $\xi_3(0<\xi_3\leq 1)$is the efficacy of antimalarial drug treatments on the average number of merozoites rupturing rate of pre-erythrocytic schizont and blood schizont. The population of merozoite will reduce due to the natural death rate μ_M. After the invasion of the red blood cells, some number of merozoites develop into male (microgametes) and female (macrogametes) gametocytes arise within-host at a rate c. The sexual form (gametocytes) are destroyed due to the administration of gametocytocide (Bruce-Chwatt, 1962) at a rate ξ_4 $(0<\xi_4\leq 1)$.

The gametocytes die naturally at a rate μ_G. Note that, $\xi_i=0,\ i=1,\ldots,4$ implies that the antimalarial drug treatments are ineffective at all, and $\xi_i=1$ means that they are 100% effective. Assume that an uninfected erythrocyte's observation of merozoites and an uninfected hepatocyte's observation of sporozoites are ignored. All the model biological parameters are listed in Table 5.1, respectively.

Based on the above assumptions, descriptions and the model schematic diagram (Figure

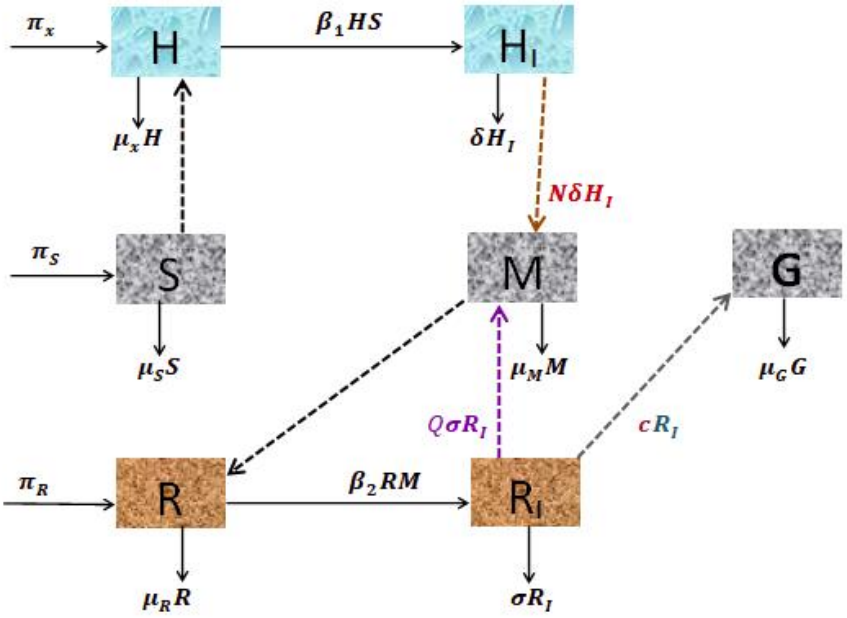

Figure 5.1: Schematic diagram of the dynamical system of hepatocytic-erythrocytic stage malaria parasite.

5.1), the formulated model equation is given by

$$\begin{aligned}
\frac{dH}{dt} &= \pi_H - (1-\xi_1)\beta_1 HS - \mu_H H,\\
\frac{dH_I}{dt} &= (1-\xi_1)\beta_1 HS - \delta H_I,\\
\frac{dR}{dt} &= \pi_R - (1-\xi_2)\beta_2 RM - \mu_R R,\\
\frac{dR_I}{dt} &= (1-\xi_2)\beta_2 RM - \sigma R_I,\\
\frac{dS}{dt} &= \pi_S - \mu_S S,\\
\frac{dM}{dt} &= (1-\xi_3)N\delta H_I + (1-\xi_3)Q\sigma R_I - \mu_M M,\\
\frac{dG}{dt} &= cR_I - \xi_4 G - \mu_G G,
\end{aligned} \tag{5.1}$$

with initial condition

$$H(0) > 0,\ H_I(0) \geq 0,\ M(0) \geq 0,\ S(0) \geq 0,\ R(0) > 0,\ R_I(0) \geq 0,\ G(0) \geq 0. \tag{5.2}$$

5.2 Qualitative analysis of the model

In this section, we investigate the non-negativity and boundedness of the developed model, equilibria, stability analysis of the equilibria, and sensitivity analysis of basic reproduction number.

Table 5.1: Model parameters and their description

Parameters	Description
π_S	The recruitment rate of sporozoites from the salivary gland of the mosquito during blood meal
π_H, π_R	Production rate of the uninfected hepatocyte and erythrocyte from the bone marrow
β_1	The infection rate of the hepatocyte by sporozoites
β_2	The infection rate of the erythrocyte by merozoites
δ	The death rate of the infected hepatocyte
N	The average number of merozoite per ruptured infected hepatocyte cells
Q	The average number of merozoites per ruptured infected erythrocyte cells
μ_H, μ_R	The natural death rate of hepatocyte, erythrocytes, respectivily
μ_M, μ_G, μ_S	The natural death rate of merozoites, gametocytes, and sporozoites, respectively
σ	The death rate of infected erythrocyte cells
c	The rate of sexual replication of merozoites
ξ_1	Efficacy of antimalarial drugs on pre-erythrocytic malaria stage
ξ_2	Efficacy of antimalarial treatment for erythrocytic invasion
ξ_3	The efficiency of antimalarial drug treatments on the bursting rate of pre-erythrocytic schizont and blood schizont
ξ_4	The efficiency of gametocytocidal on the sexual development of the merozoites

5.2.1 Non-negativity and boundedness of the solution

Theorem 5.1. *The solutions of system* (5.1) *with non-negative initial conditions,* $H_0, H_{I0}, R_0, R_{I0}, M_0, S_0$ *and* G_0*, remain non-negative for all time* $t \geq 0$.

Proof. The first equation of dynamical system (5.1) gives rise to

$$\frac{dH}{dt} = \pi_H - (1-\xi_1)\beta_1 HS - \mu_H H \geq -((1-\xi_1)\beta_1 S + \mu_H)H,$$
$$\frac{dH}{H} \geq -((1-\xi_1)\beta_1 S + \mu_H)dt, \quad \int_0^t \frac{dH}{H} \geq -\int_0^t ((1-\xi_1)\beta_1 S + \mu_H)dt,$$
$$H(t) \geq H_0 exp\left\{-\int_0^t ((1-\xi_1)\beta_1 S + \mu_H)dt\right\} > 0.$$

The second equation of dynamical system (5.1) gives rise to

$$\frac{dH_I}{dt} = (1-\xi_1)\beta_1 HS - \delta H_I \geq -\delta H_I, \quad \frac{dH_I}{H_I} \geq -\delta dt, \quad \int_0^t \frac{dH_I}{H_I} \geq -\int_0^t \delta dt,$$
$$H_I(t) \geq H_{I0} exp\{-\delta t\} \geq 0.$$

Applying the same procedure, it can be shown that the state variables $R(t), R_I(t), S(t), M(t)$ and $G(t)$ are non-negative for all $t \geq 0$. Therefore, the solution of the dynamical system (5.1) is non-negative for all $t \geq 0$. □

Theorem 5.2. *The biologically feasible region*

$$\Omega = \left\{ (H, H_I, R, R_I, S, M, G) \in R_+^7 : N_H \leq \frac{\pi_H}{d_1}, N_R \leq \frac{\pi_R}{d_2} \ \ and \ \ N_S \leq \frac{\pi_S}{d_3} \right\}$$

is positively invariant to the dynamical system (5.1).

Proof. The total hepatocyte population at a time t denoted by $N_H(t)$ and defined as

$$N_H(t) = H(t) + H_I(t). \tag{5.3}$$

By differentiating (5.3) with respect to time t, we obtained

$$\begin{aligned} \frac{dN_H}{dt} &= \pi_H - (1-\xi_1)\beta_1 HS - \mu_H H + (1-\xi_1)\beta_1 HS - \delta H_I = \pi_H - \mu_H H - \delta H_I, \\ &\leq \pi_H - d_1 N_H, \ \ where \ \ d_1 = min\{\mu_H, \delta\}, \\ N_H(t) &\leq \frac{\pi_H}{d_1} + \left(N_{H0} - \frac{\pi_H}{d_1} \right) exp\{-d_1 t\}. \end{aligned} \tag{5.4}$$

Similarly, we can apply this procedure to red-blood cells $N_R(t) = R(t) + R_I(t)$.

$$\begin{aligned} \frac{dN_R}{dt} &= \pi_R - (1-\xi_2)\beta_2 RM - \mu_R R + (1-\xi_2)\beta_2 RM - \sigma R_I - cR_I, \\ &= \pi_R - \mu_R R - \sigma R_I \leq \pi_R - d_2 N_R, \\ N_R(t) &\leq \frac{\pi_R}{d_2} + \left(N_{R0} - \frac{\pi_R}{\mu_{R'}} \right) exp\{-d_2 t\}, \end{aligned} \tag{5.5}$$

where $d_2 = min\{\mu_R, \sigma\}$.

Lastly, the total malaria parasite population in the form of sporozoites, merozoites, and gametocytes at a time t is given as $N_S(t) = S(t) + M(t) + G(t)$,

$$\begin{aligned} \frac{dN_S}{dt} &= (1-\xi_3)N\delta H_I + (1-\xi_3)Q\sigma R_I - \mu_M M + \pi_S - \mu_S S + cR_I - \mu_G G - \xi_4 G, \\ &\leq (1-\xi_3)N\delta H_I + (1-\xi_3)Q\sigma R_I + cR_I + \pi_S - d_3 N_S, \\ N_S(t) &\leq \frac{\pi_S}{d_3} + \left(N_{S0} - \frac{\pi_S}{d_3} + \int_0^t (1-\xi_3)N\delta H_I + (1-\xi_3)Q\sigma R_I + cR_I dt \right) exp\{-d_3 t\}. \end{aligned} \tag{5.6}$$

where $d_3 = min\{\mu_M, \mu_G, \mu_S\}$.

Taking the limit as $t \to \infty$ for the equations (5.4), (5.5), and (5.6), we obtained $N_H(t) \leq \frac{\pi_H}{d_1}$, $N_R(t) \leq \frac{\pi_R}{d_2}$ and $N_S(t) \leq \frac{\pi_S}{d_3}$. Therefore, the biologically feasible region Ω is positive invariant to the in-host malaria model (5.1). □

5.2.2 Parasite-free equilibrium point

The parasite-free equilibrium point is the steady-state solution where there is no parasite in the host cells. That is, $S=0,\ \ H_I=0,\ \ R_I=0,\ \ M=0,\ \ G=0$ and the recruitment rate of sporozoites from the salivary gland of the mosquito during a blood meal ($\pi_S=0$). It's obtained by setting the right-hand side of the dynamical system (5.1) to zero as

$$\begin{cases} \pi_H-(1-\xi_1)\beta_1 HS-\mu_H H=0,\\ (1-\xi_1)\beta_1 HS-\delta H_I=0,\\ \pi_R-(1-\xi_2)\beta_2 RM-\mu_R R=0,\\ (1-\xi_2)\beta_2 RM-\sigma R_I=0,\\ \pi_S-\mu_S S=0,\\ (1-\xi_3)N\delta H_I+(1-\xi_3)Q\sigma R_I-\mu_M M=0,\\ cR_I-\xi_4 G-\mu_G G=0. \end{cases}$$

After substituting the values of $S,\ H_I,\ R_I,\ M,$ and G, we obtained

$$E_0=(H^0,HI^0,R^0,RI^0,S^0,M^0,G^0)=(\frac{\pi_H}{\mu_H},0,\frac{\pi_R}{\mu_R},0,0,0,0).$$

5.2.3 The within-host basic reproduction number

Here, we compute the within-host basic reproduction number $\mathscr{R}_0$ using the technique of the next-generation matrix approach described by (Van den Driessche and Watmough, 2002) as in previous Chapter. We consider only the infected compartments H_I, R_I, M and G. Let F_i be the rate of new appearance and V_i be the rate of transfer from one compartment to another by any means and given as

$$F_i=\begin{pmatrix}(1-\xi_1)\beta_1 HS\\ (1-\xi_2)\beta_2 RM\\ 0\\ 0\\ 0\end{pmatrix},\ \ V_i=\begin{pmatrix}\delta H_I\\ \sigma R_I\\ -\pi_S+\mu_S S\\ -(1-\xi_3)N\delta H_I-(1-\xi_3)Q\sigma R_I+\mu_M M\\ -cR_I+\xi_4 G+\mu_G G\end{pmatrix}. \tag{5.7}$$

The non-negative matrix F and the non-singular matrix V are obtained via the differentiating F_i and V_i of the equation (5.7) with respect to the infected compartments at the parasite-free equilibrium point E_0 and give as

$$F=\begin{pmatrix}0&0&(1-\xi_1)\beta_1 H_0&0&0\\ 0&0&0&(1-\xi_2)\beta_2 R_0&0\\ 0&0&0&0&0\\ 0&0&0&0&0\\ 0&0&0&0&0\end{pmatrix},\ V=\begin{pmatrix}\delta&0&0&0&0\\ 0&\sigma&0&0&0\\ 0&0&\mu_S&0&0\\ -(1-\xi_3)N\delta&-(1-\xi_3)Q\sigma&0&\mu_M&0\\ 0&-c&0&0&\xi_4+\mu_G\end{pmatrix}.$$

Hence, the inverse of the matrix V is

$$V^{-1} = \begin{pmatrix} \frac{1}{\delta} & 0 & 0 & 0 & 0 \\ 0 & \frac{1}{\sigma} & 0 & 0 & 0 \\ 0 & 0 & \frac{1}{\mu_S} & 0 & 0 \\ \frac{(1-\xi_3)N\delta}{\delta\mu_M} & \frac{(1-\xi_3)Q\sigma}{\mu_M\sigma} & 0 & \frac{1}{\mu_M} & 0 \\ 0 & \frac{c}{\sigma(\mu_G+\xi_4)} & 0 & 0 & \frac{1}{\xi_4+\mu_G} \end{pmatrix}. \tag{5.8}$$

The next generation matrix FV^{-1} is

$$FV^{-1} = \begin{pmatrix} 0 & \frac{(1-\xi_1)\beta_1\pi_H}{\mu_H\mu_S} & 0 & 0 & 0 \\ \frac{(1-\xi_2)\beta_2\pi_R(1-\xi_1)N}{\mu_M\mu_R} & \frac{(1-\xi_2)\beta_2\pi_R(1-\xi_3)Q\sigma}{\mu_M\sigma\mu_R} & 0 & 0 & 0 \\ 0 & 0 & 0 & 0 & 0 \\ & 0 & 0 & 0 & 0 \\ 0 & 0 & 0 & 0 & 0 \end{pmatrix}. \tag{5.9}$$

The basic reproduction number $\mathscr{R}_0$ is the spectral radius of $\rho(FV^{-1})$. Thus,

$$\mathscr{R}_0 = \rho(FV^{-1}) = \frac{(1-\xi_2)(1-\xi_3)\beta_2\pi_R Q}{\mu_R\mu_M}. \tag{5.10}$$

The expression $\mathscr{R}_0$ is the number of secondary infections within completely susceptible RBCs due to the injection of sporozoites into a healthy individual. The within-host basic reproduction number describes explicitly infected red blood cells and merozoites populations, the inclusion of the pre-erythrocytic (liver stage).

5.2.4 Local stability analysis of parasite-free equilibrium point

In this section, we present the local stability analysis of the parasite-free equilibrium (PFE) point, by linearizing the dynamical system(5.1) at E_0. The Jacobian matrix at any point is given as

$$J(E) = \begin{pmatrix} -A_1-\mu_H & 0 & 0 & 0 & -(1-\xi_1)\beta_1 H & 0 & 0 \\ A_1 & -\delta & 0 & 0 & (1-\xi_1)\beta_1 H & 0 & 0 \\ 0 & 0 & -A_2-\mu_R & 0 & 0 & -(1-\xi_2)\beta_2 R & 0 \\ 0 & 0 & A_2 & -\sigma & 0 & (1-\xi_2)\beta_2 R & 0 \\ 0 & 0 & 0 & 0 & -\mu_S & 0 & 0 \\ 0 & (1-\xi_3)N\delta & 0 & (1-\xi_3)Q\sigma & 0 & -\mu_M & 0 \\ 0 & 0 & 0 & c & 0 & 0 & -(\xi_4+\mu_G) \end{pmatrix}, \tag{5.11}$$

where $A_1 = (1-\xi_1)\beta_1 S$ and $A_2 = (1-\xi_2)\beta_2 M$.

Theorem 5.3. *The parasite-free equilibrium E_0 is locally asymptotically stable if $\mathscr{R}_0 < 1$ and unstable if $\mathscr{R}_0 > 1$.*

Proof. The Jacobian matrix at parasite-free equilibrium point E_0 is given by

$$J(E_0) = \begin{pmatrix} -\mu_H & 0 & 0 & 0 & \frac{-(1-\xi_1)\beta_1\pi_H}{\mu_H} & 0 & 0 \\ 0 & -\delta & 0 & 0 & (\frac{-(1-\xi_1)\beta_1\pi_H}{\mu_H} & 0 & 0 \\ 0 & 0 & -\mu_R & 0 & 0 & \frac{-(1-\xi_2)\beta_2\pi_R}{\mu_R} & 0 \\ 0 & 0 & 0 & -\sigma & 0 & \frac{(1-\xi_2)\beta_2\pi_R}{\mu_R} & 0 \\ 0 & 0 & 0 & 0 & -\mu_S & 0 & 0 \\ 0 & (1-\xi_3)N\delta & 0 & (1-\xi_3)Q\sigma & 0 & -\mu_M & 0 \\ 0 & 0 & 0 & c & 0 & 0 & -(\xi_4+\mu_G) \end{pmatrix}. \tag{5.12}$$

The eigenvalues of the Jacobian matrix, $J(E^0)$ are obtained from the corresponding characteristic polynomial equation $|J(E^0) - \lambda I| = 0$. Clearly, the first, third, and seventh column of the Jacobian matrix (5.12) has only diagonal entries. Thus, the eigenvalues $\lambda_1 = -\mu_H, \lambda_3 = -\mu_R$, and $\lambda_7 = -(\xi_4 + \mu_G)$. The remaining eigenvalues are obtained from the sub-matrix

$$J^1(E_0) = \begin{pmatrix} -\delta & 0 & (\frac{-(1-\xi_1)\beta_1\pi_H}{\mu_H} & 0 \\ 0 & -\sigma & 0 & \frac{(1-\xi_2)\beta_2\pi_R}{\mu_R} \\ 0 & 0 & -\mu_S & 0 \\ (1-\xi_3)N\delta & (1-\xi_3)Q\sigma & 0 & -\mu_M \end{pmatrix}. \tag{5.13}$$

The associated characteristic equation of the Jacobian matrix (5.13) is $|J^1(E_0) - \lambda I| = 0$. That is

$$(\delta+\lambda)(\mu_S+\lambda)\left((\sigma+\lambda)(\mu_M+\lambda) - \frac{(1-\xi_3)(1-\xi_2)\beta_2\pi_R\sigma Q}{\mu_R}\right) = 0. \tag{5.14}$$

Simply, we have $\lambda_2 = -\delta, \lambda_5 = -\mu_S$, and the remaining eigenvalues are obtained from the equation

$$\lambda^2 + B_1\lambda + B_0 = 0, \tag{5.15}$$

where $$B_0 = \sigma + \mu_M, \text{ and } B_1 = \mu_M\sigma - \frac{(1-\xi_3)(1-\xi_2)\beta_2\pi_R\sigma Q}{\mu_R}.$$

Applying Routh–Hurwitz stability criterion, the characteristic equation (5.15) has roots with negative real part, if $B_0 > 0$ and $B_1 > 0$. Obviously $B_0 > 0$. We now need to show $B_1 > 0$. Now,

$$
\begin{aligned}
B_1 &= \mu_M\sigma - \frac{(1-\xi_3)(1-\xi_2)\beta_2\pi_R\sigma Q}{\mu_R},\\
&= \mu_M\sigma\left(1-\frac{(1-\xi_3)(1-\xi_2)\beta_2\pi_R Q}{\mu_R\mu_M}\right),\\
&= \mu_M\sigma\,(1-\mathscr{R}_0)\,.
\end{aligned}
$$

We observe that $B_1 > 0$ if $\mathscr{R}_0 < 1$. Therefore, the parasite-free equilibrium point is locally asymptotically if $\mathscr{R}_0 < 1$ and unstable if $\mathscr{R}_0 > 1$. □

5.2.5 Global stability of parasite-free equilibrium point

Here, we provide the global stability analysis of a parasite-free equilibrium point using a suitable Lypounove function.

Theorem 5.4. *If $\mathscr{R}_0 \le 1$ and $\pi_H(1-\xi_1)\beta_1/\mu_H\mu_S + S^0/S \le 1$ then the parasite-free equilibrium E_0 is globally asymptotically stable.*

Proof. A suitable Lyapunov functional defined as

$$
L = N(H - H^0 - H^0\ln\frac{H}{H^0}) + NH_I + Q(R - R^0 - \ln\frac{R}{R^0}) + NR_I + QR_I + S + \frac{1}{1-\xi_3}M + QG.
$$

A Lyapunov functional L is non-negative and strictly minimized to the parasite-free equilibrium point. We now compute the derivative of L as follows:

$$
\begin{aligned}
\frac{dL}{dt} =& N\left(1-\frac{H^0}{H}\right)\frac{dH}{dt} + N\frac{dH_I}{dt} + Q\left(1-\frac{R^0}{R}\right)\frac{dR}{dt} + Q\frac{dR_I}{dt} + \frac{dS}{dt} + \frac{1}{1-\xi_3}\frac{dM}{dt} + Q\frac{dG}{dt}\\
=& N\left(1-\frac{H^0}{H}\right)(\pi_H - (1-\xi_1)\beta_1 HS - \mu_H H) + N((1-\xi_1)\beta_1 HS - \delta H_I)\\
&+ Q\left(1-\frac{R^0}{R}\right)(\pi_R - (1-\xi_2)\beta_2 RM - \mu_R R) + Q((1-\xi_2)\beta_2 RM - \sigma R_I)\\
&+ \pi_S - \mu_H S + \frac{1}{1-\xi_3}((1-\xi_3)N\delta H_I + (1-\xi_3)Q\sigma R_I - \mu_M M) + cR_I - \xi_4 G - \mu_G G\\
=& N\left(1-\frac{H^0}{H}\right)(\mu_H H^0 - (1-\xi_1)\beta_1 HS - \mu_H H) + N((1-\xi_1)\beta_1 HS - \delta H_I)\\
&+ Q\left(1-\frac{R^0}{R}\right)(\mu_R R^0 - (1-\xi_2)\beta_2 RM - \mu_R R) + Q((1-\xi_2)\beta_2 RM - \sigma R_I) + \mu_S S^0 - \mu_S S\\
&\frac{1}{1-\xi_3}((1-\xi_3)N\delta H_I + (1-\xi_3)Q\sigma R_I - \mu_M M) + cR_I - \xi_4 G - \mu_G G\\
&= -\mu_H N\frac{(H-H^0)^2}{H} - N(1-\xi_1)\beta_1 HS + N(1-\xi_1)\beta_1 HS + \frac{H^0}{H}(1-\xi_1)\beta_1 HS\\
&- \mu_R Q\frac{(R-R^0)^2}{R} - Q(1-\xi_2)\beta_2 MR + Q(1-\xi_2)\beta_2 MR + \frac{R^0}{R}Q(1-\xi_2)\beta_2 MR - \frac{\mu_M M}{1-\xi_3}\\
&+ \mu_S S^0 - \mu_S S - QcR_I + QcR_I - (\xi_4 + \mu_G)G
\end{aligned}
$$

$$
\begin{aligned}
&= -\mu_H N\frac{(H-H^0)^2}{H} + \frac{\pi_H}{\mu_H}(1-\xi_1)\beta_1 S - \mu_R Q\frac{(R-R^0)^2}{R} + \frac{\pi_R}{\mu_R}Q(1-\xi_2)\beta_2 M \\
&- \mu_S S - \frac{\mu_M M}{1-\xi_3} - (\xi_4+\mu_G)G \\
&= -\mu_H N\frac{(H-H^0)^2}{H} - \mu_R Q\frac{(R-R^0)^2}{R} + \frac{\mu_M}{(1-\xi_3)}(\mathscr{R}0-1)M - \mu_S\left(1-\frac{S^0}{S}-\frac{\pi_H(1-\xi_1)\beta_1}{\mu_H\mu_S}\right)S \\
&- (\xi_4+\mu_G)G.
\end{aligned}
$$

The expression $\frac{dL}{dt} \leq 0$ if $\mathscr{R}_0 \leq 1$ and $\frac{S^0}{S} + \frac{\pi_H(1+\xi_1)\beta_1}{\mu_H\mu_S} \leq 1$ for any positive H, H_I, R, R_I, S, M, G. The equality $\frac{dL}{dt} = 0$, holds if and only if for $H = H^0$, $R = R^0$, $G = G^0$, $\mathscr{R}_0 = 1$ and $\pi_H(1-\xi_1)\beta_1/\mu_H\mu_S + S^0/S = 1$. Therefore, by LaSalle's Invariance Principle (La Salle, 1976), the parasite-free equilibrium E_0 is global asymptotically stable for $\mathscr{R}_0 \leq 1$ and $\pi_H(1-\xi_1)\beta_1/\mu_H\mu_S + S^0/S \leq 1$. □

5.2.6 Parasite persistence equilibrium point

The parasite persistence equilibrium point (PPE) is the steady-state solution at which the malaria parasite persists in the host cells. It's computed by setting the right hand side of the system equation (5.1) to zero. The parasite persistence equilibrium point E^* is investigated and given as

$$
E^*(H^*, H_I^*, R^*, R_I^*, S^*, M^*, G^*) = \begin{cases}
H^* = \frac{\pi_H}{(1-\xi_1)\beta_1\frac{\pi_S}{\mu_S}+\mu_H}, \\
H_I^* = \frac{(1-\xi_1)\beta_1\pi_S\pi_H}{\delta(\mu_S(1-\xi_1)\frac{\pi_S}{\mu_S}+\mu_H)}, \\
R^* = \frac{\pi_R}{(1-\xi_2)\beta_2 M^*+\mu_R}, \\
R_I^* = \frac{(1-\xi_2)\pi_R\beta_2 M^*}{((1-\xi_2)\beta_2 M^*+\mu_R)\sigma}, \\
S^* = \frac{\pi_S}{\mu_S}, \\
G^* = \frac{c(1-\xi_2)\pi_R\beta_2 M^*}{((1-\xi_2)\beta_2 M^*+\mu_R)\sigma(\xi_4+\mu_G)},
\end{cases}
$$

where M^* is the positive roots of

$$
P(M^*) = d_0 {M^*}^2 + d_1 M^* + d_2 = 0, \tag{5.16}
$$

and the coefficients d_2, d_1 and d_0 are given as

$$
\begin{aligned}
d_0 &= (1-\xi_1)\pi_S + \mu_H\mu_M(1-\xi_2)\beta_2\sigma, \\
d_1 &= ((1-\xi_1)\pi_S + \mu_H)\mu_M\mu_R\sigma(1-\mathscr{R}_0) - N(1-\xi_1)(1-\xi_2)(1-\xi_3)\beta_1\pi_S\pi_H\beta_2\sigma, \\
d_2 &= -(1-\xi_1)(1-\xi_3)N\beta_1\pi_S\pi_H\mu_R(\sigma+c).
\end{aligned} \tag{5.17}
$$

By Descarts' Rule of sign, the system equation (5.1) has a parasite persistence equilibrium, if $d_1 < 0$ implies that $\mathscr{R}_0 > 1$ and/or if $d_1 < 0$ implies that $\mathscr{R}_0 > 1$, and if the discriminant $\Delta = 0$, where

$$\begin{aligned}\Delta =& d_1^2 - 4d_2d_0 \\ =& (((1-\xi_1)\pi_S + \mu_H)\mu_M\mu_R\sigma(1-\mathscr{R}_0) - N(1-\xi_1)(1-\xi_2)(1-\xi_3)\beta_1\pi_S\pi_H\beta_2\sigma)^2, \\ &+4((1-\xi_1)\pi_S + \mu_H)(\mu_M(1-\xi_2)\beta_2\sigma)(1-\xi_3)N(1-\xi_1)\beta_1\pi_S\pi_H\mu_R(\sigma + c).\end{aligned}$$

From equation (5.17) it is not difficult to see that d_0 is always positive and d_2 negative. Thus, by Descarts' Rule of sign and/or discriminant a parasite persistence equilibrium point exist if $\mathscr{R}_0 > 1$.

5.2.7 Local stability analysis of parasite persistence equilibrium point

In this section, we examine the local stability analysis of parasite persistence equilibrium via linearzing the system equation (5.1) at E^*.

Theorem 5.5. *The parasite persistence equilibrium point is locally asymptotically stable if* $\mathscr{R}_0 > 1$ *and unstable if* $\mathscr{R}_0 < 1$.

Proof. The Jacobian matrix at parasite persistence equilibrium, E^* is given as

$$J(E^*) = \begin{pmatrix} -C_1 - \mu_H & 0 & 0 & 0 & -(1-\xi_1)\beta_1 H & 0 & 0 \\ C_1 & -\delta & 0 & 0 & (1-\xi_1)\beta_1 H & 0 & 0 \\ 0 & 0 & -C_2 - \mu_R & 0 & 0 & -(1-\xi_2)\beta_2 R^* & 0 \\ 0 & 0 & C_2 & -\sigma & 0 & (1-\xi_2)\beta_2 R^* & 0 \\ 0 & 0 & 0 & 0 & -\mu_S & 0 & 0 \\ 0 & (1-\xi_3)N\delta & 0 & (1-\xi_3)Q\sigma & 0 & -\mu_M & 0 \\ 0 & 0 & 0 & c & 0 & 0 & -(\xi_4 + \mu_G) \end{pmatrix}, \tag{5.18}$$

where $C_1 = (1-\xi_1)\beta_1 S^*$ and $C_2 = (1-\xi_2)\beta_2 M^*$.

The associated characteristic equation is given as $det(J(E^*) - \lambda I) = 0$. To simplify the steps now, the last column of the Jacobian matrix (5.18) has only diagonal entry, thus we have $\lambda_7 = -(\xi_4 + \mu_G)$. The fifth row of the Jacobian matrix has only a diagonal entry and we can easily obtain the $\lambda_5 = -\mu_S$. The remaining eigenvalues are obtained from the sub matrix

$$J_1(E^*) = \begin{pmatrix} -A_1 - \mu_H & 0 & 0 & 0 & 0 \\ A_1 & -\delta & 0 & 0 & 0 \\ 0 & 0 & -A_2 - \mu_R & 0 & -(1-\xi_2)\beta_2 R^* \\ 0 & 0 & A_2 & -\delta & (1-\xi_2)\beta_2 R^* \\ 0 & (1-\xi_3)N\delta & 0 & (1-\xi_3)Q\sigma & -\mu_M \end{pmatrix}. \tag{5.19}$$

The associated characteristic equation is given as $det(J_1(E^*) - \lambda I) = 0$. Thus,

$$(C_1 + \mu_H + \lambda)(\delta + \lambda)(\lambda^3 + B_0\lambda^2 + B_1\lambda + B_0) = 0, \tag{5.20}$$

where

$$\begin{aligned}
B_0 &= \delta + \mu_M + C_2 + \mu_R, \\
B_1 &= \delta\mu_M + (C_2 + \mu_R)(\delta + \mu_M), \\
B_2 &= \delta\mu_M(C_2 + \mu_R) - (1-\xi_2)(1-\xi_3)Q\delta\beta_2 R^* + (1-\xi_2)(1-\xi_3)\beta_2 C_2 Q\delta R^*.
\end{aligned}$$

From characteristic polynomial equation (5.20), we have $\lambda_1 = -C_1 - \mu_H$, $\lambda_2 = -\delta$ or

$$\lambda^3 + B_0\lambda^2 + B_1\lambda + B_2 = 0. \tag{5.21}$$

Applying Routh-Hurwitz stability criteria. The polynomial equation (5.21) has roots with negative real part if $B_0 > 0, B_1 > 0, B_2 > 0$ i.e, $\delta\mu_M(C_2 + \mu_R) + (1-\xi_2)(1-\xi_3)\beta_2 C_2 Q\delta R^* > (1-\xi_2)(1-\xi_3)Q\delta\beta_2 R^*$, and $B_0B_1 - B_2 > 0$. Therefore, the parasite persistence equilibrium point is locally asymptotically stable if $\mathscr{R}_0 > 1$. □

5.2.8 Sensitivity analysis

In this section, we present the sensitivity analysis for the basic reproduction number $\mathscr{R}_0$ to identify the parameters that have a high impact on disease elaboration within the host. The normalized forward sensitivity index of a variable to a parameter is the ratio of the relative change in the variable to the relative change in the parameter. If the variable is a differentiable function of the parameter, the sensitivity index is then defined using partial derivatives. As we have an explicit formula for $\mathscr{R}_0$ given in equation (5.10), we derive an analytical expression for the sensitivity of $\mathscr{R}_0$

$$\Theta_{\vartheta}^{\mathscr{R}_0} = \frac{\partial \mathscr{R}_0}{\partial \vartheta} \times \frac{\vartheta}{\mathscr{R}_0},$$

where ϑ is represented the model parameters which belongs to basic reproduction number $\mathscr{R}_0$. Now,

$$\begin{aligned}
\Theta_{\beta_2}^{\mathscr{R}_0} &= \frac{\partial \mathscr{R}_0}{\partial \beta_2} \times \frac{\beta_2}{\mathscr{R}_0} = +1, & \Theta_{\pi_R}^{\mathscr{R}_0} &= \frac{\partial \mathscr{R}_0}{\partial \pi_R} \times \frac{\pi_R}{\mathscr{R}_0} = +1, \\
\Theta_{Q}^{\mathscr{R}_0} &= \frac{\partial \mathscr{R}_0}{\partial Q} \times \frac{Q}{\mathscr{R}_0} = +1, & \Theta_{\mu_M}^{\mathscr{R}_0} &= \frac{\partial \mathscr{R}_0}{\partial \mu_M} \times \frac{\mu_M}{\mathscr{R}_0} = -1 \\
\Theta_{\mu_R}^{\mathscr{R}_0} &= \frac{\partial \mathscr{R}_0}{\partial \mu_R} \times \frac{\mu_R}{\mathscr{R}_0} = -1.
\end{aligned}$$

Table 5.2: Sensitivity index of within-host basic reproduction number $\mathscr{R}_0$.

Parameters	Elasticity index	Value	Parameters	Elasticity index	Value
β_2	$\Theta_{\beta_2}^{\mathscr{R}_0}$	$+1$	π_R	$\Theta_{\pi_R}^{\mathscr{R}_0}$	$+1$
Q	$\Theta_{Q}^{\mathscr{R}_0}$	$+1$	μ_M	$\Theta_{\mu_M}^{\mathscr{R}_0}$	-1
μ_R	$\Theta_{\mu_R}^{\mathscr{R}_0}$	-1			

Table 5.3: The model parameter values

Parameters	Value	Units	Source
π_S	30	sporozoite /day	Orwa et al. (2018)
μ_S	1.2×10^{-11}	/day	Selemani et al. (2016)
π_H	3000	cells/ml/day	Selemani et al. (2016)
μ_R	0.0083	/day	Anderson and May (1991b)
π_R	3×10^{5}	cells/day/μl	Orwa et al. (2018)
σ	1.0	/day	Hetzel and Anderson (1996)
β_1	$0.001\mu l$	μl/cell/day	Selemani et al. (2017a)
μ_G	0.0000625	/day	Selemani et al. (2016)
β_2	2×10^{-6}	/sporozoite	Chiyaka et al. (2008)
c	0.02	/day	Hellriegel (1992)
δ	0.02	cell/day	Orwa et al. (2018)
μ_H	0.029	cell/day	Orwa et al. (2018)
N	10000	/day	Selemani et al. (2016)
Q	16	/day	Chiyaka et al. (2008)
μ_M	48	/day	Chiyaka et al. (2008)

From Table 5.2, we see that the infection rate of the erythrocyte by merozoites β_2, average number of merozoites per ruptured infected erythrocyte cells Q, the production rate of the erythrocyte π_R, natural death rate merozoites μ_M and natural death rate of red-blood cells μ_R are the most sensitive parameters. A 10% increase (or decrease) in β_2, and Q is a 10% increase (or decrease) in $\mathscr{R}_0$. A 10% increase (decrease) in μ_M is a 10% decrease (or increase) in $\mathscr{R}_0$.

5.3 Numerical simulations

In this section, we present the numerical simulation of model (5.1) to supplement the analytical results. The initial condition we used in this simulation is $H(0) = 3000, H_I(0) = 10, R(0) = 500000, R_I(0) = 200, S(0) = 200, M(0) = 40000, G(0) = 20$ and the model parameters are given in Table 5.3. Using the model parameter values, we have within host basic reproduction number $\mathscr{R}_0 = 24.0964$ without antimalarial drug treatment ($\xi_1 = 0$, $\xi_2 = 0$) and $\mathscr{R}_0 = 6.0241$ with antimalarial drug treatment 50% effective ($\xi_1 = 50\%$, $\xi_2 = 50\%$ effective). The simulation of the system equations is integrated using the ode45 solver in MATLAB.

Figure 5.2 reveals the dynamical behavior of model (5.1) in the absence of antimalarial drug treatments, i.e., all-stage antimalarial drug treatment is not administered ($\xi_1 = 0, \xi_2 =$

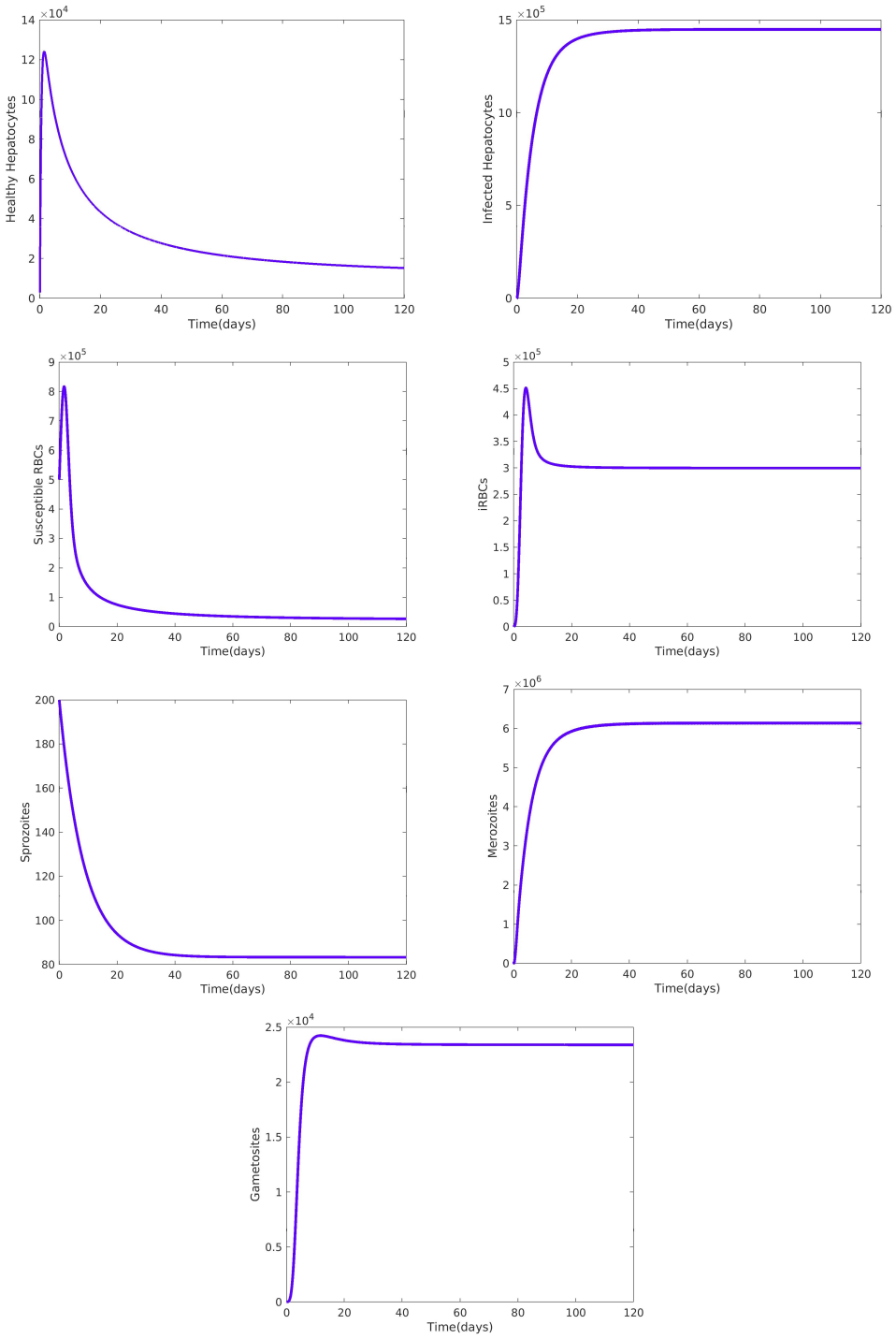

Figure 5.2: The dynamical behavior of the system equation (5.1) without malaria drug treatments i.e $\xi_1 = 0, \xi_2 = 0, \xi_3 = 0, \xi_4 = 0, \mathscr{R}_0 = 24.695$ and all the other parameters are fixed as in Table 5.3.

$0, \xi_3 = 0, \xi_4 = 0$). The vulnerable hepatocytes and red blood cells decrease over time, whereas the other state variables are rise. All the system solutions converge to an parasite persistence equilibrium point. The effect of primary tissue schizontocides on healthy and infected hepatocytes is shown in Figure 5.3. As metformin's antimalarial effectiveness rises, the number of healthy hepatocytes also rises (see Figure 5.3(a)). Figure 5.3(b) reveals when the effective-

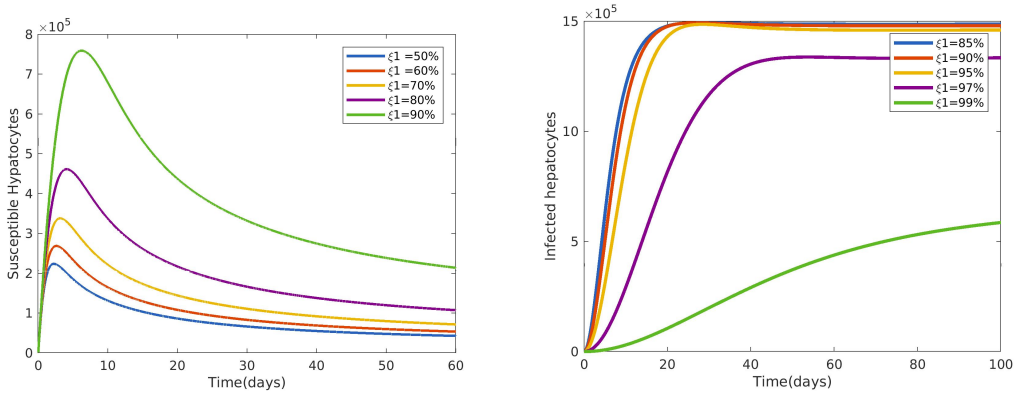

(a) (b)

Figure 5.3: The impact of primary tissue schizontocides (pre-erythrocytic treatment) ξ_1 (a) on susceptible hepatocytes (b) on infected hepatocytes using the following parameter values: $\pi_S = 30, \pi_H = 3000, \pi_R = 3 \times 10^5, \beta_1 = 0.001, \beta_2 = 2 \times 10^{-6}, \delta = 0.02, N = 10000, \mu_M = 48, \mu_S = 1.2 \times 10^{-11}, \mu_R = 0.0083, \sigma = 1.0, \mu_G = 0.0000625, c = 0.02, \mu_H = 0.029, Q = 16$ and all the other parameters are fixed as in Table 5.3.

ness of metformin antimalarial treatment rises, the number of infected hepatocytes declines. Figure 5.4(a) shows the iRBCs decrease as the efficiency of blood schizontocides increases.

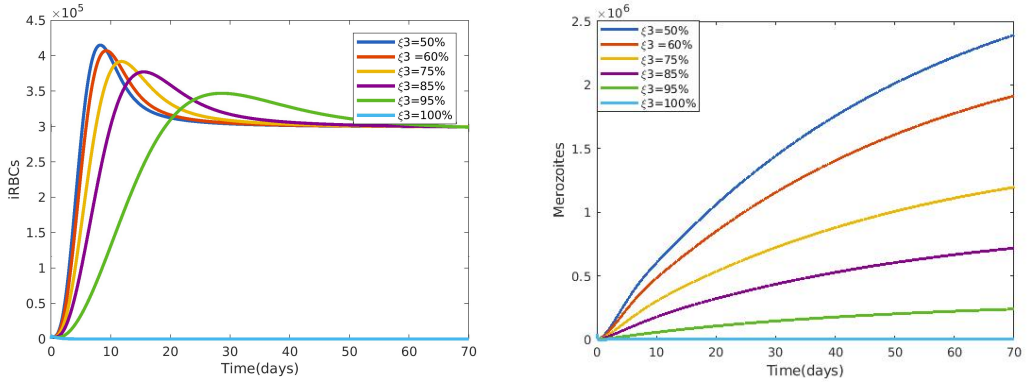

(a) (b)

Figure 5.4: (a) The impact of blood schizontocides ξ_3 on iRBCs. (b) The impact of blood schizontocides ξ_3 on merozoites using the following parameter values: $\pi_S = 30, \pi_H = 3000, \pi_R = 3 \times 10^5, \beta_1 = 0.001, \beta_2 = 2 \times 10^{-6}, \delta = 0.02, N = 10000, \mu_M = 48, \mu_S = 1.2 \times 10^{-11}, \mu_R = 0.0083, \sigma = 1.0, \mu_G = 0.0000625, c = 0.02, \mu_H = 0.029, Q = 16$ and all the other parameters are fixed as in Table 5.3.

Figure 5.4(b) indicates the impact of blood schizontocide and primary tissue schizontocide on merozoites. The merozoite population decreases as the blood schizontocides and primary tissue schizontocides efficiency increases. The impact of blood schizontocides (blood-stage antimalarial medication treatment) on red-blood cells is depicted in Figure (5.5). As blood schizontocides (blood-stage antimalarial drug therapy) increases, the number of uninfected red-blood cells rises (see Figure (5.5)(a)). As indicated in Figure (5.5)(b), the infected red blood cells gradually decline as the blood schizontocides (antimalarial drug treatment at the blood stage) increase. Figure 5.6 demonstrates that as the average number of merozoites per

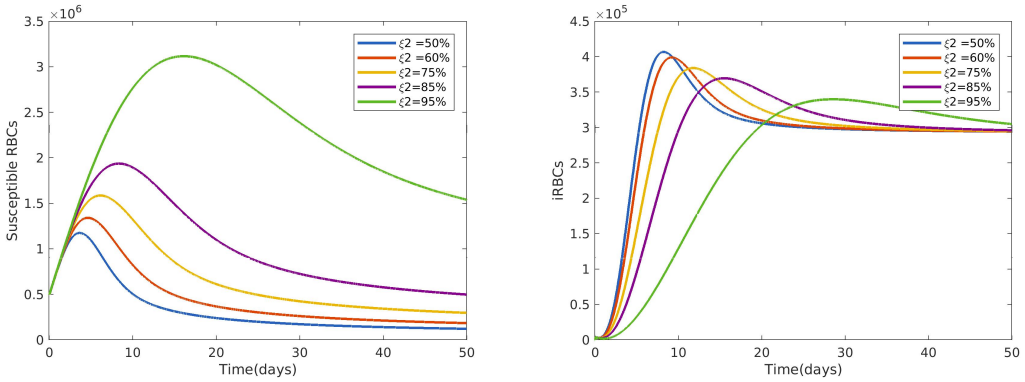

(a) (b)

Figure 5.5: The impact of the blood schizontocides ξ_2 (a) on healthy RBCs (b) on iRBCs using the following parameter values: $\pi_S = 30, \pi_H = 3000, \pi_R = 3 \times 10^5, \beta_1 = 0.001, \beta_2 = 2 \times 10^{-6}, \delta = 0.02, N = 10000, \mu_M = 48, \mu_S = 1.2 \times 10^{-11}, \mu_R = 0.0083, \sigma = 1.0, \mu_G = 0.0000625, c = 0.02, \mu_H = 0.029, Q = 16$ and all the other parameters are fixed as in Table 5.3.

ruptured infected erythrocyte grows, both the population of merozoites and the infected RBCs increase.

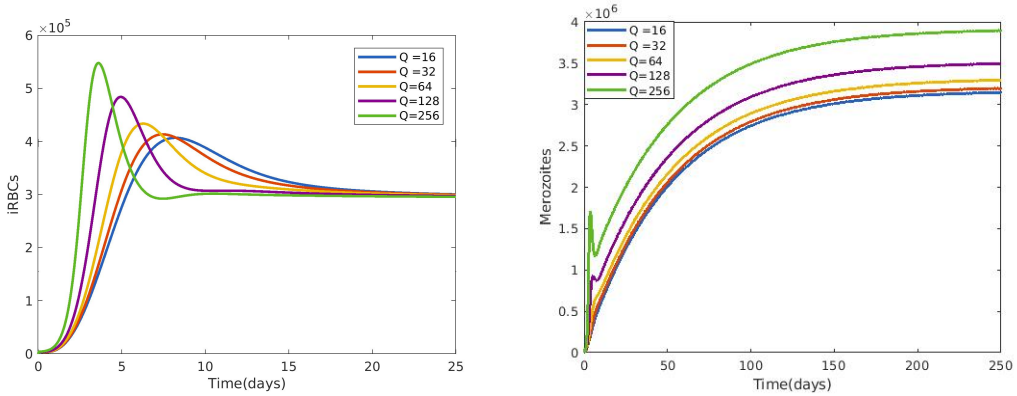

(a) (b)

Figure 5.6: The impact average number of merozoite per ruptured infected erythrocyte cells Q (a) on iRBCs and merozoites using the following parameter values: $\pi_S = 30, \pi_H = 3000, \pi_R = 3 \times 10^5, \beta_1 = 0.001, \beta_2 = 2 \times 10^{-6}, \delta = 0.02, N = 10000, \mu_M = 48, \mu_S = 1.2 \times 10^{-11}, \mu_R = 0.0083, \sigma = 1.0, \mu_G = 0.0000625, c = 0.02, \mu_H = 0.029, Q = 16$ and all the other parameters are fixed as in Table 5.3.

Figure 5.7(a) displays the gametocyte population declines as the effectiveness of gametocytocidal medication therapy (gametocytocidal) increases. Figure 5.7(b) exhibits the effect of the average number of merozoites discharged per ruptured infected hepatocytic cell on merozoites. As the average number of merozoites discharged per ruptured infected hepatocytic cell increases, the merozoite population increases. Figure 5.8(a) depicts the impact of the infection rate of erythrocyte β_2 and the antimalarial treatment on erythrocytic invasion (blood schizontocides efficacy) ξ_2 on the basic reproduction number R_0. Figure 5.8(b) displays the impact of the infection rate of the erythrocyte β_2 and blood schizontocides drug treatment ξ_3 on the basic

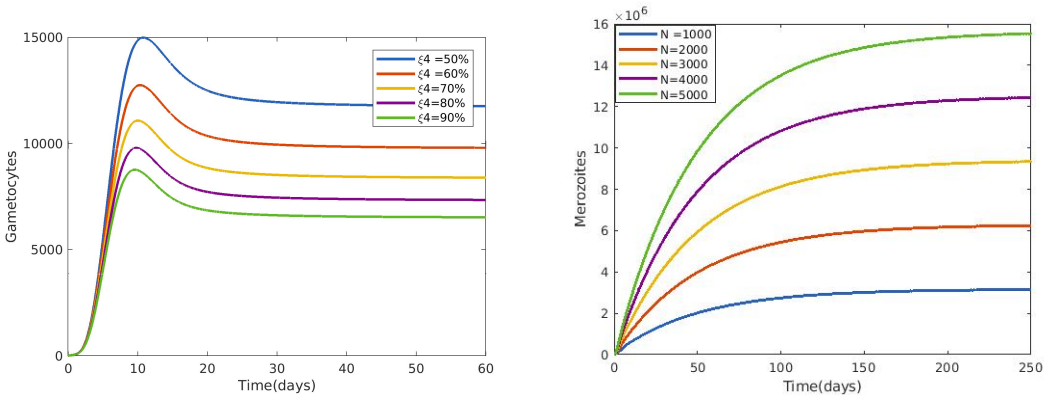

(a) (b)

Figure 5.7: (a) The impact of gametocytocidal drugs (gametocytocides) on sexual replication of malaria parasites. (b) The effect of the average number of merozoite released per ruptured infected hepatocytic cells using the following parameter values: $\pi_S = 30, \pi_H = 3000, \pi_R = 3 \times 10^5, \beta_1 = 0.001, \beta_2 = 2 \times 10^{-6}, \delta = 0.02, \mu_M = 48, \mu_S = 1.2 \times 10^{-11}, \mu_R = 0.0083, \sigma = 1.0, \mu_G = 0.0000625, c = 0.02, \mu_H = 0.029, Q = 16$ and all the other parameters are fixed as in Table 5.3.

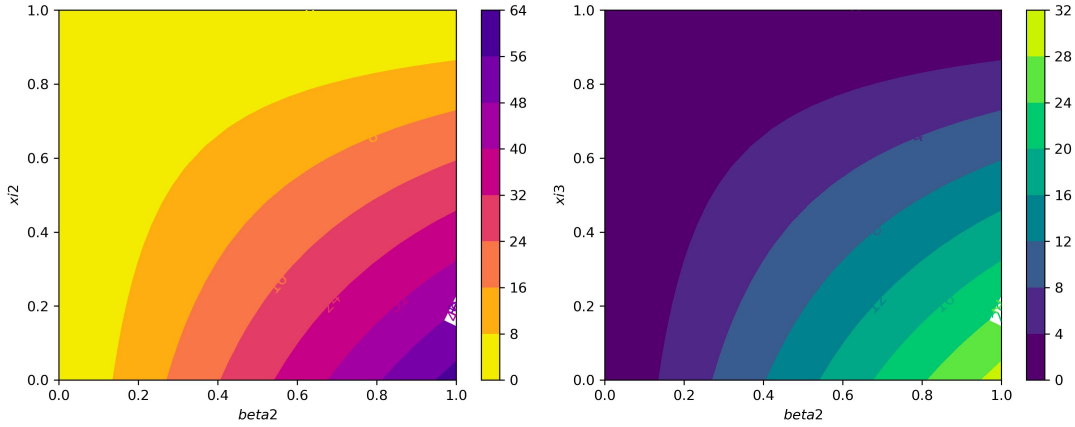

(a) (b)

Figure 5.8: (a) Contour plot of $\mathscr{R}_0$ with respect to infection rate of the erythrocyte β_2 and efficacy of antimalarial treatment on erythrocytic invasion (blood schizontocides efficacy) ξ_2. (b) Contour plot of $\mathscr{R}_0$ with respect to the infection rate of the erythrocyte β_2 and efficiency of antimalarial drug treatments on the bursting rate of erythrocytic (blood schizontocides efficacy) ξ_3.

reproduction number $\mathscr{R}_0$. As imagined, to reduce the $\mathscr{R}_0$ value below unity, the infection rate of the erythrocyte must be very low, almost irrespective of the blood schizontocides. That is, despite the availability of antimalarial treatment, inconsiderate mixing needs to be observed to prevent an excessive number of parasites inside the host cell. Figure 5.9(a) indicates the influence of the average number of merozoite per ruptured infected erythrocyte cell Q and blood-stage antimalarial drug treatment (efficacy of antimalarial treatment on erythrocytic invasion) ξ_2 on the basic reproduction number $\mathscr{R}_0$. Figure 5.9(b) shows the impact of the average number of merozoite per ruptured infected erythrocyte cells Q and efficiency of antimalarial

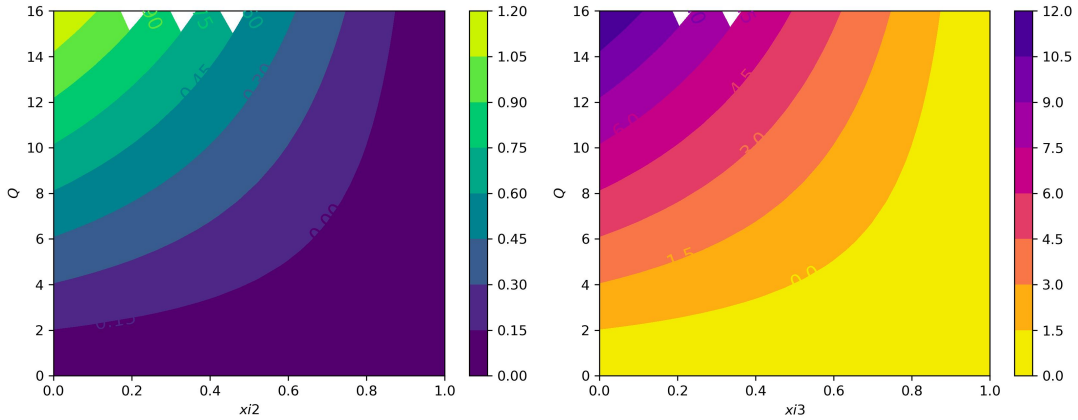

(a) (b)

Figure 5.9: (a) Contour plot of $\mathscr{R}_0$ with respect to the average number of merozoite per ruptured infected erythrocyte cells Q and blood stage antimalarial drug treatment (efficacy of antimalarial treatment on erythrocytic invasion) ξ_2. (b) Contour plot of $\mathscr{R}_0$ average number of merozoite per ruptured infected erythrocyte cells Q and efficiency of antimalarial drug treatments on the bursting rate of pre erythrocytic schizont and blood schizont ξ_3.

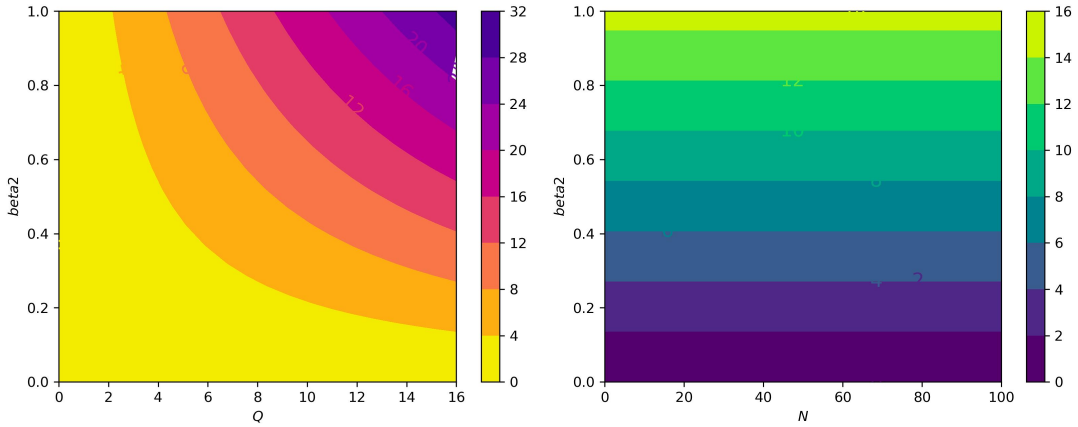

(a) (b)

Figure 5.10: (a) Contour plot of $\mathscr{R}_0$ with respect to the infection rate of the erythrocyte β_2 and an average number of merozoite per ruptured infected erythrocyte cells Q. (b) Contour plot of $\mathscr{R}_0$ with respect to an infection rate of the erythrocyte β_2 and an average number of merozoite per ruptured infected hepatocyte cells N.

drug treatments on the bursting rate of pre-erythrocytic schizont and blood schizont ξ_3. The Figures illustrate decreasing the average number of merozoites per ruptured infected erythrocyte cell Q and raising blood-stage antimalarial drug treatment ξ_2 and blood schizontocide ξ_3 decreases the in-host basic reproduction number $\mathscr{R}_0$, which, in turn, decreases the in-host malaria parasite. Figure 5.10(a) exhibits the impact of the infection rate of erythrocyte β_2 and the average number of merozoite per ruptured infected erythrocyte cells Q on the basic reproduction number, $\mathscr{R}_0$. The within-host basic reproduction number rises as both the infection rate of the erythrocyte and the average number of merozoite per ruptured infected erythrocyte cells increases. Figure 5.10(b), demonstrates the within-host reproduction number increases

as the infection rate of the erythrocyte increases, however, the average number of merozoites per ruptured infected hepatocyte cell N has no impact on the reproduction number.

5.4 Summary

In this Chapter, we investigated a cell-level mathematical model for malaria parasite infection with antimalarial drug treatment. The model includes the interactions of hepatocyte cells, red blood cells, and malaria parasites. The qualitative analysis of the developed model, such as the positivity and boundedness of the solution is discussed. The equilibria and their stability analysis are investigated, where the parasite-free equilibrium point is both local and global stable if the basic reproduction number $\mathscr{R}_0$ is less than unity. The global stability analysis of the parasite-free equilibrium point is investigated using a suitable Lyponove function. The existence of parasite persistence equilibrium is reached using Descarts' Rule of sign and its local stability is investigated by applying the Routh-Hurwitz stability criterion. We computed a sensitivity analysis of the in-host basic reproduction number to investigate the most influential parameters in the within-host malaria parasites using the normalized forward sensitivity index. As a result, the infection rate of the erythrocyte by merozoites, the average number of merozoites per ruptured infected erythrocyte, the natural death rate of merozoites, and the requirement rate of the uninfected erythrocytes are the most influential ones. Different numerical simulations are performed to supplement our analytical findings and it is observed to be in good agreement. Furthermore, the simulation result reveals that the administration of antimalarial drug treatment, such as primary tissue schizontocides, blood schizontocides, and gametocytocides are used to eliminate the malaria parasites from the human host cells. This study's findings offer guidance for antimalarial medication therapy and malaria control. By lowering the average number of merozoites per ruptured infected erythrocyte and hepatocyte, we can restrict the generation of malaria parasites within the host and prevent them from being infected. Primary tissue schizontocide and blood-stage schizontocides will be administered in order to achieve this. In this work, we considered the constant antimalarial treatment and single strains of malaria infection.

CHAPTER 6

A MATHEMATICAL MODEL FOR THE WITHIN-HOST DYNAMICS OF MALARIA PARASITE WITH ADAPTIVE IMMUNE RESPONSES

In this Chapter, we formulate a blood-stage mathematical model for within-host malaria infection with the effect of an adaptive immune system (Cytotoxic T-cells and antibodies). The within-host model is analyzed mathematically and solved numerically using Matlab software.

6.1 Model Formulation

In this section, we formulated a blood-stage mathematical model of the malaria parasite with adaptive immune responses. The model incorporates the interactions of six compartments: healthy (uninfected) red blood cells (RBCs), $X(t)$, infected red blood cells (iRBCs), $Y(t)$, merozoites, $M(t)$, gametocytes, $G(t)$, cytotoxic T-cells, $C(t)$ and antibody, $A(t)$ at a time t.

To formulate the model, the following assumptions are taken into consideration:
(i) Healthy red blood cells $X(t)$ are recruited from the bone marrow at a rate Λ_x. They may suffer natural death at a rate μ_x or get infected with the malaria parasite, in the form of merozoites $M(t)$, at a rate β and move to the iRBCs compartment $Y(t)$. (ii) The infected red blood cells $Y(t)$ are increased via the progression rate of red blood cells, and removed by cytotoxic T-cells $C(t)$ at a rate γ. Infected red blood cells die at a rate μ_y during rupturing. (iii) The merozoites $M(t)$ increase when infected red blood cells burst open and release merozoites into the bloodstream at a rate $N\mu_y$, where N is the average number of the merozoites that are released per rupture infected red blood cells $Y(t)$. The merozoite population is removed by antibodies $A(t)$ at a rate θ and by natural death at a rate μ_m. (iv) After the invasion of red blood cells, a small number of merozoites develop into sexual (female and male) gametocytes $G(t)$ at a rate c, the gametocytes are cleared via antibodies at a rate η and the gametocytes suffer natural death at a rate μ_g. (v) The adaptive immune response is activated (stimulated) during malarial *Plasmodium* infection (by the presence of merozoites) in the blood cells. Thus, antibodies $A(t)$ are stimulated when they interact with malaria merozoites and gametocytes at a rate α and ω respectively and removed by a natural death at a rate μ_a. (vi) Cytotoxic T-cells are stimulated by the presence of infected red blood cells at a rate ξ, and removed via natural death at a rate μ_c. Furthermore, all the biological parameters and their descriptions are given in Table 6.1.

Based on the above description, assumption, and schematic diagram (see Fig. 6.1), we have the leading within-host mathematical model of malaria parasites with adaptive immune responses as follows:

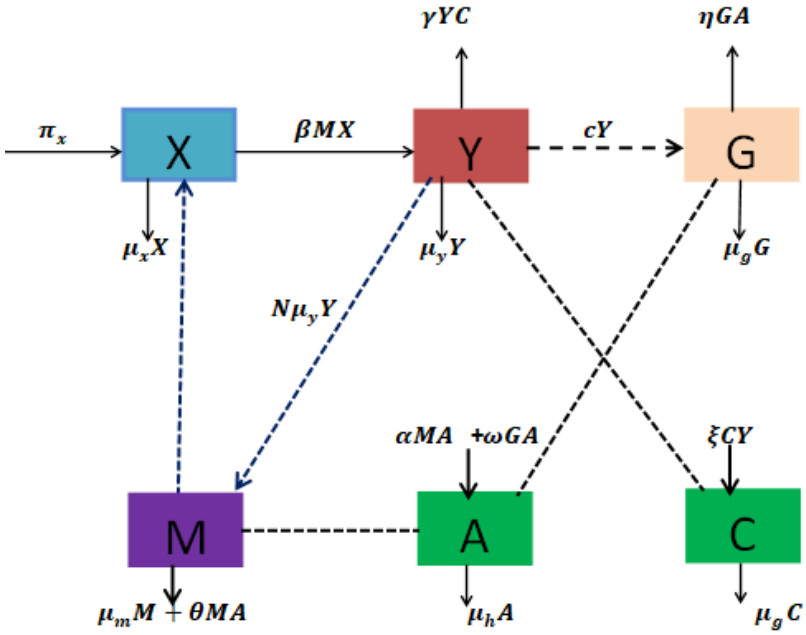

Figure 6.1: Schematic diagram of dynamical system of blood-stage malaria parasite with adaptive immune response.

$$\begin{aligned}
\frac{dX}{dt} &= \Lambda_x - \beta XM - \mu_x X,\\
\frac{dY}{dt} &= \beta XM - \gamma YC - \mu_y Y,\\
\frac{dM}{dt} &= \mu_y NY - \theta MA - \mu_m M,\\
\frac{dG}{dt} &= cY - \eta GA - \mu_g G,\\
\frac{dC}{dt} &= \xi CY - \mu_c C,\\
\frac{dA}{dt} &= \alpha MA + \omega GA - \mu_a A,
\end{aligned} \tag{6.1}$$

with initial conditions

$$X(0) > 0,\ Y(0) \geq 0,\ M(0) \geq 0,\ G(0) \geq,\ C(0) \geq 0,\ A(0) \geq 0. \tag{6.2}$$

6.2 Analysis of the model

Here, we investigate qualitatively analyze the formulated model (6.1).

6.2.1 Positivity and buondedness of the solution

Theorem 6.1. *The solution of the system equation (6.1), $X(t), Y(t), M(t), G(t), A(t)$ and $C(t)$ with non-negative initial condition (6.2) is non-negative, for all $t > 0$.*

Table 6.1: Model parameters and their descriptions

Parameters	Parameter description
Λ_x	Recruitment rate of uninfected RBCs from bone marrow
β	Infection rate of the red blood cell by merozoites
$\mu_x, \mu_m, \mu_a, \mu_c, \mu_g$	Natural death rate of RBCs, merozoites, antibodies, cytotoxic T cells, and gametocytes, respectively
μ_y	Death rate of infected red blood cells
N	Average number of merozoites per ruptured infected red blood cell
θ, η	Removal rate of merozoites and gametocytes due to antibodies, respectively
γ	Removal rate of infected red blood cells due to cytotoxic T-cells
ξ	Activation rate of cytotoxic T-cells owing to the presence of infected red blood cells
ω, α	Activation rate of antibodies due to the presence of gametocytes and merozoites, respectively

Proof. From the first equation of the system (6.1), we have

$$\frac{dX}{dt} = \Lambda_x - \beta XM - \mu_x X \geq -(\beta M + \mu_x)X.$$

By integrating this inequality, we found

$$X(t) \geq X_0 exp\left\{-\mu_x t - \int_0^t \beta M(\tau)d\tau\right\} > 0.$$

Consider the second equation of the system (6.1)

$$\frac{dY}{dt} = \beta XM - \gamma YC - \mu_y Y \geq -(\gamma C + \mu_y)Y$$

Taking integral both sides of the inequality, we get

$$Y(t) \geq Y_0 exp\left\{-\mu_y t - \int_0^t \gamma C(\tau)d\tau\right\} \geq 0$$

In the same way, we can apply for the non-negativity of state variables $M(t), G(t), C(t)$ and $A(t)$, we obtained

$$M(t) \geq M_0 exp\left\{-\mu_m t - \int_0^t \theta A(\tau)d\tau\right\} \geq 0,$$
$$G(t) \geq G_0 exp\left\{-\mu_g t - \int_0^t \eta A(\tau)d\tau\right\} \geq 0,$$
$$C(t) \geq C_0 exp\{-\mu_c t\} > 0,$$
$$A(t) \geq A_0 exp\{-\mu_a t\} > 0.$$

Therefore, the solution of the dynamical system (6.1) is non-negative with non-negative initial condition, for all $t \geq 0$. □

Theorem 6.2. *The region*

$$\Omega = \left\{ \Omega_1 \times \Omega_2 \times \Omega_3 \in R_+^6 : N_R \leq \frac{\Lambda_x}{\mu_r}; N_P(t) \leq \frac{\psi}{\mu_P}, N_I(t) \leq N_I(0) \right\}$$

is a positive invariant of the system model (6.1)*, where* $N_R(t) = X(t) + Y(t)$, $N_P(t) = M(t) + G(t)$*, and* $N_I(t) = C(t) + A(t)$.

Proof. The total size of red blood cells $N_R(t) = X(t) + Y(t)$, differentiate, this with respect to time t.

$$\begin{aligned} \frac{dN_R}{dt} &= \frac{dX}{dt} + \frac{dY}{dt} \\ &= \Lambda_x - \beta XM - \mu_x X + \beta XM - \gamma YC - \mu_y Y \\ &= \Lambda_x - \mu_x X - \gamma YC - \mu_y Y \leq \Lambda_x - \mu_R N_I, \end{aligned}$$

where, $\mu_R = min\left\{\mu_x, \mu_y\right\}$. For $N_R(0) \leq \frac{\Lambda_x}{\mu_R}$, we have

$$N_R(t) \leq \frac{\Lambda_x}{\mu_R} + \left(N_R(0) - \frac{\Lambda}{\mu_R} \right) e^{-\mu_R t} \leq \frac{\Lambda_x}{\mu_R}.$$

In the same fashion, we can compute for the malaria parasite $N_P(t) = M(t) + G(t)$, and immune response $N_I(t) = C(t) + A(t)$, we get

$$\begin{aligned} N_P(t) &\leq \frac{(\mu_y N + c)\Lambda_x}{\mu_R \mu_P} + \left(N_P(0) - \frac{(\mu_y N + c)\Lambda_x}{\mu_R \mu_P} \right) e^{-\mu_P t} \leq \frac{\psi}{\mu_P}, \\ N_I(t) &\leq N_I(0), \quad for \;\; N_I(0) > 0. \end{aligned}$$

where $\psi = \frac{(\mu_y N + c)\Lambda_x}{\mu_R}$ is the maximum production rate of malaria merozoites in the red blood cells. Therefore, the region Ω is a positive invariant for the dynamical system (6.1). □

6.2.2 Parasite-free equilibrium point and the in-host basic reproduction number

The parasite-free equilibrium point, E^0, is the steady-state solution in the absence of the parasite in-host cells. It is obtained by setting the right-hand sides of equations in the model system (6.1) to zero. Thus, we found that

$$E^0 = (X^0, Y^0, M^0, G^0, C^0, A^0) = \left(\frac{\Lambda_x}{\mu_x}, 0, 0, 0, 0, 0 \right).$$

Next, we examine the within-host basic reproduction number using the next-generation matrix approach method Van den Driessche and Watmough (2002). Let $\mathscr{F}_i$ and $\mathscr{V}_i$ be the rate of

new appearance and the rate of transfer from one compartment to another by any means, respectively, and given as

$$\mathscr{F}_i = \begin{pmatrix} \beta XM \\ 0 \\ 0 \end{pmatrix}, \quad \mathscr{V}_i = \begin{pmatrix} \gamma YC + \mu_y Y \\ -\mu_y NY + \theta MA + \mu_m M \\ -cY + \eta GA + \mu_g G \end{pmatrix}. \tag{6.3}$$

The non negative matrix $\mathscr{F}$ and non-singular matrix $\mathscr{V}$ are obtained by differentiating $\mathscr{F}_i$ and $\mathscr{V}_i$ at parasite-free equilibrium point, E^0, respectively as follows:

$$\mathscr{F} = \begin{pmatrix} 0 & \frac{\beta\Lambda_x}{\mu_x} & 0 \\ 0 & 0 & 0 \\ 0 & 0 & 0 \end{pmatrix}, \quad \mathscr{V} = \begin{pmatrix} \mu_y & 0 & 0 \\ -N\mu_y & \mu_m & 0 \\ -c & 0 & \mu_g \end{pmatrix}.$$

Thus,

$$V^{-1} = \begin{pmatrix} \frac{1}{\mu_y} & 0 & 0 \\ \frac{N}{\mu_m} & \frac{1}{\mu_m} & 0 \\ \frac{c}{\mu_y\mu_g} & 0 & \frac{1}{\mu_g} \end{pmatrix}, \quad \mathscr{F}\mathscr{V}^{-1} = \begin{pmatrix} \frac{N\beta\Lambda_x}{\mu_x\mu_m} & \frac{\beta\Lambda_x}{\mu_x\mu_m} & 0 \\ 0 & 0 & 0 \\ 0 & 0 & 0 \end{pmatrix}.$$

The basic reproduction number is the dominant eigenvalue of $\mathscr{F}\mathscr{V}^{-1}$. Hence,

$$\mathscr{R}_0 = \rho(\mathscr{F}\mathscr{V}^{-1}) = \frac{N\beta\Lambda_x}{\mu_x\mu_m}.$$

The term $\beta\Lambda_x N$ of $\mathscr{R}_0$ is the number of infected red blood cells during entry of malaria merozoites, $1/\mu_x$ and $1/\mu_m$ are the life expectancy of uninfected red blood cells and merozoites, respectively.

6.2.3 Local and global stability of parasite -free equilibrium point

In this section, we investigate the local and global stability analysis of the parasite-free equilibrium point model (6.1). The local stability of the parasite-free equilibrium point is obtained by linearizing the system equation (6.1) at E^0. The Jacobian matrix at any point $E = (X, Y, M, G, C, A)$ is given as

$$J(E) = \begin{pmatrix} -\beta M - \mu_x & 0 & -\beta X & 0 & 0 & 0 \\ \beta M & -\mu_y - \gamma C & \beta X & 0 & -\gamma C & 0 \\ 0 & N\mu_y & -\mu_m - \theta A & 0 & 0 & -\theta M \\ 0 & c & 0 & -\mu_g - \eta A & 0 & -\eta G \\ 0 & \xi C & 0 & 0 & -\mu_c & 0 \\ 0 & 0 & \alpha A & \omega A & 0 & -\mu_a \end{pmatrix}.$$

Theorem 6.3. *The parasite-free equilibrium is locally asymptotically stable if* $\mathscr{R}_0 < 1$*, and unstable if* $\mathscr{R}_0 > 1$.

Proof. The Jacobian matrix at parasite-free equilibrium E^0 is

$$J(E^0) = \begin{pmatrix} -\mu_x & 0 & -\frac{\beta\Lambda_x}{\mu_x} & 0 & 0 & 0 \\ 0 & -\mu_y & \frac{\beta\Lambda_x}{\mu_x} & 0 & 0 & 0 \\ 0 & N\mu_y & -\mu_m & 0 & 0 & 0 \\ 0 & c & 0 & -\mu_g & 0 & 0 \\ 0 & 0 & 0 & 0 & -\mu_c & 0 \\ 0 & 0 & 0 & 0 & 0 & -\mu_a \end{pmatrix} \tag{6.4}$$

□

Applying the Routh-Hurwitz stability criteria, the parasite-free equilibrium is locally asymptotically stable, if all the eigenvalues of the Jacobian matrix (6.4) have a negative real part. Obviously, the first, fourth, fifth, and sixth columns of the Jacobian matrix (6.4) have only diagonal entries. Thus, $\lambda_1 = -\mu_x, \lambda_4 = -\mu_g, \lambda_5 = -\mu_c$, and $\lambda_6 = -\mu_a$, and the remaining eigenvalues are obtained from the following sub-matrix:

$$J_1(E^0) = \begin{pmatrix} -\mu_y & \frac{\beta\Lambda_x}{\mu_x} \\ N\mu_y & -\mu_m \end{pmatrix}. \tag{6.5}$$

The associated characteristic polynomial equation (6.5) is given as

$$\lambda^2 + a_1\lambda + a_2 = 0, \tag{6.6}$$

where $a_1 = \mu_m + \mu_y$ and $a_2 = \mu_m\mu_x(1 - \mathscr{R}_0)$. The characteristic equation (6.6) has negative real parts if a_1, and a_2 are positive.

Therefore, the parasite-free equilibrium is locally asymptotically stable if $\mathscr{R}_0 < 1$ and unstable if $\mathscr{R}_0 > 1$.

Next, we investigate the global stability of parasite-free equilibrium points using constructing Lyapunov functions. The global stability analysis of parasite-free equilibrium E^0 is established by the following theorem.

Theorem 6.4. *The parasite-free equilibrium* E^0 *of system* (6.1) *is globally asymptotically stable when* $\mathscr{R}_0 \leq 1$.

Proof. For the parasite-free equilibrium E^0, define the Lyapunov function

$$L_0(X,Y,M,G,C,M) = X - X^0 - X^0 \ln\frac{X}{X^0} + Y + \frac{1}{N}M + \frac{\omega\theta}{\alpha\eta N}G + \frac{\gamma}{\xi}C + \frac{\theta}{\alpha N}A. \tag{6.7}$$

Then the derivative of L_0 along solutions of system equation (6.1) is

$$\begin{aligned}
\frac{dL_0}{dt} &= \left(1-\frac{X^0}{X}\right)\frac{dX}{dt}+\frac{dY}{dt}+\frac{1}{N}\frac{dM}{dt}+\frac{\omega\theta}{\alpha\eta N}\frac{dG}{dt}+\frac{\gamma}{\xi}\frac{dC}{dt}+\frac{\theta}{\alpha N}\frac{dA}{dt}\\
&= \left(1-\frac{X^0}{X}\right)(\pi_x-\beta XM-\mu_x X)+\beta XM-\gamma YC-\mu_y Y+\frac{1}{N}(\mu_y NY-\theta MA-\mu_m M)\\
&\quad+\frac{\omega\theta}{\alpha\eta N}(cY-\eta GA-\mu_g G)+\frac{\gamma}{\xi}(\xi CY-\mu_c C)+\frac{\theta}{\alpha N}(\alpha MA+\omega GA-\mu_h A)\\
&= \left(1-\frac{X^0}{X}\right)(\mu_x X^0-\beta XM-\mu_x X)+\beta XM-\frac{\mu_m}{N}M-\frac{\mu_g\omega\theta}{\eta\alpha N}G-\frac{\mu_a\theta}{\alpha N}A-\frac{\gamma\mu_c}{\xi}C\\
&= -\mu_x\frac{(X-X^0)^2}{X}+\frac{\Lambda_x\beta}{\mu_x}M-\frac{\mu_m}{N}M-\frac{\mu_g\omega\theta}{\eta\alpha N}G-\frac{\mu_a\theta}{\alpha N}A-\frac{\gamma\mu_c}{\xi}C\\
&= -\mu_x\frac{(X-X^0)^2}{X}+\frac{\mu_m}{N}\left(\frac{\Lambda_x\beta N}{\mu_x\mu_m}-1\right)M-\frac{\mu_g\omega\theta}{\eta\alpha N}G-\frac{\mu_a\theta}{\alpha N}A-\frac{\gamma\mu_c}{\xi}C\\
&= -\mu_x\frac{(X-X^0)^2}{X}+\frac{\mu_m}{N}(\mathscr{R}_0-1)M-\frac{\mu_g\omega\theta}{\eta\alpha N}G-\frac{\mu_a\theta}{\alpha N}A-\frac{\gamma\mu_c}{\xi}C.
\end{aligned}$$

Therefore, $\frac{dL_0}{dt}<0$ for $\mathscr{R}_0<1$, and the equality $\frac{dL_0}{dt}=0$ holds if and only if $X=X^0$, $M=M^0$, $G=G^0$, $C=C^0$, $A=A^0$, and $\mathscr{R}_0=1$. Therefore, by LaSalle invariant principle (LaSalle, 1976) parasite-free equilibrium E^0 is global asymptotically stable in Ω. □

6.2.4 Parasite-persistence equilibria

The parasite-persistence equilibrium point is the steady-state solution at which parasites persist in-host cells, and it is obtained by setting the right-hand side system equation (6.1) to zero and solving for the state variables. Thus,

$$\begin{aligned}
&\Lambda_x-\beta XM-\mu_x X=0,\\
&\beta XM-\gamma YC-\mu_y Y=0,\\
&\mu_y NY-\theta MA-\mu_m M=0,\\
&cY-\eta GA-\mu_g G=0,\\
&\xi CY-\mu_c C=0,\\
&\alpha MA+\omega GA-\mu_a A=0.
\end{aligned}\tag{6.8}$$

From the last two equation of (6.8), we have $C=0$ or $Y=\frac{\mu_c}{\xi}$ and $A=0$ or $\alpha M+\omega G=\mu_a$, so we have four cases.

Case I: If $C=0$ and $A=0$. In this case, the parasite-persistence equilibrium point $E_1^*=(X_1^*,Y_1^*,M_1^*,G_1^*,0,0)$ without adaptive immune response exists if and only if, the basic reproduction number $R_0>1$, where

$$X_1^*=\frac{\mu_m}{\beta N},\ Y_1^*=\frac{\mu_m\mu_x}{\beta\mu_y N}(\mathscr{R}_0-1),M_1^*=\frac{\mu_x}{\beta}(\mathscr{R}_0-1),G_1^*=\frac{c\mu_m\mu_x}{\beta\mu_g\mu_y N}(\mathscr{R}_0-1).$$

Case II: If $C \neq 0$, $A = 0$. In this case, $Y_2^* = \frac{\mu_c}{\xi}$, and thus we have the endemic equilibrium point $E_2^* = (X_2^*, Y_2^*, M_2^*, G_2^*, C_2^*, 0)$ in the presence of cytotoxic T-cells, where

$$X_2^* = \frac{\Lambda_x \xi \mu_m}{\beta N \mu_y \mu_c + \mu_x \mu_m \xi}, \quad Y_2^* = \frac{\mu_c}{\xi}, \quad M_2^* = \frac{N \mu_y \mu_c}{\mu_m \xi}, G_2^* = \frac{c \mu_c}{\mu_g \xi}, \quad C_2^* = \frac{\mu_y}{\gamma}(R_0^c - 1).$$

And $R_0^c = \frac{\beta \Lambda_x N \xi}{\beta N \mu_y \mu_c + \mu_x \mu_m \xi}$ is the basic reproduction number of the system model (6.1) in the presence of cytotoxic T-cells. The parasite-persistence equilibrium point E_2^* exists if $1 < R_0^c \leq R_0$.

Case III: If $C = 0$, $A \neq 0$. In this case, $\alpha M + \omega G = \mu_a$. Thus, we have parasite-persistence equilibrium point $E_3^* = (X_3^*, Y_3^*, M_3^*, G_3^*, 0, A_3^*)$ in the presence of antibodies, where

$$X_3^* = \frac{\mu_m + \theta A_3^*}{\beta N}, \qquad Y_3^* = \frac{\mu_a(\mu_m + \theta A_3^*)(\mu_g + \eta A_3^*)}{\alpha N \mu_y(\mu_g + \eta A_3^*) + \omega c(\mu_m + \theta A_3^*)},$$
$$M_3^* = \frac{N \mu_y \mu_a(\mu_g + \eta A_3^*)}{\alpha N \mu_y(\mu_g + \eta A_3^*) + \omega c(\mu_m + \theta A_3^*)}, \quad G_3^* = \frac{c \mu_a(\mu_m + \theta A_3^*)}{\alpha N \mu_y(\mu_g + \eta A_3^*) + \omega c(\mu_m + \theta A_3^*)}.$$

And A_3^* is the positive roots of the characteristic equation

$$b_0 A_3^{*2} + b_1 A_3^* + b_2 = 0, \tag{6.9}$$

where

$$\begin{aligned}
b_0 =& N \mu_a \mu_g \theta \eta + \mu_x \theta \alpha \mu_y \eta N + \mu_x \theta^2 \omega c, \\
b_1 =& N \mu_a \mu_m \mu_y \eta + N \mu_a \mu_g \mu_y \theta + N \alpha \mu_g \mu_y \theta + \omega c \Lambda_x \mu_m \theta + (N \mu_m \mu_x \mu_y \eta + \mu_m \mu_x \omega c \theta)(1 - R_0), \\
b_2 =& \mu_x \mu_m \mu_g \mu_y \alpha N (1 - R_0) + (\mu_a \mu_y \mu_m \mu_g N + \mu_x \mu_m \mu_y \mu_g \alpha N)(1 - R_0^A).
\end{aligned}$$

And $\mathscr{R}_0^A = \frac{\beta N \omega \Lambda_x c}{N \mu_y \mu_g \mu_m \mu_a \alpha + \mu_x \mu_m^2 \omega c}$ is the basic reproduction number of the system model (6.1) in presence antibodies.Therefore, the parasite-persistence equilibrium point E_3^* is exist if $1 < \mathscr{R}_0^A \leq \mathscr{R}_0$.

Case IV: If $C \neq 0, A \neq 0$. In this case $Y = \frac{\mu_c}{\xi}$ and $\alpha M + \omega G = \mu_a$. Thus, we have the parasite-persistence equilibrium point $E_4^* = (X_4^*, Y_4^*, M_4^*, G_4^*, C_4^*, A_4^*)$ with adaptive immune response, where

$$X_4^* = \frac{\Lambda_x \xi(\mu_m + \theta A_4^*)}{\beta N \mu_y N \mu_c + \xi \mu_x(\mu_m + \theta A_4^*)}, \quad Y_4^* = \frac{\mu_c}{\xi}, \quad M_4^* = \frac{N \mu_y \mu_c}{\xi(\mu_m + \theta A_4^*)}, \quad G_4^* = \frac{c \mu_c}{\xi(\mu_g + \eta A_4^*)}$$
$$C_4^* = \frac{N \mu_y \beta \Lambda_x}{\gamma \beta N \mu_y \xi + \gamma c \mu_x(\mu_m + \theta A_4^*)} - \frac{\mu_y}{\gamma},$$

And A_4^* is a positive roots of the characteristic equation

$$c_0 A_4^{*2} + c_1 A_4^* + c_2 = 0, \tag{6.10}$$

where

$$c_0 = \mu_a \xi \theta \eta,$$
$$c_1 = (N\mu_c\mu_y\eta\xi + \omega\mu_c\theta c\xi)\left(\frac{\mu_a\theta\xi\mu_g}{N\mu_c\mu_y\eta\xi + \omega\mu_c\theta c\xi} + \frac{\mu_m\mu_a\eta\xi}{N\mu_c\mu_y\eta\xi + \omega\mu_c\theta c\xi} - 1\right),$$
$$c_2 = (N\mu_y\mu_c\theta\mu_g\xi + \omega\mu_c\mu_m c)\left(\frac{\mu_a\mu_c\mu_m^2\mu_g}{N\mu_y\mu_c\theta\mu_g\xi + \omega\mu_c\mu_m c} - 1\right).$$

The above discussions are summarized in the following Theorem.

Theorem 6.5. *(Existence of the parasite-persistence equilibria)*

i. If $\mathscr{R}_0 < 1$, then the system has only parasite-free equilibrium point E^0.

ii. If $\mathscr{R}_0 > 1$, then the system has a parasite-persistence equilibrium point in the absence of adaptive immune response E_1^*.

iii. If $1 < \mathscr{R}_0^C \leq \mathscr{R}_0$, then the system has a parasite-persistence equilibrium point with cytotoxic T-cells response E_2^*.

iv. If $1 < \mathscr{R}_0^A \leq \mathscr{R}_0$, then the system has a parasite-persistence equilibrium point with antibodies response E_3^*.

v. If $\frac{\mu_a\mu_c\mu_m^2\mu_g}{N\mu_y\mu_c\alpha\mu_g\xi+\omega\mu_c\mu_m^2 c} < 1$ or $\frac{\mu_a\theta\xi\mu_g}{N\mu_c\mu_y\eta\xi+\omega\mu_c\theta c\xi} + \frac{\mu_m\mu_a\eta\xi}{N\mu_c\mu_y\eta\xi+\omega\mu_c\theta c\xi} < 1$, then the system has a parasite-persistence equilibrium point with adaptive immune response E_4^*.

6.2.5 Local stability analysis of parasite-persistence equilibria

In this section, we explore the local stability analysis of the parasite-persistence equilibria using the Routh-Hurwitz stability criterion.

Theorem 6.6. *The parasite-persistence equilibrium E_1^* is locally asymptotically stable if $\mathscr{R}_0 > 1$, and unstable if $\mathscr{R}_0 < 1$.*

Proof. The Jacobian matrix at parasite-persistence equilibrium point E_1^* is

$$J(E_1^*) = \begin{pmatrix} -\beta M_1^* - \mu_x & 0 & -\beta X_1^* & 0 & 0 & 0 \\ \beta M_1^* & -\mu_y & \beta X_1^* & 0 & 0 & 0 \\ 0 & N\mu_y & -\mu_m & 0 & 0 & -\theta M_1^* \\ 0 & c & 0 & -\mu_g & 0 & -\eta G_1^* \\ 0 & 0 & 0 & 0 & -\mu_c & 0 \\ 0 & 0 & 0 & 0 & 0 & -\mu_a \end{pmatrix}. \tag{6.11}$$

Applying the Routh-Hurwitz stability criteria to the parasite-persistence equilibrium point without adaptive immune response E_1^* is locally asymptotically stable if all the eigenvalues of the Jacobian matrix (6.11) have a negative real part. Clearly, it is not difficult to see that

the fourth, and fifth columns of the Jacobian matrix (6.11) have only diagonal entries. Thus, the eigenvalues $\lambda_4 = -\mu_g$, $\lambda_5 = -\mu_c$, and the Jacobian reduced again easily, so we obtained $\lambda_6 = -\mu_a$. The remaining eigenvalues are investigated from the sub-matrix

$$J_1(E_1^*) = \begin{pmatrix} -\beta M_1^* - \mu_x & 0 & -\beta X^* \\ \beta M_1^* & -\mu_y & \beta X_1^* \\ 0 & N\mu_y & -\mu_m \end{pmatrix}. \tag{6.12}$$

The associated characteristic polynomial equation of (6.12) is

$$\lambda^3 + D_0\lambda^2 + D_1\lambda + D_2 = 0, \tag{6.13}$$

where, $D_0 = \mu_m + \mu_y + \mu_x + \frac{\beta\Lambda_x N}{\mu_m}\left(1 - \frac{1}{\mathscr{R}_0}\right)$, $D_1 = \mu_x(\mu_m + \mu_x)(\mathscr{R}_0 + 1)$ and $D_2 = \left(\frac{\beta\Lambda_x N}{\mu_x} + \beta\Lambda_x\right)\left(1 - \frac{1}{\mathscr{R}_0}\right) + \mu_m$.
The characteristic equation (6.13) has a negative real roots if $D_0 > 0$, $D_1 > 0$, $D_2 > 0$, and $D_0D_1 - D_2 > 0$. Clearly $D_1 > 0$, the coefficient $D_0 > 0$ and $D_2 > 0$, if and only if $\mathscr{R}_0 > 1$.

Therefore, the parasite-persistence equilibrium point E_1^* is locally asymptotically stable if $\mathscr{R}_0 > 1$, and unstable if $\mathscr{R}_0 < 1$. □

Theorem 6.7. *The parasite-persistence equilibrium point E_2^* is locally asymptotically stable if $\mathscr{R}_0^c > 1$, and unstable if $\mathscr{R}_0^c < 1$.*

Proof. The Jacobian matrix at parasite-persistence equilibrium point E_2^* is

$$J(E_2^*) = \begin{pmatrix} -\beta M_2^* - \mu_x & 0 & -\beta X_2^* & 0 & 0 & 0 \\ \beta M_2^* & -\mu_y - \gamma C_2^* & \beta X_2^* & 0 & -\gamma C_2^* & 0 \\ 0 & N\mu_y & -\mu_m & 0 & 0 & -\theta M_2^* \\ 0 & c & 0 & -\mu_g & 0 & -\eta G_2^* \\ 0 & \xi C_2^* & 0 & 0 & -\mu_c & 0 \\ 0 & 0 & 0 & 0 & 0 & -\mu_a \end{pmatrix}. \tag{6.14}$$

The fourth column of the Jacobian matrix (6.14) has only diagonal entry, Thus, we have $\lambda_4 = -\mu_g$ and the last row of the Jacobian matrix has only one non-zero entry so, we can simply get $\lambda_6 = -\mu_a$, the remaining eigenvalues are obtained from the sub-matrix

$$J_1(E_2^*) = \begin{pmatrix} -\beta M_2^* - \mu_x & 0 & -\beta X_2^* & 0 \\ \beta M_2^* & -\mu_y - \gamma C_2^* & \beta X_2^* & -\gamma C_2^* \\ 0 & N\mu_y & -\mu_m & 0 \\ 0 & c & 0 & 0 \\ 0 & \xi C_2^* & 0 & -\mu_c \end{pmatrix}. \tag{6.15}$$

The corresponding characteristic equation of (6.15) is

$$\lambda^4 + A_0\lambda^3 + A_1\lambda^2 + A_2\lambda + A_3 = 0, \tag{6.16}$$

where

$$\begin{aligned}
A_0 &= \beta M_2^* + \mu_x + \mu_y + \mu_c + \gamma(\mathscr{R}_0^c - 1) + \mu_m,\\
A_1 &= \mu_m\mu_c + \mu_m + \mu_c + \mu_y + \gamma\xi\gamma(\mathscr{R}_0^c - 1)\left(\frac{1+\xi}{\xi} - \mathscr{R}_0^c\right) + \beta\mu_y N X_2^* + (\beta M_2^* + \mu_x)(\mu_m + \mu_c)\\
&\quad + \gamma(\mathscr{R}_0^c - 1)),\\
A_2 &= \mu_m\mu_y\mu_c + \mu_m\xi\gamma(\mathscr{R}_0^c - 1)\left(\frac{\mu_c+\xi}{\xi} - \mathscr{R}_0^c\right) + \beta X_2^* N\mu_y\mu_c\\
&\quad + (\beta M_2^* + \mu_x)(\mu_c\mu_m + \mu_m + \mu_c + \mu_y + \beta N\mu_y X_2^*) + (\beta M_2^* + \mu_x)(\xi\gamma(\mathscr{R}_0^c - 1)\left(\frac{1+\xi}{\xi} - \mathscr{R}_0^c\right)),\\
A_3 &= \beta^2 N\mu_c\mu_y X_2^* M_2^* + (\mu_c\mu_m\mu_y + N\mu_c\mu_y\beta X_2^*) + \mu_m\xi\gamma(\mathscr{R}_0^c - 1)\left(\frac{\mu_c+\xi}{\xi} - \mathscr{R}_0^c\right)(\beta M_2^* + \mu_x).
\end{aligned}$$

The characteristic equation (6.16) has an eigenvalue with a negative real part if A_0, A_1, A_2, and A_3 are non-negative, and

$$H_1 = A_3 > 0,\ \ H_2 = \begin{vmatrix} A_1 & A_3 \\ 1 & A_2 \end{vmatrix} > 0 \ \textit{and}\ \ H_3 = \begin{vmatrix} A_0 & A_2 & 0 \\ 1 & A_1 & A_3 \\ 0 & A_0 & A_2 \end{vmatrix} > 0.$$

Let the $max\left\{\frac{\mu_c+\xi}{\xi}, \frac{1+\xi}{\xi}\right\}$ is $\frac{1+\xi}{\xi}$. Obviously $A_0 > 0$, for $\mathscr{R}_0^c > 1$ and $A_1 > 0, A_2 > 0$ and $A_3 > 0$, if $1 < \mathscr{R}_0^c \leq \frac{1+\xi}{\xi} \leq \mathscr{R}_0$. Therefore, by Routh–Hurwitz stability criteria, the parasite-persistence equilibrium point E_2^* is locally asymptotically stable, if $1 < \mathscr{R}_0^c \leq \mathscr{R}_0$. □

Theorem 6.8. *The parasite-persistence equilibrium point E_3^* is locally asymptotically stable if $\mathscr{R}_0^A > 1$ and unstable if $\mathscr{R}_0^A < 1$.*

Proof. The Jacibian matrix at parasite-persistence equilibrium E_3^* is

$$J(E_2^*) = \begin{pmatrix}
-\beta M_3^* - \mu_x & 0 & -\beta X_3^* & 0 & 0 & 0 \\
\beta M_3^* & -\mu_y & \beta X_3^* & 0 & 0 & 0 \\
0 & N\mu_y & -\mu_m - \theta A_3^* & 0 & 0 & -\theta M_3^* \\
0 & c & 0 & -\mu_g - \eta A_3^* & 0 & -\eta G_3^* \\
0 & 0 & 0 & 0 & -\mu_c & 0 \\
0 & 0 & \alpha A_3^* & \omega A_3^* & 0 & -\mu_a
\end{pmatrix}. \tag{6.17}$$

The corresponding characteristic equation of Jacobian matrix (6.17) is

$$(-\mu_c-\lambda)(\lambda^5+B_0\lambda^4+B_1\lambda^3+B_2\lambda^2+B_3\lambda+B_4)=0, \tag{6.18}$$

where

$$\begin{aligned}
B_0 &= \beta M_3^*+\mu_x+\mu_m+\mu_y+\theta A_3^*+\mu_g+\mu_a+\eta A_3^*,\\
B_1 &= (\beta M_3^*+\mu_x)(\mu_m+\mu_y+\theta A_3^*+\mu_g+\mu_a+\eta A_3^*)+\mu_y(\mu_m+\theta A_3^*)+\mu_a(\mu_g+\eta A_3^*)\\
&\quad (\mu_y+\mu_m+\theta A_3^*)(\mu_g+\mu_a+\eta A_3^*)-N\mu_y X_3^*,\\
B_2 &= (\beta M_3^*+\mu_x)(\mu_y(\mu_m+\theta A_3^*)+\mu_a(\mu_g+\eta A_3^*)(\mu_y+\mu_m+\theta A_3^*)(\mu_g+\mu_a+\eta A_3^*))\\
&\quad +\mu_a(\mu_m+\mu_y+\theta A_3^*)(\mu_g+\eta A_3^*)+\mu_y(\mu_m+\theta A_3^*)(\mu_g+\mu_a+\eta A_3^*)-\alpha\theta M_3^*A_3^*\\
&\quad -(N\mu_y X_3^*(\beta M_3^*+\mu_x)+N\mu_y(\mu_g+\eta A_3^*+\mu_a)X_3^*)+\beta^2 M_3^*X_3^*N\mu_y,\\
B_3 &= (\beta M_3^*+\mu_x)(\mu_a(\mu_m+\mu_y+\theta A_3^*)(\mu_g+\eta A_3^*)+\mu_y(\mu_m+\theta A_3^*)(\mu_g+\mu_a+\eta A_3^*)\\
&\quad -\alpha\theta M_3^*A_3^*)+\mu_y\mu_a(\mu_m+\theta A_3^*)(\mu_g+\eta A_3^*)-\alpha\theta M_3^*A_3^*(\mu_g+\eta A_3^*)-((\beta M_3^*+\mu_x)X_3^*\\
&\quad +N\mu_y(\mu_g+\eta A_3^*+\mu_a)X_3^*+N\mu_g\mu_a(\mu_g+\eta A_3^*+\mu_a)X_3^*+\beta^2M_3^*X_3^*N\mu-y(\mu_g+\eta A_3^*+\mu_a)),\\
B_4 &= (\beta M_3^*+\mu_x)(\mu_y(\mu_m+\theta A_3^*)+\mu_a(\mu_g+\eta A_3^*)(\mu_y+\mu_m+\theta A_3^*)(\mu_g+\mu_a+\eta A_3^*))\\
&\quad +\mu_a(\mu_m+\mu_y+\theta A_3^*)(\mu_g+\eta A_3^*)+\mu_y(\mu_m+\theta A_3^*)(\mu_g+\mu_a+\eta A_3^*)-\alpha\theta M_3^*A_3^*\\
&\quad -N\mu_y X_3^*-(\beta^2M_3^*X_3^*N\mu_y+\mu_a(\mu_g+\eta A_3^*+\mu_a)+\beta^2M_3^*X_3^*\omega\eta A_3^*X_3^*).
\end{aligned}$$

Applying the Routh–Hurwitz stability criteria the characteristic equation (6.18) has eigenvalues with negative real parts, if $B_i>0$, for $i=0,1,\cdots,4$ and

$$H_1=B_4>0,\ \ H_2=\begin{vmatrix}B_2 & B_4\\ 1 & B_3\end{vmatrix}>0, H_3=\begin{vmatrix}B_1 & B_3 & 0\\ 1 & B_2 & B_4\\ 0 & B_1 & B_3\end{vmatrix}>0,\quad \textit{and}\ \ H_4=\begin{vmatrix}B_0 & B_2 & B_4 & 0\\ 1 & B_1 & B_3 & 0\\ 0 & B_0 & B_2 & B_4\\ 0 & 1 & B_1 & B_3\end{vmatrix}>0.$$

Therefore, parasite-persistence equilibrium point E_3^* is locally asymptotically stable if $1<R_0^A\leq R_0$. The stability of the parasite-persistence equilibrium point in the presence of adaptive immune response (cytotoxic T-cells and antibodies) responses E_4^* is presented in numerical simulation. □

6.3 Numerical Simulation

In this section, we present a numerical simulation of the dynamical system (6.1) to supplement our theoretical results. The model parameter values used during the simulation are given in Table 6.2 and the remains are listed in the previous Chapters. The initial data which is used for the simulation is $X_0=500000,\ Y_0=0,\ M_0=16,\ G_0=20, C_0=0.001\ , H_0=0.001$. The

Table 6.2: The values for model parameters utilized in the simulation, where *mero* represents merozoites.

Parameters	Value	Source
Λ_x	$2.5 \times 10^8 cells/\mu l/day$	Hetzel and Anderson (1996)
μ_c	0.05/day	Anderson et al. (1989)
μ_a	0.05/day	Anderson et al. (1989)
μ_y	0.03 /day	Kamangira et al. (2014)
μ_m	48/day	Hetzel and Anderson (1996); Annan (2020)
ω	0.005/day	Elaiw and Al Agha (2020)
α	0.00005/day	Chiyaka et al. (2008)
γ	0.0009 cell μ l/day	Elaiw and Al Agha (2020)
ξ	0.0.0005/day	Chiyaka et al. (2008)
θ	0.3 mero $\mu l/day$	Chiyaka et al. (2008)
η	0.003 mero μl/day	Assumed

simulations are performed using ode45 solver in MATLAB software. Figure 6.2 displays the global stability of parasite-free equilibrium, for different initial values, and $\mathscr{R}_0 = 0.00250 < 1$. All the solutions of the state variables converge to parasite-free equilibrium $E^0 = (3.0120 \times 10^7, 0, 0, 0, 0, 0)$. Hence, by Theorem 6.3 and Theorem 6.4, the parasite-free equilibrium point E^0 is globally asymptotically stable. The stability of the parasite-persistence equilibrium E_1^* is shown in Figure 6.3, for $\mathscr{R}_0 = 1.2048 > 1$. The solution of the state variables from different initial conditions converges to $E_1^* = (3.00 \times 10^5, 51.4525, 17.6375, 10.1345, 0, 0)$. Thus, by Theorem 6.5(ii) and Theorem 6.7, the parasite-persistence equilibrium in the absence of adaptive immune response E_1^* exists and is stable for the basic reproduction number, $\mathscr{R}_0$ is greater than unity.

Figure 6.4, despites the stability analysis of the parasite-persistence equilibrium point in the presence of *cytotoxic T-cells* E_2^*. All the solutions of the state variables converge to $E_2^* = (2.9240 \times 10^5, 100.00, 1.00, 10.36210, 47.8867, 0)$, for $\mathscr{R}_0 = 2.5100 > 1$ and $\mathscr{R}_0^C = 2.4366 > 1$. Hence, due to Theorem 6.5(iii) and Theorem 6.7 the parasite-persistence equilibrium point with *cytotoxic T-cells* exists and is stable, when $1 < \mathscr{R}_0^C \leq \mathscr{R}_0$. Figure 6.5 describes the stability of the parasite-persistence equilibrium point in the presence of antibodies E_3^*. The solution of the state variables converge to the point $E_3^* = (2.4895 \times 10^6, 1000.00, 4.23510, 1.36210, 0, 7000)$, for $\mathscr{R}_0 = 56.4759 > 1$ and $\mathscr{R}_0^A = 1.1756 > 1$. So, by Theorem 6.5(iv) and Theorem 6.8 the parasite-persistence equilibrium point in the presence of antibodies exists and is stable when $1 < \mathscr{R}_0^A \leq \mathscr{R}_0$.

Figure 6.6 reveals the existence and stability of the parasite-persistence equilibrium point in the presence of an adaptive immune response E_4^*. The equilibrium point exists if and only if the basic reproduction numbers: basic reproduction $\mathscr{R}_0$, basic reproduction number in the

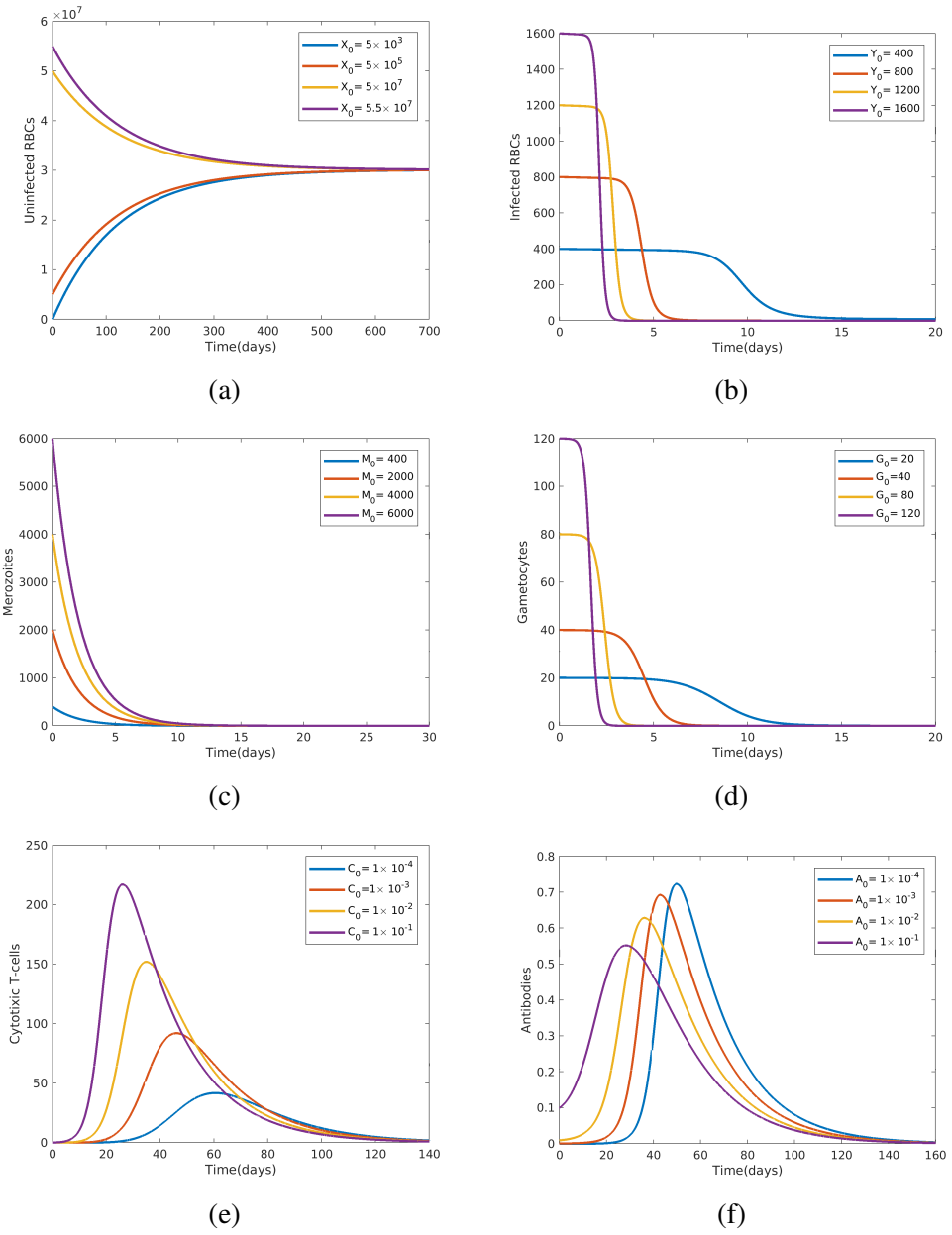

(a) (b) (c) (d) (e) (f)

Figure 6.2: Shows the global stability analysis of the parasite-free equilibrium point $E^0 = (3.0120 \times 10^7, 0, 0, 0, 0, 0)$ for different initial values of state variables. The basic reproduction number $R_0 = 0.0025 < 1$, all the biological parameter values are constant and given as in Table 6.2.

presence of cytotoxic T-cells, $\mathscr{R}_0^C$ and basic reproduction number in the presence of antibodies $\mathscr{R}_0^A$ are greater than unity, and if Theorem 6.5(v) is satisfied. All the state solutions are roughly converge to $E_4^* = (2.6595 \times 10^6, 100.00, 3.8512, 1.0325, 1100.2578, 700.3325)$. Hence, by Theorem 6.5(v) the parasite-persistence equilibrium point E_4^* exists, and from this simulation, we confirm that it is stable. The solutions of the state variables oscillate and decay to parasite-persistence steady states (see Figure 6.3-8.7). This demonstrates that oscillation fevers are associated with malaria parasites. The fever occurs when infected erythrocytes rupture and release the malaria parasites (merozoites). The period of the fever is roughly the same

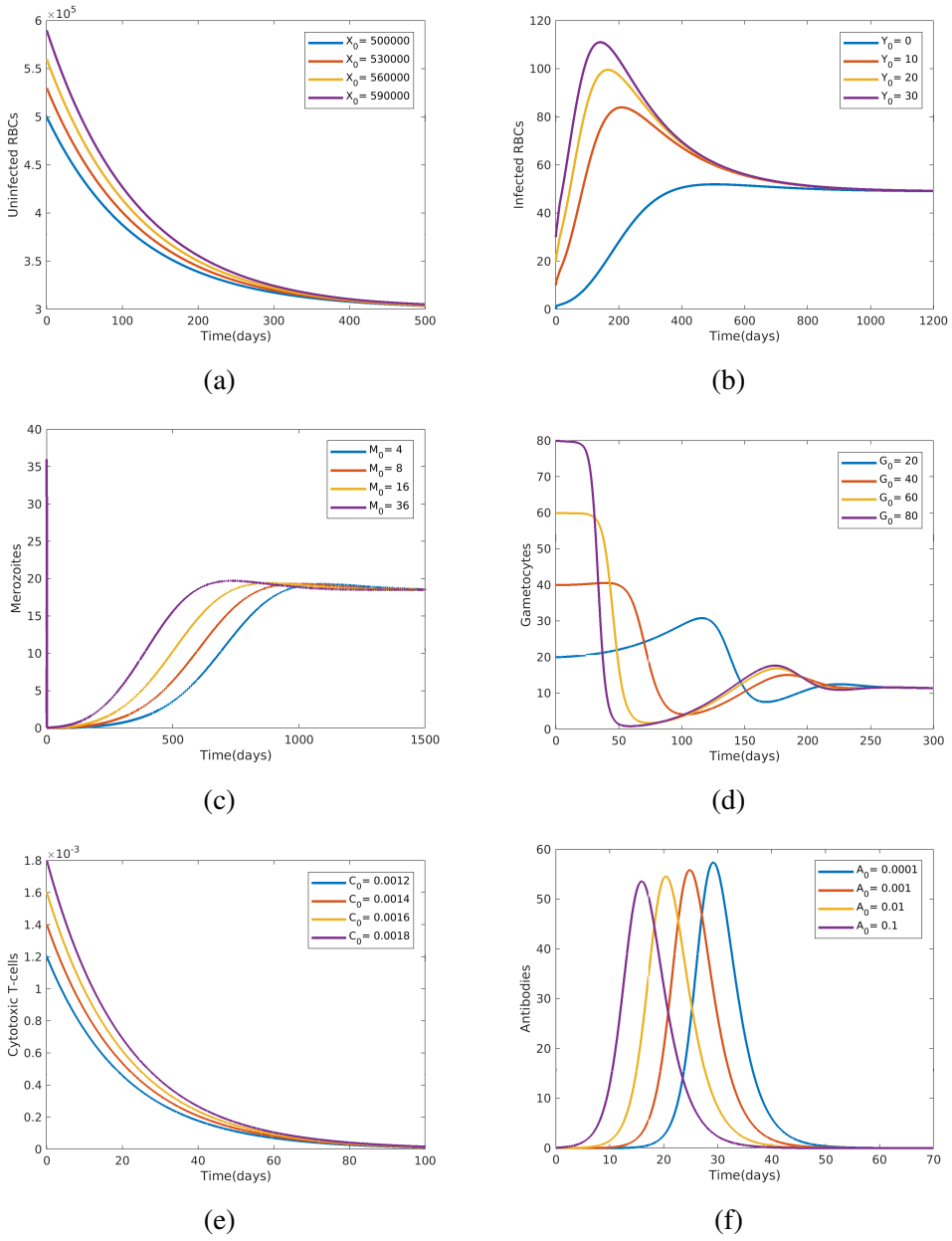

Figure 6.3: Shows the stability of parasite-persistence equilibrium point in the absence of adaptive immune response $E_1^* = (3.00 \times 10^5, 51.4525, 17.6375, 10.1345$
$0, 0)$ for different initial values of state variables. The basic reproduction number $R_0 = 1.2048 > 1$, by taking $\beta = 2.5 \times 10^{-6}$, $\Lambda_x = 2.5 \times 10^3, N = 24, \omega = 0.05$, and all the other biological parameter values are constant and given as in Table 6.2.

as the parasite's asexual reproduction cycle, which offers a fundamental underpinning mechanism for the periodicity of the fever. The period of oscillation has been identified with the length of the replication cycle Figure 6.7 reveals the effect of the adaptive immune response on the infected red blood cells and malaria parasites in the form of gametocytes. Figure (6.7)(a) describes that the infected red blood cell drop-off as the removal rate of infected red blood cells due to cytotoxic T-cells increases. From 6.7(b), we confirm that the gametocyte population decreases as the removal rate of gametocytes due to antibodies is increasing.

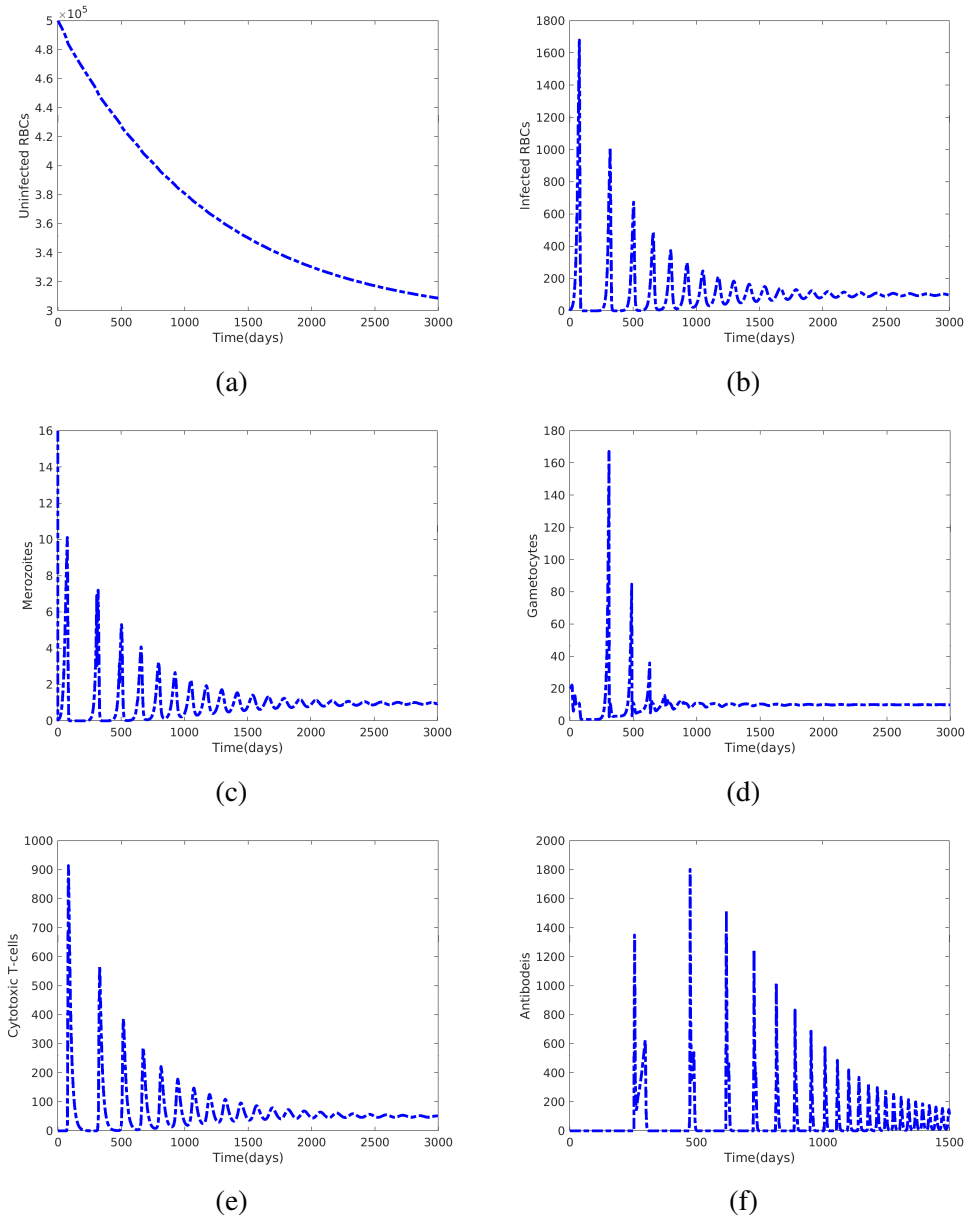

Figure 6.4: Shows the stability analysis of the parasite-persistence equilibrium point in the presence of Cytotoxic T-cells $E_2^* = (2.924 \times 10^5, 100, 1.00, 10.362, 47.887, 0)$, for different initial values . The basic reproduction number $\mathscr{R}_0 = 2.5100 > 1$ and $\mathscr{R}_0^C = 2.4366 > 1$, by taking $\beta = 2.5 \times 10^{-6}, \Lambda_x = 2.5 \times 10^3, N = 24$, and all the other parameter values are constant and given as in Table 6.2.

The average number of merozoites per ruptured infected red blood cells on merozoites is demonstrated in 6.8(a). The population of merozoites is rising as the average number of merozoites per ruptured infected red blood cell increases. The number of cytotoxic T-cells increases with the activation rate of cytotoxic T-cells owing to infected red blood cells is increases (see Figure 6.8(b)). Figure 6.9 displays the effect of activation rate antibody due to the presence of merozoites 6.9(a) and gametocytes 6.9(b). The antibodies' immune response increases as both activation rates antibody due to the presence of merozoites and gametocytes are increasing.

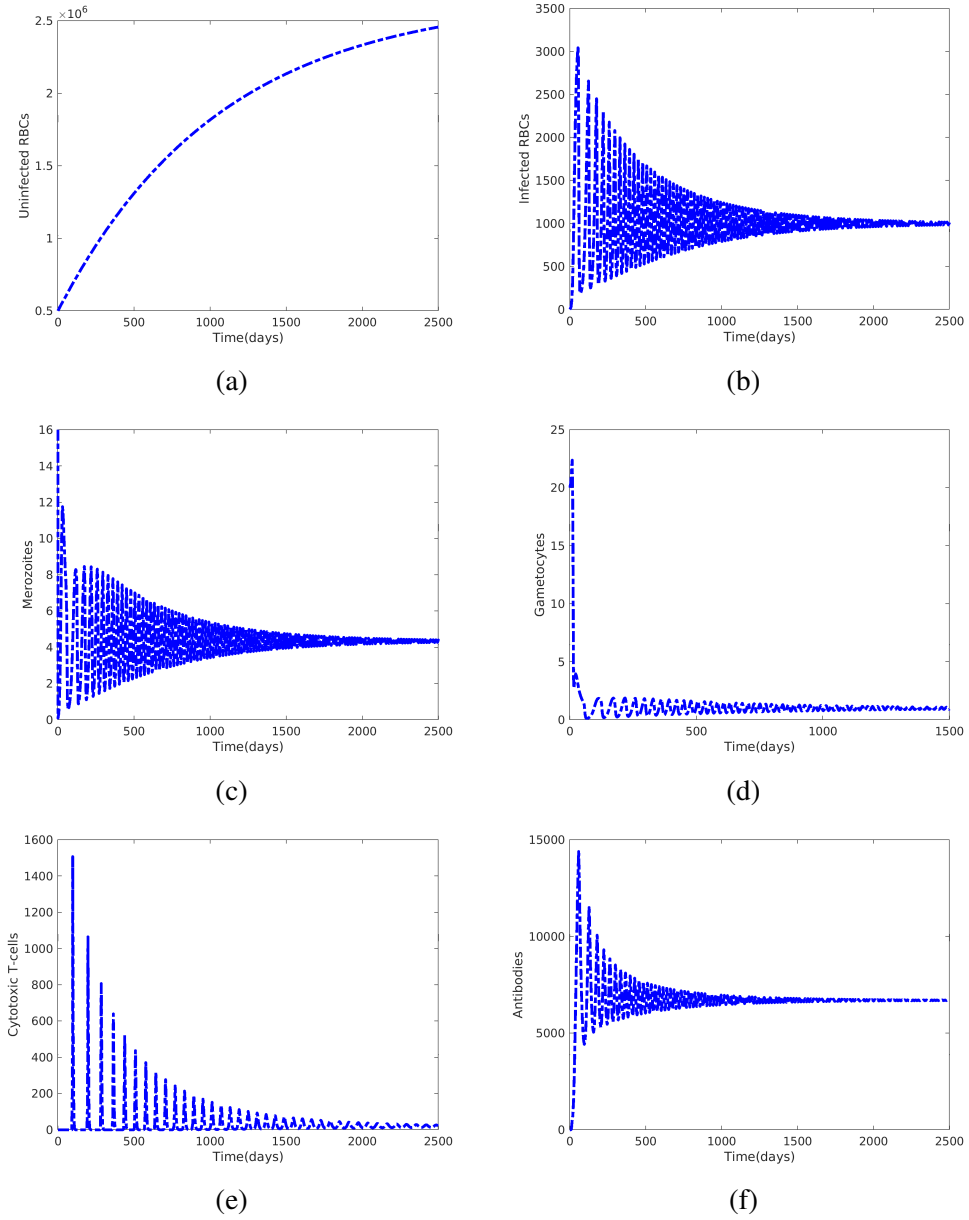

Figure 6.5: Shows the stability analysis of the parasite-persistence equilibrium point in the presence of antibodies $E_3^* = (2.4895 \times 10^6, 1000.00, 4.23510, 1.36210, 0,$
$7000)$, for different initial values of state variables. The basic reproduction number $\mathscr{R}_0 = 56.4759 > 1$ and $\mathscr{R}_0^A = 1.1756 > 1$, $\beta = 2.5 \times 10^{-6}$, by taking $\Lambda_x = 2.5 \times 10^3, N = 36$, and all the parameter values are constant and given as in Table 6.2.

6.4 Summary

This Chapter covers a mathematical model of the malaria parasite during its blood stage with an adaptive immune system is investigated. The model includes the interactions of six cell populations: uninfected red blood cells, infected red blood cells, merozoites, gametocytes, cytotoxic T-cells, and antibodies. The qualitative analysis of the developed model, such as the positivity and boundedness of the solution is discussed. The model equilibria and their

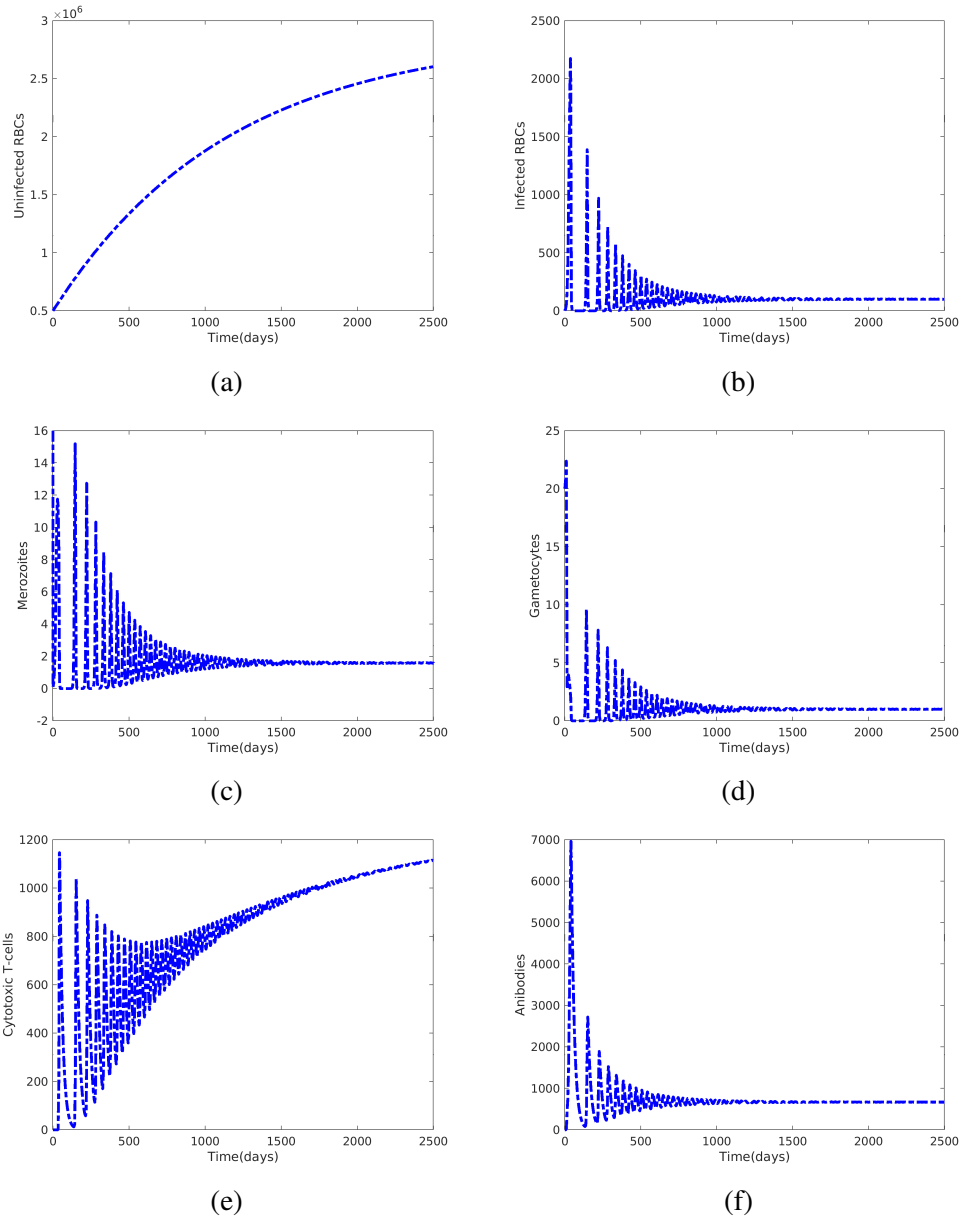

Figure 6.6: Shows the stability analysis of the parasite-persistence equilibrium in the presence of cytotoxic T-cells and antibodies $E_4^* = (2.66 \times 10^6, 100, 3.85, 1.03$ $, 1100.26, 700.33)$, for the basic reproduction numbers $\mathscr{R}_0 = 56.4759 > 1$, $\mathscr{R}_0^A = 1.1756 > 1$, and $\mathscr{R}_0^c = 52.8914 > 1$, by taking $\beta = 2.5 \times 10^{-5}$, $\Lambda_x = 2.5 \times 10^3$, $N = 36, \mu_x = 0.00083$ and all the other biological parameter values are constant and given as in Table 6.2.

stability are investigated. The parasite-free equilibrium exists and it is locally and globally stable if $\mathscr{R}_0 < 1$. The dynamical system (6.1) has four parasite-persistence steady states: Adaptive immune-free parasite-persistence equilibrium point E_1^*, which is stable if $\mathscr{R}_0 > 1$. The parasite-persistence equilibrium point in the presence of *cytotoxic T-cells*, E_2^*, which is locally asymptotically stable if $1 < \mathscr{R}_0^C \leq \mathscr{R}_0$. The parasite-persistence equilibrium point in the presence of antibodies, E_3^*, it is locally asymptotically stable if $1 < \mathscr{R}_0^A \leq \mathscr{R}_0$. The parasite-persistence equilibrium point in the presence of an adaptive immune response (cytotoxic T-cells and antibodies) E_4^*, which is locally asymptotically stable if the basic reproduction

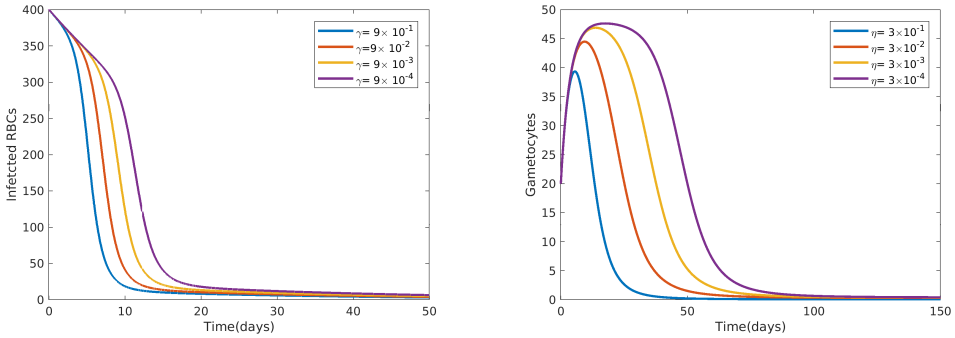

(a) (b)

Figure 6.7: (a) The impact of removal rate infected red blood cell due to cytotoxic T-cells, and (b) The impact of removal rate gametocytes due to antibodies, for $\mathscr{R}_0 = 0.0025$. All the other biological parameters are constant and given as in Table 6.2.

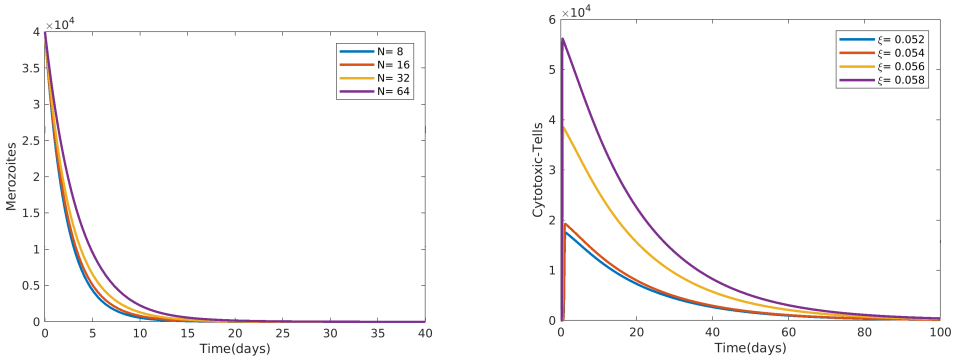

(b)

Figure 6.8: (a) The impact of an average number of merozoite per ruptured infected red blood cells on merozoites, and (b) The impact of activation rate cytotoxic T-cells owing to infected red blood cells on cytotoxic T-cells, for $\mathscr{R}_0 = 0.0025$. All the other biological parameters are constant and given as in Table 6.2.

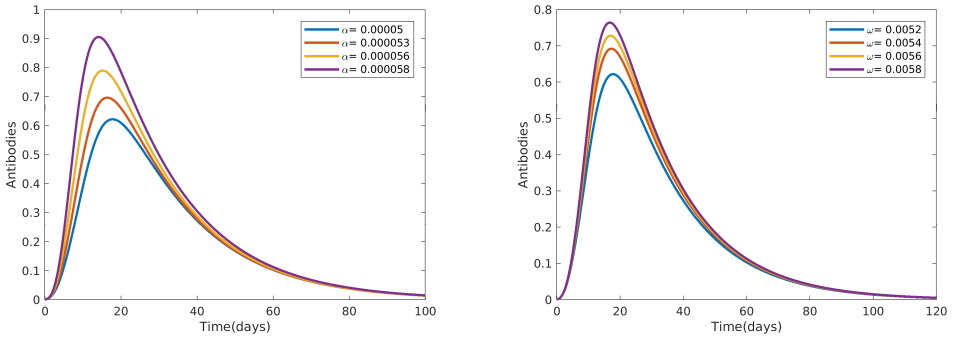

Figure 6.9: (a) The impact of activation rate antibody due to presence of merozoites, and (b) The impact of activation rate antibodies due to presence of gametocytes, for $\mathscr{R}_0 = 0.0025$. All the other biological parameters are constant and given as in Table 6.2.

numbers are greater than one, and Theorem 6.5(v) is satisfied. The stability of the equilibria is investigated using the Routh-Hurwitz stability criterion. To supplement our theoretical and analytical findings, many numerical simulations are offered. Figures 6.2 through 8.7 demonstrate the presence and constancy of the model's steady stats. Furthermore, the impact of the *cytotoxic T-cells* on the infected red blood cells and antibodies on the malaria parasites are presented in the simulation. The simulation findings suggested that an adaptive immune response has a high impact on the elimination of the parasite infection.

CHAPTER 7

OPTIMAL CONTROL ANALYSIS OF WITHIN-HOST MALARIA PARASITE INFECTION

In this chapter, we develop a mathematical model within-host dynamics of malaria infection with optimal control strategies. The within-host malaria model that describes the dynamics of the malaria infection during the liver-blood stages and their interactions with the immune system is presented. The most reasonable nonlinear bounded Michaelis-Menten-Monod function is used to show the interaction between liver hepatocyte cells, erythrocyte cells, malaria parasites, and the immunological system. We used a time-dependent malaria vaccine and antimalarial drug therapy such as a pre-erythrocytic vaccine, blood-stage vaccine, primary tissue schizontocides, and blood-schizontocides and gametocytocidal drugs (gametocytocides) as control strategies for the within-host dynamics of malaria infection.

7.1 Model Formulation

The within-host mathematical model of malaria infection dynamics is presented. The deterministic model is an extension of the within-host malaria model in Chapter 4 of this dissertation. The hepatocyte and erythrocyte stages of the malaria infection are investigated. The developed model considers the interaction of eight cell populations: sporozoites $P(t)$, uninfected hepatocytes $H(t)$, infected hepatocytes $H_I(t)$, red blood cells $R(t)$, iRBCs $R_I(t)$, merozoites $M(t)$, gametocyte $G(t)$ and immune response $E(t)$ at a time t. The formulated in-host model is governed by the assumptions given in the previous Chapters: The description of each compartment is given as follows:

Sporozoite $P(t)$: Assume that the female *Anopheles* mosquito deposits sporozoites into the human skin during blood meal at a constant rate Λ_p. These sporozoites invade the liver hepatocyte cell through blood vessels at a rate β_1 and sporozoites can die naturally at a rate $\mu_p P$. The sporozoites can observed by uninfected hepatocytes at a rate $\frac{\beta_1 HP}{1+b_0 E}$. Thus, the rate change of sporozoite per unit time is given by

$$\frac{dP}{dt} = \Lambda_p - \mu_p P - \frac{\beta_1 HP}{1+b_0 E}.$$

Uninfected hepatocyte $H(t)$: Healthy/uninfected hepatocyte is produced from bone marrow at a constant rate Λ_h and get infected at a rate $\frac{\beta_1 HP}{1+b_0 E}$. The term $\frac{1}{1+b_0 E}$ indicates the inhibition rate of hepatocyte invasion due to immune response against the parasite. The uninfected hepatocyte suffers natural death at a rate $\mu_h H$. Thus, the healthy hepatocyte at a time t is given

as

$$\frac{dH}{dt} = \Lambda_h - \frac{\beta_1 HP}{1+b_0E} - \mu_h H.$$

Infected hepatocyte $H_I(t)$: Infected hepatocyte increase when healthy hepatocytes get infection at a rate $\frac{\beta_1 HP}{1+b_0E}$ and mature into liver-schizonts. The liver-schizonts burst and die at a rate δH_I as well as removed by the immune response at a rate $\vartheta_1 H_I E$. Hence, the rate change of infected hepatocyte at time t is given by

$$\frac{dH_I}{dt} = \frac{\beta_1 HP}{1+b_0E} - \delta H_I - \vartheta_1 H_I E.$$

Uninfected red blood cells (RBCs) $R(t)$: The RBCs are produced at a constant rate Λ_r from the bone marrow and get infection by merozoites that are released from liver schizonts at a rate $\frac{\beta_2 RM}{1+b_1E}$ and die naturally at a rate $\mu_r R$. The expression $\frac{1}{1+b_1E}$ indicates the invasion of RBCs is inhibited due to the immune response against the parasite. Hence, the rate change of RBCs at a time t is given as

$$\frac{dR}{dt} = \Lambda_r - \frac{\beta_2 RM}{1+b_1E} - \mu_r R.$$

Infected red blood cell(iRBCs) $R_I(t)$: The healthy RBCs get the infection to propagate to the formation of iRBCs at a rate $\frac{\beta_2 RM}{1+b_1E}$ and infected red blood cells die at a rate αR_I as well as removed by immune system at a rate $\vartheta_2 R_I E$. So, the rate change of iRBCs at a time t is given by

$$\frac{dR_I}{dt} = \frac{\beta_2 RM}{1+b_1E} - \alpha R_I - \vartheta_2 R_I E.$$

Merozoite $M(t)$: The merozoite populations are produced when the infected hepatocyte and iRBCs rupture and release merozoites in the bloodstream at the rates of $\frac{N\delta H_I}{1+b_2E}$ and $\frac{Q\alpha R_I}{1+b_3E}$ respectively, where N is the average number of merozoites that produced per rupture liver-schizonts and Q is the average number of merozoites that are produced per burst of iRBCs (blood–schizonts). The merozoites die naturally at a rate $\mu_m M$ and are removed by the immune response at a rate $\vartheta_m ME$. Assume that the merozoite is observed by uninfected erythrocytes at a rate $\frac{\beta_2 RM}{1+b_1E}$. Hence, the rate change of merozoites per unit time is given as

$$\frac{dM}{dt} = \frac{N\delta H_I}{1+b_2E} + \frac{Q\alpha R_I}{1+b_3E} - \mu_m M - \vartheta_m ME - \frac{\beta_2 RM}{1+b_1E}.$$

Gametocyte $G(t)$: After the invasion of RBCs, some of the merozoites develop under sexual replication (gametocytes) at the rate cG. Also, the gametocytes suffer natural death at a rate $\mu_g G$ and are killed by the immune response at the rate $\vartheta_g GE$. Thus, the rate change of gametocytes is given by

$$\frac{dG}{dt} = \frac{cR_I}{1+b_4E} - \mu_g G - \vartheta_g GE.$$

Immune responses $E(t)$: Immune responses against malaria infections are complex and stage-specific. The malaria parasite induces a specific immune response which can stimulate

the release of cytokines and activate the host's monocytes, neutrophils, T-cells, B-cells, and natural killer cells to react to the hepatocyte and erythrocyte stages parasite infection (Holz et al., 2016; McQueen and McKenzie, 2008). However, for the seek of simplicity and analysis, we only consider the immunity response $E(t)$ as the total capacity of the immune response of the human to infected cells (infected red blood cells and liver cells) as well as malaria parasites. The immune response recruits at a constant rate Λ_e from bone marrow, and stimulates (activate) in the presence of malaria infection, that is the immune cells activate at the rate $\frac{\xi H_I}{1+a_0 H_I}$, $\frac{\nu R_I}{1+a_2 R_I}$, $\frac{\sigma M}{1+a_1 M}$, and $\frac{\theta G}{1+a_3 G}$ during the immune response against infected hepatocytes, iRBCs, merozoites, and gametocytes, respectively. The immune response is suffered natural death at a rate $\mu_e E$. Thus, the rate change of the immune system at a time t is given by

$$\frac{dE}{dt} = \Lambda_e + E\left(\frac{\xi H_I}{1+a_0 H_I} + \frac{\nu R_I}{1+a_2 R_I} + \frac{\sigma M}{1+a_1 M} + \frac{\theta G}{1+a_3 G}\right) - \mu_e E$$

All the biological parameters and their description are presented in Table 7.1. The above

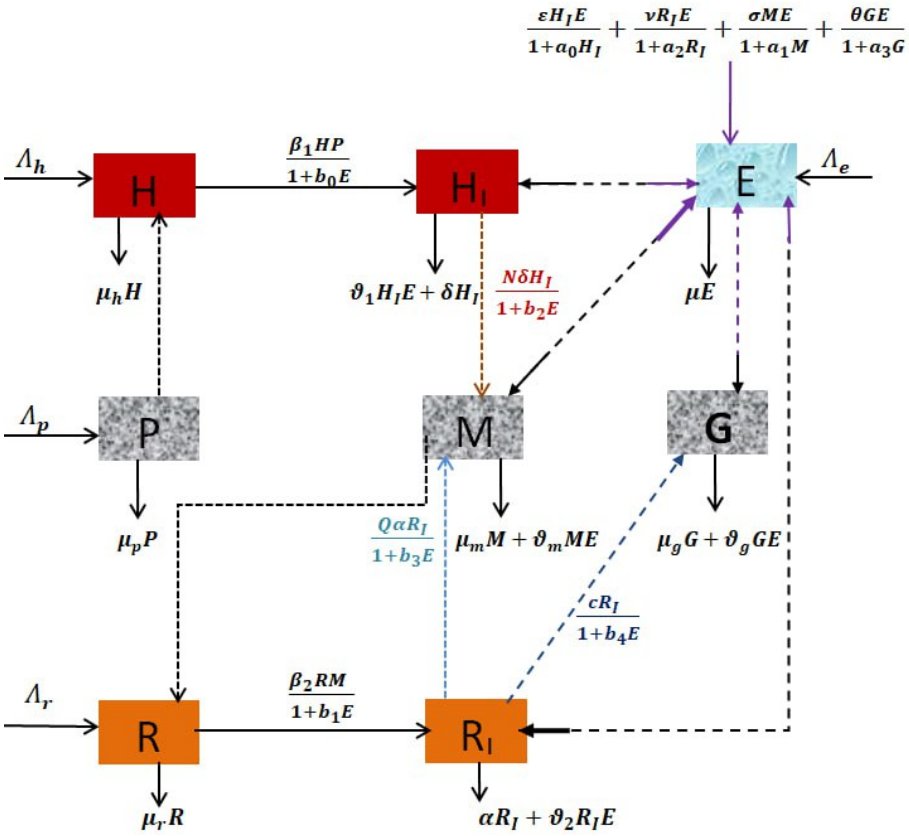

Figure 7.1: Schematic diagram of the within-host mathematical model of malaria parasite infection with the immune system. The dashed line indicates the interaction of infected red cells and infected hepatocytes with malaria parasites and immune system as well as malaria parasites with the immune system. A solid array line indicates the transfer or removal of compartments.

assumptions and schematic diagram Figure 7.1 lead to the following deterministic system of nonlinear ordinary differential equations, which describe the within-host dynamics of malaria

parasites.

$$
\begin{aligned}
\frac{dH}{dt} &= \Lambda_h - \frac{\beta_1 HP}{1+b_0E} - \mu_h H,\\
\frac{dH_I}{dt} &= \frac{\beta_1 HP}{1+b_0E} - \delta H_I - \vartheta_1 H_I E,\\
\frac{dR}{dt} &= \Lambda_r - \frac{\beta_2 RM}{1+b_1E} - \mu_r R,\\
\frac{dR_I}{dt} &= \frac{\beta_2 RM}{1+b_1E} - \alpha R_I - \vartheta_2 R_I E,\\
\frac{dM}{dt} &= \frac{N\delta H_I}{1+b_2E} + \frac{Q\alpha R_I}{1+b_3E} - \mu_m M - \vartheta_m ME - \frac{\beta_2 RM}{1+b_1E},\\
\frac{dP}{dt} &= \Lambda_p - \mu_p P - \frac{\beta_1 HP}{1+b_0E},\\
\frac{dG}{dt} &= \frac{cR_I}{1+b_4E} - \mu_g G - \vartheta_g GE,\\
\frac{dE}{dt} &= \Lambda_e + E\left(\frac{\xi H_I}{1+a_0H_I} + \frac{\nu R_I}{1+a_2R_I} + \frac{\sigma M}{1+a_1M} + \frac{\theta G}{1+a_3G}\right) - \mu_e E,
\end{aligned}
\tag{7.1}
$$

with initial condition

$$
H(0)>0, H_I(0)\geq 0, M(0)\geq 0, P(0)\geq 0, R(0)>0, R_I(0)\geq 0, G(0)\geq 0, E(0)>0. \tag{7.2}
$$

7.2 Model Analysis

In this section, we provide an explanation of the biological significance and mathematical validity of the model's solution, as well as a qualitative analysis of the model proposed.

7.2.1 Non-negativity and boundedness

Here, we present the biological feasibility and mathematical well-posedness of the model system (7.1) by showing the non-negativity and boundedness of the solutions.

Theorem 7.1. *If the initial data (7.2): $H(0), H_I(0), M(0), P(0), R(0), R_I(0), G(0)$,and $E(0)$ are non-negative, then the solutions of the system model (7.1):*
$H(t), H_I(t), R(t), R_I(t), M(t), P(t), G(t)$, and $E(t)$ are non-negative, for all time $t \geq 0$.

Proof. Consider the first equation of the dynamical system (7.1)

$$
\frac{dH}{dt} = \Lambda_h - \frac{\beta_1 HP}{1+b_0E} - \mu_h H \geq -\frac{\beta_1 HP}{1+b_0E} - \mu_h H = -\left(\frac{\beta_1 P}{1+b_0E} + \mu_h\right) H.
$$

Integrating both side from 0 to t, we found that

$$
H(t) \geq H(0) exp\left\{-\int_0^t \left(\frac{\beta_1 HP}{1+b_0E} + \mu_h\right) dt\right\} > 0.
$$

Table 7.1: The biological model parameters and their descriptions

Parameters	Description
Λ_h	Recruitment rate of hepatocyte from bone marrow
Λ_r	Recruitment rate of erythrocyte from bone marrow
Λ_p	The rate of injection of sporozoites into the liver due to mosquito bites
β_1	Infection rate of the hepatocyte by sporozoites
β_2	Infection rate of the red blood cell by merozoites
μ_h, μ_r	Natural death rate of uninfected hepatocytes and red blood cells, respectively
δ	Death rate infected hepatocytes
N	Average number of merozoite per ruptured infected hepatocytes
Q	Average number of merozoite per ruptured infected red blood cells
α	Death rate infected red blood cell
μ_m, μ_p	Natural death rate of merozoites and sporozoites, respectively
μ_g	Natural death rate gametocytes
μ_e	Natural death rate of immune system
b_0	Efficacy of immune response on hepatocytic invasion
b_1	Efficacy of the immune response on erythrocyte invasion
b_2	Effectiveness of the immune system on merozoites synthesis during hepatic schizont burst
b_3	Immune response's influence on merozoite production during blood schizonts' burst
b_4	Efficacy of the immune response on productions of gametocytes
ϑ_1	Removal rate of infected hepatocytes due to immune system
ϑ_2	Removal rate of infected erythrocytes due to immune system
ϑ_g	Removal rate gametocyte due to immune system
ϑ_m	Removal rate merozoites immune system
ξ	Activation rate immune system owing to infected hepatocytes
ν	Activation rate immune response due to the presence of infected red blood cells
σ	Activation rate immune response due to the presence of merozoites
θ	Activation rate immune response due to presence of gametocytes
a_0	Efficacy of the infected hepatocytes on the activation of the immune system
a_1	Efficacy of the infected erythrocyte on the activation of immune system
a_2	Efficacy of the merozoites on the activation of immune system
a_3	Efficacy of the gametocytes on the activation of immune system

Similarly, we can proceed with the non-negativity of the solution of the remaining state variables, we have

$$P(t) \geq P(0)exp\left\{-\mu_p t - \int_0^t \left(\frac{\beta_1 H}{1+b_0 E}\right) dt\right\} > 0,$$
$$H_I(t) \geq H_I(0)exp\left\{-\delta t - \int_0^t \vartheta_x E dt\right\} \geq 0,$$
$$R(t) \geq R(0)exp\left\{-\mu_r t - \int_0^t \left(\frac{\beta_2 M}{1+b_1 E}\right) dt\right\} > 0,$$
$$R_I(t) \geq R_I(0)exp\left\{-\alpha t - \int_0^t \vartheta_x E dt\right\} \geq 0,$$

$$M(t) \geq M_0 exp\left\{-\mu_m t - \int_0^t \left(\vartheta_m + \frac{\beta_1 R}{1+b_0 E}\right) dt\right\} \geq 0,$$
$$E(t) \geq E(0) exp\{-\mu_e t\} \geq 0.$$
$$G(t) \geq G(0) exp\left\{-\mu_g t - \int_0^t \vartheta_g E dt\right\} \geq 0,$$

Therefore, all the solutions of the dynamical system (7.1) will remain non-negative with non-negative initial data (7.2), for all $t \geq 0$. □

Theorem 7.2. *The region*

$$\Omega = \left\{ \begin{array}{c} \Omega_H \times \Omega_R \times \Omega_P \times \Omega_E \subseteq R_+^2 \times R_+^2 \times R_+^3 \times R_+^1 : \Omega_H = \left\{(H,H_I) \in R_+^2 : H(t) + H_I(t) \leq \frac{\Lambda_h}{\chi}\right\}, \\ \Omega_R = \left\{(R,R_I) \in R_+^2 : R(t) + R_I(t) \leq \frac{\Lambda_r}{\psi}\right\}, \Omega_P = \left\{(P,M,G) \in R_+^3 : P(t) + M(t) + G(t) \leq \frac{\mathscr{N}}{\varphi}\right\}, \\ \Omega_E = \left\{E \in R_+^1 : E(t) \leq \frac{\Lambda_e}{r}\right\} \end{array} \right\}$$

is a positive invariant of system model (7.1).

Proof. Let, $N_H(t) = H(t) + H_I(t)$ be the total size of the hepatocyte population. From the equation system (7.1), we have

$$\begin{aligned} \frac{dN_H}{dt} = \frac{dH}{dt} + \frac{dH_I}{dt} &= \Lambda_h - \frac{\beta_1 HP}{1+b_0 E} - \mu_h H + \frac{\beta_1 HP}{1+b_0 E} - \delta H_I - \vartheta_1 H_I E \\ &= \Lambda_h - \mu_h H - \delta H_I - \vartheta_1 H_I E \leq \Lambda_h - \mu_h H - \delta H_I \leq \Lambda_h - \chi N_H, \end{aligned}$$

where $\chi = min\{\mu_h, \delta\}$. Solving this inequality, we get

$$N_H(t) \leq \frac{\Lambda_h}{\chi} + \left(N_H(0) - \frac{\Lambda_h}{\chi}\right) e^{-\chi t} \leq \frac{\Lambda_h}{\chi}, \quad for \;\; N_H(0) \leq \frac{\Lambda_h}{\chi}$$

Also, we can apply the same procedure for the red blood cells $N_R(t) = R(t) + R_I(t)$, malaria parasites $N_P(t) = P(t) + M(t) + G(t)$, and immune responses $N_E(t) = E(t)$. That is the total population of red blood cells is given by $N_R(t) = R(t) + R_I(t)$.

$$\begin{aligned} \frac{dN_R}{dt} = \frac{dR}{dt} + \frac{dR_I}{dt} &= \Lambda_r - \frac{\beta_2 RM}{1+b_1 E} - \mu_r R + \frac{\beta_2 RM}{1+b_1 E} - \alpha R_I - \vartheta_2 R_I E \\ &\Lambda_r - \mu_r R - \alpha R_I - \vartheta_2 R_I E \leq \Lambda_r - \psi N_R, \end{aligned}$$

where $\psi = min\{\mu_r, \alpha\}$. Solving this inequality, we found

$$N_R(t) \leq \frac{\Lambda_r}{\psi} + \left(N_R(0) - \frac{\Lambda_r}{\psi}\right) e^{-\psi t} \leq \frac{\Lambda_r}{\psi}$$

Next, the total size of malaria parasites is $N_P(t) = P(t) + M(t) + G(t)$. Differentiating both side with respect to time t.

Now,

$$\begin{aligned}
\frac{dN_P}{dt} &= \frac{dP}{dt} + \frac{dM}{dt} + \frac{dG}{dt} \\
&= \Lambda_p - \mu_p P - \frac{\beta_1 HP}{1+b_0E} + \frac{N\delta H_I}{1+b_2E} + \frac{Q\alpha R_I}{1+b_3E} - \mu_m M - \vartheta_m ME - \frac{\beta_2 RM}{1+b_1E} + \frac{cR_I}{1+b_4E} - \mu_g G - \vartheta_g GE \\
&\leq \Lambda_p - \varphi N_P + \frac{N\delta H_I}{1+b_2E} + \frac{Q\alpha R_I}{1+b_3E} + \frac{cR_I}{1+b_4E}, \ \ where \ \ \varphi = min\{\mu_p, \mu_m, \mu_g\} \\
&\leq \Lambda_p - \varphi N_P + N\delta H_I + (Q\alpha + c)R_I \\
&\leq \Lambda_p - \varphi N_P + \frac{N\delta\Lambda_h}{\chi} + \frac{(Q\alpha+c)\Lambda_r}{\psi} = \mathscr{Y} - \varphi N_P, \ \ since \ \ H_I \leq \frac{\Lambda_h}{\chi} \ \ and \ \ R_I \leq \frac{\Lambda_r}{\psi},
\end{aligned}$$

where $\mathscr{Y} = \Lambda_p + \frac{N\delta\Lambda_h}{\chi} + \frac{(Q\alpha+c)\Lambda_r}{\psi}$ is the maximum production of malaria parasites during malaria infection within infected individual. After solving the inequality, we have

$$N_P(t) \leq \frac{\mathscr{Y}}{\varphi} + \left(N_P(0) - \frac{\mathscr{Y}}{\varphi}\right) e^{-\varphi t} \leq \frac{\mathscr{Y}}{\varphi}.$$

Lastly, the total size of immune system is $N_E(t) = E(t)$. Now,

$$\begin{aligned}
\frac{dN_E(t)}{dt} = \frac{dE}{dt} &= \Lambda_e + E\left(\frac{\xi H_I}{1+a_0H_I} + \frac{\nu R_I}{1+a_2R_I} + \frac{\sigma M}{1+a_1M} + \frac{\theta G}{1+a_3G}\right) - \mu_e E \\
&\leq \Lambda_e + (\xi + \nu + \sigma + \theta)E - \mu_e E \leq \Lambda_e - rE.
\end{aligned}$$

After solving the inequality, we have

$$N_E(t) \leq \frac{\Lambda_e}{r} + \left(E(0) - \frac{\Lambda_e}{r}\right) e^{-rt} \leq \frac{\Lambda_e}{r},$$

where $\mathscr{Q} = \xi + \nu + \sigma + \theta$ is the maximum stimulation rate of immune system during malaria infection and $r = \mu_e - \mathscr{Q}$, for $\mu_e > \mathscr{Q}$.

Therefore, the region Ω is a positive invariant of the system equation (7.1). All the solutions of the system remain in the region Ω, for all time $t \geq 0$. □

7.2.2 Parasite-free equilibrium point

The parasite-free equilibrium point (PFE) is the steady-state solution at which no malaria parasites are in the host cell, and it will be obtained by setting the right-hand side of equation (7.1) to zero. Thus, we found that

$$\mathscr{E}^0 = (H^0, H_I^0, R^0, R_I^0, M^0, P^0, G^0, E^0) = \left(\frac{\Lambda_h}{\mu_h}, 0, \frac{\Lambda_r}{\mu_r}, 0, 0, 0, 0, \frac{\Lambda_e}{\mu_e}\right).$$

7.2.3 The within-host basic reproduction number

Here, we utilized the next-generation matrix approach that was invented by (Van den Driessche and Watmough, 2002) to determine the within-host basic reproduction number, $\mathscr{R}_0$ similar to the previous Chapters. In order to investigate the within-host reproduction number we consider only the infected compartments. Let

$$\frac{dX}{dt} = \mathscr{F}_i - \mathscr{V}_i,$$

where X is the infected compartment, $\mathscr{F}_i$ is the rate of new appearance, $\mathscr{V}_i$ is the rate of transfer of individuals from one compartment to another compartment via any other means and given as

$$\mathscr{F}_i = \begin{pmatrix} \frac{\beta_1 HP}{1+b_0E} \\ \frac{\beta_2 RM}{1+b_1E} \\ 0 \\ 0 \\ 0 \end{pmatrix}, \quad \mathscr{V}_i = \begin{pmatrix} \delta H_I + \vartheta_1 H_I E \\ \alpha R_I + \vartheta_2 R_I E \\ -\frac{N\delta H_I}{1+b_2E} - \frac{Q\alpha R_I}{1+b_3E} + \mu_m M + \vartheta_m ME + \frac{\beta_2 RM}{1+b_1E} \\ -\Lambda_p + \mu_p P + \frac{\beta_1 HP}{1+b_0E} \\ -\frac{cR_I}{1+b_4E} + \mu_g G + \vartheta_g GE \end{pmatrix}.$$

The Jacobian matrix $\mathscr{F}$ and $\mathscr{V}$ is obtained by differentiating the vectors $\mathscr{F}_i$ and $\mathscr{V}_i$ at PFE, $\mathscr{E}^0$. Hence, we found that

$$\mathscr{F} = \begin{pmatrix} 0 & 0 & 0 & \frac{\beta_1 \Lambda_h \mu_e}{\mu_h \mu_e + b_0 \mu_h \Lambda_e} & 0 \\ 0 & 0 & \frac{\beta_2 \Lambda_r \mu_e}{\mu_r \mu_e + b_1 \mu_r \Lambda_e} & 0 & 0 \\ 0 & 0 & 0 & 0 & 0 \\ 0 & 0 & 0 & 0 & 0 \\ 0 & 0 & 0 & 0 & 0 \end{pmatrix},$$

$$\mathscr{V} = \begin{pmatrix} \delta + \frac{\vartheta_1 \Lambda_e}{\mu_e} & 0 & 0 & 0 & 0 \\ 0 & \alpha + \frac{\vartheta_2 \Lambda_e}{\mu_e} & 0 & 0 & 0 \\ -\frac{N\delta\mu_e}{\mu_e + b_2\Lambda_e} & -\frac{Q\alpha\mu_e}{\mu_e + b_3\Lambda_e} & \mu_m + \frac{\beta_2 \Lambda_r \mu_e}{\mu_e \mu_r + b_1 \Lambda_e \mu_r} + \frac{\vartheta_m \Lambda_e}{\mu_e} & 0 & 0 \\ 0 & 0 & 0 & \mu_p + \frac{\beta_1 \Lambda_e \mu_e}{\mu_e \mu_h + b_0 \Lambda_e \mu_h} & 0 \\ 0 & -\frac{c\mu_e}{\mu_e + b_4 \Lambda_e} & 0 & 0 & \mu_g + \frac{\vartheta_g \Lambda_e}{\mu_e} \end{pmatrix}.$$

The inverse of matrix $\mathscr{V}$ is hence given as

$$\mathscr{V}^{-1} = \begin{pmatrix} \frac{\mu_e}{\delta\mu_c + \vartheta_1 \Lambda_e} & 0 & 0 & 0 & 0 \\ 0 & \frac{\mu_e}{\alpha\mu_c + \vartheta_2 \Lambda_e} & 0 & 0 & 0 \\ \frac{N\delta\mu_e^2}{(\mu_e + b_2\Lambda_e)(\delta\mu_e + \vartheta_1\Lambda_e)C_{33}} & \frac{Q\alpha\mu_e^2}{(\mu_e + b_3\Lambda_e)(\alpha\mu_e + \vartheta_1\Lambda_e)C_{33}} & \frac{1}{C_{33}} & 0 & 0 \\ 0 & 0 & 0 & \frac{\mu_h\mu_e + b_0\Lambda_e\mu_h}{\mu_p\mu_h\mu_e + b_0\Lambda_e\mu_p\mu_h} & 0 \\ 0 & \frac{c\mu_e^3}{(\mu_e + b_4\Lambda_e)(\alpha\mu_e + \vartheta_2\Lambda_e)(\mu_g\mu_e + \vartheta_g\Lambda_e)} & 0 & 0 & \frac{\mu_e}{\mu_g\mu_e + \vartheta_g\Lambda_e} \end{pmatrix},$$

where $C_{33} = \mu_m + \frac{\beta_2\Lambda_r\mu_e}{\mu_r\mu_e+b_1\Lambda_e\mu_r} + \frac{\vartheta_m\Lambda_e}{\mu_e}$. The basic reproduction number is denoted by $\mathscr{R}_0$, it's the dominant eigenvalue of the matrix $\mathscr{F}\mathscr{V}^{-1}$. Thus,

$$\mathscr{R}_0 = \frac{\alpha Q\beta_2\Lambda_r}{\left(1+\frac{b_3\Lambda_e}{\mu_e}\right)\mu_r\left(1+\frac{b_2\Lambda_e}{\mu_e}\right)\left(\alpha+\frac{\vartheta_2\Lambda_e}{\mu_e}\right)\left(\mu_m+\frac{\beta_2\Lambda_r\mu_e}{\mu_r\mu_e+b_1\Lambda_e\mu_r}+\frac{\vartheta_m\Lambda_e}{\mu_e}\right)}. \tag{7.3}$$

Remark: The biological interpretations of the within-host basic reproduction number $\mathscr{R}_0$ is the average number of secondary infections caused by the entrance of malaria parasites called merozoites into a population of uninfected red blood cells. The term $\frac{\alpha Q}{\left(1+\frac{b_1\Lambda_e}{\mu_e}\right)\left(\mu_m+\frac{\beta_2\Lambda_r\mu_e}{\mu_r\mu_e+b_1\Lambda_e\mu_r}+\frac{\vartheta_m\Lambda_e}{\mu_e}\right)}$ is the expected number of merozoites that are released during rupturing of the infected erythrocytes in the presence of an immune response, $\beta_2\Lambda_r/(\mu_r(1+\frac{b_2\Lambda_e}{\mu e}))$ is the expected number of infected red blood cells during malaria parasite infection in the presence of the immune system and the term $\frac{b_2\Lambda_e}{\mu e}$ represents the inhibition of the invasion of uninfected red blood cells owing to immune responses, $1/\mu_r(\alpha+\frac{\vartheta_2\Lambda_e}{\mu_e})$ is the life span of infected erythrocytes and $1/(\mu_m+\frac{\beta_2\Lambda_r\mu_e}{\mu_r\mu_e+b_1\Lambda_e\mu_r}+\frac{\vartheta_m\Lambda_e}{\mu_e})$ is the life span of the malaria parasite in the form of merozoites in the presence of an immune response.

7.2.4 Local stability of parasite-free equilibrium point

Theorem 7.3. *The parasite-free equilibrium point is locally asymptotically stable if $\mathscr{R}_0 < 1$ and unstable if $\mathscr{R}_0 > 1$.*

Proof. The Jacobian matrix at a PFE is given as

$$J(\mathscr{E}^0) = \begin{pmatrix}
-\mu_h & 0 & 0 & 0 & 0 & \frac{\beta_1\Lambda_h}{\mu_h(1+\frac{b_0\Lambda_e}{\mu_e})} & 0 & 0 \\
0 & -\delta-\frac{\vartheta_1\Lambda_e}{\mu_e} & 0 & 0 & 0 & \frac{\beta_1\Lambda_h}{\mu_h(1+\frac{b_0\Lambda_e}{\mu_e})} & 0 & 0 \\
0 & 0 & -\mu_r & 0 & -\frac{\beta_2\Lambda_r}{\mu_r(1+\frac{b_1\Lambda_e}{\mu_e})} & 0 & 0 & 0 \\
0 & 0 & 0 & -\alpha-\frac{\vartheta_2\Lambda_e}{\mu_e} & \frac{\beta_2\Lambda_r}{\mu_r(1+\frac{b_1\Lambda_e}{\mu_e})} & 0 & 0 & 0 \\
0 & \frac{N\delta}{1+\frac{b_2\Lambda_e}{\mu_e}} & 0 & \frac{Q\alpha}{1+\frac{b_3\Lambda_e}{\mu_e}} & -\mu_m-\frac{\vartheta_m\Lambda_e}{\mu_e}-\frac{\beta_2\Lambda_r}{\mu_r(1+\frac{b_1\Lambda_e}{\mu_e})} & 0 & 0 & 0 \\
0 & 0 & 0 & 0 & 0 & -\mu_p-\frac{\beta_1\Lambda_h}{\mu_h(1+b_0E)} & 0 & 0 \\
0 & 0 & 0 & \frac{c}{1+\frac{b_4\Lambda_e}{\mu_e}} & 0 & 0 & -\mu_g-\frac{\vartheta_g\Lambda_e}{\mu_e} & 0 \\
0 & \frac{\xi\Lambda_e}{\mu_e} & 0 & \frac{\nu\Lambda_e}{\mu_e} & \frac{\sigma\Lambda_e}{\mu_e} & 0 & \frac{\theta\Lambda_e}{\mu_e} & -\mu_e
\end{pmatrix}. \tag{7.4}$$

The first, third, and last columns of the Jacobian matrix has only the diagonal entry. Thus, we can easily obtained the $\lambda_1 = -\mu_h, \lambda_3 = -\mu_r$, and $\lambda_8 = -\mu_e$. After removing those columns and respective rows of the Jacobian matrix, we can easily obtain the eigenvalues $\lambda_7 = -\mu_g - \frac{\vartheta_g\Lambda_e}{\mu_e}$, $\lambda_6 = -\mu_p - \frac{\beta_1\Lambda_h}{\mu-h(1+\frac{b_0\Lambda_e}{\mu_e})}$, and $\lambda_2 = -\delta - \frac{\vartheta_1\Lambda_e}{\mu_e}$. The remaining eigenvalues are obtained from

the sub matrix

$$J_1(\mathscr{E}^0) = \begin{pmatrix} -\alpha - \frac{\vartheta_2\Lambda_e}{\mu_e} & \frac{\beta_2\Lambda_r}{\mu_r\left(1+\frac{b_1\Lambda_e}{\mu_e}\right)} \\ \frac{Q\alpha}{1+\frac{b_3\Lambda_e}{\mu_e}} & -\mu_m - \frac{\vartheta_m\Lambda_e}{\mu_e} - \frac{\beta_2\Lambda_r}{\mu_r(1+\frac{b_1\Lambda_e}{\mu_e})} \end{pmatrix}.$$

The corresponding characteristic equation is

$$\lambda^2 + b_1\lambda + b_0 = 0, \tag{7.5}$$

where $b_1 = \alpha + \frac{\vartheta_2\Lambda_e}{\mu_e} + \mu_m + \frac{\vartheta_m\Lambda_e}{\mu_e} + \frac{\beta_2\Lambda_r}{\mu_r(1+\frac{b_1\Lambda_e}{\mu_e})}$, and

$b_0 = (\alpha + \frac{\vartheta_2\Lambda_e}{\mu_e})\left(\mu_m + \frac{\vartheta_m\Lambda_e}{\mu_e} + \frac{\beta_2\Lambda_r}{\mu_r(1+\frac{b_1\Lambda_e}{\mu_e})}\right) - \frac{\beta_2\Lambda_r Q\alpha}{\left(1+\frac{b_3\Lambda_e}{\mu_e}\right)\mu_r\left(1+\frac{b_1\Lambda_e}{\mu_e}\right)}$

$= (\alpha + \frac{\vartheta_2\Lambda_e}{\mu_e})\left(\mu_m + \frac{\vartheta_m\Lambda_e}{\mu_e} + \frac{\beta_2\Lambda_r}{\mu_r(1+\frac{b_1\Lambda_e}{\mu_e})}\right)(1-\mathscr{R}_0).$

Applying Routh–Hurwitz stability criteria the PFE is locally asymptotically stable if all the eigenvalues of the Jacobian matrix (7.4) have a negative real part. Hence, from the above discussion, all the eigenvalues of the Jacobian matrix have a negative real part if the coefficients of the characteristic equation (7.5) are positive. Clearly $b_1 > 0$, and $b_0 > 0$, if the basic reproduction number, $\mathscr{R}_0 < 1$. Therefore the PFE is locally asymptotically stable if the $\mathscr{R}_0 < 1$, and unstable if $\mathscr{R}_0 > 1$. □

7.2.5 Global stability parasite-free equilibrium point

Here, we investigate the global stability analysis of the PFE using the method which is presented in Castillo-Chavez and Song (2004).

Theorem 7.4. *The parasite-free equilibrium $\mathscr{E}^0$ is globally asymptotically stable if $\mathscr{R}_0 < 1$.*

Proof. Initially, we divide the system equation (7.1) into uninfected and infected compartments as follows

$$\frac{d\mathscr{U}}{dt} = \mathscr{F}(\mathscr{U},\mathscr{W}), \tag{7.6}$$

$$\frac{d\mathscr{W}}{dt} = \mathscr{G}(\mathscr{U},\mathscr{W}),\ \ \mathscr{G}(\mathscr{U},0) = 0, \tag{7.7}$$

where $\mathscr{U} = (H,R,E) \in R^3$ is denotes healthy compartments and $\mathscr{W} = (H_I,R_I,M,P,G) \in R^5$ is infected compartment. The global stability analysis of PFE $\mathscr{E}^0$ is exist, if the following condition $\mathscr{H}_1$ and $\mathscr{H}_2$ are satisfied.

($\mathscr{H}_1$) For $\frac{d\mathscr{U}}{dt} = \mathscr{F}(\mathscr{U},0)$ is globally asymptotically stable, where $\mathscr{F}(\mathscr{U}^0,0) = 0$.

($\mathscr{H}_2$) $\mathscr{G}(\mathscr{U},\mathscr{W}) = \mathscr{D}\mathscr{W} - \widehat{\mathscr{G}}(\mathscr{U},\mathscr{W}), \widehat{\mathscr{G}}(\mathscr{U},\mathscr{W}) > 0$, for $(\mathscr{U},\mathscr{W}) \in \Omega$, where $\mathscr{D} = D_{\mathscr{W}}\mathscr{G}(\mathscr{U}^0,0)$ is an **M** matrix i.e the off diagonal elements of matrix $\mathscr{D}$ is non-negative. Now, from system

equation (7.1), we have

$$\mathscr{F}(\mathscr{U},\mathscr{W}) = \begin{pmatrix} \Lambda_h - \frac{\beta_1 HP}{1+b_0E} - \mu_h H \\ \Lambda_r - \frac{\beta_2 RM}{1+b_1E} - \mu_r R \\ \Lambda_e + E\left(\frac{\xi H_I}{1+a_0H_I} + \frac{\nu R_I}{1+a_2R_I} + \frac{\sigma M}{1+a_1M} + \frac{\theta G}{1+a_3G}\right) - \mu_e E \end{pmatrix}. \tag{7.8}$$

$$\mathscr{F}(\mathscr{U},0) = \begin{pmatrix} \Lambda_h - \mu_h H \\ \Lambda_r - \mu_r R \\ \Lambda_e - \mu_e E \end{pmatrix}, \text{ and } \mathscr{F}(\mathscr{U}^0,0) = 0, \text{ where } \mathscr{U} = \left(\frac{\Lambda_h}{\mu_h}, \frac{\Lambda_r}{\mu_r}, \frac{\Lambda_e}{\mu_e}\right). \tag{7.9}$$

Thus, the equation (8.29) has a unique PFE , $\mathscr{U}^0 = \left(\frac{\Lambda_h}{\mu_h}, \frac{\Lambda_r}{\mu_r}, \frac{\Lambda_e}{\mu_e}\right)$, which is globally asymptotically stable. That is all the solution of the state variables $H(t), R(t)$ and $E(t)$ are converges to $\frac{\Lambda_h}{\mu_h}, \frac{\Lambda_r}{\mu_r}$,and $\frac{\Lambda_e}{\mu_e}$, respectively. The $\mathscr{H}_1$ is satisfied.

Next, we preform the condition $\mathscr{H}_2$. From system equation (7.1), we have □

$$\mathscr{G}(\mathscr{U},\mathscr{W}) = \begin{pmatrix} \frac{\beta_1 HP}{1+b_0E} - \delta H_I - \vartheta_1 H_I E \\ \frac{\beta_2 RM}{1+b_1E} - \alpha R_I - \vartheta_2 R_I E \\ \frac{N\delta H_I}{1+b_2E} + \frac{Q\alpha R_I}{1+b_3E} - \mu_m M - \vartheta_m ME - \frac{\beta_2 RM}{1+b_1E} \\ \Lambda_p - \mu_p P - \frac{\beta_1 HP}{1+b_0E} \\ \frac{cR_I}{1+b_4E} - \mu_g G - \vartheta_g GE \end{pmatrix}, \tag{7.10}$$

$$\mathscr{D} = \mathscr{D}_{\mathscr{W}}\mathscr{G}(\mathscr{U}^0,0) = \begin{pmatrix} -\delta - \vartheta_1 E^0 & 0 & 0 & \frac{\beta_1 H^0}{1+b_0E^0} & 0 \\ 0 & -\alpha - \vartheta_2 E^0 & \frac{\beta_2 R^0}{1+b_1E^0} - & 0 & 0 \\ \frac{N\delta}{1+b_2E^0} + \frac{Q\alpha}{1+b_3E^0} & -\mu_m - \vartheta_m E^0 & -\frac{\beta_2 R^0}{1+b_1E^0} & 0 & 0 \\ 0 & 0 & 0 & -\mu_p P - \frac{\beta_1 H^0}{1+b_0E^0} & 0 \\ 0 & \frac{c}{1+b_4E^0} & 0 & 0 & -\mu_g - \vartheta_g E^0 \end{pmatrix}, \tag{7.11}$$

which is $\mathbf{M}-$ matrix. The off diagonal elements of the $\mathscr{D}$ is non-negative. Finally,

$$\begin{aligned} \widehat{\mathscr{G}}(\mathscr{U},\mathscr{W}) &= \mathscr{D}\mathscr{W} - \mathscr{G}(\mathscr{U},\mathscr{W}) \\ &= \begin{pmatrix} \frac{\beta_1 H^0 P}{1+b_0E^0}\left(1 - \frac{(1+b_0E^0)H}{(1+b_0E)H^0}\right) + \vartheta_1 H_I E\left(1 - \frac{E^0}{E}\right) \\ \frac{\beta_2 R^0 M}{1+b_1E^0}\left(1 - \frac{(1+b_1E^0)R}{(1+b_1E)R^0}\right) + \vartheta_2 R_I E\left(1 - \frac{E^0}{E}\right) \\ \frac{\delta N H_I}{1+b_2E^0}\left(1 - \frac{(1+b_2E^0)}{d(1+b_2E)}\right) \frac{\alpha Q R_I}{1+b_3E^0}\left(1 - \frac{(1+b_3E^0)}{(1+b_2E)}\right) + \frac{\beta_2 RM}{1+b_1E}\left(1 - \frac{(1+b_1E)R^0}{(1+b_1E^0)R}\right) \\ \frac{\beta_1 HP}{1+b_0E} - \Lambda_p \\ \frac{cG}{1+b_4E^0}\left(1 - \frac{1+b_4E^0}{1+b_4E}\right) + \vartheta_g GE\left(1 - \frac{E^0}{E}\right) \end{pmatrix}, \end{aligned} \tag{7.12}$$

which implies that $\widehat{\mathscr{G}}(\mathscr{U},\mathscr{W}) \geq 0$, for all $(\mathscr{U},\mathscr{W}) \in \Omega$ the conditions $(\mathscr{H}_1)$ and $(\mathscr{H}_2)$ are satisfied. Therefore, PFE is globally asymptotically stable if $\mathscr{R}_0 < 1$. The PFE is violated if $\mathscr{R}_0 > 1$, and the system (7.1) has the parasite persistence equilibrium point (PPE). Although, it would be challenging to establish the explicit form of the PPE in this context.

7.3 Sensitivity Analysis

The within-host basic reproduction number in the absence of control is given as in equation (7.3). As a result, we demonstrate the sensitivity analysis of basic reproduction number in the absence of control mechanisms as

$$\Delta_{\theta}^{\mathscr{R}_0} = \frac{\partial \mathscr{R}_0}{\partial \theta} \times \frac{\theta}{\mathscr{R}_0},$$

were θ is the parameters which belongs to $\mathscr{R}_0$. The sensitivity index of the basic reproduction number, $\mathscr{R}_0$ is listed in Table 7.2 based on the parameter value in Table 7.3. The results reveal that the infection rate of RBCs β_2, the death rate of iRBCs α, average number of merozoite per rupture iRBCs Q, and the recruitment of RBCs Λ_r have a positive impact on the basic reproduction number, $\mathscr{R}_0$, whereas the other parameters have a negative impact on $\mathscr{R}_0$. The parameters β_2 and Q have a high impact on the spread of in-host parasite infection. That is, a 10% increase or decrease β_2 and Q is a 2.6347% and 10% increase or decrease in $\mathscr{R}_0$, respectively. Thus, we apply the controls to reduce the β_2 and Q in the following section. In addition, we apply the controls to reduce the average number of merozoite per ruptured infected hepatocytes, N and infection rate hepatocytes, β_1 (Orwa et al., 2022). These parameters do not belong to an expression $\mathscr{R}_0$, however, from the biological point of view reducing the parameters β_1 and N is reducing in-host parasite infection.

7.4 Numerical solution of proposed model

Here, we perform the numerical simulation of the model equation (7.1). In this, we used the initial values of the state variables for the model equations given as $H(0) = 5000, H_I(0) = 40, R(0) = 500000, R_I(0) = 100, M(0) = 40000, P(0) = 50, G(0) = 30$, and $E(0) = 0.001$ and all the biological parameter values listed in Table 7.3. The time series plots of the dynamical system equation (7.1) are demonstrated in Figure 7.2. The Figures also demonstrate the existence of parasite persistence equilibrium. Figures 7.2(a) 7.2(b), 7.2(c), and 7.2(d) reveal the time series of hepatocyte cells (uninfected hepatocyte and infected hepatocyte), malaria parasites (merozoites, sporozoites, and gametocytes), red blood cells (uninfected red blood cells and infected red blood cells), and human immunity system, respectively.

The uninfected hepatocytes grow and become constant as the time interval increases and the infected hepatocytes initially rise and get over constant (see 7.2(a)). The density of un-

Table 7.2: Elasticity indices of within-host basic reproduction number, $\Re_0$ concerning parameters in within-host model (7.1) using parameter values in Table 7.3.

Parameters	Elasticity index	Value
β_2	$\Delta_{\beta_2}^{\Re_0}$	$+0.26347$
Q	$\Delta_{Q}^{\Re_0}$	$+1$
α	$\Delta_{\alpha}^{\Re_0}$	$+0.1697$
Λ_r	$\Delta_{\Lambda_r}^{\Re_0}$	$+0.02050$
ϑ_2	$\Delta_{\vartheta_2}^{\Re_0}$	-0.350918
ϑ_m	$\Delta_{\vartheta_m}^{\Re_0}$	-0.0000128
b_2	$\Delta_{b_2}^{\Re_0}$	-0.020500
b_3	$\Delta_{b_3}^{\Re_0}$	-0.004975
μ_m	$\Delta_{\mu_m}^{\Re_0}$	-0.020487
μ_r	$\Delta_{\mu_r}^{\Re_0}$	-0.323645

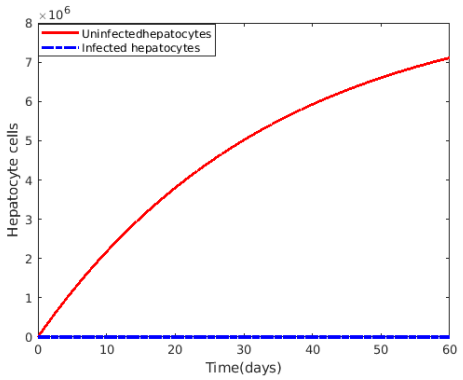

(a) Red blood (erythrocyte) cells.

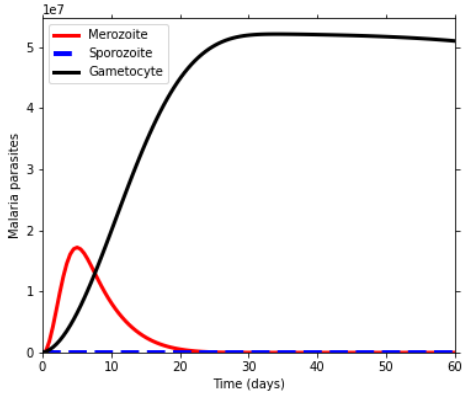

(b) Malaria parasites.

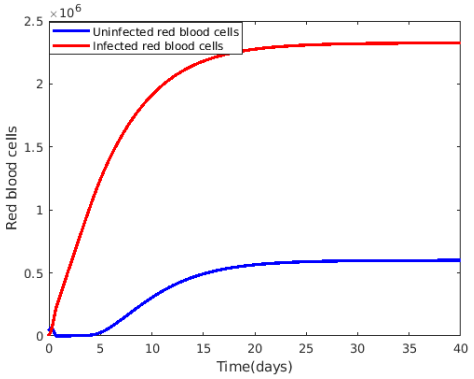

(c) Liver hepatocyte cells.

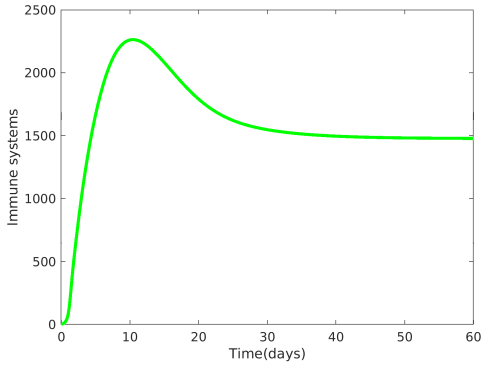

(d) Immune system.

Figure 7.2: The time serious plot of proposed model equation (7.1).

infected red blood cells declines with time interval and becomes constant as the time interval increases, whereas the infected red blood cells rise in the time series and become constant after some time interval (see 7.2(b)). The merozoite populations initially rise and drop off and

Table 7.3: The values for model parameters utilized in the simulation, where mero represents merozoites.

Parameters	Value	Interval	Unit	Reference
Λ_r	2.5×10^6	$2.5 \times 10^5 - 2.5 \times 10^{10}$	$cells/\mu l/day$	Hetzel and Anderson (1996)
Λ_h	2.5×10^8	$2.5 \times 10^5 - 2.5 \times 10^{10}$	$cells/\mu l/day$	Hetzel and Anderson (1996)
Λ_p	20	$20 - 200$	$sporo/day$	Selemani et al. (2016,0)
β_1	0.001	$1 \times 10^{-5} - 1 \times 10^{-3}$	$\mu l/cell/day$	Selemani et al. (2016)
β_2	0.008	$8 \times 10^{-5} - 8 \times 10^{-3}$	$\mu l/cell/day$	Hetzel and Anderson (1996)
δ	0.95	$0.0095 - 0.95$	$cell/day$	Selemani et al. (2016)
α	0.03	$0.0003 - 0.3$	$cell/day$	Kamangira et al. (2014)
Q	16	$16 - 32$	$mero/\mu l$	Chiyaka et al. (2008)
b_0	0.05	$0.0005 - 0.5$	$cell/\mu l$	Selemani et al. (2016)
b_1	0.05	$0.0005 - 0.5$	$cell/\mu l$	De Roode et al. (2005)
b_2	0.005	$0.00005 - 0.05$	$cell/\mu l$	Selemani et al. (2016)
b_3	0.005	$0.00005 - 0.05$	$cell/\mu l$	De Roode et al. (2005)
b_4	0.004	$0.0005 - 0.5$	$cell/\mu l$	Chiyaka et al. (2008)
ϑ_1	9×10^{-11}	$9 \times 10^{-11} - 9 \times 10^{-3}$	$cell\mu l/day$	Selemani et al. (2017a)
ϑ_2	9×10^{-5}	$9 \times 10^{-8} - 9 \times 10^{-3}$	$cell\mu l/day$	Chiyaka et al. (2008)
ϑ_m	0.03	$0.0003 - 0.3$	$cell\mu l/day$	Chiyaka et al. (2008)
ϑ_g	3×10^{-3}	$3 \times 10^{-5} - 3 \times 10^{-2}$	$cell\mu l/day$	Anderson (1998)
σ	5×10^{-4}	$5 \times 10^{-6} - 5 \times 10^{-2}$	$/day$	Orwa et al. (2022)
ν	5×10^{-5}	$5 \times 10^{-6} - 5 \times 10^{-3}$	$/day$	Orwa et al. (2018)
θ	5×10^{-4}	$5 \times 10^{-6} - 5 \times 10^{-2}$	$/day$	Orwa et al. (2018)
μ_r	0.0083	$8.3 \times 10^{-5} - 8.3 \times 10^{-2}$	$cell/day$	Anderson et al. (1989)
μ_h	0.029	$0.0029 - 0.029$	$cell/day$	Selemani et al. (2016)
μ_p	1.2×10^{-11}	$1.2 \times 10^{-11} - 1.2 \times 10^{-5}$	$cell/day$	Selemani et al. (2016)
μ_m	48		$cell/day$	Annan (2020)
μ_g	6.25×10^{-3}	$6.25 \times 10^{-6} - 6.25 \times 10^{-2}$	$cell/day$	Selemani et al. (2016)
μ_e	2		cell/day	Selemani et al. (2017a)
Λ_e	20		$\mu l/day$	Selemani et al. (2017a)
a_0	4×10^{-3}	$4 \times 10^{-6} - 4 \times 10^{-2}$	$\mu l/day$	Anderson (1998)
a_1	6.67×10^{-3}	$6.67 \times 10^{-6} - 6.25 \times 10^{-2}$	$\mu l/day$	Anderson (1998)
a_2	6.67×10^{-3}	$6.67 \times 10^{-6} - 6.25 \times 10^{-2}$	$\mu l/day$	Anderson (1998)
a_3	6.67×10^{-3}	$6.67 \times 10^{-6} - 6.25 \times 10^{-2}$	$\mu l/day$	Orwa et al. (2018)
ξ	5×10^{-5}	$5 \times 10^{-6} - 5 \times 10^{-2}$	mm^{-1}/day	Orwa et al. (2018)
τ	2		$unitless$	Selemani et al. (2017a)
c	0.02	0.0002-0.2	$/day$	Hellriegel (1992)

become constant after approximately 25 days. The malaria sporozoites are eradicated from the infected host cells and gametocytes increase initially in time intervals (see 7.2(c)). The

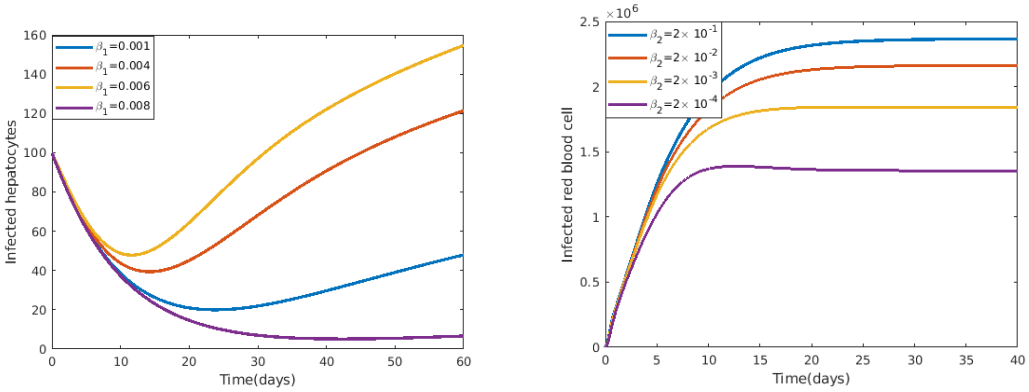

(a) Infected hepatocyte cells. (b) Infected red blood cells.

Figure 7.3: Impact of invention rate of hepatocytes and red blood cells.

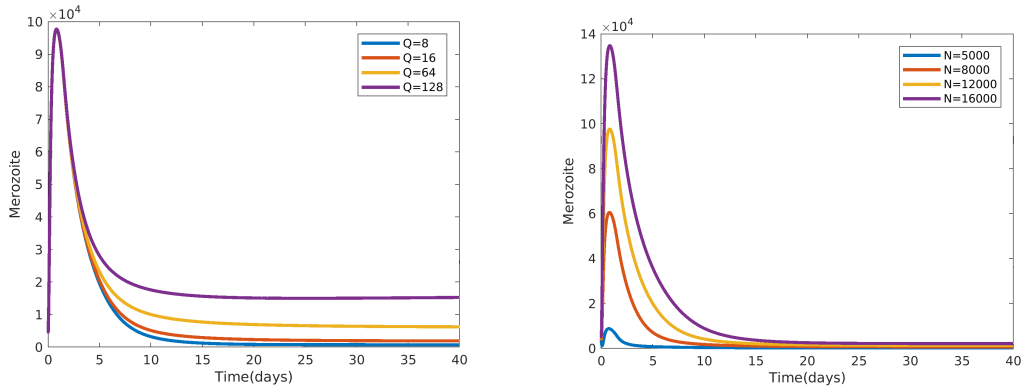

Figure 7.4: Impact of average number of merozoites per ruptured blood-schizont and liver schizont on malaria merozoites.

human immunity system against malaria parasite infection is initially growing exponentially. This is because most human immunity systems are stimulated due to the presence of infection (7.2(d)).

Figure 7.3 reveals the impact of the invasion rate of hepatocyte by sporozoites and red blood cell by meroziotes on infected hepatocytes and infected red blood cells, respectively. The density of the infected hepatocytes and red blood cells are decreases as the invasion rate are decreases. Figure 7.4, shows the effect of the average number of merozoites per rupture blood-schizont Q and liver-schizont N on the malaria merozoite populations. The merozoites population growth as both the average number of merozoites per rupture blood-schizont and liver-schizont are rising. Figure 7.5 demonstrates the impact of the immune sensitivity of infected hepatocytes, infected red blood cells, merozoites, and gametocytes. As the removal rates increase the infected cells and malaria parasites are reduced.

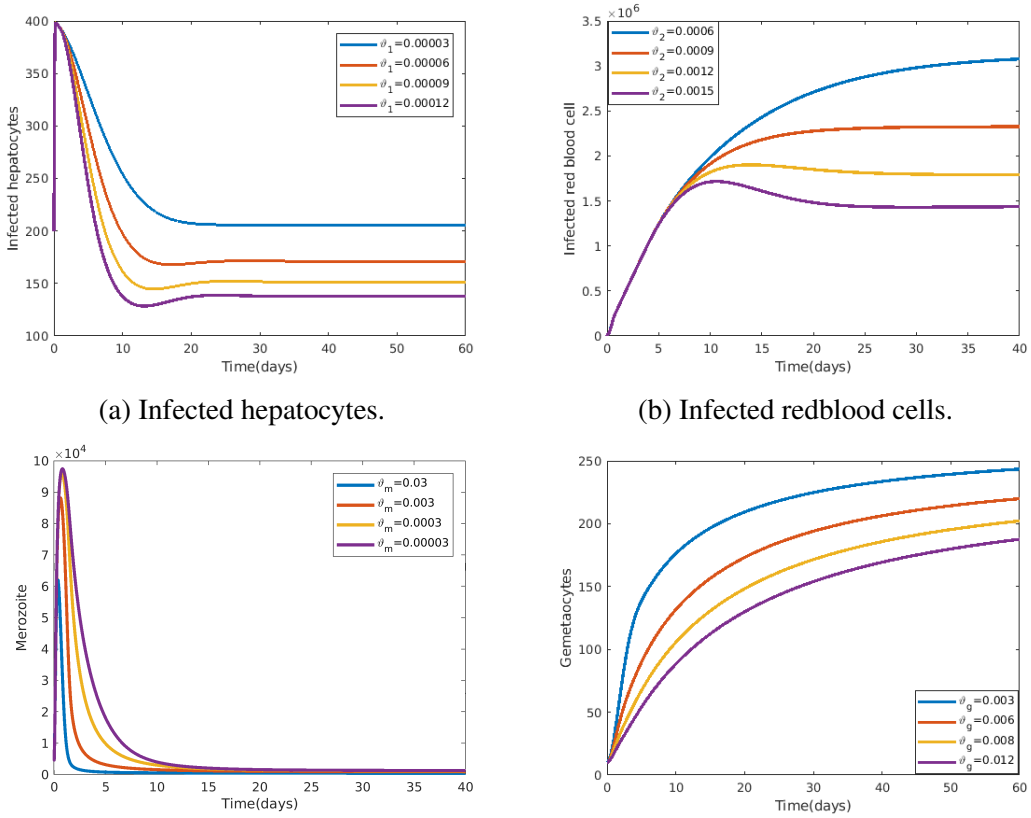

(a) Infected hepatocytes.

(b) Infected redblood cells.

(c) Merozoites.

(d) Gammetocytes.

Figure 7.5: The time serious plot of proposed model equation (7.1).

7.5 Optimal Control Problem

In this section, we extend the model (7.1) into optimal control by incorporating time-dependent controls. We consider the four control variables such as pre-erythrocytic vaccine ($u_1(t)$), blood-stage vaccine ($u_2(t)$), primary tissue schizontocides ($u_3(t)$), and blood-schizontocides and gametocytocidal drugs (gametocytocides) ($u_4(t)$). The administration of these controls reduces the invasion of hepatocytes by sporozoites and erythrocytes by merozoites, as well as the average number merozoites per rupturing infected hepatocytes, infected erythrocyte cells and sexual replication of the merozoites (gametocytes) . Furthermore, pry-erythrocytic vaccine and blood stage vaccine reduces the rates of invasion of healthy hepatocytes and healthy erythrocytes, respectively. The hepatocyte invasion rate by sporozoites β_1 and the erythrocyte invasion rate by merozoites β_2 are hence reduced as $(1-u_1(t))\beta_1$ and $(1-u_2(t))\beta_2$, respectively. The use of primary tissue schizontocides (primaquine) reduces the burst size N of liver schizonts with $(1-u_3(t))N$. The administration of blood-schizontocides reduces the burst size Q of infected erythrocytes to $(1-u_4(t))Q$. Similarly, the administration of gametocytocides removes the gametocytes by a rate $u_4(t)$. Also, the malaria vaccine enhances the immune system at a rate $\tau > 1$.

The in-host dynamical system of the malaria parasite (7.1) with antimalarial drugs and malaria vaccines is hence bestowed as follows:

$$\begin{aligned}
\frac{dH}{dt} &= \Lambda_h - \frac{(1-u_1(t))\beta_1 HP}{1+b_0E} - \mu_h H,\\
\frac{dH_I}{dt} &= \frac{(1-u_1(t))\beta_1 HP}{1+b_0E} - \delta H_I - \vartheta_1 H_I E,\\
\frac{dR}{dt} &= \Lambda_r - \frac{(1-u_2(t))\beta_2 RM}{1+b_1E} - \mu_r R,\\
\frac{dR_I}{dt} &= \frac{(1-u_2(t))\beta_2 RM}{1+b_1E} - \alpha R_I - \vartheta_2 R_I E,\\
\frac{dM}{dt} &= \frac{(1-u_3(t))N\delta H_I}{1+b_2E} + \frac{(1-u_4(t))Q\alpha R_I}{1+b_3E} - \mu_m M - \vartheta_m ME - \frac{\beta_2 RM}{1+b_1E},\\
\frac{dP}{dt} &= \Lambda_p - \mu_p P - \frac{\beta_1 HP}{1+b_0E},\\
\frac{dG}{dt} &= \frac{cR_I}{1+b_4E} - u_4(t)G - \mu_g G - \vartheta_g GE,\\
\frac{dE}{dt} &= \tau\Lambda_e + E\left(\frac{\xi H_I}{1+a_0H_I} + \frac{\nu R_I}{1+a_2R_I} + \frac{\sigma M}{1+a_1M} + \frac{\theta G}{1+a_3G}\right) - \mu_e E,
\end{aligned} \tag{7.13}$$

with initial condition

$$H(0)>0, H_I(0)\geq 0, M(0)\geq 0, P(0)\geq 0, R(0)>0, R_I(0)\geq 0, G(0)\geq 0, E(0)>0. \tag{7.14}$$

We then apply the optimal control method using Pontryagin's Minimum Principle to determine the conditions under which disease eradication can be achieved in finite time $[0,t_f]$. We seek to minimize the number of infected hepatocytes, infected red blood cells, merozoites, and gametocytes plus the cost of applying treatment and vaccination controls. The objective function that we consider is defined as

$$J(u_1,u_2,u_3,u_4) = \int_0^{t_f}\left(A_1H_I + A_2R_I + A_3M + A_4G + \frac{1}{2}\sum_{i=1}^{4}B_iu_i^2\right)dt, \tag{7.15}$$

subjected to the dynamical system equation (7.13), where t_f is the final time and A_1, A_2, A_3, A_4, and B_i, for $i = 1,2,\cdots,4$ are positive weight. A linear function is used to cost infected hepatocytes, infected red blood cells, merozoites, and gametocytes. The cost of the controls $B_1u_1^2$, Bu_2^2, $B_3u_3^2$, and $B_4u_4^2$ are the quadratic form such that the terms $\frac{1}{2}B_1u_1^2$, $\frac{1}{2}B_2u_2^2$, $\frac{1}{2}B_3u_3^2$, and $\frac{1}{2}B_4u_4^2$ cost spending on the pre-erythrocyte vaccination, blood-stage vaccine, primary tissue schizonticides, and blood-stage schizontocides and gametocytocidal treatments, respectively. We look to find the optimal control u_1^*, u_2^*, u_3^*, and u_4^* such that

$$J(u_1^*,u_2^*,u_3^*,u_4^*) = min_{(u_1,u_2,u_3,u_4)\in\mathscr{U}}\ \{J(u_1,u_2,u_3,u_4)\},$$

where $\mathscr{U} = (u_1,u_2,u_3,u_4)$ such that u_i is Lesbegue measurable with $0\leq u_i\leq 1$, for all $t\in[0,t_f]$

is control set, $i = 1, 2, \cdots, 4$.

7.5.1 Existence of an optimal control

An optimal control problem exists if the five necessary conditions that define the optimal solutions $J(u_1^*, u_2^*, u_3^*, u_4^*) = min_{(u_1,u_2,u_3,u_4)\in\mathscr{U}} \{J(u_1, u_2, u_3, u_4)\}$ of problem (7.13) derived using the Pontryagin's Maximum Principle are satisfied.

Theorem 7.1. *Consider the objective functional (7.15), subjected to of system equation (7.13) and its initial boundary condition for state variable $Y(t) \in R^8$ and a control variable $u_i(t) \in U$, for $i = 1, \ldots, 4$ then there exists an optimal solution $J(u_1^*, u_2^*, u_3^*, u_4^*)$, such that*

$$J(u_1^*, u_2^*, u_3^*, u_4^*) = min_{(u_1,u_2,u_3,u_4)\in\mathscr{U}} \{J(u_1, u_2, u_3, u_4)\}$$

if the following necessary conditions are satisfied.

1. *The set of controls and the corresponding state variables are nonempty.*
2. *The control set U is convex and closed.*
3. *The right hand side of the state system is bounded by the linear function in the state and control variables.*
4. *The integrand of the objective function is convex.*
5. *There exist the non-negative constant numbers c_1, c_2 and $\vartheta > 1$ such that the integrand of the objective function is bounded below by $c_1 \left(\sum_{i=1}^{4} |u_i|\right)^{\frac{\vartheta}{2}} - c_2$, for $i = 1, 2, 3, 4$.*

Proof. The existence of an optimal control is verified by conditions stated in Fleming and Rishel (2012). From our the objective functional (7.15) of system equation (7.13), the set of all state variables $Y(t) \in R^8$ and the control variables $\{u_i(t) \in U : 0 \leq u_i(t) \leq 1\}, t \in [t_0, t_f]$ are non-negative. Thus, the first condition is satisfied. By the definition, the optimal solution $u^*(t)$ is convex and bounded in U and thus the second condition is also satisfied (Mlay et al., 2015; Collins et al., 2009). The optimal system (7.13) is bounded which evaluates the compactness needed for the existence of the optimal control (Athithan and Ghosh, 2015) and hence the third condition holds. Also, the integrand in the objective functional (7.15) is clearly convex on the control set U which proves the fourth condition. According to (Mlay et al., 2015), since the state variables are bounded, therefore the integrand is also bounded below by $c_1 \left(|u_1| + |u_2| + |u_3| + |u_4|\right)^{\frac{\vartheta}{2}} - c_2$. That is

$$A_1 H_I + A_2 R_I + A_3 M + A_4 G + \frac{1}{2} B_1 u_1^2 + \frac{1}{2} B_2 u_2^2 + \frac{1}{2} B_3 u_3^2 + \frac{1}{2} B_4 u_4^2 \geq c_1 \left(|u_1| + |u_2| + |u_3| + |u_4|\right)^{\frac{\vartheta}{2}} - c_2,$$

which satisfies the fifth condition. With those five conditions satisfied we therefore conclude that there exist control variables u_1^*, u_2^*, u_3^* and u_4^* such that

$$J(u_1^*, u_2^*, u_3^*, u_4^*) = min_{(u_1,u_2,u_3,u_4)\in\mathscr{U}} \{J(u_1, u_2, u_3, u_4)\}$$

□

7.5.2 Characterization of the optimal control

Here, we characterize the optimal controls $u^* = (u_1^*, u_2^*, u_3^*, u_4^*)$ which gives the optimal values for the control measures and the corresponding state variables $(H^*, H_I^*, R^*, R_I^*, M^*, P^*, G^*, E^*)$. The necessary conditions that an optimal solution must satisfy come from the Pontryagin Maximum Principle (Lenhart and Workman, 2007). The dynamical system equations (7.13) and the objectives function (7.15) are transformed by Pontryagin's Maximum Principle into a problem of minimizing a Hamiltonian, $\mathscr{H}$ pointwise concerning u_1, u_2, u_3, and u_4.

$$\begin{aligned}
\mathscr{H} =& A_1 H_I + A_2 R_I + A_3 M + A_4 G + \frac{1}{2}B_1 u_1^2 + \frac{1}{2}B_2 u_2^2 + \frac{1}{2}B_3 u_3^2 + \frac{1}{2}B_3 u_3^2 + \frac{1}{2}B_4 u_4^2 \\
&+ \lambda_1 \left(\Lambda_h - \frac{(1-u_1(t))\beta_1 HP}{1+b_0 E} - \mu_h H \right) + \lambda_2 \left(\frac{(1-u_1(t))\beta_1 HP}{1+b_0 E} - \delta H_I - \vartheta_1 H_I E \right) \\
&+ \lambda_3 \left(\Lambda_r - \frac{(1-u_2(t))\beta_2 RM}{1+b_1 E} - \mu_r R \right) + \lambda_4 \left(\frac{(1-u_2(t))\beta_2 RM}{1+b_1 E} - \alpha R_I - \vartheta_2 R_I E \right) \\
&+ \lambda_5 \left(\frac{(1-u_3(t))N\delta H_I}{1+b_2 E} + \frac{(1-u_4(t))Q\alpha R_I}{1+b_3 E} - \mu_m M - \vartheta_m M E - \frac{\beta_2 RM}{1+b_1 E} \right) \\
&+ \lambda_6 \left(\Lambda_p - \mu_p P - \frac{\beta_1 HP}{1+b_0 E} \right) + \lambda_7 \left(\frac{cR_I}{1+b_4 E} - u_4(t) G - \mu_g G - \vartheta_g G E \right) \\
&+ \lambda_8 \left(\tau \Lambda_e + E \left(\frac{\xi H_I}{1+a_0 H_I} + \frac{\nu R_I}{1+a_2 R_I} + \frac{\sigma M}{1+a_1 M} + \frac{\theta G}{1+a_3 G} \right) - \mu_e E \right),
\end{aligned} \tag{7.16}$$

where $\lambda_1, \lambda_2, \lambda_3, \lambda_4, \lambda_5, \lambda_6, \lambda_7$, and λ_8 are the adjoint variables or co-state variables. The system of equations is obtained by taking the appropriate partial derivatives of the Hamiltonian (7.16) concerning the associated state variable. Thus, the adjoint equations can be written as

$$\frac{d\lambda_i}{dt} = -\frac{\partial \mathscr{H}}{\partial j}, \tag{7.17}$$

where $i = 1, 2, \cdots, 8$, and $j = H, H_I, R, R_I, M, P, G, E$. This implies that

$$\begin{aligned}
\frac{d\lambda_1}{dt} &= -\frac{\partial \mathscr{H}}{\partial H} = \frac{(1-u_1)\beta_1 P}{1+b_0 E}(\lambda_1 + \lambda_6 - \lambda_2) - \mu_h \lambda_1, \\
\frac{d\lambda_2}{dt} &= -\frac{\partial \mathscr{H}}{\partial HI} = -A1 + (\delta + \theta_1 E)\lambda_2 - \frac{(1-u_3)N\delta}{1+b_2 E}\lambda_5 - \frac{\xi E}{(1+a_0 HI)^2}\lambda_8, \\
\frac{d\lambda_3}{dt} &= -\frac{\partial \mathscr{H}}{\partial R} = \frac{(1-u_2)\beta_2 M}{1+b_1 E}(\lambda_3 + \lambda_5 - \lambda_4) + \mu_r \lambda_3, \\
\frac{d\lambda_4}{dt} &= -\frac{\partial \mathscr{H}}{\partial RI} = -A2 + (\alpha + \vartheta_2 E)\lambda_4 - \frac{(1-u_4)Q\alpha}{1+b_3 E}\lambda_5 - \frac{\nu E \lambda_8}{(1+a_2 R_I)^2}, \\
\frac{d\lambda_5}{dt} &= -\frac{\partial \mathscr{H}}{\partial M} = -A3 + \frac{(1-u_2)\beta_2 R}{1+b_1 E}(\lambda_3 + \lambda_5 - \lambda_4) + (\mu_m + \vartheta_m E)\lambda_5 - \frac{\sigma E}{(1+a_1 M)^2}\lambda_8, \\
\frac{d\lambda_6}{dt} &= -\frac{\partial \mathscr{H}}{\partial P} = \frac{(1-u_1)\beta_1 H}{1+b_0 E}(\lambda_6 + \lambda_1 - \lambda_2) + \mu_p \lambda_6, \\
\frac{d\lambda_7}{dt} &= -\frac{\partial \mathscr{H}}{\partial G} = -A4 + (u_4 + \mu_g + \vartheta_g E)\lambda_7 - \frac{\theta E}{(1+a_3 G)^2}\lambda_8,
\end{aligned} \tag{7.18}$$

$$\frac{d\lambda_8}{dt} = -\frac{\partial \mathscr{H}}{\partial E} = \frac{(1-u_1)\beta_1 b_0 HP}{(1+b_0E)^2}(\lambda_2-\lambda_1-\lambda_6) + \frac{(1-u_2)\beta_2 b_1 MR}{(1+b_1E)^2}(\lambda_4-\lambda_3-\lambda_5) + \vartheta_1 H_I\lambda_2,$$
$$+ \vartheta_2 R_I\lambda_4 + \vartheta_m M\lambda_5 + \vartheta_g G\lambda_7 - \left(\frac{\xi H_I}{1+a_0H_I} + \frac{\nu R_I}{1+a_2R_I} + \frac{\sigma M}{1+a_1M} + \frac{\theta G}{1+a_2G}\right)\lambda_8,$$

and with transversality conditions

$$\lambda_1(t_f) = \lambda_2(t_f) = \lambda_3(t_f) = \lambda_4(t_f) = \lambda_5(t_f) = \lambda_6(t_f) = \lambda_7(t_f) = \lambda_8(t_f) = 0. \tag{7.19}$$

Theorem 7.2. *Given the optimal controls u_1^*, u_2^*, u_3^*, and u_4^* with optimal solutions H^*, H_I^*, R^*, R_I^*, M^*, P^*, G^*, and E^*, the adjoint variables λ_i, for $i = 1, 2, \cdots, 8$ exist and satisfying equations (7.18) and (7.19). Furthermore, the optimality conditions*

$$\begin{aligned}
u_1^* &= max\left\{0, min\left(\frac{(\lambda_2-\lambda_1-\lambda_6)\beta_1 H^*P^*}{B_1(1+b_0E^*)}, 1\right)\right\},\\
u_2^* &= max\left\{0, min\left(\frac{(\lambda_4-\lambda_3-\lambda_5)\beta_2 M^*R^*}{B_2(1+b_1E^*)}, 1\right)\right\},\\
u_3^* &= max\left\{0, min\left(\frac{\lambda_5 N\delta H_I^*}{B_3(1+b_2E^*)}, 1\right)\right\},\\
u_4^* &= max\left\{0, min\left(\frac{\lambda_5 \alpha Q R_I^*}{B_4(1+b_3E^*)}, 1\right)\right\},
\end{aligned} \tag{7.20}$$

is satisfied by the optimal control $(u_1^*, u_2^*, u_3^*, u_4^*)$ that minimizes objective function J over Ω.

Proof. The Fleming and Rishel (2012) gives the existence of an optimal control owing to the convexity of the integrand of the objective function J with respect to u_1, u_2, u_3, and u_4 , a priori boundedness of the state solutions, and the Lipschitz property of the state system with respect to the state variables. The adjoint system equation (7.18) is obtained by differentiating the Hamiltonian function, evaluated at the optimal control. Moreover, the derivatives of the Hamiltonian concerning the controls and equating to zero to obtain the optimal control variables as follows

$$\begin{aligned}
\frac{\partial \mathscr{H}}{\partial u_1} &= B_1u_1^* + (\lambda_1-\lambda_2+\lambda_6)\frac{\beta_1 H^*P^*}{1+b_0E^*} = 0,\\
\frac{\partial \mathscr{H}}{\partial u_2} &= B_2u_2^* + (\lambda_3-\lambda_4+\lambda_5)\frac{\beta_2 M^*R^*}{1+b_1E^*} = 0,\\
\frac{\partial \mathscr{H}}{\partial u_3} &= B_3u_3^* - \lambda_5\frac{N\delta H_I^*}{1+b_2E^*} = 0,\\
\frac{\partial \mathscr{H}}{\partial u_4} &= B_4u_4^* - \lambda_5\frac{\alpha Q R_I^*}{1+b_3E^*} = 0.
\end{aligned}$$

Hence, we obtain (detail see Lenhart and Workman (2007))

$$u_1^* = \frac{(\lambda_2-\lambda_1-\lambda_6)\beta_1 H^*P^*}{B_1(1+b_0E^*)}, \qquad u_3^* = \frac{\lambda_5 N\delta H_I^*}{B_3(1+b_2E^*)},$$

$$u_2^* = \frac{(\lambda_4 - \lambda_3 - \lambda_5)\beta_2 M^* R^*}{B_2(1+b_1E^*)}, \qquad u_4^* = \frac{\lambda_5 \alpha Q R_I^*}{B_4(1+b_3E^*)}.$$

Through standard control arguments involving the bounds of the controls, we found that

$$u_1^* = \begin{cases} 0 & if \quad \widetilde{u_1^*} \leq 0 \\ \widetilde{u_1^*} & if \quad 0 < \widetilde{u_1^*} < 1 \\ 1 & if \quad \widetilde{u_1^*} \geq 1 \end{cases} \quad u_2^* = \begin{cases} 0 & if \quad \widetilde{u_2^*} \leq 0 \\ \widetilde{u_2^*} & if \quad 0 < \widetilde{u_2^*} < 1 \\ 1 & if \quad \widetilde{u_2^*} \geq 1 \end{cases}$$

$$u_3^* = \begin{cases} 0 & if \quad \widetilde{u_3^*} \leq 0 \\ \widetilde{u_3^*} & if \quad 0 < \widetilde{u_3^*} < 1 \\ 1 & if \quad \widetilde{u_3^*} \geq 1 \end{cases} \quad u_4^* = \begin{cases} 0 & if \quad \widetilde{u_4^*} \leq 0 \\ \widetilde{u_4^*} & if \quad 0 < \widetilde{u_4^*} < 1 \\ 1 & if \quad \widetilde{u_4^*} \geq 1 \end{cases},$$

which leads to (7.20), where

$$\widetilde{u_1^*} = \frac{(\lambda_2 - \lambda_1 - \lambda_6)\beta_1 H^* P^*}{B_1(1+b_0E^*)}, \widetilde{u_2^*} = \frac{(\lambda_4 - \lambda_3 - \lambda_5)\beta_2 M^* R^*}{B_2(1+b_1E^*)}, \widetilde{u_3^*} = \frac{\lambda_5 N \delta H_I^*}{B_3(1+b_2E^*)}, \widetilde{u_4^*} = \frac{\lambda_5 \alpha Q R_I^*}{B_4(1+b_3E^*)}.$$

One way to confirm that the optimal control is a minimizer is to compute the Hessian matrix of the Hamiltonian $\mathscr{H}$ function and verify its positive definiteness with respect to the control u. The Hessian matrix of Hamiltonian $\mathscr{H}$ with respect to the control variables u is given as

$$\frac{\partial^2 \mathscr{H}}{\partial u^2} = \begin{bmatrix} \frac{\partial^2 \mathscr{H}}{\partial u_1^2} & \frac{\partial^2 \mathscr{H}}{\partial u_1 \partial u_2} & \frac{\partial^2 \mathscr{H}}{\partial u_1 \partial u_3} & \frac{\partial^2 \mathscr{H}}{\partial u_1 \partial u_4} \\ \frac{\partial^2 \mathscr{H}}{\partial u_2 \partial u_1} & \frac{\partial^2 \mathscr{H}}{\partial u_2^2} & \frac{\partial^2 \mathscr{H}}{\partial u_2 \partial u_3} & \frac{\partial^2 \mathscr{H}}{\partial u_2 \partial u_4} \\ \frac{\partial^2 \mathscr{H}}{\partial u_3 \partial u_1} & \frac{\partial^2 \mathscr{H}}{\partial u_3 \partial u_2} & \frac{\partial^2 \mathscr{H}}{\partial u_3^2} & \frac{\partial^2 \mathscr{H}}{\partial u_3 \partial u_4} \\ \frac{\partial^2 \mathscr{H}}{\partial u_4 \partial u_1} & \frac{\partial^2 \mathscr{H}}{\partial u_4 \partial u_2} & \frac{\partial^2 \mathscr{H}}{\partial u_4 \partial u_3} & \frac{\partial^2 \mathscr{H}}{\partial u_4^2} \end{bmatrix} = \begin{bmatrix} B_1 & 0 & 0 & 0 \\ 0 & B_2 & 0 & 0 \\ 0 & 0 & B_3 & 0 \\ 0 & 0 & 0 & B_4 \end{bmatrix},$$

which is a positive definite matrix as a consequence of the positive weights B_1, B_2, B_3, B_4 the Hamiltonian $\mathscr{H}$ is convex with respect to control variables and as a result optimal control $(u_1^*, u_2^*, u_3^*, u_4^*)$ is minimizer. □

7.5.3 Uniqueness of optimal control

In this section, we prove the uniqueness of an optimal control. According to Joshi et al. (2006), to show the uniqueness of an optimal control is the same as to show the uniqueness of an optimality system. The dynamical system (7.13) with properties of optimality system can be written as:

$$H^{'} = g_1(t, H, H_I, R, R_I, M, G, P, E)$$
$$H_I^{'} = g_2(t, H, H_I, R, R_I, M, G, P, E)$$
$$R^{'} = g_3(t, H, H_I, R, R_I, M, G, P, E)$$
$$R_I^{'} = g_4(t, H, H_I, R, R_I, M, G, P, E)$$

$$
\begin{aligned}
M^{'} &= g_5(t,H,H_I,R,R_I,M,G,P,E)\\
G^{'} &= g_6(t,H,H_I,R,R_I,M,G,P,E)\\
P^{'} &= g_7(t,H,H_I,R,R_I,M,G,P,E)\\
E^{'} &= g_5(t,H,H_I,R,R_I,M,G,P,E)
\end{aligned}
$$

$H(0),H_I(0),M(0),P(0),R(0),R_I(0),G(0),E(0)$ given, $H(t_f),H_I(t_f),M(t_f),P(t_f),R(t_f),R_I(t_f)$, $G(t_f),E(t_f)$ is given and fixed, where $H \in \mathbb{R}^{n_1},H_I \in \mathbb{R}^{n_2},R \in \mathbb{R}^{n_3},R_I \in \mathbb{R}^{n_4},M \in \mathbb{R}^{n_5},G \in \mathbb{R}^{n_6},P \in \mathbb{R}^{n_7},E \in \mathbb{R}^{n_8},n_i$, for $i = 1,2,\ldots,8$ is a dimension of vector space $\mathbb{R}^{n_i}$ and

$$
\begin{aligned}
g_1 &: \mathbb{R}\times\mathbb{R}^{n_1}\times\mathbb{R}^{n_2}\times\mathbb{R}^{n_3}\times\mathbb{R}^{n_4}\times\mathbb{R}^{n_5}\times\mathbb{R}^{n_6}\times\mathbb{R}^{n_7}\times\mathbb{R}^{n_8}\to\mathbb{R}^{n_1}\\
g_2 &: \mathbb{R}\times\mathbb{R}^{n_1}\times\mathbb{R}^{n_2}\times\mathbb{R}^{n_3}\times\mathbb{R}^{n_4}\times\mathbb{R}^{n_5}\times\mathbb{R}^{n_6}\times\mathbb{R}^{n_7}\times\mathbb{R}^{n_8}\to\mathbb{R}^{n_2}\\
g_3 &: \mathbb{R}\times\mathbb{R}^{n_1}\times\mathbb{R}^{n_2}\times\mathbb{R}^{n_3}\times\mathbb{R}^{n_4}\times\mathbb{R}^{n_5}\times\mathbb{R}^{n_6}\times\mathbb{R}^{n_7}\times\mathbb{R}^{n_8}\to\mathbb{R}^{n_3}\\
g_4 &: \mathbb{R}\times\mathbb{R}^{n_1}\times\mathbb{R}^{n_2}\times\mathbb{R}^{n_3}\times\mathbb{R}^{n_4}\times\mathbb{R}^{n_5}\times\mathbb{R}^{n_6}\times\mathbb{R}^{n_7}\times\mathbb{R}^{n_8}\to\mathbb{R}^{n_4}\\
g_5 &: \mathbb{R}\times\mathbb{R}^{n_1}\times\mathbb{R}^{n_2}\times\mathbb{R}^{n_3}\times\mathbb{R}^{n_4}\times\mathbb{R}^{n_5}\times\mathbb{R}^{n_6}\times\mathbb{R}^{n_7}\times\mathbb{R}^{n_8}\to\mathbb{R}^{n_5}\\
g_6 &: \mathbb{R}\times\mathbb{R}^{n_1}\times\mathbb{R}^{n_2}\times\mathbb{R}^{n_3}\times\mathbb{R}^{n_4}\times\mathbb{R}^{n_5}\times\mathbb{R}^{n_6}\times\mathbb{R}^{n_7}\times\mathbb{R}^{n_8}\to\mathbb{R}^{n_6}\\
g_7 &: \mathbb{R}\times\mathbb{R}^{n_1}\times\mathbb{R}^{n_2}\times\mathbb{R}^{n_3}\times\mathbb{R}^{n_4}\times\mathbb{R}^{n_5}\times\mathbb{R}^{n_6}\times\mathbb{R}^{n_7}\times\mathbb{R}^{n_8}\to\mathbb{R}^{n_7}\\
g_8 &: \mathbb{R}\times\mathbb{R}^{n_1}\times\mathbb{R}^{n_2}\times\mathbb{R}^{n_3}\times\mathbb{R}^{n_4}\times\mathbb{R}^{n_5}\times\mathbb{R}^{n_6}\times\mathbb{R}^{n_7}\times\mathbb{R}^{n_8}\to\mathbb{R}^{n_8}
\end{aligned}
$$

are continuous.

Theorem 7.3. *Assume that g_i, for $i = 1,2,\ldots,8$ are bounded and satisfy a Lipschitz condition relative to H,H_I,R,R_I,M,G,P, and E with constant $K > 0$. Then system (7.13) has a unique solutions if t_f is sufficiently small.*

Proof. Suppose the system equation (7.13) has two solutions $(H_1(t),H_{I1}(t),R_1(t),R_{I1}(t),M_1(t),G_1(t),P_1(t),E_1(t))$ and $(H_2(t),H_{I2}(t),R_2(t),R_{I2}(t),M_2(t),G_2(t),P_2(t),E_2(t))$. The Lipschitz condition on g_1 implies

$$
\begin{aligned}
||H_1(t)-H_2(t)|| \le \int_0^{t_1} K(&||H_1(s)-H_2(s)||+||H_{I1}(s)-H_{I2}(s)||+||R_1(s)-R_2(s)||\\
&+||R_{I1}(s)-R_{I2}(s)||+||M_1(s)-M_2(s)||+||G_1(s)-G_2(s)||\\
&+||P_1(s)-P_2(s)||+||E_1(s)-E_2(s)||)ds
\end{aligned}
\tag{7.21}
$$

Lipschitz condition on solutions $H_{I1}(t)$ and $H_{I2}(t)$ result to:

$$
\begin{aligned}
||H_{I1}(t)-H_{I2}(t)|| \le \int_{t_1}^{t_2} K(&||H_1(s)-H_2(s)||+||H_{I1}(s)-H_{I2}(s)||+||R_1(s)-R_2(s)||\\
&+||R_{I1}(s)-R_{I2}(s)||+||M_1(s)-M_2(s)||+||G_1(s)-G_2(s)||\\
&+||P_1(s)-P_2(s)||+||E_1(s)-E_2(s)||)ds
\end{aligned}
\tag{7.22}
$$

In the similar ways, we can perform the Lipschitz condition on solutions of the remain state

variables and we obtained.

$$\begin{aligned}||R_1(t)-R_2(t)|| \leq \int_{t_2}^{t_3} K(&||H_1(s)-H_2(s)||+||H_{I1}(s)-H_{I2}(s)||+||R_1(s)-R_2(s)|| \\ &+||R_{I1}(s)-R_{I2}(s)||+||M_1(s)-M_2(s)||+||G_1(s)-G_2(s)|| \\ &+||P_1(s)-P_2(s)||+||E_1(s)-E_2(s)||)ds\end{aligned} \tag{7.23}$$

$$\begin{aligned}||R_{I1}(t)-R_{I2}(t)|| \leq \int_{t_3}^{t_4} K(&||H_1(s)-H_2(s)||+||H_{I1}(s)-H_{I2}(s)||+||R_1(s)-R_2(s)|| \\ &+||R_{I1}(s)-R_{I2}(s)||+||M_1(s)-M_2(s)||+||G_1(s)-G_2(s)|| \\ &+||P_1(s)-P_2(s)||+||E_1(s)-E_2(s)||)ds\end{aligned} \tag{7.24}$$

$$\begin{aligned}||M_1(t)-M_2(t)|| \leq \int_{t_4}^{t_5} K(&||H_1(s)-H_2(s)||+||H_{I1}(s)-H_{I2}(s)||+||R_1(s)-R_2(s)|| \\ &+||R_{I1}(s)-R_{I2}(s)||+||M_1(s)-M_2(s)||+||G_1(s)-G_2(s)|| \\ &+||P_1(s)-P_2(s)||+||E_1(s)-E_2(s)||)ds\end{aligned} \tag{7.25}$$

$$\begin{aligned}||G_1(t)-G_2(t)|| \leq \int_{t_5}^{t_6} K(&||H_1(s)-H_2(s)||+||H_{I1}(s)-H_{I2}(s)||+||R_1(s)-R_2(s)|| \\ &+||R_{I1}(s)-R_{I2}(s)||+||M_1(s)-M_2(s)||+||G_1(s)-G_2(s)|| \\ &+||P_1(s)-P_2(s)||+||E_1(s)-E_2(s)||)ds\end{aligned} \tag{7.26}$$

$$\begin{aligned}||P_1(t)-P_2(t)|| \leq \int_{t_6}^{t_7} K(&||H_1(s)-H_2(s)||+||H_{I1}(s)-H_{I2}(s)||+||R_1(s)-R_2(s)|| \\ &+||R_{I1}(s)-R_{I2}(s)||+||M_1(s)-M_2(s)||+||G_1(s)-G_2(s)|| \\ &+||P_1(s)-P_2(s)||+||E_1(s)-E_2(s)||)ds\end{aligned} \tag{7.27}$$

Finally, Lipschitz condition on solutions $E_1(t)$ and $E_2(t)$, where t_f is final time is given by:

$$\begin{aligned}||E_1(t)-E_2(t)|| \leq \int_{t_7}^{t_f} K(&||H_1(s)-H_2(s)||+||H_{I1}(s)-H_{I2}(s)||+||R_1(s)-R_2(s)|| \\ &+||R_{I1}(s)-R_{I2}(s)||+||M_1(s)-M_2(s)||+||G_1(s)-G_2(s)|| \\ &+||P_1(s)-P_2(s)||+||E_1(s)-E_2(s)||)ds\end{aligned} \tag{7.28}$$

Adding (7.21), (7.22), (7.23), (7.24), (7.25), (7.26), (7.27), and (7.28) together yields:

$$\begin{aligned}&||H_1(t)-H_2(t)||+||H_{I1}(t)-H_{I2}(t)||+||R_1(t)-R_2(t)||+||R_{I1}(t)-R_{I2}(t)||+||M_1(t)-M_2(t)|| \\ &+||G_1(t)-G_2(t)||+||P_1(t)-P_2(t)||+||E_1(t)-E_2(t)|| \\ &\quad\leq \int_0^{t_f} K(||H_1(s)-H_2(s)||+||H_{I1}(s)-H_{I2}(s)||+||R_1(s)-R_2(s)||+||R_{I1}(s)-R_{I2}(s)|| \\ &\qquad +||M_1(s)-M_2(s)||+||G_1(s)-G_2(s)||+||P_1(s)-P_2(s)||+||E_1(s)-E_2(s)||)ds\end{aligned}$$

Applying Mean Value Theorem (MVT) for integrals, there exists a ℓ, $0 \leq \ell \leq t_f$, such that

$$||H_1(t)-H_2(t)||+||H_{I1}(t)-H_{I2}(t)||+||R_1(t)-R_2(t)||+||R_{I1}(t)-R_{I2}(t)||+||M_1(t)-M_2(t)||$$
$$+||G_1(t)-G_2(t)||+||P_1(t)-P_2(t)||+||E_1(t)-E_2(t)||\leq t_f K(||H_1(\ell)-H_2(\ell)||+||H_{I1}(\ell)-H_{I2}(\ell)||$$
$$+||R_1(\ell)-R_2(\ell)||+||R_{I1}(\ell)-R_{I2}(\ell)||+||M_1(\ell)-M_2(\ell)||+||G_1(\ell)-G_2(\ell)||+||P_1(\ell)-P_2(\ell)||$$
$$+||E_1(\ell)-E_2(\ell)||),$$

for all $t\in[0,t_f]$. If t_f is so small that $t_f K<1$, we arrive at a contradiction, completing the proof. □

7.6 Numerical solution of the optimal control problem

In this section, we present the numerical simulation of the optimal control problem (7.13), to illustrate the effectiveness of control intervention using PYTHON software. The simulation is computed using the forward-backward sweep algorithm and the fourth-order Runge-Kutta scheme is applied to solve the optimality system. The forward-backward sweep method is implemented as follows: First, we initialize the control parameters as zeros and solve for the state variables (7.13) using the forward fourth-order Runge-Kutta method in time using the initial conditions. Then, we solve the adjoint equation (7.18) using backward in time with the transversality conditions (7.19) according to their differential equations in the optimality system (Lenhart and Workman (2007)). The procedure is carried out until the stopping requirement is achieved. The parameter values utilized in the simulations are listed in Table 7.3. The weight constants that we utilized during the simulation are given as $A_1=1, A_2=1, A_3=1, A_4=1, B_1=2900, B_2=9000, B_3=4600$, and $B_4=800$. Using combinations of double controls, triple controls, and all four controls, we have identified eleven control strategies. However, our analysis indicates that seven of these strategies are the most effective in mitigating the malaria parasite within host cells. Therefore, we will focus on implementing the following most effective control strategies:

1. Double control strategy
   - Strategy 1: Combination of pre-erythrocytic vaccine, $u_1(t)\neq 0$ and blood-stage vaccine, $u_2\neq 0$, $u_3=0$, $u_4=0$.
   - Strategy 2: Combination of pre-erythrocytic vaccine, $u_1(t)\neq 0$ and blood-schizontocides and gametocytocides, $u_4\neq 0$, $u_2=0$, $u_3=0$.
   - Strategy 3: Combination of blood-stage vaccine, $u_2(t)\neq 0$ and blood-schizontocides and gametocytocides, $u_4\neq 0$, $u_1=0$, $u_3=0$.
2. Triple control strategy
   - Strategy 4: Combination of pre-erythrocytic vaccine, $u_1\neq 0$, blood-stage vaccine $u_2\neq 0$, and blood-schizontocides and gametocytocides, $u_4(t)\neq 0$, $u_3=0$.

- Strategy 5: Combination of pre-erythrocytic vaccine, $u_1 \neq 0$, primary tissue schizontocides $u_3 \neq 0$, and blood-schizontocides and gametocytocides, $u_4(t) \neq 0$, $u_2 = 0$.
- Strategy 6: Combination of blood-stage vaccine, $u_2 \neq 0$, primary tissue schizontocides $u_3 \neq 0$, and blood-schizontocides and gametocytocides, $u_4(t) \neq 0$, $u_1 = 0$.

3. All four control strategy
   - Strategy 7: Combination of pre-erythrocytic vaccine, $u_1 \neq 0$, blood-stage vaccine $u_2 \neq 0$, primary tissue schizontocides, $u_3(t) \neq 0$, and blood-schizontocides and gametocytocides $u_4 \neq 0$.

7.6.1 Strategy 1: $u_1 \neq 0,\ u_2 \neq 0,\ u_3 = 0,\ u_4 = 0$

The implementation of strategy 1 (combination of pre-erythrocytic vaccine and blood-stage vaccine) in the prevention of malaria parasite infection in human hosts is presented in Figure 7.6. As seen in Figures 7.6(a)-(d), malarial prevention with such a combination is highly effective in mitigating the infected hepatocytes, infected erythrocytes, merozoites, and gametocytes within the host cell. The control profile corresponding the Strategy 1 is displayed in Figure 7.7. From Figure 7.7, we see that the pre-erythrocytic vaccine (u_1) will start decreasing after about 35 days throughout the intervention period, while the blood-stage vaccine (u_2) will start decreasing after about 58 days. Thus, pre-erythrocytic vaccine prevention (control u_1) should be optimally implemented.

7.6.2 Strategy 2: $u_1 \neq 0,\ u_2 = 0,\ u_3 = 0,\ u_4 \neq 0$

The impact of pre-erythrocytic vaccine and blood schizontocides and gametocytocides in the control of the malaria parasite infection are shown in Figure 7.8. The implementation of the combination of these controls will slightly reduce the infected hepatocytes, and infected red blood cells (see Figures 7.8(a) and (b)). The gametocytes were reducing exponentially within a time interval (Figure (7.8(c))), and merozoites were eradicated over approximately twenty days (see Figure 7.8(d)). Figure 7.9 demonstrates the control profile of the pre-erythrocytic vaccine, and blood schizontocides and gametocytocides. The control u_1 is effect for 48 days before declining to zero, but the control u_2 begins to decrease after 22 days.

7.6.3 Strategy 3: $u_1 = 0,\ u_2 \neq 0,\ u_3 = 0,\ u_4 \neq 0$

Figure 7.10 illustrates the implementation of the blood-stage vaccine and blood schizontocides and gametocytocides in the maximization of the eradication of malaria infection within the human host. The application of this control strategy has no impact on infected hepatocytes due to the inactivation of the blood-stage vaccine, and blood schizontocides and gametocytocides at the liver stage of infection (see Figure 7.10)(a). Following Figures 7.10(c)-(d), note

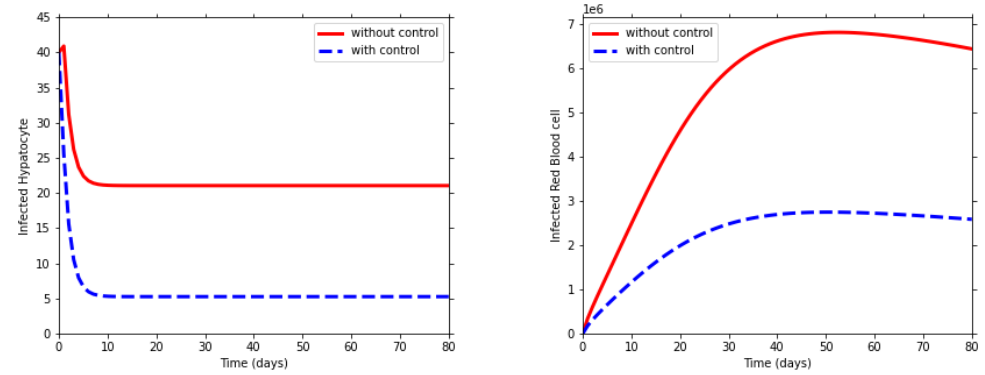

(a)

(b)

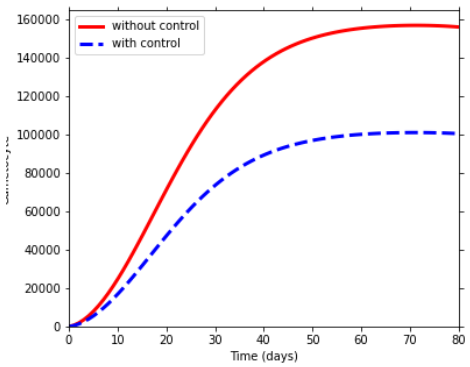

(c)

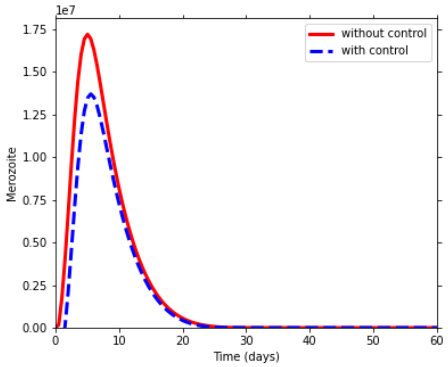

(d)

Figure 7.6: Simulation of infected hepatocytes, iRBCs, gametocytes and merozoites with double controls strategy pre-erythrocytic vaccine, $u_1(t) \neq 0$ and blood-stage vaccine, $u_2 \neq 0$, $u_3 = 0,\ u_4 = 0$. Utilized parameter values are given in Table 7.3.

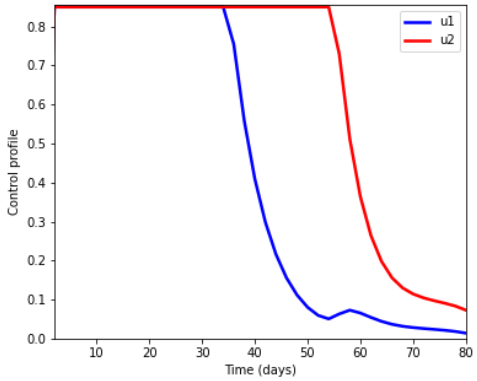

Figure 7.7: Control profiles of pre-erythrocytic vaccine (u_1) and blood-stage vaccine (u_2). Here, $u_3 = 0, u_4 = 0$.

that the infected red blood cells, gametocytes, and merozoites are reducing in period. Figure 7.11 exhibits the control profiles of blood stage vaccine (u_2) and blood-schizontocides and gametocytocidal (u_4).

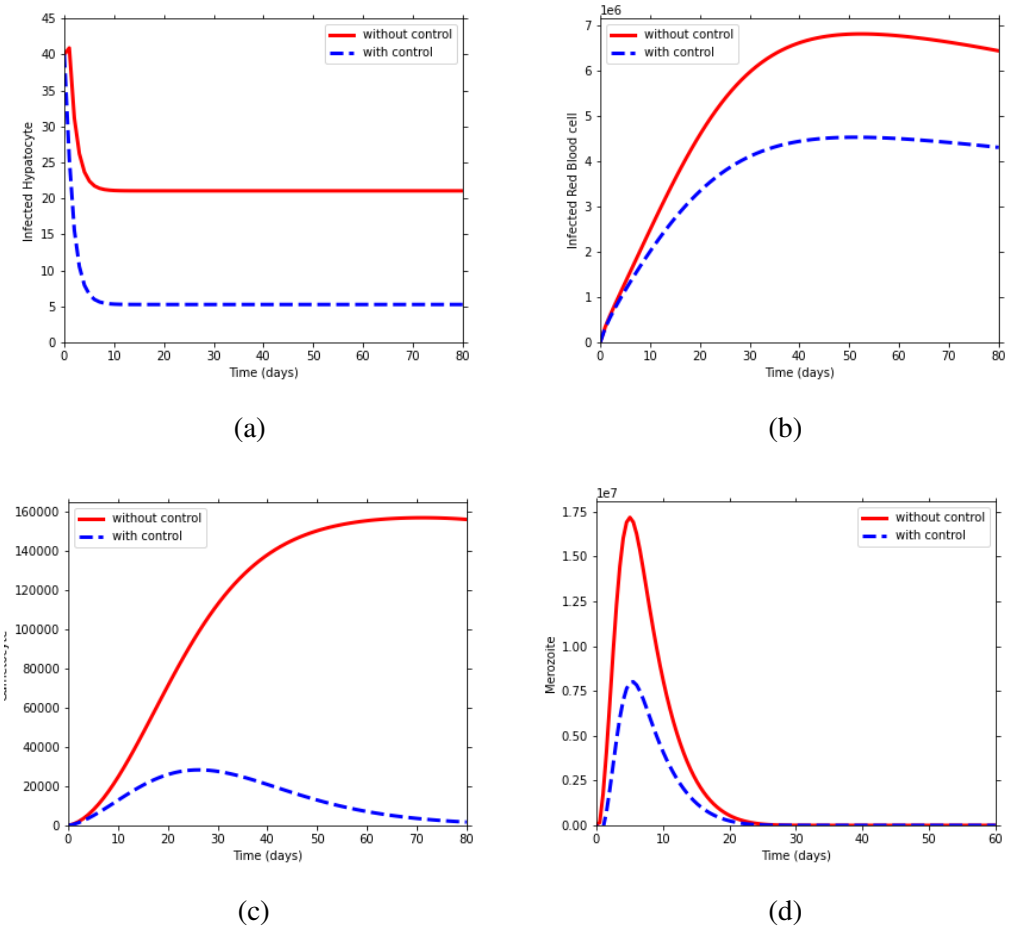

Figure 7.8: Simulation of infected hepatocytes, iRBCs, gametocytes, and merozoites with double controls strategy pre-erythrocytic vaccine, $u_1(t) \neq 0$ and blood-schizontocides, $u_4 \neq 0$, $u_2 = 0,\ u_3 = 0$. Utilized parameter values are given in Table 7.3.

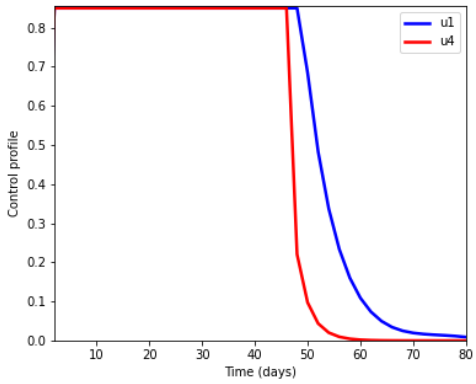

Figure 7.9: Control profiles of pre-erythrocytic vaccine (u_1) and blood schizontocides (u_4). Here, $u_2 = 0, u_3 = 0$.

7.6.4 Strategy 4: $u_1 \neq 0,\ u_2 \neq 0,\ u_3 = 0,\ u_4 \neq 0$

The administration of a combination of three controls, such as a pre-erythrocytic vaccine, blood-stage vaccine, and blood schizontocides and gametocytocidal in control of malaria in-

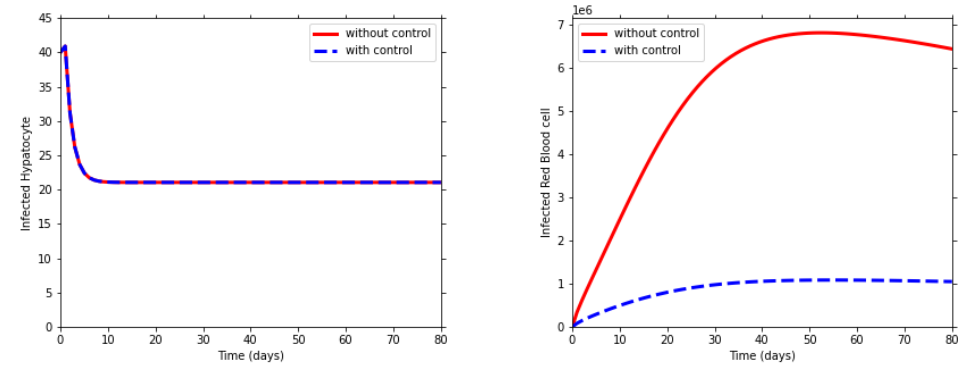

(a) (b)

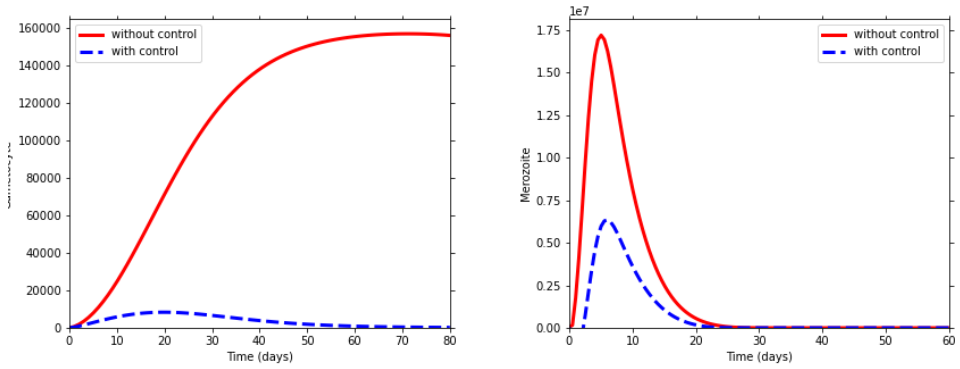

(c)

Figure 7.10: Simulation of infected hepatocytes, iRBCs, gametocytes and merozoites with double controls strategy blood-stage vaccine, $u_2(t) \neq 0$ and blood-schizontocides and gametocytocides, $u_4 \neq 0$, $u_1 = 0$ $u_3 = 0$. Utilized parameter values are given in Table 7.3.

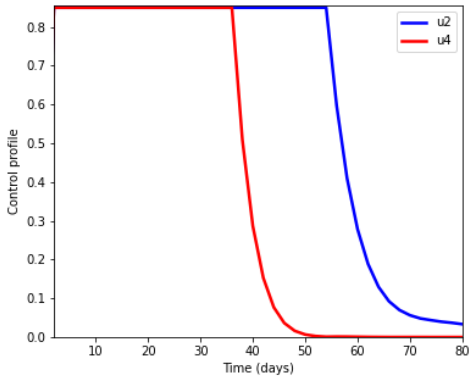

Figure 7.11: Control profiles of blood-stage vaccine (u_2) and blood-schizontocides and gametocytocides (u_4). Here $u_1 = 0, u_3 = 0$.

fection is shown in Figure 7.12. The administration of such a control strategy has strongly affected the dynamics of the infected hepatocytes, infected red blood cells, gametocytes, and merozoites (Figures 7.12(a)-(d)). Furthermore, the merozoite population is eliminated within the time of intervention after twenty days, while the gametocyte population is eliminated af-

ter 70 days. Figure 7.13 visually illustrates the control profiles for the pre-erythrocytic vaccination, blood-stage vaccines, blood schizontocides, and gametocytocides. The simulation demonstrates that the blood schizontocides and gametocytocides are functioning at their best.

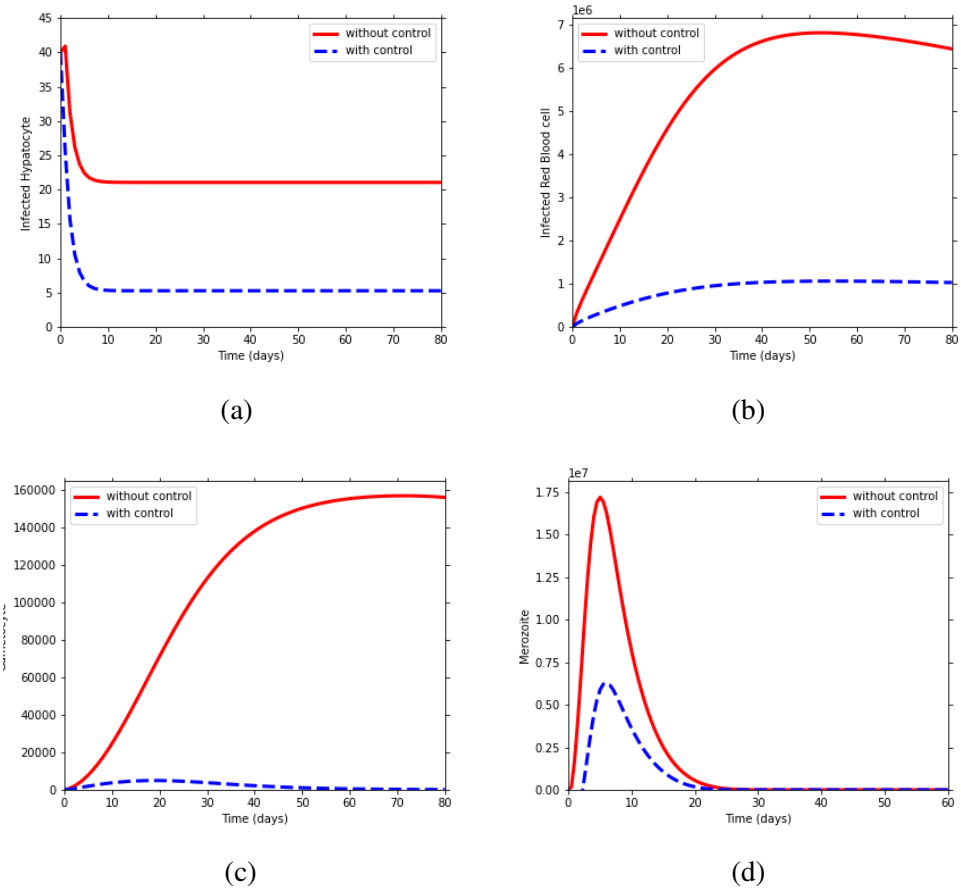

Figure 7.12: Simulation of infected hepatocytes, iRBCs, gametocytes, and merozoites with triple controls strategy pre-erythrocytic vaccine, $u_1 \neq 0$, blood-stage vaccine $u_2 \neq 0$, and blood-schizontocides, and gametocytocides, $u_4 \neq 0$, $u_3 = 0$. Utilized parameter values are given in Table 7.3.

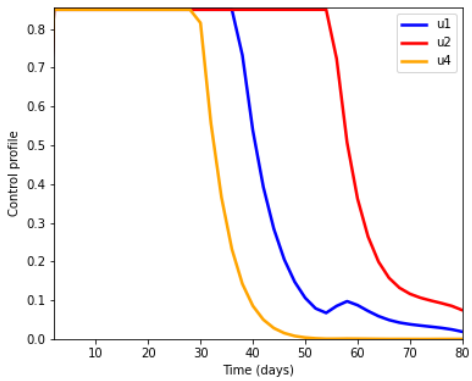

Figure 7.13: Control profiles of pre-erythrocytic vaccine (u_1) , blood-stage vaccine (u_2), and blood-schizontocides, and gametocytocides (u_4). Here, $u_3 = 0$.

7.6.5 Strategy 5: $u_1 \neq 0,\ u_2 = 0,\ u_3 \neq 0,\ u_4 \neq 0$

Figure 7.14 represents the results of the employment of the triple control techniques, which include pre-erythrocytic vaccine, primary tissue schizontocides, and blood-schizontocides, and gametocytocides. According to the results, employing these controls lowers the levels of infected hepatocytes and infected red blood cells in the human host (see Figures 7.14(a) and (b)). Furthermore, the simulation shows that the implementation of the strategy is more effective on merozoites and gametocyte parasites (Figures 7.14(c) and (d)). The associated control profile is presented in Figure 7.15.

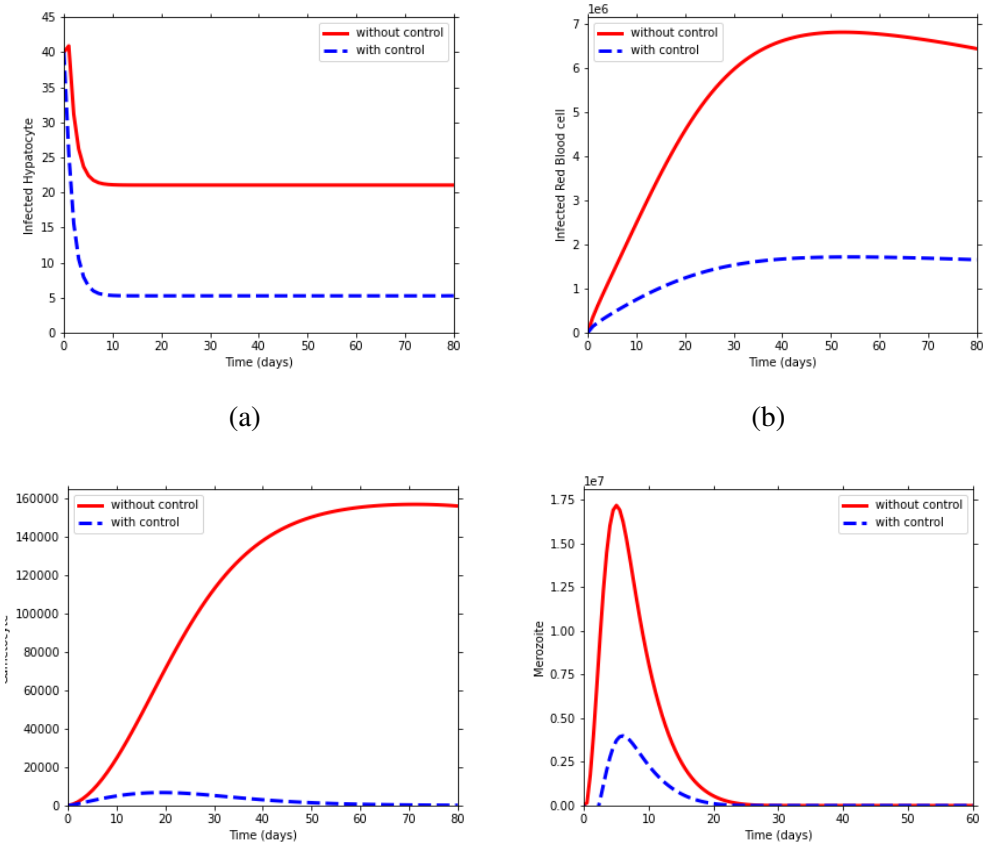

Figure 7.14: Simulation of infected hepatocytes, iRBCs, gametocytes, and merozoites with triple controls strategy pre-erythrocytic vaccine, $u_1 \neq 0$, primary tissue schizontocides $u_3 \neq 0$, and blood-schizontocides, and gametocytocides, $u_4 \neq 0$, $u_2 = 0$. Utilized parameter values are given in Table 7.3.

7.6.6 Strategy 6: $u_1 = 0,\ u_2 \neq 0,\ u_3 \neq 0,\ u_4 \neq 0$

The impact of the implementation of the combination of the blood-stage vaccine, primary tissue schizon-tocides, and blood schizontocides and gametocytocides in the control of the malaria parasite in humans is presented in Figure 7.16. The implementation of the control strategy does not affect the infected hepatocytes, because the blood-stage vaccine, blood sch-

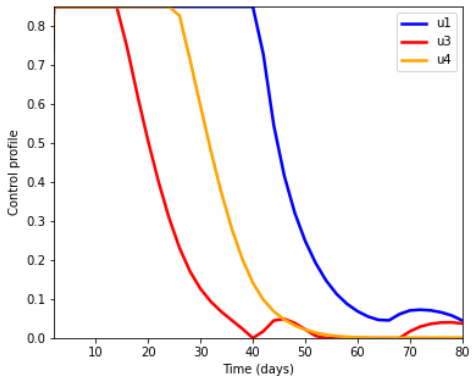

Figure 7.15: Control profiles of pre-erythrocytic vaccine (u_1) , primary tissue schizontocides (u_3), and blood-schizontocides, and gametocytocides (u_4), $u_2 = 0$.

izontocides and gametocytocidal are inactive at liver-stage infection, and primary tissue schizontocides are effective in reducing the rate of rupture of infected hepatocytes but do not occupy the hepatocyte invasion (Figure 7.16(a)). However, the population of infected gametocytes, merozoites, and infected red blood cells is decreasing over time (Figure 7.16(c)-(d)). In Figure 7.17, the associated control profile is presented. The control strategy reveals that the blood schizontocides and gametocytocidal considered as optimal.

7.6.7 Strategy 7: $u_1 \neq 0,\ u_2 \neq 0,\ u_3 \neq 0,\ u_4 \neq 0$

Figure 7.18 demonstrates the impact of carrying out all four measures together on preventing malaria infection in human hosts. The result suggests that the infection will be reduced within the infected individual, which means that all populations of gametocytes, and merozoites will be eradicated within the infected individual (Figure 7.18 (c)-(d)). The infected hepatocytes and infected red blood cells are reduced to small amounts (Figure 7.18 (a)-(b)). This strategy is the most effective controlling the in-host malaria parasite infection when compared to the other ones. Figure 7.19 reveals the control profiles of pre-erythrocytic vaccines, blood-stage vaccines, primary tissue schizontocides, and blood schizontocides and gametocytocides.

7.7 Summary

In this Chapter, we investigate the deterministic within-host malaria parasite infection model with an optimal control strategy. The well-posedness and epidemiological meaningfulness of the developed model were proved by demonstrating the positivity and boundedness of all solutions in the feasible region. The parasite-free equilibrium point and its stability analysis are performed. The parasite-free equilibrium point is locally and globally stable if the within-host basic reproduction number is less than unity. A sensitivity analysis of the basic reproduction number is investigated using a normalized forward sensitivity index. The infection rate of the red blood cell by merozoites, the average number of merozoites per ruptured

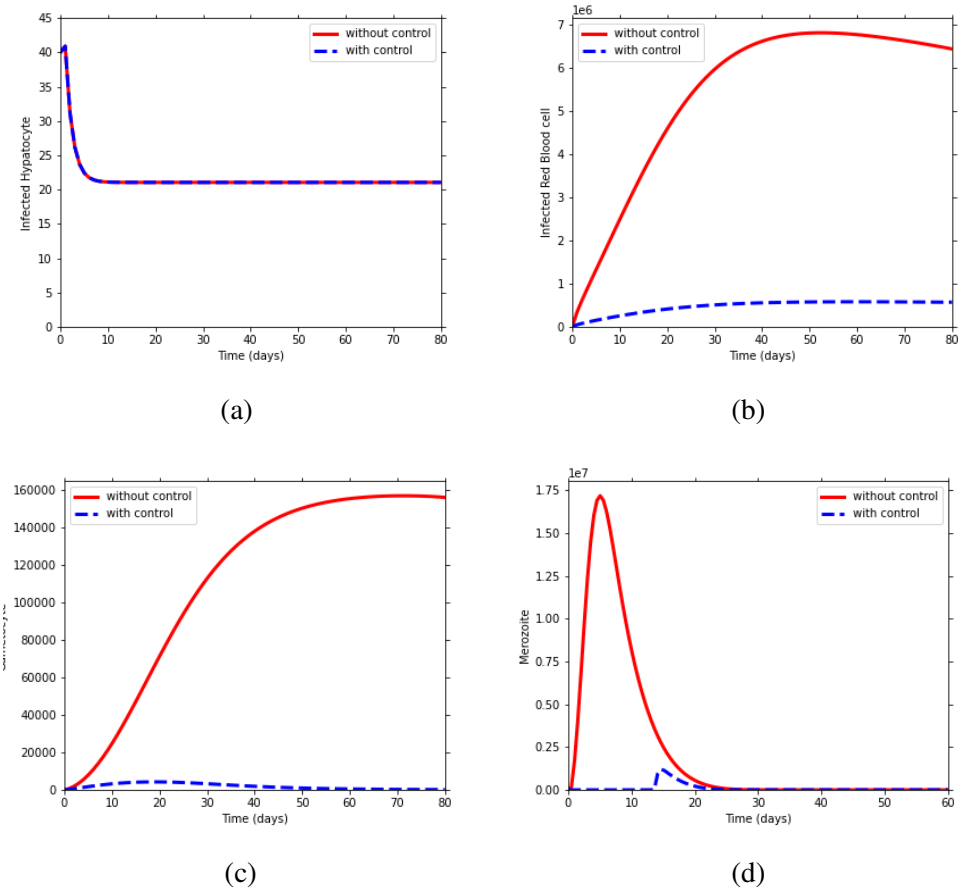

Figure 7.16: Simulation of infected hepatocytes, iRBCs, gametocytes, and merozoites with triple controls strategy blood-stage vaccine, $u_2 \neq 0$, primary tissue schizontocides $u_3 \neq 0$, and blood-schizontocides, and gametocytocides, $u_4 \neq 0$, $u_1 = 0$. Utilized parameter values are given in Table 7.3.

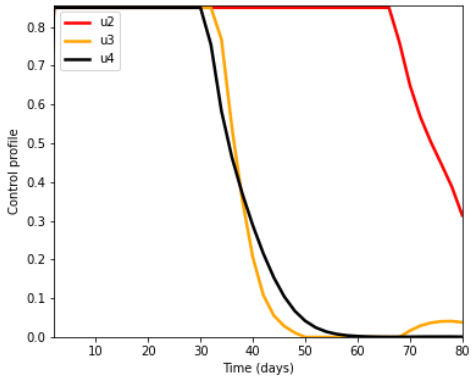

Figure 7.17: Control profiles of blood-stage vaccine (u_2) , primary tissue schizontocides (u_3), and blood-schizontocides, and gametocytocides (u_4), $u_1 = 0$.

infected red blood cells, and the removal rate of infected erythrocytes due to the immune system are the most influential parameters in the model. To mitigate the in-human host infection of the malaria parasite, we extended an optimal control model by integrating four control

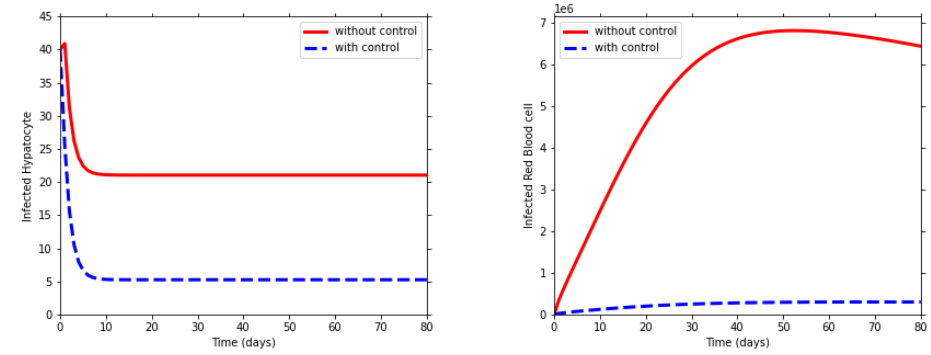

(a)

(b)

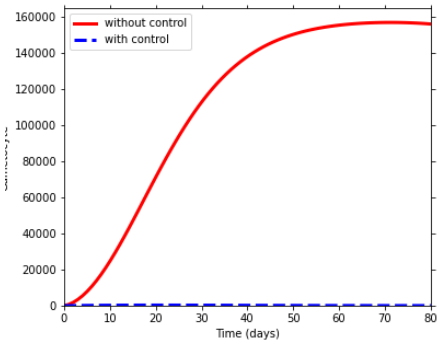

(c)

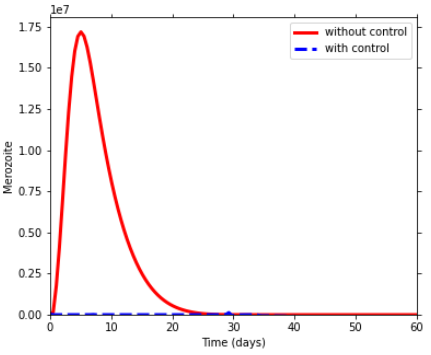

(d)

Figure 7.18: Simulation of infected hepatocytes, iRBCs, gametocytes, and merozoites with triple controls strategy pre-erythrocytic vaccine, $u_1 \neq 0$, blood-stage vaccine, $u_2 \neq 0$, primary tissue schizontocides $u_3 \neq 0$, and blood-schizontocides, and gametocytocides, $u_4 \neq 0$. Utilized parameter values are given in Table 7.3.

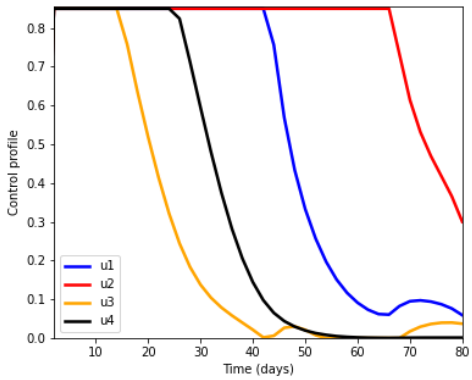

Figure 7.19: Control profiles of pre-erythrocytic vaccine (u_1) blood-stage vaccine (u_2) , primary tissue schizontocides (u_3), and blood-schizontocides, and gametocytocides (u_4).

variables: pre-erythrocytic vaccine, blood stage vaccine, primary tissue schizontocides, and blood-schizontocides and gametocytocidal drugs (gametocytocides). The control functions are implemented to maximize the eradication of the infected hepatocytes, infected red blood cells, gametocytes, and merozoites in the human host with minimum cost of malaria vaccine and an-

timalarial drug treatment. Then, the optimal control characterization is computed analytically. We characterized the optimal control via the application of Pontryagin's Minimum Principle and obtained an optimality system that satisfied the necessary conditions. Furthermore, to control within-host parasite infection, we considered the double control strategy, triple control strategy, and all four control strategies. Finally, several numerical simulation is investigated, to support our analytical findings. We used PYTHON software to investigate the numerical simulation. The simulation is computed using the forward-backward sweep algorithm and the fourth-order Runge-Kutta scheme is applied to solve the optimality system. The result shows that the implementation of all four control strategies is powerful for the eradication of in-host malaria infection.

CHAPTER 8

FRACTIONAL-ORDER MATHEMATICAL MODEL FOR THE WITHIN-HOST DYNAMICS OF MALARIA PARASITE INFECTION

In this chapter, we develop a fractional order mathematical model within-host dynamics of malaria infection. The within-host malaria model that describes the dynamics of the malaria infection during the erythrocyte-hepatocyte stages with memory effect is presented using Caputo fractional derivative. The model consider the interactions of liver hepatocyte cells, erythrocytes cells, malaria parasites, and immunological system. The basic properties and qualitative analysis of the in-host model are discussed.

8.1 Model Formulation

In this section, we developed a fractional-order mathematical model of within-host cell malaria parasite dynamics within the immune response. The developed model considers the interaction of eight cell populations: sporozoites $S(t)$, uninfected hepatocytes $H(t)$, infected hepatocytes $X(t)$, uninfected red blood cells (RBCs) $R(t)$, infected red blood cells (iRBCs) $Y(t)$, merozoites $M(t)$, gametocytes $G(t)$ and immune response $I(t)$ at a time t.
The formulated mathematical model is governed by the following assumptions.

i. The infection (invasion) of hepatocyte and erythrocyte cells is inhibited at a rate $1/(1+b_0I)$.

ii. The production of merozoites from liver schizontoside and blood schizontoside as well as gametocytes are inhibited by the rate of $1/(1+b_1I)$.

iii. The stimulation rate of immunological response is inhibited by infected red blood cells, infected hepatocyte cells, merozoite, and gametocyte at a rate $1/(1+a_0k_i)$, for $k_i = X, Y, M$ and G.

The female Anopheles mosquito injects sporozoites into the human skin during blood feeding at a constant rate π_s, and invades the hepatocyte at a rate β_1. The invasion of hepatocytes is inhibited owing to the host immune defense at a rate $\beta_1/(1+b_0I)$ and assumes that sporozoite can die naturally at a rate μ_s. The hepatocyte is produced from bone marrow at a constant rate π_h and dies naturally at a rate μ_h. Infected hepatocytes mature into liver schizonts and burst open releasing a thousand merozoites into the blood cells at a rate $N\delta$, where N is the average number of merozoites that are generated per ruptured liver schizonts. They are removed during burst at a rate δ and by immune response at a rate ϖ_x. The uninfected red blood cells (RBCs) are produced at a constant rate π_r from the bone marrow and get infected when invited by merozoites that are released from liver-stage schizonts at a rate β_2. The invasion is inhabited

by the immune response at a rate of $\beta_2/(1+b_0I)$. The uninfected RBCs die naturally at a rate μ_r. Due to invasion by merozoites, the healthy RBCs get infected, and propagate to the formation of infected red blood cells. The iRBCs rupture and release 8-32 daughters of merozoites into the bloodstream at a rate $Q\gamma$, the parameter Q represents the average number of merozoites that are produced per burst of infected red blood cells.

The merozoite populations are produced when the infected hepatocyte (liver-schizonts) and infected erythrocyte (blood-schizonts) rupture and release merozoites in the blood system at the rates $N\delta$ and $Q\alpha$, respectively. The production is haunted due to the presence of the immune system at a rate of $(N\delta+Q\alpha)/(1+b_1I)$. The merozoites die naturally at a rate μ_m and are killed (removed) by the immune response at a rate ϖ_m. During blood invasion, some of the merozoites go under sexual replication (gametocytes) at the rate c. Also, the gametocytes suffer natural death at a rate μ_g and are removed by the immune response at the rate ϖ_g. An immune system recruited from bone marrow at a rate π_i and stimulated owing to the presence of malaria infection at the rates ξ, ν, σ, θ, and the stimulation is inhibited at a rate $1/(1+a_0k_i)$, where $k_i = X,Y,M$, and G. The immune system suffers natural death at a rate μ_i. We assume that the observation of sporozoites by uninfected hepatocytes and merozoites by healthy erythrocytes is neglected.

Using the above assumptions and descriptions, we have the following governed integer-order compartmental mathematical model for the within-host malaria parasite infection.

$$\begin{aligned}
\frac{dS}{dt} &= \pi_s - \mu_s S,\\
\frac{dH}{dt} &= \pi_h - \frac{\beta_1 HS}{1+b_0I} - \mu_h H,\\
\frac{dX}{dt} &= \frac{\beta_1 HS}{1+b_0I} - \delta X - \varpi_x XI,\\
\frac{dR}{dt} &= \pi_r - \frac{\beta_2 RM}{1+b_oI} - \mu_r R,\\
\frac{dY}{dt} &= \frac{\beta_2 RM}{1+b_0I} - \gamma Y - \varpi_y YI,\\
\frac{dM}{dt} &= \frac{N\delta X}{1+b_1I} + \frac{Q\gamma Y}{1+b_1I} - \mu_m M - \varpi_m MI,\\
\frac{dG}{dt} &= \frac{cY}{1+b_1I} - \mu_g G - \varpi_g GI,\\
\frac{dI}{dt} &= \pi_i + I\left(\frac{\xi X}{1+a_0X} + \frac{\nu Y}{1+a_0Y} + \frac{\sigma M}{1+a_0M} + \frac{\theta G}{1+a_0G}\right) - \mu_i I,
\end{aligned} \tag{8.1}$$

with initial condition

$$S(0)\geq 0, H(0)>0, X(0)\geq 0, R(0)>0, Y(0)=>0, M(0)>0, G(0)>0, I(0)>0. \tag{8.2}$$

Next, we extend the within-host malaria parasite infection model (8.1) into fractional order model using a Caputo fractional-order derivative in order to observe the memory effects and

gain more insights about the in-host dynamics of parasite infection.
Dynamical system (8.1) in terms of integral form is followed by substituting the value of kernel as a power-law correlation function. So, applying fractional integral of order $(1-\alpha)$ to the right-hand sides of system (8.1), we found that

$$\begin{aligned}
\frac{dS}{dt} &= I^{-(\alpha-1)}\left[\pi_s - \mu_s S\right] ds,\\
\frac{dH}{dt} &= I^{-(\alpha-1)}\left[\pi_h - \frac{\beta_1 HS}{1+b_0 I} - \mu_h H\right] ds,\\
\frac{dX}{dt} &= I^{-(\alpha-1)}\left[\frac{\beta_1 HS}{1+b_0 I} - \delta X - \varpi_x XI\right] ds,\\
\frac{dR}{dt} &= I^{-(\alpha-1)}\left[\pi_r - \frac{\beta_2 RM}{1+b_{bo} I} - \mu_r R\right] ds,\\
\frac{dY}{dt} &= I^{-(\alpha-1)}\left[\frac{\beta_2 RM}{1+b_0 I} - \gamma Y - \varpi_y YI\right] ds,\\
\frac{dM}{dt} &= I^{-(\alpha-1)}\left[\frac{N\delta X}{1+b_1 I} + \frac{Q\gamma Y}{1+b_1 I} - \mu_m M - \varpi_m MI\right] ds,\\
\frac{dG}{dt} &= I^{-(\alpha-1)}\left[\frac{cY}{1+b_1 I} - \mu_g G - \varpi_g GI\right] ds,\\
\frac{dE}{dt} &= I^{-(\alpha-1)}\left[\pi_i + I\left(\frac{\xi X}{1+a_0 X} + \frac{\nu Y}{1+a_0 Y} + \frac{\sigma M}{1+a_0 M} + \frac{\theta G}{1+a_0 G}\right) - \mu_i I\right] ds,
\end{aligned} \tag{8.3}$$

where

$$I^{-(\alpha-1)} = \frac{1}{\Gamma(1-\alpha)}\int_0^t (t-s)^{(2-\alpha)} dt$$

and the term $\frac{1}{\Gamma(1-\alpha)}(t-s)^{(2-\alpha)}$ is time dependent kernal power law correlation, where $0<\alpha\leq 1$ and $\Gamma(x)$ is gamma function. Applying the Caputo fractional derivative of order $(\alpha-1)$. Thus,

$$\begin{aligned}
{}_0^C D_t^{\alpha-1}\left[\frac{dS}{dt}\right] &= {}_0^C D_t^{\alpha-1} I^{-(\alpha-1)}\left[\pi_s - \mu_s S\right],\\
{}_0^C D_t^{\alpha-1}\left[\frac{dH}{dt}\right] &= {}_0^C D_t^{\alpha-1} I^{-(\alpha-1)}\left[\pi_h - \frac{\beta_1 HS}{1+b_0 I} - \mu_h H\right],\\
{}_0^C D_t^{\alpha-1}\left[\frac{dX}{dt}\right] &= {}_0^C D_t^{\alpha-1} I^{-(\alpha-1)}\left[\frac{\beta_1 HS}{1+b_0 I} - \delta X - \varpi_x XI\right],\\
{}_0^C D_t^{\alpha-1}\left[\frac{dR}{dt}\right] &= {}_0^C D_t^{\alpha-1} I^{-(\alpha-1)}\left[\pi_r - \frac{\beta_2 RM}{1+b_{bo} I} - \mu_r R\right],\\
{}_0^C D_t^{\alpha-1}\left[\frac{dY}{dt}\right] &= {}_0^C D_t^{\alpha-1} I^{-(\alpha-1)}\left[\frac{\beta_2 RM}{1+b_0 I} - \gamma Y - \varpi_y YI\right],\\
{}_0^C D_t^{\alpha-1}\left[\frac{dM}{dt}\right] &= {}_0^C D_t^{\alpha-1} I^{-(\alpha-1)}\left[\frac{N\delta X}{1+b_1 I} + \frac{Q\gamma Y}{1+b_1 I} - \mu_m M - \varpi_m MI\right],\\
{}_0^C D_t^{\alpha-1}\left[\frac{dG}{dt}\right] &= {}_0^C D_t^{\alpha-1} I^{-(\alpha-1)}\left[\frac{cY}{1+b_1 I} - \mu_g G - \varpi_g GI\right],\\
{}_0^C D_t^{\alpha-1}\left[\frac{dE}{dt}\right] &= {}_0^C D_t^{\alpha-1} I^{-(\alpha-1)}\left[\pi_i + I\left(\frac{\xi X}{1+a_0 X} + \frac{\nu Y}{1+a_0 Y} + \frac{\sigma M}{1+a_0 M} + \frac{\theta G}{1+a_0 G}\right) - \mu_i I\right].
\end{aligned} \tag{8.4}$$

Then, we obtain the within-host malaria infection model in the Caputo sense as follows:

$$
\begin{aligned}
{}^{C}D_t^{\alpha}S &= \pi_s - \mu_s S,\\
{}^{C}D_t^{\alpha}H &= \pi_h - \frac{\beta_1 HS}{1+b_0 I} - \mu_h H,\\
{}^{C}D_t^{\alpha}X &= \frac{\beta_1 HS}{1+b_0 I} - \delta X - \varpi_x XI,\\
{}^{C}D_t^{\alpha}R &= \pi_r - \frac{\beta_2 RM}{1+b_0 I} - \mu_r R,\\
{}^{C}D_t^{\alpha}Y &= \frac{\beta_2 RM}{1+b_0 I} - \gamma Y - \varpi_y YI,\\
{}^{C}D_t^{\alpha}M &= \frac{N\delta X}{1+b_1 I} + \frac{Q\gamma Y}{1+b_1 I} - \mu_m M - \varpi_m MI,\\
{}^{C}D_t^{\alpha}G &= \frac{cY}{1+b_1 I} - \mu_g G - \varpi_g GI,\\
{}^{C}D_t^{\alpha}I &= \pi_i + I\left(\frac{\xi X}{1+a_0 X} + \frac{\nu Y}{1+a_0 Y} + \frac{\sigma M}{1+a_0 M} + \frac{\theta G}{1+a_0 G}\right) - \mu_i I,
\end{aligned}
\tag{8.5}
$$

with initial condition

$$
S(0)\geq 0, H(0)>0, X(0)\geq 0, R(0)>0, Y(0)\geq 0, M(0)>0, G(0)>0, I(0)>0. \tag{8.6}
$$

8.2 Basic properties of the model

Here, we discuss the existence, uniqueness, well-posedness and biological meaningfulness of the solution of the developed model. The existence and uniqueness of the solution is proved using the Banach fixed point theorem, whereas the well-posedness and biological meaningfulness of the solution is examined by showing the non-negativity and boundedness of the solution of system equation (8.5) in feasible region in the following subsections.

8.2.1 Existence and uniqueness of the solution

We present the existence and uniqueness of the solution of the proposed model (8.5) in this section. Let us rewrite the model equation (8.5) as follows:

$$
\begin{aligned}
{}^{C}D_t^{\alpha}S &= g_1(t,S,H,X,R,Y,M,G,I) = \pi_s - \mu_s S,\\
{}^{C}D_t^{\alpha}H &= g_2(t,S,H,X,R,Y,M,G,I) = \pi_h - \frac{\beta_1 HS}{1+b_0 I} - \mu_h H,\\
{}^{C}D_t^{\alpha}X &= g_3(t,S,H,X,R,Y,M,G,I) = \frac{\beta_1 HS}{1+b_0 I} - \delta X - \varpi_x XI,\\
{}^{C}D_t^{\alpha}R &= g_4(t,S,H,X,R,Y,M,G,I) = \pi_r - \frac{\beta_2 RM}{1+b_0 I} - \mu_r R,\\
{}^{C}D_t^{\alpha}Y &= g_5(t,S,H,X,R,Y,M,G,I) = \frac{\beta_2 RM}{1+b_0 I} - \gamma Y - \varpi_2 YI,
\end{aligned}
\tag{8.7}
$$

$$
\begin{aligned}
{}^{C}D_t^{\alpha}M &= g_6(t,S,H,X,R,Y,M,G,I) = \frac{N\delta X}{1+b_1 I} + \frac{Q\gamma Y}{1+b_1 I} - \mu_m M - \varpi_m M I,\\
{}^{C}D_t^{\alpha}G &= g_7(t,S,H,X,R,Y,M,G,I) = \frac{cY}{1+b_1 I} - \mu_g G - \varpi_g G I,\\
{}^{C}D_t^{\alpha}I &= g_8(t,S,H,X,R,Y,M,G,I) = \pi_i + I\left(\frac{\xi X}{1+a_0 X} + \frac{\nu Y}{1+a_0 Y} + \frac{\sigma M}{1+a_0 M} + \frac{\theta G}{1+a_0 G}\right) - \mu_i I,
\end{aligned}
$$

The model equation (8.7) can be written as

$$
\begin{cases}
{}^{C}D_t^{\alpha}U(t) = g_i(t,U)\\
U(0) = U_0,
\end{cases}
\tag{8.8}
$$

The equation (8.8) has an integral representation

$$
U(t) = U_0 + \frac{1}{\Gamma(\alpha)}\int_0^t g_i(s,U(s))(t-s)^{\alpha-1}ds, \tag{8.9}
$$

where

$$
U(t) = \begin{cases} S(t)\\ H(t)\\ X(t)\\ R(t)\\ Y(t)\\ M(t)\\ G(t)\\ I(t) \end{cases}, \quad U_0 = \begin{cases} S_0\\ H_0\\ X_0\\ R_0\\ Y_0\\ M_0\\ G_0\\ I_0 \end{cases}, \quad g_i(t,U(t)) = \begin{cases} g_1(t,U)\\ g_2(t,U)\\ g_3(t,U)\\ g_4(t,U)\\ g_5(t,U)\\ g_6(t,U)\\ g_7(t,U)\\ g_8(t,U) \end{cases}. \tag{8.10}
$$

For a Banach space $\mathscr{L} = C([0,T],\mathscr{R})$ of a continuous function with the norm defined as

$$
||U||_{\mathscr{L}} = ||(S(t),H(t),X(t),R(t),Y(t),M(t),G(t),I(t))|| = sup_{t\in\mathscr{L}}|U(t)|,
$$

where $|U(t)| = [|S(t)| + |H(t)| + |X(t)| + |R(t)| + |Y(t)| + |M(t)| + |G(t)| + |I(t)|]$ and all the state variables in $C([0,T],\mathscr{R})$.

Theorem 8.1. *(Existence of the solution)*
For every g_i of equation (8.7) there exist Δ_i such that $||g_i(t,U) - g_i(t,U_1)|| \le \Delta_i||U(t) - U_1(t)||$ are contractions for $0 \le \Delta_i \le 1$, for $i = 1,2,\ldots,8$.

Proof. Let
$||S(t)|| = sup_{t\in[0,T]}|S(t)| = \mathscr{K}_1$, $||H(t)|| = sup_{t\in[0,T]}|H(t)| = \mathscr{K}_2$,
$||X(t)|| = sup_{t\in[0,T]}|X(t)| = \mathscr{K}_3$, $||R(t)|| = sup_{t\in[0,T]}|R(t)| = \mathscr{K}_4$,
$||Y(t)|| = sup_{t\in[0,T]}|Y(t)| = \mathscr{K}_5$, $||M(t)|| = sup_{t\in[0,T]}|M(t)| = \mathscr{K}_6$,

$||G(t)|| = sup_{t\in[0,T]}|G(t)| = \mathscr{K}_7,\ \ ||I(t)|| = sup_{t\in[0,T]}|I(t)| = \mathscr{K}_8.$

Taking variable S, we have

$$\begin{aligned}||g_1(t,S) - g_1(t,S_1)|| &= ||\Pi_s - \mu_s S - (\Pi_s + \mu_s S_1)|| \\ &= ||-\mu_s(S-S_1)|| \leq \mu_s||S-S_1|| = \Delta_1||S-S_1||,\end{aligned}$$

where $\Delta_1 = \mu_s$.

Taking variable H, we have

$$\begin{aligned}||g_2(t,H) - g_2(t,H_1)|| &= \left|\left|\Pi_H - \frac{\beta_1 SH}{1+b_0 I} - \mu_h H - (\Pi_H + \frac{\beta_1 SH_1}{1+b_0 I} + \mu_h H_1)\right|\right| \\ &= \left|\left|-\frac{\beta_1 S}{1+b_0 I}(H-H_1) - \mu_h(H-H_1)\right|\right| \\ &\leq \left(\frac{\beta_1||S||}{1+b_0||I||} + \mu_h\right)||H-H_1|| \leq \Delta_2||H-H_1||,\end{aligned}$$

where $\Delta_2 = \frac{\beta_1 \mathscr{K}_1}{1+b_0\mathscr{K}_8} + \mu_h$. Then $g_1(t,S)$ and $g_2(t,H)$ are satisfies the Lipschitz condition with Lipschitz constant Δ_1 and Δ_2, respectively. Furthermore, if $0 \leq \Delta_{1,2} < 1$, then $g_1(t,S)$ and $g_2(t,H)$ are contraction. In same procedure, we can be shown the Lipschitz constant Δ_i and contraction of $g_i(t,U)$, for $i = 3,4,\ldots,8$.

Next, for $j = 1,2,3,\ldots$, defined the following recursive form of equation (8.9) as follows:

$$U_j(t) - U_{j-1}(t) = \frac{1}{\Gamma(\alpha)}\int_0^t (g_i(s,U_{j-1}))(t-s)^{\alpha-1}ds \tag{8.11}$$

The difference between subsequent terms in the above equation and taking the norm on both sides of the resulting equation, we obtained

$$||U_j(t) - U_{j-1}(t)|| = \frac{1}{\Gamma(\alpha)}\int_0^t ||g_i(s,U_{j-1}) - g_i(s,U_{j-2})||(t-s)^{\alpha-1}|ds \tag{8.12}$$

Taking variable $S(t)$, we found that

$$\begin{aligned}||S_j(t) - S_{j-1}(t)|| &= \frac{1}{\Gamma(\alpha)}\int_0^t ||g_i(s,S_{j-1}) - g_i(s,S_{j-2})||(t-s)^{\alpha-1}|ds \\ &\leq \frac{1}{\Gamma(\alpha)}\int_0^t \Delta_1||S_{j-1}(t) - S_{j-2}(t)||(t-s)^{\alpha-1}|ds \\ &= \Delta_1||S_{j-1}(t) - S_{j-2}(t)||\frac{1}{\Gamma(\alpha)}\int_0^t |(t-s)^{\alpha-1}|ds \\ &\leq \Delta_1||S_{j-1}(t) - S_{j-2}(t)||\left|\frac{t^\alpha}{\Gamma(\alpha+1)}\right|.\end{aligned}$$

Thus, S satisfies the Lipschitz condition with Lipschitz constant Δ_1. We have

$$||S_j(t) - S_{j-1}(t)|| \leq \Delta_1||S_{j-1}(t) - S_{j-2}(t)||\left|\frac{t^\alpha}{\Gamma(\alpha+1)}\right|.$$

In similar ways, we can show for the state variables $H(t), X(t), R(t), Y(t), M(t), G(t)$, and $I(t)$, we found

$$\begin{aligned}
||H_j(t) - H_{j-1}(t)|| &\leq \Delta_2 ||H_{j-1}(t) - H_{j-2}(t)|| \left| \frac{t^\alpha}{\Gamma(\alpha+1)} \right| \\
||X_j(t) - X_{j-1}(t)|| &\leq \Delta_3 ||X_{j-1}(t) - X_{j-2}(t)|| \left| \frac{t^\alpha}{\Gamma(\alpha+1)} \right| \\
||R_j(t) - R_{j-1}(t)|| &\leq \Delta_4 ||R_{j-1}(t) - R_{j-2}(t)|| \left| \frac{t^\alpha}{\Gamma(\alpha+1)} \right| \\
||Y_j(t) - Y_{j-1}(t)|| &\leq \Delta_5 ||Y_{j-1}(t) - Y_{j-2}(t)|| \left| \frac{t^\alpha}{\Gamma(\alpha+1)} \right| \\
||M_j(t) - M_{j-1}(t)|| &\leq \Delta_6 ||M_{j-1}(t) - M_{j-2}(t)|| \left| \frac{t^\alpha}{\Gamma(\alpha+1)} \right| \\
||G_j(t) - G_{j-1}(t)|| &\leq \Delta_7 ||G_{j-1}(t) - G_{j-2}(t)|| \left| \frac{t^\alpha}{\Gamma(\alpha+1)} \right| \\
||I_j(t) - I_{j-1}(t)|| &\leq \Delta_8 ||I_{j-1}(t) - I_{j-2}(t)|| \left| \frac{t^\alpha}{\Gamma(\alpha+1)} \right|.
\end{aligned} \tag{8.13}$$

Thus, equation (8.12) can be reduced to the form

$$||U_j(t) - U_{j-1}(t)|| \leq \Delta_i \left| \frac{t^\alpha}{\Gamma(\alpha+1)} \right| ||U_{j-1}(t) - U_{j-2}(t)||, \; i = 1,2,3,\ldots,8. \tag{8.14}$$

□

Theorem 8.2. *The model equation (8.5) has the solution if we can find $\mathscr{W}$ satisfying the inequality*

$$\frac{\mathscr{W}^\alpha}{\Gamma(\alpha+1)} \Delta_i < 1, \quad for \;\; i = 1,2,\ldots,8$$

Proof. From equation (8.14), we have

$$||U_{ij}|| \leq ||U(0)|| \left[\frac{t^\alpha}{\Gamma(\alpha+1)} \right]^j.$$

The existence of the solution (the existence of fixed point) is confirmed Theorem (8.1). Now, we need to show that $S(t), H(t), X(t), R(t), Y(t), M(t), G(t)$, and $I(t)$ are the solution of the model equation. Now, we will show that $U_j(t)$ converge to system of solutions of (8.5). Assume the following condition hold:

$$U(t) - U(0) = U_j(t) - \mathscr{M}_{ij}, \tag{8.15}$$

where the $\mathscr{M}_{ij}$, $for \;\; i = 1,2,\ldots,8$, remainder terms after j iterations. Using the equations

(8.9) and (8.11), we found

$$||\mathscr{M}_{ij}|| = \frac{1}{\Gamma(\alpha+1)}\int_0^t ||g_i(s,U_j) - g_i(s,U_{j-1})||(t-s)^{\alpha-1}|ds \leq \frac{t^\alpha}{\Gamma(\alpha+1)}\Delta_i||U_j - U_{j-1}||.$$

Repeating the process recursively lead to

$$||\mathscr{M}_{ij}|| \leq \left[\frac{t^\alpha}{\Gamma(\alpha+1)}\right]^{j+1}\Delta_i^j||U_j - U_{j-1}||^j.$$

Taking as $t = \mathscr{W}$ yields

$$||\mathscr{M}_{ij}|| \leq \left[\frac{\mathscr{W}^\alpha}{\Gamma(\alpha+1)}\right]^{j+1}\Delta_i^j||U_j - U_{j-1}||^j.$$

Using hypothesis $\frac{\mathscr{W}^\alpha}{\Gamma(\alpha+1)}\Delta_i < 1, \quad for \quad i = 1,2,\ldots,8$, then $||\mathscr{M}_{ij}|| \to 0$ as $j \to \infty$. Combination of Theorems 8.1 and 8.2 shows the system equation (8.5) has solution by Banach fixed theorem. Therefore, the solution is exist. □

Theorem 8.3. *(Uniqueness of the solution)*
A model equation (8.5) *has a unique solution provided that*

$$\left|\frac{\mathscr{W}^\alpha}{\Gamma(\alpha+1)}\right|\Delta_i < 1, \quad i = 1,2,\ldots,8.$$

Proof. Assume that $S(t), H(t), X(t), R(t), Y(t), M(t), G(t)$, and $I(t)$ are solution to model equation (8.5), then

$$S(t) - S_1(t) = \frac{1}{\Gamma(\alpha)}\int_0^t (g_1(s,S) - g_1(s,S_1))(t-s)^{\alpha-1}ds$$

Taking the norm both sides, we found

$$\begin{aligned}||S(t) - S_1(t)|| =& \frac{1}{\Gamma(\alpha+1)}\int_0^t ||g_1(s,S) - g_1(s,S_1)||(t-s)^{\alpha-1}|ds \\ &\leq \Delta_1||S - S_1||\int_0^t |(t-s)^{\alpha-1}|ds \leq \Delta_1||S - S_1||\left|\frac{t^\alpha}{\Gamma(\alpha+1)}\right|.\end{aligned}$$

Taking $t = \mathscr{W}$

$$||S(t) - S_1(t)|| \leq \Delta_1||S - S_1||\left|\frac{\mathscr{W}^\alpha}{\Gamma(\alpha+1)}\right|.$$

Since, $1 - \left|\frac{\mathscr{W}^\alpha}{\Gamma(\alpha+1)}\right| > 0$, we obtain $||S(t) - S_1(t)|| = 0$. Thus, we have $S(t) = S_1(t)$. In the same procedure we can show that for $H(t), X(t), R(t), Y(t), M(t), G(t)$, and $I(t)$.

Therefore, by Banach fixed point theorem the model equation has a unique solution. □

8.2.2 Invariant region

The dynamics system of Caputo fractional order model (8.5) is evaluated in a feasible region $\Omega \subset R_+^8$, such that

$$\Omega = \left\{ \begin{array}{c} (S(t),H(t),X(t),R(t),Y(t),M(t),G(t),I(t)) \in R_+^8 : \; N_h(t) = H(t)+X(t) \leq \frac{\pi_h}{\chi}; \\ N_r(t) = R(t)+Y(t) \leq \frac{\pi_r}{\varphi}; \; N_s(t) = S(t)+M(t)+G(t) \leq \frac{\pi_s+\mathscr{Z}}{\psi}; \; I(t) \leq \frac{\pi_i}{\varkappa-\mu_i} \end{array} \right\} \tag{8.16}$$

Theorem 8.4. *The region Ω of equation (8.16) is a positive invariant of the system equation (8.5) with non-negative initial condition (8.6).*

Proof. The total size of the hepatocyte cell populations at a time t is given as $N_h(t) = H(t) + X(t)$. Now,

$$^{C}D_t^{\alpha} N_h(t) = {}^{C}D_t^{\alpha} H(t) + {}^{C}D_t^{\alpha} X(t) = \Pi_h - \mu_h H - \delta X - \varpi_1 XI \leq \pi_h - \chi N_h,$$

where $\chi = min\{\mu_h, \delta\}$, then we have

$$^{C}D_t^{\alpha} N_h(t) + \chi N_h(t) \leq \pi_h.$$

Applying the Laplace transform as

$$\begin{aligned} &\mathscr{L}\{{}^{C}D_t^{\alpha} N_h(t) + \chi N_h(t)\} \leq \mathscr{L}\{\pi_h\} \\ &s^{\alpha}\mathscr{L}\{N_h(t)\} - s^{\alpha-1}N_h(0) + \chi\mathscr{L}\{N_h(t)\} \leq \Pi_H \mathscr{L}\{1\} \\ &(s^{\alpha}+\chi)\mathscr{L}\{N_h(t)\} \leq \frac{\pi_h}{s} + s^{\alpha-1}N_h(0) \\ &\mathscr{L}\{N_h(t)\} \leq \frac{\pi_h}{s(s^{\alpha}+\chi)} + \frac{s^{\alpha-1}N_h(0)}{s^{\alpha}+\chi} \end{aligned}$$

Next, apply the inverse Laplace transform as

$$\begin{aligned} &\mathscr{L}^{-1}\{\mathscr{L}\{N_h(t)\}\} \leq \mathscr{L}^{-1}\left\{\frac{\pi_h}{s(s^{\alpha}+\chi)} + \frac{s^{\alpha-1}N_h(0)}{s^{\alpha}+\chi}\right\} \\ &N_h(t) \leq N_h(0)E_{\alpha,1}(-\chi t^{\alpha}) + \pi_h t^{\alpha} E_{\alpha,\alpha+1}(-\chi t^{\alpha}), \end{aligned}$$

where $E_{\alpha,1}$ is Mittag-Leffler function. Using the relation $E_{\alpha,\beta}(z) = zE_{\alpha,\alpha+\beta}(z) + \frac{1}{\Gamma(\beta)}$, we have $t^{\alpha}E_{\alpha,\alpha+1}(-\chi t^{\alpha}) = \frac{1}{\chi}(1 - E_{\alpha,1}(-\chi t^{\alpha}))$. Thus,

$$N_h(t) \leq N_h(0)E_{\alpha,1}(-\chi t^{\alpha}) + \frac{\pi_h}{\chi}(1 - E_{\alpha,1}(-\chi t^{\alpha})).$$

The Mittag-Leffler function $E_{\alpha,1}(-\chi t^{\alpha}) \to 0$ as $t \to \infty$. Hence,

$$N_h(t) \leq N_h(0)E_{\alpha,1}(-\chi t^{\alpha}) + \frac{\pi_h}{\chi}(1 - E_{\alpha,1}(-\chi t^{\alpha})) \leq \frac{\pi_h}{\chi}.$$

In the same manner, we can perform for the population of the red blood cells, malaria parasites, and immune system. The red blood cell population is given $N_r(t) = R(t) + Y(t)$. Now,

$$\begin{aligned}
{}^{C}D_t^{\alpha} N_r(t) =& {}^{C}D_t^{\alpha} R(t) + {}^{C}D_t^{\alpha} Y(t) \\
&= \pi_r - \frac{\beta_2 RM}{1+b_0 I} - \mu_r R + \frac{\beta_2 RM}{1+b_0 I} - \gamma Y - \varpi_y YI \\
&\leq \pi_r - \mu_r R - \gamma Y \leq \pi_r - \varphi N_r(t),
\end{aligned}$$

where $\varphi = min\{\mu_r, \varpi_y\}$. Taking the Laplace transform both sides of ${}^{C}D_t^{\alpha} N_r(t) \leq \pi_r - \varphi N_r(t)$, we found that

$$\mathscr{L}\{N_r(t)\} \leq \frac{\pi_r}{s(s^{\alpha}+\varphi)} + \frac{N_r(0)s^{\alpha-1}}{s^{\alpha}+\varphi}.$$

By applying the inverse Laplace, we have

$$N_r(t) \leq \pi_r t^{\alpha} E_{\alpha,\alpha+1}(-\varphi t^{\alpha}) + N_r(0) E_{\alpha,1}(-\varphi t^{\alpha}) \leq \frac{\pi_r}{\varphi}.$$

Next, the total size of malaria parasites $N_p(t) = S(t) + M(t) + G(t)$. Now,

$$\begin{aligned}
{}^{C}D_t^{\alpha} N_p(t) =& {}^{C}D_t^{\alpha} S(t) + {}^{C}D_t^{\alpha} M(t) + {}^{C}D_t^{\alpha} G(t) \\
&= \pi_s - \mu_s S + \frac{N\delta X}{1+b_1 I} + \frac{Q\gamma Y}{1+b_1 I} - \mu_m M - \varpi_m MI + \frac{cY}{1+b_0 I} - \mu_g G - \varpi_g GI \\
&\leq \pi_s - \psi N_p(t) + \frac{N\delta X}{1+b_1 I} + \frac{Q\gamma Y}{1+b_1 I} + \frac{cY}{1+b_1 I} \leq \pi_s - \psi N_p(t) + N\delta X + (Q\gamma + c)Y \\
&\leq \pi_s - \psi N_p(t) + \frac{N\delta \pi_h}{\chi} + \frac{(Q\gamma+c)\pi_r}{\varphi}, \ \ since \ \ X \leq \frac{\pi_h}{\chi}, \ \ Y \leq \frac{\pi_r}{\varphi} \\
&= \pi_s + \mathscr{Z} - \psi N_p(t),
\end{aligned}$$

where $\psi = min\{\mu_s, \mu_m, \mu_g\}$ is the minimum death rate of malaria parasite and $\mathscr{Z} = \frac{N\delta\pi_h}{\chi} + \frac{(Q\gamma+c)\pi_r}{\varphi}$ is the production rate of malaria parasites by infected hepatocytes and infected red blood cells. Applying the Laplace transform, we found that

$$\mathscr{L}\{N_p(t)\} \leq \frac{\Pi_r + \mathscr{Z}}{s(s^{\alpha}+\psi)} + \frac{s^{\alpha-1} N_p(0)}{s^{\alpha}+\psi}.$$

After applying the inverse Laplace, we obtained

$$N_p(t) \leq (\Pi_s + \mathscr{Z}) t^{\alpha} E_{\alpha,\alpha+1}(-\psi t^{\alpha}) + N_p(0) E_{\alpha,1}(-\psi t^{\alpha}) \leq \frac{\Pi_s + \mathscr{Z}}{\psi}.$$

Finally,

$$\begin{aligned}
{}^{C}D_t^{\alpha} I(t) =& \Pi_i + I\left(\frac{\xi X}{1+a_0 X} + \frac{\nu Y}{1+a_0 Y} + \frac{\sigma M}{1+a_0 M} + \frac{\theta G}{1+a_0 G}\right) - \mu_i I \\
\leq& \Pi_i + I(\xi X + \nu Y + \sigma M + \theta G) - \mu_i I \\
\leq& \Pi_i + I\left(\frac{\xi \Pi_h}{\chi} + \frac{\nu \Pi_r}{\varphi} + \frac{(\sigma+\theta)(\Pi_s + \mathscr{Z})}{\psi}\right) - \mu_i I \leq \Pi_i - (\mu_i - \varkappa) I,
\end{aligned}$$

where $\varkappa = \frac{\xi\Pi_h}{\chi} + \frac{\nu\Pi_r}{\varphi} + \frac{(\sigma+\theta)(\Pi_s+\mathscr{Z})}{\psi}$ represents the stimulation rate of immune response in the presence of malaria infection. Using Laplace transform, we have

$$\mathscr{L}\{I(t)\} \leq \frac{\Pi_i}{s(s^\alpha + \mu_i - \varkappa)} + \frac{I_0 s^{\alpha-1}}{s^\alpha + \mu_i - \varkappa}.$$

After we use the inverse Laplace, we found that

$$I(t) \leq \Pi_i t^\alpha E_{\alpha+1,\alpha}(\varkappa - \mu_i) + I_0 E_{\alpha,1}(\varkappa - \mu_i) \leq \frac{\Pi_i}{\varkappa - \mu_i}, \quad for \quad \varkappa > \mu_i.$$

Thus, the solution of the dynamical system (8.5) with the nonnegative conditions in Ω remains in the region Ω. Therefore, the region Ω is positively invariant and attracts all the solutions in R^8_+. □

8.2.3 Non-negativity of the solution

Now, for the non-negativity of the system solution, let

$$\Omega \subset R^8_+ = \left\{x \in R^8_+ : x \geq 0\right\} \quad and \quad x(t) = (S(t), H(t), X(t), R(t), Y(t), M(t), G(t), I(t))^T \tag{8.17}$$

Theorem 8.5. *The model equation* (8.5) *is non-negative for non-negative initial condition* (8.6)*, for all* $t \geq 0$.

Proof. To show the solution of the model is non-negative, it is required to show that for each hyper-plane bounding the positive orthant there is vector field R^8_+, from system equation (8.5), we have

$$\begin{aligned}
{}^C D_t^\alpha S|_{S=0} &= \Pi_s \geq 0, & {}^C D_t^\alpha H|_{H=0} &= \Pi_h > 0,\\
{}^C D_t^\alpha X|_{X=0} &= \frac{\beta_1 SH}{1+b_0 I} \geq 0, & {}^C D_t^\alpha R|_{R=0} &= \Pi_r > 0,\\
{}^C D_t^\alpha Y|_{Y=0} &= \frac{\beta_2 RM}{1+b_0 I} \geq 0, & {}^C D_t^\alpha M|_{M=0} &= \frac{\delta NX}{1+b_1 I} + \frac{\gamma Y}{1+b_1 I} \geq 0 > 0,\\
{}^C D_t^\alpha G|_{G=0} &= \frac{cY}{1+b_1 I} \geq 0 & {}^C D_t^\alpha I|_{I=0} &= \Pi_e > 0
\end{aligned}$$

Hence, using Corollary A.2 the solutions of the dynamical system will remain in $\Omega \subset R^8_+$. This completes the proof. □

8.3 Model Analysis

In this section the qualitative analysis of the proposed fractional-order model (8.5) such as equilibria and their stability as well as sensitivity analysis of the in-host reproduction number are investigated.

8.3.1 Parasite-free equilibrium point

The point that no parasite in the human host cell is known as the parasite-free equilibrium point (parasite-free steady state). We obtained it by equating the right-hand side of the system equation (8.5) to zero. That is,

$$\begin{aligned}
&\pi_s - \mu_s S = 0\\
&\pi_h - \frac{\beta_1 HS}{1+b_0 I} - \mu_h H = 0\\
&\frac{\beta_1 HS}{1+b_0 I} - \delta X - \varpi_x XI = 0\\
&{}^{C}D_t^{\alpha} R = \pi_r - \frac{\beta_2 RM}{1+b_0 I} - \mu_r R = 0\\
&\frac{\beta_2 RM}{1+b_0 I} - \gamma Y - \varpi_y YI = 0\\
&\frac{N\delta X}{1+b_1 I} + \frac{Q\gamma Y}{1+b_1 I} - \mu_m M - \varpi_m MI = 0\\
&\frac{cY}{1+b_1 I} - \mu_g G - \varpi_g GI = 0\\
&\pi_i + I\left(\frac{\xi X}{1+a_0 X} + \frac{\nu Y}{1+a_0 Y} + \frac{\sigma M}{1+a_0 M} + \frac{\theta G}{1+a_0 G}\right) - \mu_i I = 0,
\end{aligned} \tag{8.18}$$

Applying the required conditions $S = 0, X = Y = M = G = 0$ and $\pi_s = 0$ to the system (8.18) for parasite-free equilibrium, then the parasite-free equilibrium point of the within-host model (8.5) is given as:

$$E^0 = (S^0, H^0, X^0, R^0, Y^0, M^0, G^0, I^0) = \left(0,\ \frac{\pi_h}{\mu_h},\ 0,\ \frac{\pi_r}{\mu_r},\ 0,\ 0,\ 0,\ \frac{\pi_i}{\mu_i}\right).$$

8.3.2 The basic reproduction number

To compute the basic reproduction number we use the next-generation matrix approach that was discussed by (Van den Driessche and Watmough, 2002). Therefore, the infected compartments of our model equation are

$$\begin{aligned}
{}^{C}D_t^{\alpha} S &= \Pi_s - \mu_s S,\\
{}^{C}D_t^{\alpha} X &= \frac{\beta_1 HS}{1+b_0 I} - \delta X - \varpi_x XI,\\
{}^{C}D_t^{\alpha} Y &= \frac{\beta_2 RM}{1+b_0 I} - \gamma Y - \varpi_y YI,\\
{}^{C}D_t^{\alpha} M &= \frac{N\delta X}{1+b_1 I} + \frac{Q\gamma Y}{1+b_1 I} - \mu_m M - \varpi_m MI,\\
{}^{C}D_t^{\alpha} G &= \frac{cY}{1+b_1 I} - \mu_g G - \varpi_g GI.
\end{aligned} \tag{8.19}$$

Let

$$\frac{dY}{dt} = F_j - V_j,$$

where Y represents the infected compartments (S,X,Y,M,G) of equation (8.19), F_j is the rate of new appearance and V_j is the rate of movement from one compartment to other through any other means. Now,

$$F_j = \begin{pmatrix} 0 \\ \frac{\beta_1 HS}{1+b_0 I} \\ \frac{\beta_2 RM}{1+b_0 I} \\ 0 \\ 0 \end{pmatrix}, \quad V_j = \begin{pmatrix} -\pi_s + \mu_s S \\ \delta X + \varpi_x XI \\ \gamma Y + \varpi_y YI \\ -\frac{N\delta X}{1+b_1 I} - \frac{A\gamma Y}{1+b_1 I} + \mu_m M + \varpi_m MI \\ -\frac{cY}{1+b_1 I} + \mu_g G + \varpi_g GI \end{pmatrix}.$$

Hence, the non-negative matrix F and non singular matrix V are investigated by differentiating the vectors F_j and V_j at PFE, E^0. Thus, we obtained

$$F = \begin{pmatrix} 0 & 0 & 0 & 0 & 0 \\ \frac{\beta_1 \pi_h}{\mu_h\left(1+\frac{b_0\pi_i}{\mu_i}\right)} & 0 & 0 & 0 & 0 \\ 0 & 0 & 0 & \frac{\beta_2 \pi_r}{\mu_r\left(1+\frac{b_0\pi_i}{\mu_i}\right)} & 0 \\ 0 & 0 & 0 & 0 & 0 \\ 0 & 0 & 0 & 0 & 0 \end{pmatrix}, \tag{8.20}$$

$$V = \begin{pmatrix} \mu_s & 0 & 0 & 0 & 0 \\ 0 & \delta + \frac{\varpi_x \pi_i}{\mu_i} & 0 & 0 & 0 \\ 0 & 0 & \gamma + \frac{\varpi_y \pi_i}{\mu_i} & 0 & 0 \\ 0 & -\frac{\delta N}{1+\frac{b_1\pi_i}{\mu_i}} & -\frac{\gamma Q}{1+\frac{b_1\pi_i}{\mu_i}} & 0 & \\ 0 & 0 & -\frac{c}{1+\frac{b_1\pi_i}{\mu_i}} & 0 & \mu_g + \frac{\varpi_g \pi_i}{\mu_i} \end{pmatrix} \tag{8.21}$$

Hence,

$$V^{-1} = \begin{pmatrix} \frac{1}{\mu_s} & 0 & 0 & 0 & 0 \\ 0 & \frac{1}{\delta+\frac{\varpi_x\pi_i}{\mu_i}} & 0 & 0 & 0 \\ 0 & 0 & \frac{1}{\gamma+\frac{\varpi_y\pi_i}{\mu_i}} & 0 & 0 \\ 0 & \frac{\delta N}{(1+\frac{b_1\pi_i}{\mu_i})(\delta+\frac{\varpi_x\pi_i}{\mu_i})(\mu_m+\frac{\varpi_m\pi_i}{\mu_i})} & \frac{\gamma Q}{(1+\frac{b_1\pi_i}{\mu_i})(\gamma+\frac{\varpi_y\pi_i}{\mu_i})(\mu_m+\frac{\varpi_m\pi_i}{\mu_i})} & \frac{1}{\mu_m+\frac{\varpi_m\pi_i}{\mu_i}} & 0 \\ 0 & 0 & \frac{c}{(1+\frac{b_1\pi_i}{\mu_i})(\gamma+\frac{\varpi_y\pi_i}{\mu_i})(\mu_g+\frac{\varpi_g\pi_i}{\mu_i})} & 0 & \frac{1}{\mu_g+\frac{\varpi_g\pi_i}{\mu_i}} \end{pmatrix}.$$

The basic reproduction number is the spectral radius of FV^{-1}. Thus,

$$R_0 = \frac{\beta_2 \pi_r \gamma Q}{\mu_r \left(1+\frac{b_0\pi_i}{\mu_i}\right)\left(1+\frac{b_1\pi_i}{\mu_i}\right)\left(\gamma+\frac{\varpi_y\pi_i}{\mu_i}\right)\left(\mu_m+\frac{\varpi_m\pi_i}{\mu_i}\right)}. \tag{8.22}$$

In the absence of human immunity against malaria infection the within-host basic reproduction number become

$$R_0^{WI} = \frac{\beta_2 Q \pi_r}{\mu_m \mu_r}. \tag{8.23}$$

8.3.3 Local and global stability of parasite-free equilibrium point

In section, we investigate the local and global stability analysis of the PFE. The local stability analysis PFE is obtained by linearizing the system equation (8.5) at PFE E^0.

Theorem 8.1. *The parasite-free equilibrium point is locally asymptotically stable if* $R_0 < 1$ *and unstable if* $R_0 > 1$.

Proof. To show the local stability of the PFE, we need to show all the eigenvalues of Jacobian matrix J of the system equation (8.5) evaluated at PFE E^0 satisfy the condition $|arg(\lambda_i)| \geq \frac{\alpha\pi}{2}$. The Jacobian matrix at E^0 is given as

$$J(E^0) = \begin{pmatrix}
-\mu_s & 0 & 0 & 0 & 0 & 0 & 0 & 0 \\
-\frac{\beta_1\pi_h}{\mu_h(1+\frac{b_1\pi_i}{\mu_i})} & -\mu_h & 0 & 0 & 0 & 0 & 0 & 0 \\
\frac{\beta_1\pi_h}{\mu_h(1+\frac{b_1\pi_i}{\mu_i})} & 0 & -\delta-\frac{\varpi_x\pi_i}{\mu_i} & 0 & 0 & 0 & 0 & 0 \\
0 & 0 & 0 & -\mu_r & 0 & -\frac{\beta_2\pi_r}{\mu_r(1+\frac{b_0\pi_i}{\mu_i})} & 0 & 0 \\
0 & 0 & 0 & 0 & -\gamma-\frac{\varpi_y\pi_i}{\mu_i} & \frac{\beta_2\pi_r}{\mu_r(1+b_0\frac{\pi_i}{\mu_i})} & 0 & 0 \\
0 & 0 & \frac{\delta N}{1+\frac{b_1\pi_i}{\mu_i}} & 0 & \frac{\gamma Q}{1+\frac{b_1\pi_i}{\mu_i}} & -\mu_m-\frac{\varpi_m\pi_i}{\mu_i} & 0 & 0 \\
0 & 0 & 0 & 0 & \frac{c}{1+\frac{b_1\pi_i}{\mu_i}} & 0 & -\mu_g-\frac{\varpi_g\pi_i}{\mu_i} & 0 \\
0 & 0 & \frac{\xi\pi_i}{\mu_i} & 0 & \frac{\nu\pi_i}{\mu_i} & \frac{\sigma\pi_i}{\mu_i} & \frac{\theta\pi_i}{\mu_i} & -\mu_i
\end{pmatrix} \tag{8.24}$$

The eigenvalues can be determined by solving the characteristic equation $det(J(E^0)-\lambda I)=0$. That is

$$(\lambda+\mu_s)(\lambda+\mu_h)(\lambda+\delta+\frac{\varpi_x\pi_i}{\mu_i})(\lambda+\mu_r)(\lambda+\mu_i)(\lambda+\mu_g+\frac{\varpi_g\pi_i}{\mu_i})(\lambda^2+a_1\lambda+a_0)=0,$$

where

$$a_1 = \gamma+\frac{\varpi_y\pi_i}{\mu_i}+\mu_m+\frac{\varpi_m\pi_i}{\mu_i}, \qquad a_0 = \left(\gamma+\frac{\varpi_y\pi_i}{\mu_i}\right)\left(\mu_m+\frac{\varpi_m\pi_i}{\mu_i}\right)(1-R_0).$$

The roots of the characteristic equation are $\lambda_1=-\mu_s, \lambda_2=-\mu_h, \lambda_3=-\delta-\frac{\varpi_x\pi_i}{\mu_i}, \lambda_4=-\mu_r, \lambda_7=$

$-\mu_g - \frac{\varpi_g \pi_i}{\mu_i}, \lambda_8 = -\mu_i$ and

$$\lambda^2 + a_1\lambda + a_0 = 0. \tag{8.25}$$

The eigenvalues $\lambda_1, \lambda_2, \lambda_3, \lambda_4, \lambda_7$ and λ_8 are satisfies the condition $|arg(\lambda)| > \frac{\alpha\pi}{2}$. In order to show the all roots of polynomial (8.25) is satisfies $|arg(\lambda_i)| > \frac{\alpha\pi}{2}$, we use the fractal Ruoth-Hurwitz conditions that presented in Theorem A.4. Thus, we use either Routh-Hurwitz stability conditions or $a_1 < 0, 4a_0^2 > (a_1)^2$, $\tan^{-1}|\sqrt{4a_0^2 > (a_1)^2}/a_1| > \alpha\frac{\pi}{2}$. Since $a_1 > 1$, we use Routh-Hurwitz stability conditions. The characteristic polynomial equation (8.25) has roots with negative real parts if $a_1 > 0$ and $a_0 > 1$. Clearly $a_1 > 0$ and $a_0 > 0$ if and only if $R_0 < 1$. Thus, the eigenvalues λ_5 and λ_6 satisfy the condition $|arg(\lambda)| > \alpha\frac{\pi}{2}$. Therefore, the PFE E^0 is locally asymptotically stable if $R_0 < 1$ and if $R_0 > 1$ at least one of the eigenvalue has a positive real part, thus PFE E^0 is unstable.

Next, we investigate the global stability analysis of the PFE utilize the method discussed in (Castillo-Chavez and Song, 2004). □

Theorem 8.2. *The parasite-free equilibrium point of the model (8.5) is global asymptotically stable if $R_0 < 1$.*

Proof. Let, we divided the model compartment in to uninfected and infected compartments as follows

$$\frac{d\mathscr{W}}{dt} = \mathscr{F}(\mathscr{W}, \mathscr{Z}) \tag{8.26}$$

$$\frac{d\mathscr{Z}}{dt} = \mathscr{H}(\mathscr{W}, \mathscr{Z}), \quad \mathscr{H}(\mathscr{W}, 0) = 0, \tag{8.27}$$

where $\mathscr{W} = (H, R, E) \in R_+^3$ is represent healthy compartments and $\mathscr{Z} = (S, X, Y, M, G) \in R_+^5$ is infected compartment. The global stability analysis of PFE E^0 is exist, if the following condition $\mathscr{C}_1$ and $\mathscr{C}_2$ are satisfied.
($\mathscr{C}_1$) For $\frac{d\mathscr{W}}{dt} = \mathscr{F}(\mathscr{W}, 0)$ is globally asymptotically stable, where $\mathscr{F}(\mathscr{W}^0, 0) = 0$.
($\mathscr{C}_2$) $\mathscr{H}(\mathscr{W}, \mathscr{Z}) = \mathscr{D}\mathscr{Z} - \widehat{\mathscr{H}}(\mathscr{W}, \mathscr{Z}), \widehat{\mathscr{H}}(\mathscr{W}, \mathscr{Z}) > 0$, for $(\mathscr{W}, \mathscr{Z}) \in \Omega$, where $\mathscr{D} = D_{\mathscr{Z}}\mathscr{H}(\mathscr{W}^0, 0)$ is an **M** matrix i.e the off diagonal elements of matrix $\mathscr{D}$ is non-negative. Now, from system equation (8.5), we have

$$\mathscr{F}(\mathscr{W}, \mathscr{Z}) = \begin{pmatrix} \pi_h - \frac{\beta_1 HP}{1+b_0 E} - \mu_h H \\ \pi_r - \frac{\beta_2 RM}{1+b_1 E} - \mu_r R \\ \pi_i + I\left(\frac{\xi X}{1+a_0 X} + \frac{\nu Y}{1+a_0 Y} + \frac{\sigma M}{1+a_0 M} + \frac{\theta G}{1+a_0 G}\right) - \mu_i I \end{pmatrix} \tag{8.28}$$

$$\mathscr{F}(\mathscr{W}, 0) = \begin{pmatrix} \pi_h - \mu_h H \\ \pi_r - \mu_r R \\ \Pi_i - \mu_i I \end{pmatrix}, \text{ and } \mathscr{F}(\mathscr{W}^0, 0) = 0, \text{ where } \mathscr{W}^0 = \left(\frac{\pi_h}{\mu_h}, \frac{\pi_r}{\mu_r}, \frac{\pi_i}{\mu_i}\right). \tag{8.29}$$

Thus, the equation (8.29) has a unique PFE , $\mathscr{W}^0 = \left(\frac{\pi_h}{\mu_h}, \frac{\pi_r}{\mu_r}, \frac{\pi_i}{\mu_i}\right)$, which is globally asymptotically stable. The condition $\mathscr{C}_1$ is satisfied.

Next, we compute the condition $\mathscr{C}_2$. From system equation (8.5), we have

$$\mathscr{H}(\mathscr{W},\mathscr{Z}) = \begin{pmatrix} \pi_s - \mu_s S \\ \frac{\beta_1 HS}{1+b_0 I} - \delta X - \varpi x XI \\ \frac{\beta_2 RM}{1+b_0 I} - \alpha Y - \varpi_y YI \\ \frac{N\delta X}{1+b_1 I} + \frac{Q\alpha Y}{1+b_1 I} - \mu_m M - \varpi_m MI \\ \frac{cY}{1+b_1 I} - \mu_g G - \varpi_g GI \end{pmatrix} \tag{8.30}$$

$$\mathscr{D} = \mathscr{D}_{\mathscr{Z}}\mathscr{H}(\mathscr{W}^0,0) = \begin{pmatrix} -\mu_s & 0 & 0 & 0 & 0 \\ \frac{\beta_1 H^0}{1+b_0 I^0} & -\delta - \varpi_x I^0 & 0 & 0 & 0 \\ 0 & 0 & -\gamma - \varpi_y I^0 & \frac{\beta_2 R^0}{1+b_0 I^0} & 0 \\ 0 & \frac{\delta N}{1+b_1 I^0} & \frac{\gamma Q}{1+b_1 I^0} & -\mu_m - \varpi_m I^0 & 0 \\ 0 & 0 & \frac{c}{1+a_1 I^0} & 0 & -\mu_g - \varpi_g I^0 \end{pmatrix},$$

which is $\mathbf{M}-$ matrix. The off diagonal elements of the $\mathscr{D}$ is non-negative. Lastly

$$\widehat{\mathscr{H}}(\mathscr{W},\mathscr{Z}) = \mathscr{D}\mathscr{Z} - \mathscr{G}(\mathscr{W},\mathscr{Z}) = \begin{pmatrix} -\pi_s \\ \frac{\beta_1 H^0 S}{1+b_0 I^0}\left(1 - \frac{(1+b_0 I^0 H)}{(1+b_0 I)H^0}\right) + \varpi_x XI\left(1 - \frac{I^0}{I}\right) \\ \varpi_y IY\left(1 - \frac{I^0}{I}\right) + \frac{\beta_2 R^0 M}{1+b_0 I^0}\left(1 - \frac{(1+b_0 I^0)R}{(1+b_0 I)R^0}\right) \\ \frac{(\delta NX + \gamma QY)}{1+b_0 I^0}\left(1 - \frac{1+b_0 I^0}{1+b_0 I}\right) + \varpi_m MI(1 - \frac{I^0}{I}) \\ \frac{cY}{1+b_0 I^0}\left(1 - \frac{1+b_0 I^0}{1+b_0 I}\right) + \varpi_g YI\left(1 - \frac{I^0}{I}\right) \end{pmatrix}.$$

This implies that $\widehat{\mathscr{H}}(\mathscr{W},\mathscr{Z}) \ngeq 0$, for all $(\mathscr{W},\mathscr{Z}) \in \Omega$ the conditions $(\mathscr{C}_2)$ is not satisfied. Therefore, PFE E^0 is not globally asymptotically stable for $R_0 \leq 1$. □

8.3.4 Existence of the parasite persistence equilibria

The parasite persistence equilibrium point (PPE) is the steady-state solution where the malaria parasites exist in the human host cells. There are two parasite persistence equilibria: the PPE without and the PPE with immune response against malaria infection. In this, we compute only the PPE without an immune response against malaria infection. In the absence of a human immune response against parasite infection ($I = 0$) the model equation (8.5) become

$$\begin{aligned} {}^C D_t^\alpha S &= \pi_s - \mu_s S, \\ {}^C D_t^\alpha H &= \pi_h - \beta_1 HS - \mu_h H, \\ {}^C D_t^\alpha X &= \beta_1 HS - \delta X, \\ {}^C D_t^\alpha R &= \pi_r - \beta_2 RM - \mu_r R, \\ {}^C D_t^\alpha Y &= \beta_2 RM - \gamma Y, \\ {}^C D_t^\alpha M &= N\delta X + Q\gamma Y - \mu_m M, \\ {}^C D_t^\alpha G &= cY - \mu_g G. \end{aligned} \tag{8.31}$$

Thus, we found that PPE without immune response as

$$E_1^* = (S_1^*, H_1^*, X_1^*, R_1^*, Y_1^*, M_1^*, G_1^*, 0) = \begin{cases} S_1^* = \frac{\pi_s}{\mu_s}, \\ H_1^* = \frac{\pi_h \mu_s}{\beta_1 \pi_s + \mu_h \mu_m}, \\ X_1^* = \frac{\beta_1 \pi_h}{\delta \beta_1 \pi_s + \mu_h \mu_m \delta} \\ R_1^* = \frac{\pi_r}{\beta_2 M + \mu_r}, \\ M_1^* = \frac{\beta_1 N \pi_h \pi_s}{\mu_m (\beta_1 \pi_s + \mu_h \mu_m)} + \frac{\gamma Q Y_1^*}{\mu_m}, \\ G_1^* = \frac{c Y_1^*}{\mu_g}, \end{cases}$$

where Y_1^* is the positive roots the polynomial equation

$$D_2 Y_1^{*2} + D_1 Y_1^* + D_0 = 0, \tag{8.32}$$

where $D_2 = \gamma^2 \beta_2 Q$, $D_1 = \frac{\beta_1 \beta_2 \gamma N \pi_h \pi_s}{\beta_1 \pi_s + \mu_h \mu_m} + \gamma \mu_m \mu_r (1 - R_0^{WI})$, and $D_0 = -\frac{\beta_1 \beta_2 \pi_r N \pi_h \pi_s}{\beta_1 \pi_s + \mu_h \mu_m}$.

Theorem 8.3. *(Existence of PPE without immune response): The PPE without immune response exists*
(i) If $D_1 < 0$ implies that $R_0^{WI} > 1$ and discriminant equal to zero, i.e $D_1^2 - 4D_0D_2 = 0$.
(ii) If $D_1 < 0$ implies that $R_0^{WI} > 1$ and discriminant greater than zero, i.e $D_1^2 - 4D_0D_2 > 0$.
(iii) Otherwise not exist.

To perform the PPE of the dynamical system (8.5) with immune defense against the parasite infection, is difficult in this context. However, we can investigate its existence and stability using numerical simulation.

8.3.5 Sensitivity analysis

Here, the index measures indicate how significantly the parameters have changed relative to with respect to changes in R_0 (Chitnis et al., 2008). The normalized forward sensitivity index of the reproduction number concerning parameters is defined as

$$\Gamma_{\mathscr{M}}^{R_0} = \frac{\partial R_0}{\partial \mathscr{M}} \times \frac{\mathscr{M}}{R_0},$$

where $\mathscr{M}$ is denoted the parameters that belongs to R_0. The sensitivity index of the basic reproduction number is presented in Table 8.1. From the findings, it can be concluded that, among the factors taken into account when determining the basic reproduction number, R_0 is more sensitive to β_2, π_r, N, Q and ϖ_m in order. The basic reproduction number, R_0 is impacted negatively by the parameter ϖ_m, which means that increasing this parameter will cause a decrease in R_0, while positively impacted by the parameters β_2, N, and Q, which means that decreasing their value will cause a decrease in R_0.

Table 8.1: Sensitivity indices of within-host basic reproduction number using parameter values in Table 8.2.

Parameter	Value	Parameter	Value
β_2	$+1$	Q	$+1$
γ	$+0.00269927$	π_r	$+1$
b_0	-0.069767	π_i	-1.007281223
b_1	-0.428571429	ϖ_y	-0.0000135
μ_m	-0.066574202	ϖ_m	-0.998613037

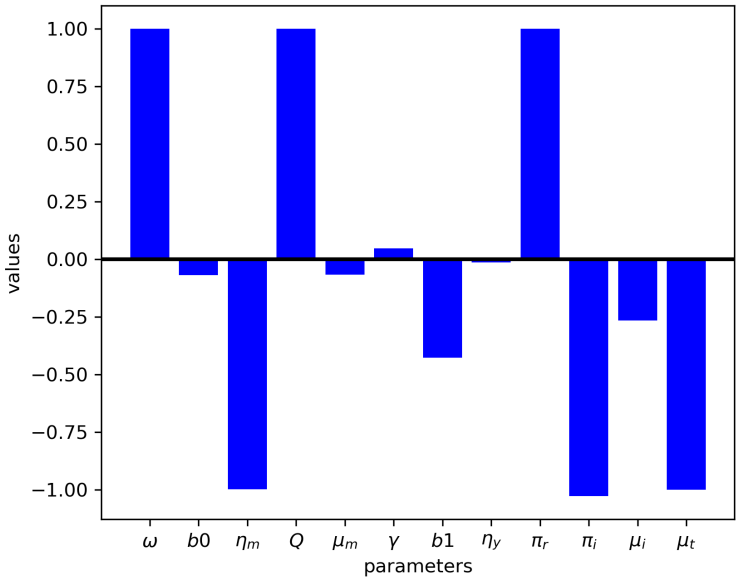

Figure 8.1: Sensitivity index of the biological parameters of the in-host basic reproduction number, R_0.

Figure 8.1 illustrates the sensitivity index of the within-host basic reproduction number.

8.4 Numerical results

In this section, we present several numerical simulations to validate our theoretical results and investigate the memory effect on within-host malaria infection dynamics. The model equation is solved numerically by a generalized predictor-corrector of the Adams-Bashforth-Moulton method using parameter values listed in Table 8.2. The initial data used during the simulation is given as $S(t) = 200, H(t) = 1000, X(t) = 100, R(t) = 55000, Y(t) = 100, M(t) = 10000, G(t) = 10, I(t) = 0.001$. Figures 8.2-8.4 present the evolutionary dynamics with different fractional order, whereas, Figures 7.8-8.9 present the effect of parameters on the evolutionary dynamics of parasite infection.

8.4.1 Impact of fractional order derivative

Figures 8.2-8.4 show the impact of the order derivative on the dynamical behavior of the system equation (8.5). The order of the fractional derivative order α does not affect the stability

Table 8.2: The values for model parameters utilized in the simulation, where *mero* represents merozoites.

Parameters	Value	Range	Unit	Source
π_r	2.5×10^6	$2.5 \times 10^5 - 2.5 \times 10^{10}$	$cell/\mu l/day$	Hetzel and Anderson (1996)
π_h	2.5×10^8	$2.5 \times 10^5 - 2.5 \times 10^{10}$	$cell/\mu l/day$	Orwa et al. (2018)
π_p	20	$20 - 200$	$sporo/day$	Selemani et al. (2016,0)
β_1	0.001	$1 \times 10^{-5} - 1 \times 10^{-3}$	$\mu l/cell/day$	Selemani et al. (2016)
β_2	0.008	$8 \times 10^{-5} - 8 \times 10^{-3}$	$\mu l/cell/day$	Hetzel and Anderson (1996)
δ	0.95	$0.0095 - 0.95$	$cell/day$	Orwa et al. (2018)
γ	0.03	$0.0003 - 0.3$	$cell/day$	Kamangira et al. (2014)
Q	16	$16 - 32$	$mero/\mu l$	Chiyaka et al. (2008)
b_0	0.05	$0.0005 - 0.5$	$cell/\mu l$	Selemani et al. (2016)
b_1	0.05	$0.0005 - 0.5$	$cell/\mu l$	De Roode et al. (2005)
ϖ_1	9×10^{-11}	$9 \times 10^{-11} - 9 \times 10^{-3}$	$cell\mu l/day$	Selemani et al. (2017a)
ϖ_2	9×10^{-5}	$9 \times 10^{-8} - 9 \times 10^{-3}$	$cell\mu l/day$	Chiyaka et al. (2008)
ϖ_m	0.03	$0.0003 - 0.3$	$cell\mu l/day$	Chiyaka et al. (2008)
ϖ_g	3×10^{-5}	$3 \times 10^{-5} - 3 \times 10^{-2}$	$cell\mu l/day$	Anderson et al. (1989)
σ	5×10^{-4}	$5 \times 10^{-6} - 5 \times 10^{-2}$	$/day$	Orwa et al. (2022)
ν	5×10^{-5}	$5 \times 10^{-6} - 5 \times 10^{-3}$	$/day$	Orwa et al. (2018)
θ	5×10^{-4}	$5 \times 10^{-6} - 5 \times 10^{-2}$	$/day$	Orwa et al. (2018)
μ_r	0.0083	$8.3times10^{-5} - 8.3 \times 10^{-2}$	$cell/day$	Anderson et al. (1989)
μ_h	0.029	$0.0029 - 0.029$	$cell/day$	Selemani et al. (2016)
μ_p	1.2×10^{-11}	$1.2times10^{-11} - 1.2 \times 10^{-5}$	$cell/day$	Selemani et al. (2016)
μ_m	48		$cell/day$	Hetzel and Anderson (1996)
μ_g	6.25×10^{-3}	$6.25 \times 10^{-6} - 6.25 \times 10^{-2}$	$cell/day$	Selemani et al. (2016)
μ_e	2		cell/day	Dube et al. (2010)
Λ_e	20		$\mu l/day$	Dube et al. (2010)
a_0	4×10^{-3}	$4 \times 10^{-6} - 4 \times 10^{-2}$	$\mu l/day$	Orwa et al. (2018)
ξ	5×10^{-5}	$5 \times 10^{-6} - 5 \times 10^{-2}$	mm^{-1}/day	Orwa et al. (2018)
c	0.02	0.0002-0.2	$/day$	Hellriegel (1992)

of the steady state. However, for small values of α, which describes the behavior of long memory, solutions converge more quickly towards the parasite persistence steady state. That is the fractional order derivative influences only the convergence speed towards the steady states. Accordingly, the fractional order α impacts the time it takes to attain steady states. Therefore, the fractional order derivative should be included in the epidemiological/immunological model, especially when studying parasite infection dynamics before infection equilibrium is reached.

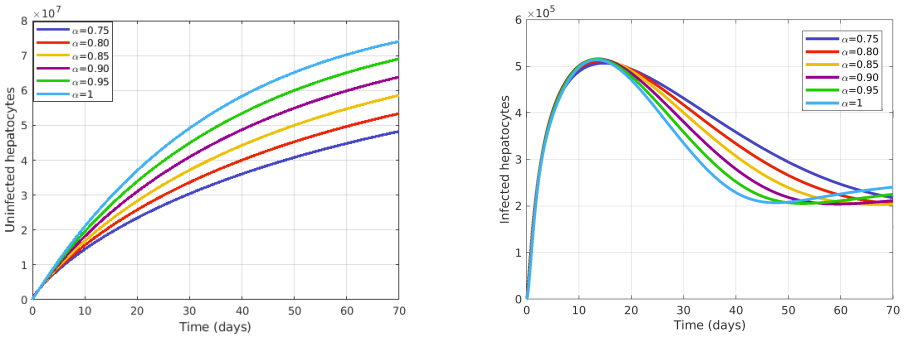

(a) (b)

Figure 8.2: Impact of fractional-order on (a) uninfected hepatocyte cells, (b) infected hepatocyte cells, for $R_0 = 3.1062$ and all the model parameter values are listed as in Table 8.2.

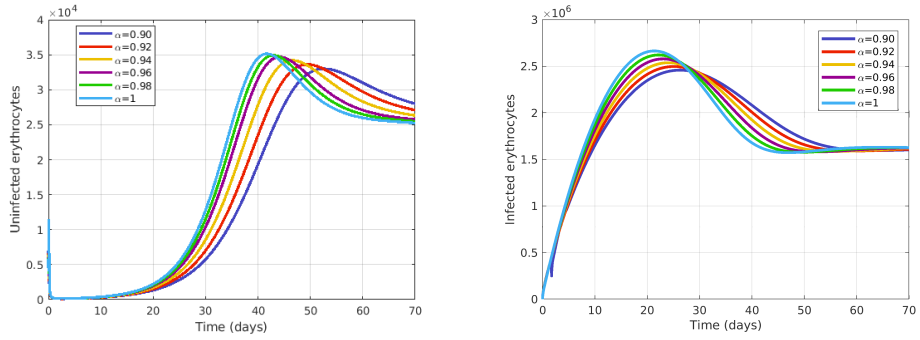

(a) (b)

Figure 8.3: Impact of fractional-order on (a) uninfected erythrocytes, (b) infected erythrocytes, for $R_0 = 3.1062$ and all the model parameter values are listed as in Table 8.2.

8.4.2 Effect of immunological response on hepatocyte and erythrocyte invasion

Figure 8.5 reveals the effect of the efficacy of immune response on hepatocytes and erythrocytes (red blood cells) invasion. The healthy erythrocyte increases as the efficacy of immune response on hepatocytic and erythrocytic invasion increases (see Figure 8.5 (a)). The infected hepatocytes decrease as the efficacy of immune response on hepatocytic and erythrocytic invasion increases (Figure 8.5 (b) and (d)). Thus, the human immunological response can eliminate the malaria parasite infection by blocking the invasion of human liver hepatocyte cells and red blood cells (erythrocytes). Also, human immunity may cure the infected individual.

8.4.3 Effect of infection rate of erythrocyte and hepatocyte

The effect of the infection rate of red blood cells by the malaria parasite in the form of merozoites, β_2 on the dynamics of uninfected erythrocytes and infected erythrocytes is shown in Figure 8.6. The uninfected erythrocytes decrease as the infection rate increases (Figure 8.6

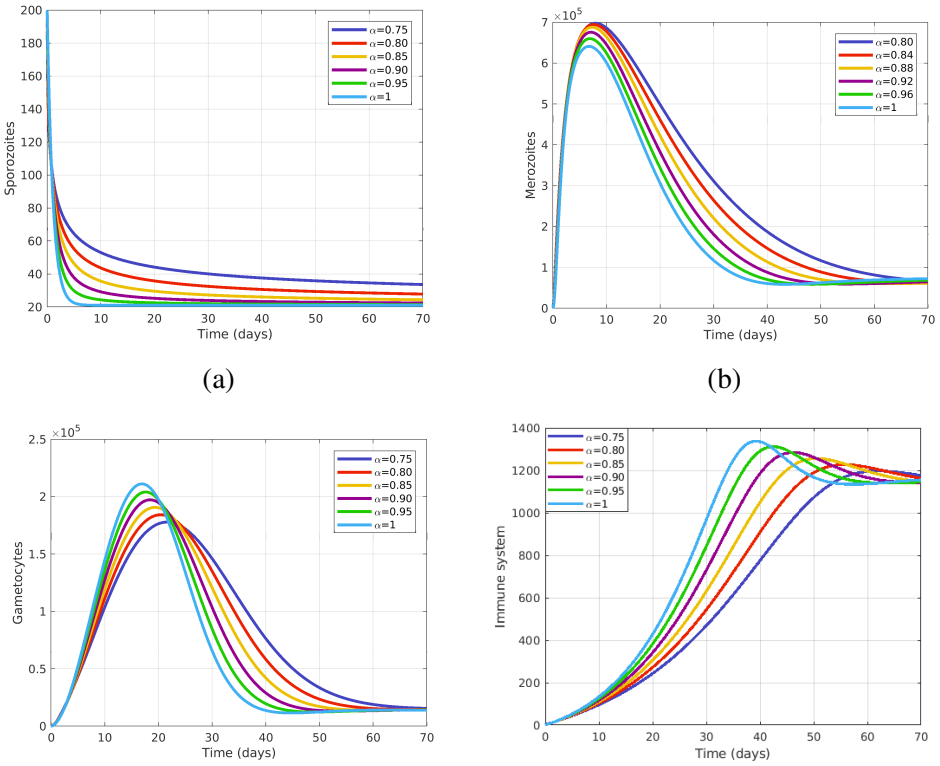

Figure 8.4: Impact of the fractional order on (a) sporozoites, (b) merozoites, (c) gametocytes), (d) immune system, for $R_0 = 3.1062$ and all the model parameter values are listed as in Table 8.2.

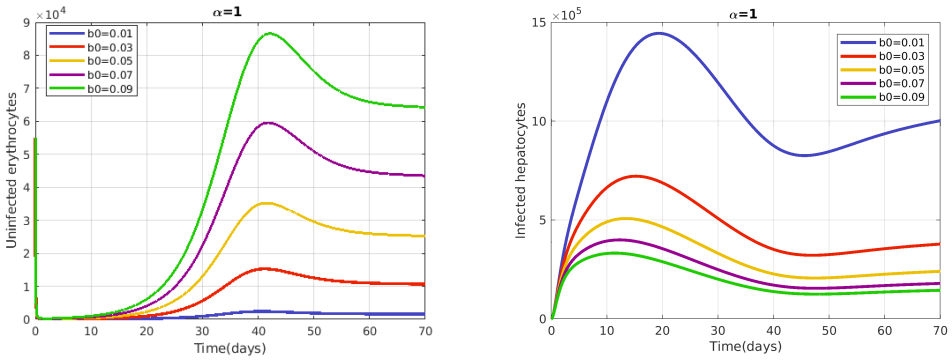

Figure 8.5: The effect of the efficacy of immune response on hepatocytic and erythrocytic invasion on the dynamical behavior of liver hepatocytes and erythrocytes, for $R_0 = 3.1062$ and integer order $\alpha = 1$. All the model parameter values are listed in Table 8.2.

(a)) because uninfected erythrocytes get infected due to merozoite that is released from infected hepatocytes and become infected erythrocytes. Thus, infected erythrocytes slightly rise as the infection rate increases (Figure 8.6 (b)). Figure 8.7 exhibits the effect of the infection rate of hepatocyte cells by sporozoites, β_1 on the dynamical behavior of uninfected hepatocyte cells and infected hepatocyte cells. The uninfected hepatocytes slightly decline as the

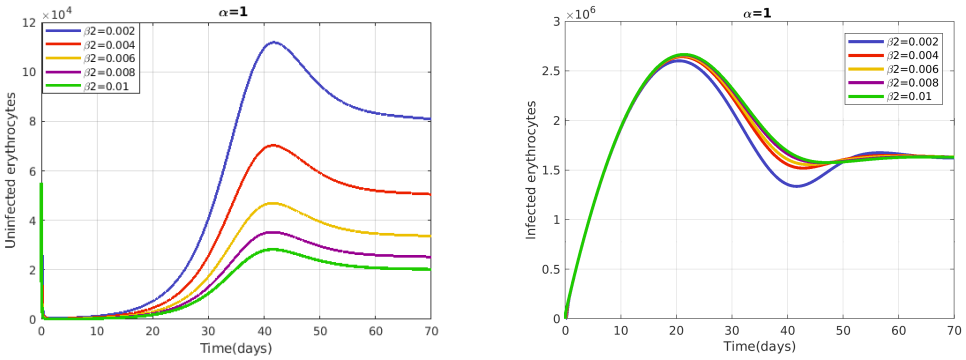

(a) (b)

Figure 8.6: The effect of infection rate of red blood cells on the dynamical behavior of healthy erythrocytes and infected erythrocytes, for $R_0 = 3.1062$ and integer order $\alpha = 1$. All the model parameter values are listed in Table 8.2.

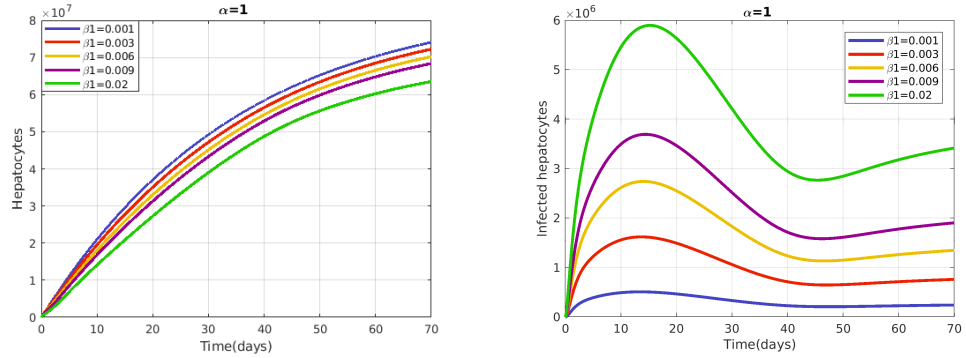

(a) (b)

Figure 8.7: The effect of infection rate of the hepatocyte by sporozoites on the dynamical behavior of healthy hepatocytes and infected hepatocytes, for $R_0 = 3.1062$ and integer order $\alpha = 1$. All the model parameter values are listed in Table 8.2.

infection rate rises (Figure 8.7 (a)), whereas infected hepatocytes rise as the infection rate of hepatocytes by sporozoites increases (Figure 8.7 (b)). This is because the hepatocyte cell acquires infection by sporozoites that are introduced by vector into the liver and get along with infected hepatocytes.

8.4.4 Effect of an average number of merozoites produced per rupturing infected hepatocytes and iRBCs

Figure 8.8 illustrates the effect of an average number of merozoites generated per rupturing infected hepatocytes and infected erythrocytes (iRBCs) on the production of malaria merozoites. The merozoite populations increases as both the average number of merozoites generated per bursting infected hepatocyte cells (liver-schizonts) and infected erythrocytes (blood-schizonts) rises. That is the liver-schizont bursts open and release thousands of merozoites, and the blood-schizont bursts open and release sixteen-thirty six malaria merozoites in the blood system. Again, each of these merozoites invades fresh red blood cells. The cycle repeats if control is

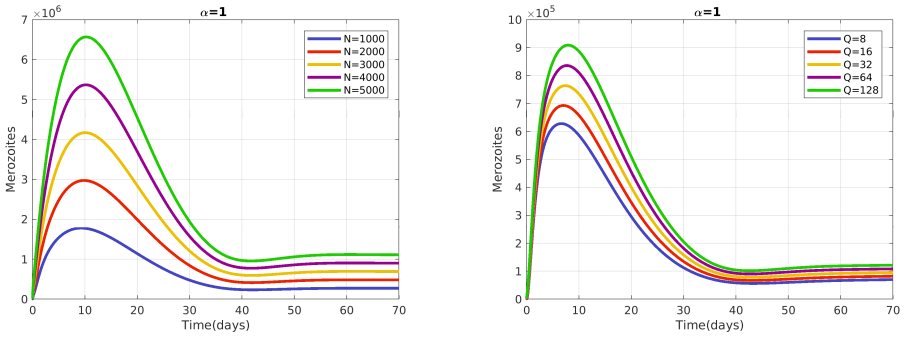

(a) (b)

Figure 8.8: Impact of an average number of merozoites generated per rupturing infected hepatocytes (liver-schizont) and infected erythrocytes (blood-schizont), for $R_0 = 3.1062$ and integer order $\alpha = 1$. All the model parameter values are listed in Table 8.2.

not applied and generates the malaria merozoites.

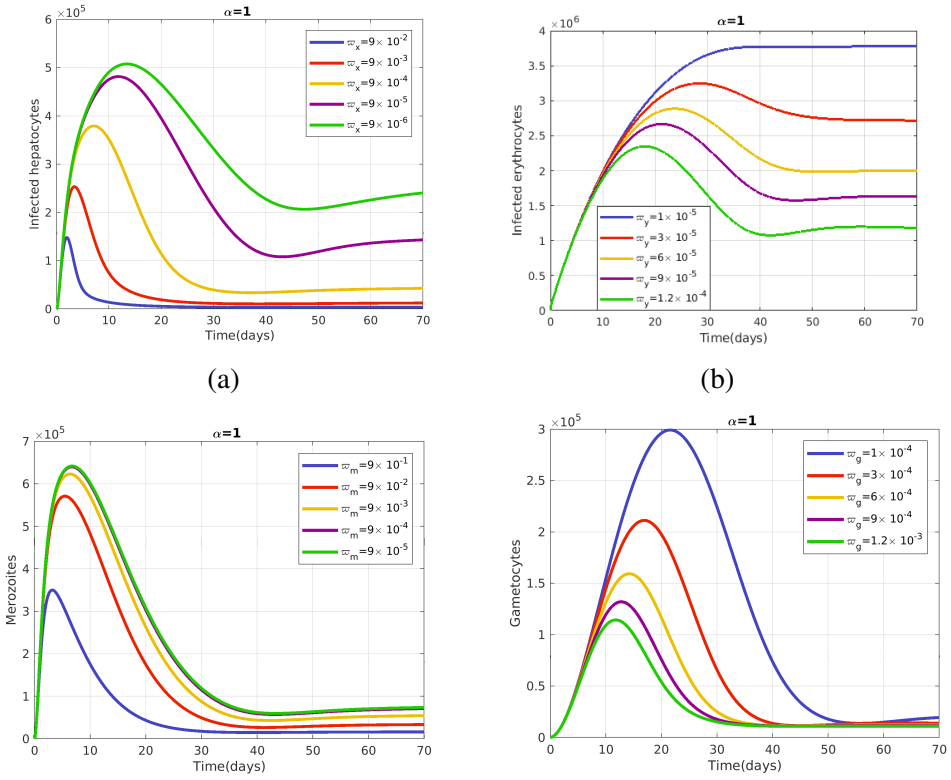

(a) (b)

(c) (d)

Figure 8.9: The effect of removal rate (immunosensitivity) of infected hepatocytes, infected erythrocytes, merozoites, and gametocytes, for $R_0 = 3.1062$ and integer order $\alpha = 1$. All the model parameter values are listed in Table 8.2.

8.4.5 Effect of immune sensitivity of infected cells and malaria parasites

Here, Figure 8.9 depicts the effect of the removal rate (immunosensitivity) of iRBCs, infected hepatocytes, merozoites, and gametocytes owing to an immune response against the parasite

infection. The infected hepatocytes rapidly decline as the removal rate of infected hepatocytes due to human immunity (immunosensitivity of infected hepatocyte cells) ϖ_x rises (Figure 8.9(a)). Infected erythrocytes (iRBCs) decline as the immunosensitivity of infected erythrocytes ϖ_y rises (Figure 8.9(b)), as well as the merozoites and gametocytes are falls as the immunosensitivity of merozoites, ϖ_m and gametocytes, ϖ_g growth (see Figure 8.9(c) and (d)). Here, we conclude that human immunity against parasite infection can prevent the infection by killing (removing) malaria merozoites, gametocytes, infected hepatocytes, and erythrocytes (iRBCs).

8.5 Summary

In this chapter, we developed and analyzed a fractional order mathematical model for the within-host cell dynamics of malaria parasites using Caputo fractional order derivative. Initially, the model is presented with integer-order (classical) differential equations and then reformulated using the fractional order operator in the sense of Caputo. The basic properties of the model such as existence and uniqueness, boundedness, and positivity of the solutions of the model are performed. The existence and uniqueness of the solution are proved using the Banach fixed point theorem. The most important threshold quantity, known as the within-host basic reproduction number R_0, is performed. The model equilibria and their stability analysis are investigated with the parasite-free equilibrium point being both local and global stable if the $R_0 < 1$ and unstable if $R_0 > 1$. The parasite persistence equilibrium point without immune response is exist if $R_0^{WI} > 1$. Sensitivity analysis of the within-host basic reproduction number is conferred. The results indicated that the infection rate of red blood cells by merozoites, the recruitment rate of red blood cells, and the average number of merozoites per rupturing of infected red blood cells are the most influential parameters in the dynamics of the within-host parasite infection. Furthermore, to support our theoretical findings different numerical simulations are presented using a generalized predictor-corrector of the Adams-Bashforth-Moulton method. The simulation results show that an average number of merozoites per rupturing infected hepatocytes and infected erythrocytes as well as the inhibition rate of the invasion of healthy hepatocytes and erythrocytes have a high effect on the within-host dynamics of the parasite. When this rate is reduced, there is a noticeable decrease in the number of infected cells, indicating that primary tissue and blood schizontocides are effective in curing the infection.

CHAPTER 9

SUMMARY, CONCLUSION AND RECOMMENDATIONS

9.1 Summary

Malaria is the most fatal infectious disease after the HIV/ADIS and TB diseases. The WHO is still finding the best control for the malaria disease. This study was intended to develop and analyze mathematical models for within-host dynamics with the aim of investigating effective control strategies. In this study, the in-host mathematical models for malaria parasite infection were investigated. The models consider the dynamics and interactions of the malaria parasites, red blood cells (erythrocytes), liver hepatocyte cells, and immune cells using non-linear differential equations. The stage-specific control efforts of immunological systems are incorporated into the models. The extended models are subjected to antimalaria drug treatment and malaria vaccines. Optimal control theory is also applied to establish the effective medical combination strategy against within-host malaria infection.

The first model of this study is a deterministic model of within-host malaria infection dynamics. The model considers the blood stage dynamics of the parasite infection. The stage-specific cell-mediated and antibody-mediated immunological responses are considered. The cell-mediated immune system is used to eliminate the iRBCs from infected individuals and the antibody-mediated immune response is deployed to eliminate malaria parasites such as merozoites and gametocytes as well as reduce the infection (invasion) rate of healthy red blood cells. The basic properties and qualitative analysis of the model are investigated. The very important threshold value in the epidemic model known as the basic reproduction number R_0 is examined. The parasite-free equilibrium point is shown to be local and global stable if the within-host basic reproduction number is less than R_0 unit.

The results based on the simulation show that intervention during malaria infection should target the merozoite invasion rate on uninfected red blood cells and the density of merozoites in circulation that are responsible for the invasion of vulnerable red blood cells. The cell-mediated and antibody-mediated immune systems are shown to be vital in the elimination of infected red blood cells, merozoites, and gametocytes. The potential role of efficacious antimalarial medication in within-host malaria infection control and elimination is presented in the second model of this study. The model takes into account the tissue schizontocides, blood-schizontocides, and gametocytocide antimalarial treatments. The model is mathematically analyzed to provide useful insights into the infected individual and combine antimalarial treatment's impact on eradicating the severity of parasite infection. The model presented that a highly efficacious antimalarial therapy (efficacy 95%) is likely to offer much-needed protection against malaria infection. In general, antimalarial treatment eliminates iRBCs, and

infected hepatocytes, as well as reduces the concentrations of malaria parasites by blocking the rupturing rate of liver-schozont and blood schizont.

The parameters such as the invention rate of both healthy hepatocytes and erythrocytes, and the average number of merozoites released per rupturing blood-schizont and liver-schizont are also revealed to have a considerable impact on the severity of malaria infection. The efficacy of antimalarial drugs is shown to have a direct negative impact on the density of infected erythrocytes. The higher the efficacy of the administered antimalarial drug, the lower the population of infective merozoites and the smaller the density of infected erythrocytes. This ensures prompt recovery from malaria infection. Using contour plots and results from sensitivity analysis, it is observed that the efficacy of antimalarial drug used, the density of blood floating merozoites produced per infected erythrocytes and the rate of infection by merozoites are the most important parameters in blood-stage malaria infection and control efforts.

The effect of the adaptive immune system in within-host dynamics of malaria infection is also investigated in this study. The blood-stage dynamics of the parasite infection are provided with cytotoxic- T cells and antibodies. We assumed that the adaptive immune cells are activated only during the presence of parasite infection. The mass-action incidence rate is used to show the interaction between healthy red blood cells and hepatocyte cells with malaria parasites, as well as the interaction between immunological responses and infected cells. The qualitative analysis of the model is performed using mathematical analysis. The threshold value R_0 of the model is evaluated. When the within-host basic reproduction number R_0 is less than one the parasite-free equilibrium point exists and it's local and global stable and when the within-host basic reproduction number R_0 greater than one parasite-free equilibrium point is violated and four parasite persistence equilibria are inhibited.

To validate and supplement the analytical findings the model is simulated for different values of initial conditions and parameters. It observed that if $R_0 < 1$ parasite-free equilibrium is globally asymptotically stable, if $R_0 > 1$ a parasite persistence equilibrium without adaptive immune response is stable, if $1 \leq R_0^C \leq R_0$ a parasite persistence equilibrium in the presence of cytotoxic T-cells is stable, if $1 \leq R_0^A \leq R_0$ a parasite persistence equilibrium in the presence of antibodies is stable, and if $1 \leq R_0^A, R_0^C \leq R_0$ a parasite persistence equilibrium with adaptive immune response is stable.

The optimal control theory is applied to the within-host dynamics malaria infection model in this study. The model takes into account antimalarial drug treatment and malaria vaccine antigens as a control strategy against malaria parasite infection. The target is to present the best combination of control strategies. The model contains the Pre-erythrocytic vaccine (PEV), blood-stage vaccine (BSV), transmission-blocking vaccines (TBVs), primary tissue schizontocides, blood schizontocides, and gametocytocidal drugs against in-host parasite infection. Using a combination of two controls, three controls, and all four controls the model incorporates the most effective control strategies as: (i) combinations of the Pre-erythrocytic vaccine and

blood schizontocides, (ii) combination of Pre-erythrocytic vaccine and blood schizontocides, (iii) combinations of blood-stage vaccine and blood schizontocides and gametocytocides, (iv) combinations pre-erythrocytic vaccine, blood-stage vaccine, and blood schizontocides as well as gametocytocidal, (v) combinations of pre-erythrocytic vaccine, primary tissue schizontocides, and blood-schizontocides, and gametocytocides, (vi) combination of the blood-stage vaccine, primary tissue schizon-tocides, and blood schizontocides and gametocytocides and (vii) combination all four measures together on preventing malaria infection in human hosts.

The Pontryagin's Maximum Principle was used to characterize and discuss control strategies that substantially reduced the populations of infected erythrocytes, infected hepatocytes, and malaria parasites. The necessary conditions were derived and analyzed for the existence of optimal control therapy for malaria infection. For sufficiently small values of intervention time, the uniqueness of the optimality system was proved. Numerical results showed that a combination of pre-erythrocytic vaccine antigen, blood schizontocide, and gametocytocide drugs offers the best control strategy against malaria parasite infection.

Finally, in this study, the within-host dynamic of the malaria infection model with memory effect is considered. The model is formulated and analyzed using fractional order derivative in the sense of Caputo fractional derivative to observe the memory effects and obtain more insight into the in human host dynamics of malaria infection. The existence, and uniqueness of the model solution, as well as the biological feasibility and mathematical well-posedness of the model, is performed in this study. The qualitative analysis of the model is examined. The model equilibria and their stability analysis are investigated. Several numerical simulations are presented to validate and supplement our analytical results. It observed that the order of derivative has no affect stability of the steady states, however, it affects the speed of the convergence toward the steady states. The small values of fractional order derivative, which describe the behavior of long memory, solutions converge more quickly towards the parasite persistence steady state.

9.2 Conclusion

In this study, the deterministic mathematical models for the within-host dynamics of the malaria parasite are formulated utilizing a system of non-leaner ordinary differential equations. The models consider the effect of different stage-specific human immunological systems in the transmission dynamics of within-host malaria parasites. Particularly, the effect of cell-mediated, antibody-mediated, cytotoxic T-cells, and antibodies immunological responses are provided in this study. The findings suggested that immunology is vital in the elimination of malaria parasite infections by blocking the invasion of the liver hepatocyte cells, red blood cells (erythrocytes), and killing/ removing the infected cells (infected liver hepatocytes and erythrocytes) and malaria parasites (merozoites and gametocytes) from infected individuals.

When the within-host basic reproduction number is R_0 is greater than one the human immunological response is not responsible for eliminating the parasite infection. Thus, antimalarial medication is required to treat infected individuals. This study also examined the effect of the antimalarial treatment in within-host parasite infection dynamics. The primary tissue(pre-erythrocytic) schizontocides, blood schizontocides, and gametocytocide antimalarial drugs medication are incorporated into the model. It observed the blood stage antimalarial treatment (blood schzontocide) is the most effective in influencing the malaria parasite infection.

The theory of optimal control is applied to the in-host dynamics of the malaria infection model. The study takes into account the malaria vaccine and antimalarial therapy as a control strategy against malaria infection. The main target of this theory of optimal control is to examine the most effective control strategies to eliminate in-host malaria infection with minimum cost spending during infected individual medication. Nearly seven control strategies are considered in this study, it observed that implementation of all the controls is the most effective control strategy to eradicate the within-host malaria infection. The memory effect of the within-host malaria infection is investigated in this study, using a fractional order differential equation in the sense of Caputo fractional derivative. The small values of fractional order derivative indicate the behavior of long memory, solutions converge more fastly towards the parasite persistence steady state. That is, it affects the time it takes to attain parasite steady states.

9.3 Recommendations

In this study, we explore various models to gain insight into the within-host dynamics of the malaria parasite. We analyze the impact of human immunological responses and antimalarial treatment, as well as the effectiveness of control measures in preventing within-host malaria infection. Our investigation includes an analysis of the results, leading to the following recommendations based on our findings. Blood schizontocides are effective in eliminating malarial parasites during clinical infections, and health workers should administer them. Understanding the efforts of the immunological system is used to develop malaria prevention. Hence, policymakers can use this work to develop malaria prevention. In this work, we focus solely on drug-sensitive antimalarial treatment. The drug-resistant treatment can aid in understanding the complexity of within-host malaria infection. Thus, the scholars can consider the within-host dynamics of malaria parasite infection with drug-resistant. Furthermore, to better understand the in-host dynamics of malaria parasite infection the researchers can use the reaction-diffusion model, delay differential equation, and stochastic model.

9.4 Limitations and future work

This study utilizes mathematical modeling and analysis to gain valuable insights necessary understanding the dynamics of malaria parasite infection within the host and for improving the most effective control measures against malaria parasite infection. The within-host malaria infection models, like many other epidemic models, are based on various assumptions. These assumptions are made to simplify the model and make the analytical results more manageable. However, the malaria parasite life cycle is extremely complex and there are many unknown biological functions. To improve the model's accuracy, some of the assumptions made in this study could be reconsidered.

The values of the parameters used in this study were either obtained from existing literature or simply assumed. This was due to a lack of data and some unknown dynamics within the complex malaria parasite life cycle. The availability of clinical data on within-host malaria dynamics, both with and without vaccines and antimalarial drugs, could be very helpful in estimating model parameter values for improved results. The time delay from invasion to schizont rupture is not captured in this study. This is another key area that could improve the results presented here. A time-dependent delay parameter would be a plausible addition to future within-host malaria models. Furthermore, reaction-diffusion is not considered. It plays a key role in understanding the transport of blood, allowing cells of multicellular organisms to receive nutrients, and remove waste through the human circulatory system. Model validation is an essential step in disease modeling. In this study, we can extend the models by validating them using accurate data on within-host malaria dynamics and therapeutic control.

REFERENCES

Aba Oud, M. A., Ali, A., Alrabaiah, H., Ullah, S., Khan, M. A., and Islam, S. (2021). A fractional order mathematical model for covid-19 dynamics with quarantine, isolation, and environmental viral load. *Advances in Difference Equations*, 2021(1):1–19.

Abiodun, O., Olukayode, A., and Ndako, J. (2023). Mathematical modeling and optimal control strategies of hiv/aids with haart. In *2023 International Conference on Science, Engineering and Business for Sustainable Development Goals (SEB-SDG)*, volume 1, pages 1–9. IEEE.

Abioye, A. I., Peter, O. J., Ogunseye, H. A., Oguntolu, F. A., Ayoola, T. A., and Oladapo, A. O. (2023). A fractional-order mathematical model for malaria and covid-19 co-infection dynamics. *Healthcare Analytics*, 4:100210.

Abramson, G. (2001). Mathematical modeling of the spread of infectious diseases. *A series of lectures given at PANDA, UNM*.

Acharya, P., Garg, M., Kumar, P., Munjal, A., and Raja, K. (2017). Host–parasite interactions in human malaria: clinical implications of basic research. *Frontiers in microbiology*, 8:889.

Adi, Y. A. (2021). A within-host tuberculosis model using optimal control. *JTAM (Jurnal Teori dan Aplikasi Matematika)*, 5(1):162–170.

Adu, I. K., Aidoo, A. Y., Darko, I. O., and Osei-Frimpong, E. (2014). Mathematical model of hepatitis b in the bosomtwe district of ashanti region, ghana. *Applied Mathematical Sciences*, 8(67):3343–3358.

Adugna, A. (2011). Malaria in ethiopia.

Ahmed, E., El-Sayed, A., and El-Saka, H. A. (2006). On some routh–hurwitz conditions for fractional order differential equations and their applications in lorenz, rössler, chua and chen systems. *Physics Letters A*, 358(1):1–4.

Al Basir, F. and Abraha, T. (2023). Mathematical modelling and optimal control of malaria using awareness-based interventions. *Mathematics*, 11(7):1687.

Al-Refai, M. and Pal, K. (2019). New aspects of caputo–fabrizio fractional derivative. *Prog. Fract. Differ. Appl*, 5(2):157–166.

Alrabaiah, H., Safi, M. A., DarAssi, M. H., Al-Hdaibat, B., Ullah, S., Khan, M. A., and Shah, S. A. A. (2020). Optimal control analysis of hepatitis b virus with treatment and vaccination. *Results in Physics*, 19:103599.

Alsahafi, S. and Woodcock, S. (2022). Exploring hiv dynamics and an optimal control strategy. *Mathematics*, 10(5):749.

Anderson and May (1991a). Infectious diseases of humans. *Aust J Public Health*, 16:208–212.

Anderson, R., May, R., and Gupta, S. (1989). Non-linear phenomena in host—parasite interactions. *Parasitology*, 99(S1):S59–S79.

Anderson, R. M. (1998). Complex dynamic behaviours in the interaction between parasite populations and the host's immune system. *International Journal for Parasitology*, 28(4):551–566.

Anderson, R. M. and May, R. M. (1991b). Infectious diseases of humans, vol. 1 oxford. *UK: Oxford University Press.[Google Scholar]*.

Annan, K. (2020). In-host analysis of malaria dynamics in humans. *Open Journal of Applied Sciences*, 10(5):191–209.

Arafa, A., Rida, S., and Khalil, M. (2012). Fractional modeling dynamics of hiv and cd4+ t-cells during primary infection. *Nonlinear biomedical physics*, 6(1):1–7.

Arafa, A., Rida, S., and Khalil, M. (2014). A fractional-order model of hiv infection with drug therapy effect. *Journal of the Egyptian Mathematical Society*, 22(3):538–543.

Arama, C. and Troye-Blomberg, M. (2014). The path of malaria vaccine development: challenges and perspectives. *Journal of internal medicine*, 275(5):456–466.

Assebe, L. F., Kwete, X. J., Wang, D., Liu, L., Norheim, O. F., Jbaily, A., Verguet, S., Johansson, K. A., and Tolla, M. T. (2020). Health gains and financial risk protection afforded by public financing of selected malaria interventions in ethiopia: an extended cost-effectiveness analysis. *Malaria journal*, 19(1):1–10.

Athithan, S. and Ghosh, M. (2015). Stability analysis and optimal control of a malaria model with larvivorous fish as biological control agent. *Applied Mathematics & Information Sciences*, 9(4):1893.

Audran, R., Cachat, M., Lurati, F., Soe, S., Leroy, O., Corradin, G., Druilhe, P., and Spertini, F. (2005). Phase i malaria vaccine trial with a long synthetic peptide derived from the merozoite surface protein 3 antigen. *Infection and immunity*, 73(12):8017–8026.

Augustine, A. D., Hall, B. F., Leitner, W. W., Mo, A. X., Wali, T. M., and Fauci, A. S. (2009). Niaid workshop on immunity to malaria: addressing immunological challenges. *Nature immunology*, 10(7):673–678.

Austin, D., White, N., and Anderson, R. (1998). The dynamics of drug action on the within-host population growth of infectious agents: melding pharmacokinetics with pathogen population dynamics. *Journal of theoretical biology*, 194(3):313–339.

Ayele, T. K., Goufo, E. F. D., and Mugisha, S. (2021). Mathematical modeling of hiv/aids with optimal control: a case study in ethiopia. *Results in Physics*, 26:104263.

Badmos, A. O., Alaran, A. J., Adebisi, Y. A., Bouaddi, O., Onibon, Z., Dada, A., Lin, X., and Lucero-Prisno, D. E. (2021). What sub-saharan african countries can learn from malaria elimination in china. *Tropical Medicine and Health*, 49(1):1–6.

Baihaqi, M. A. and Adi-Kusumo, F. (2020). Modelling malaria transmission in a population with seirs p method. In *AIP Conference Proceedings*, volume 2264, page 020002. AIP Publishing LLC.

Barnes, K. I., Chanda, P., and Ab Barnabas, G. (2009). Impact of the large-scale deployment of artemether/lumefantrine on the malaria disease burden in africa: case studies of south africa, zambia and ethiopia. *Malaria journal*, 8(1):1–7.

Belachew, E. B. (2018). Immune response and evasion mechanisms of plasmodium falciparum parasites. *Journal of immunology research*, 2018.

Bernoulli, D. (1760). Essai d'une nouvelle analyse de la mortalité causée par la petite vérole, et des avantages de l'inoculation pour la prévenir.

Bhatt, S., Weiss, D., Cameron, E., Bisanzio, D., Mappin, B., Dalrymple, U., Battle, K., Moyes, C., Henry, A., Eckhoff, P., et al. (2015). The effect of malaria control on plasmodium falciparum in africa between 2000 and 2015. *Nature*, 526(7572):207–211.

Boukhouima, A., Hattaf, K., and Yousfi, N. (2018). A fractional order model for viral infection with cure of infected cells and humoral immunity. *International Journal of Differential Equations*, 2018.

Bruce-Chwatt, L. J. (1962). Classification of antimalarial drugs in relation to different stages in the life-cycle of the parasite: commentary on a diagram. *Bulletin of the World Health Organization*, 27(2):287.

Bugssa, G. and Tedla, K. (2020). Feasibility of malaria elimination in ethiopia. *Ethiopian Journal of Health Sciences*, 30(4).

Burrack, K. S., Hart, G. T., and Hamilton, S. E. (2019). Contributions of natural killer cells to the immune response against plasmodium. *Malaria Journal*, 18(1):1–9.

Bussell, E. H., Dangerfield, C. E., Gilligan, C. A., and Cunniffe, N. J. (2019). Applying optimal control theory to complex epidemiological models to inform real-world disease management. *Philosophical Transactions of the Royal Society B*, 374(1776):20180284.

Carr, J. (1981). Applications of center manifold theory springer-verlag: Newyork. *Heidelberg, Berlin*.

Carter, R. (2001). Transmission blocking malaria vaccines. *Vaccine*, 19(17-19):2309–2314.

Carter, R., Mendis, K. N., Miller, L. H., Molineaux, L., and Saul, A. (2000). Malaria transmission-blocking vaccines—how can their development be supported? *Nature medicine*, 6(3):241–244.

Castillo-Chavez, C. and Song, B. (2004). Dynamical models of tuberculosis and their applications. *Mathematical Biosciences & Engineering*, 1(2):361.

Cauchemez, S., Fraser, C., Van Kerkhove, M. D., Donnelly, C. A., Riley, S., Rambaut, A., Enouf, V., van der Werf, S., and Ferguson, N. M. (2014). Middle east respiratory syndrome coronavirus: quantification of the extent of the epidemic, surveillance biases, and transmissibility. *The Lancet infectious diseases*, 14(1):50–56.

Chatterjee, A. N. and Ahmad, B. (2021). A fractional-order differential equation model of covid-19 infection of epithelial cells. *Chaos, Solitons & Fractals*, 147:110952.

Chen, H., Wang, W., Fu, R., and Luo, J. (2015). Global analysis of a mathematical model on malaria with competitive strains and immune responses. *Applied Mathematics and Computation*, 259:132–152.

Cheneke, K. R. et al. (2023). Optimal control and bifurcation analysis of hiv model. *Computational and Mathematical Methods in Medicine*, 2023.

Chernin, E. (1988). Sir ronald ross, malaria, and the rewards of research. *Medical history*, 32(2):119–141.

Chitnis, N., Hyman, J. M., and Cushing, J. M. (2008). Determining important parameters in the spread of malaria through the sensitivity analysis of a mathematical model. *Bulletin of mathematical biology*, 70:1272–1296.

Chiyaka, C., Garira, W., and Dube, S. (2008). Modelling immune response and drug therapy in human malaria infection. *Computational and Mathematical Methods in Medicine*, 9(2):143–163.

Cibulskis, R. E., Alonso, P., Aponte, J., Aregawi, M., Barrette, A., Bergeron, L., Fergus, C. A., Knox, T., Lynch, M., Patouillard, E., et al. (2016). Malaria: global progress 2000–2015 and future challenges. *Infectious diseases of poverty*, 5:1–8.

Coban, C., Ishii, K. J., Horii, T., and Akira, S. (2007). Manipulation of host innate immune responses by the malaria parasite. *Trends in microbiology*, 15(6):271–278.

Collins, C., Fister, K. R., Key, B., and Williams, M. (2009). Blasting neuroblastoma using optimal control of chemotherapy. *Mathematical Biosciences & Engineering*, 6(3):451–467.

Dalir, M. and Bashour, M. (2010). Applications of fractional calculus. *Applied Mathematical Sciences*, 4(21):1021–1032.

De Boer, R. J. and Perelson, A. S. (1995). Towards a general function describing t cell proliferation. *Journal of theoretical biology*, 175(4):567–576.

De Roode, J. C., Helinski, M. E., Anwar, M. A., and Read, A. F. (2005). Dynamics of multiple infection and within-host competition in genetically diverse malaria infections. *The American Naturalist*, 166(5):531–542.

Dehingia, K., Mohsen, A. A., Alharbi, S. A., Alsemiry, R. D., and Rezapour, S. (2022). Dynamical behavior of a fractional order model for within-host sars-cov-2. *Mathematics*, 10(13):2344.

Dhangadamajhi, G., Kar, S. K., and Ranjit, M. (2010). The survival strategies of malaria parasite in the red blood cell and host cell polymorphisms. *Malaria research and treatment*, 2010.

Diekmann, O., Heesterbeek, J. A. P., and Metz, J. A. (1990). On the definition and the computation of the basic reproduction ratio r 0 in models for infectious diseases in heterogeneous populations. *Journal of mathematical biology*, 28:365–382.

Diethelm, K., Ford, N. J., and Freed, A. D. (2002). A predictor-corrector approach for the numerical solution of fractional differential equations. *Nonlinear Dynamics*, 29:3–22.

Dietz, K. (1993). The estimation of the basic reproduction number for infectious diseases. *Statistical methods in medical research*, 2(1):23–41.

Ding, Y. and Ye, H. (2009). A fractional-order differential equation model of hiv infection of cd4+ t-cells. *Mathematical and Computer Modelling*, 50(3-4):386–392.

Donnelly, C. A., Fisher, M. C., Fraser, C., Ghani, A. C., Riley, S., Ferguson, N. M., and Anderson, R. M. (2004). Epidemiological and genetic analysis of severe acute respiratory syndrome. *The Lancet infectious diseases*, 4(11):672–683.

Dube, S., Chiyaka, C., and Garira[1], W. (2010). Using mathematics to understand malaria infection during erythrocytic stages. *Zimbabwe journal of science and technology*, 5(1):1–11.

Duffy, P. E., Sahu, T., Akue, A., Milman, N., and Anderson, C. (2012). Pre-erythrocytic malaria vaccines: identifying the targets. *Expert review of vaccines*, 11(10):1261–1280.

Elaiw, A. and Al Agha, A. (2020). Global analysis of a reaction-diffusion within-host malaria infection model with adaptive immune response. *Mathematics*, 8(4):563.

Fischer, P. R. and Bialek, R. (2002). Prevention of malaria in children. *Clinical infectious diseases*, 34(4):493–498.

Fleming, W. H. and Rishel, R. W. (2012). *Deterministic and stochastic optimal control*, volume 1. Springer Science & Business Media.

Fontaine, R. E., Najjar, A. E., Prince, J. S., et al. (1961). The 1958 malaria epidemic in ethiopia. *American journal of tropical medicine and hygiene*, 10(6):795–803.

Gahamanyi, M., Banzi, W., and Ntaganda, J. M. (2021). Solving an optimal control problem of hepatitis b virus dynamics: Efficacy of fuzzy logic strategy. *Rwanda Journal of Engineering, Science, Technology and Environment*, 4(1):1–18.

Gao, D.-p. and Huang, N.-j. (2018). Optimal control analysis of a tuberculosis model. *Applied Mathematical Modelling*, 58:47–64.

Girum, T., Shumbej, T., and Shewangizaw, M. (2019). Burden of malaria in ethiopia, 2000-2016: findings from the global health estimates 2016. *Tropical Diseases, Travel Medicine and Vaccines*, 5(1):1–7.

Gowda, D. C. and Wu, X. (2018). Parasite recognition and signaling mechanisms in innate immune responses to malaria. *Frontiers in immunology*, 9:3006.

Hamer, W. H. (1906). *The milroy lectures on epidemic diseases in england: The evidence of variability and of persistency of type; delivered before the royal college of physicians of london, march 1st, 6th, and 8th, 1906*. Bedford Press.

Heller, L. E. and Roepe, P. D. (2019). Artemisinin-based antimalarial drug therapy: molecular pharmacology and evolving resistance. *Tropical medicine and infectious disease*, 4(2):89.

Hellriegel, B. (1992). Modelling the immune response to malaria with ecological concepts: short-term behaviour against long-term equilibrium. *Proceedings of the Royal Society of London. Series B: Biological Sciences*, 250(1329):249–256.

Helmersson, J. (2012). Mathematical modeling of dengue-temperature effect on vectorial capacity.

Hethcote, H. W. (2000). The mathematics of infectious diseases. *SIAM review*, 42(4):599–653.

Hetzel, C. and Anderson, R. (1996). The within-host cellular dynamics of bloodstage malaria: theoretical and experimental studies. *Parasitology*, 113(1):25–38.

Holz, L. E., Fernandez-Ruiz, D., and Heath, W. R. (2016). Protective immunity to liver-stage malaria. *Clinical & translational immunology*, 5(10):e105.

Iggidr, A., Kamgang, J.-C., Sallet, G., and Tewa, J.-J. (2006). Global analysis of new malaria intrahost models with a competitive exclusion principle. *SIAM Journal on Applied Mathematics*, 67(1):260–278.

Illingworth, J. J., Alanine, D. G., Brown, R., Marshall, J. M., Bartlett, H. E., Silk, S. E., Labbé, G. M., Quinkert, D., Cho, J. S., Wendler, J. P., et al. (2019). Functional comparison of blood-stage plasmodium falciparum malaria vaccine candidate antigens. *Frontiers in immunology*, 10:1254.

Joshi, H. R., Lenhart, S., Li, M. Y., and Wang, L. (2006). Optimal control methods applied to disease models. *Contemporary Mathematics*, 410:187–208.

Kamangira, B., Nyamugure, P., and Magombedze, G. (2014). A theoretical mathematical assessment of the effectiveness of coartemether in the treatment of plasmodium falciparum malaria infection. *Mathematical Biosciences*, 256:28–41.

Kazem, S. (2013). Exact solution of some linear fractional differential equations by laplace transform. *International Journal of nonlinear science*, 16(1):3–11.

Kendie, F. A., Nibret Semegn, E., Ferede, M. W., et al. (2021). Prevalence of malaria among adults in ethiopia: a systematic review and meta-analysis. *Journal of tropical medicine*, 2021.

Keno, T. D., Dano, L. B., and Makinde, O. D. (2022). Modeling and optimal control analysis for malaria transmission with role of climate variability. *Computational and Mathematical Methods*, 2022:1–18.

Khan, T., Rihan, F. A., and Ahmad, H. (2023). Modelling the dynamics of acute and chronic hepatitis b with optimal control. *Scientific reports*, 13(1):14980.

Kotola, B. S., Teklu, S. W., and Abebaw, Y. F. (2023). Bifurcation and optimal control analysis of hiv/aids and covid-19 co-infection model with numerical simulation. *Plos one*, 18(5):e0284759.

La Salle, J. P. (1976). *The stability of dynamical systems*. SIAM.

Laishram, D. D., Sutton, P. L., Nanda, N., Sharma, V. L., Sobti, R. C., Carlton, J. M., and Joshi, H. (2012). The complexities of malaria disease manifestations with a focus on asymptomatic malaria. *Malaria journal*, 11(1):1–15.

LaSalle, J. (1976). The stability of dynamical systems, society for industrial and applied mathematics, philadelphia, pa., 1976. In *With an appendix:"Limiting equations and stability of nonautonomous ordinary differential equations" by Z. Artstein, Regional Conference Series in Applied Mathematics*.

Layek, G. et al. (2015). *An introduction to dynamical systems and chaos*, volume 449. Springer.

Lenhart, S. and Workman, J. T. (2007). *Optimal control applied to biological models*. CRC press.

Li, Y., Ruan, S., and Xiao, D. (2011). The within-host dynamics of malaria infection with immune response. *Mathematical Biosciences & Engineering*, 8(4):999.

Long, C. A. and Zavala, F. (2017). Immune responses in malaria. *Cold Spring Harbor perspectives in medicine*, 7(8):a025577.

Malaguarnera, L. and Musumeci, S. (2002). The immune response to plasmodium falciparum malaria. *The Lancet infectious diseases*, 2(8):472–478.

Malaria, R. B. (2011). Economic costs of malaria. *World Health Organization*, 20(1).

Mandala, W. L., Harawa, V., Dzinjalamala, F., and Tembo, D. (2021). The role of different components of the immune system against plasmodium falciparum malaria: Possible contribution towards malaria vaccine development. *Molecular and biochemical parasitology*, 246:111425.

Mbacham, W., Ayong, L., Guewo-Fokeng, M., and Makoge, V. (2019). Current situation of malaria in africa. In *Malaria Control and Elimination*, pages 29–44. Springer.

McQueen, P. G. and McKenzie, F. E. (2008). Host control of malaria infections: constraints on immune and erythropoeitic response kinetics. *PLoS computational biology*, 4(8):e1000149.

McQueen, P. G., Williamson, K. C., and McKenzie, F. E. (2013). Host immune constraints on malaria transmission: insights from population biology of within-host parasites. *Malaria journal*, 12(1):1–18.

Miao, H., Abdurahman, X., Teng, Z., and Kang, C. (2017). Global dynamics of a fractional order hiv model with both virus-to-cell and cell-to-cell transmissions and therapy effect. *IAENG International Journal of Applied Mathematics*, 47(1):75–81.

Mlay, G. M., Luboobi, L., Kuznetsov, D., and Shahada, F. (2015). Optimal treatment and vaccination control strategies for the dynamics of pulmonary tuberculosis. *International Journal of Advances in Applied Mathematics and Mechanics*, 2(3):196–207.

Moorthy, V. S., Good, M. F., and Hill, A. V. (2004). Malaria vaccine developments. *The lancet*, 363(9403):150–156.

Moualeu, D. P., Weiser, M., Ehrig, R., and Deuflhard, P. (2015). Optimal control for a tuberculosis model with undetected cases in cameroon. *Communications in Nonlinear Science and Numerical Simulation*, 20(3):986–1003.

Munro, B. A. and McMorran, B. J. (2022). Antimalarial drug strategies to target plasmodium gametocytes. *Parasitologia*, 2(2):101–124.

Mwanga, G. G., Haario, H., and Nannyonga, B. K. (2014). Optimal control of malaria model with drug resistance in presence of parameter uncertainty. *Applied Mathematical Sciences*, 8(55):2701–2730.

Nath, B. J., Dehingia, K., Mishra, V. N., Chu, Y.-M., and Sarmah, H. K. (2021). Mathematical analysis of a within-host model of sars-cov-2. *Advances in difference equations*, 2021:1–11.

Nazir, G., Shah, K., Debbouche, A., and Khan, R. A. (2020). Study of hiv mathematical model under nonsingular kernel type derivative of fractional order. *Chaos, Solitons & Fractals*, 139:110095.

Nepomuceno, E. G., Peixoto, M. L., Lacerda, M. J., Campanharo, A. S., Takahashi, R. H., and Aguirre, L. A. (2021). Application of optimal control of infectious diseases in a model-free scenario. *SN Computer Science*, 2(5):405.

Ngina, P., Mbogo, R. W., Luboobi, L. S., et al. (2018). Modelling optimal control of in-host hiv dynamics using different control strategies. *Computational and Mathematical Methods in Medicine*, 2018.

Nishiura, H. (2010). Correcting the actual reproduction number: a simple method to estimate from early epidemic growth data. *International journal of environmental research and public health*, 7(1):291–302.

Odibat, Z. M. and Shawagfeh, N. T. (2007). Generalized taylor's formula. *Applied Mathematics and Computation*, 186(1):286–293.

Ogutu, B. R., Apollo, O. J., McKinney, D., Okoth, W., Siangla, J., Dubovsky, F., Tucker, K., Waitumbi, J. N., Diggs, C., Wittes, J., et al. (2009). Blood stage malaria vaccine eliciting high antigen-specific antibody concentrations confers no protection to young children in western kenya. *PloS one*, 4(3):e4708.

Oke, S. I., Ojo, M. M., Adeniyi, M. O., and Matadi, M. B. (2020). Mathematical modeling of malaria disease with control strategy. *Commun. Math. Biol. Neurosci.*, 2020:Article–ID.

Okosun, K. and Makinde, O. D. (2011). Modelling the impact of drug resistance in malaria transmission and its optimal control analysis.

Okosun, K. O., Rachid, O., and Marcus, N. (2013). Optimal control strategies and cost-effectiveness analysis of a malaria model. *BioSystems*, 111(2):83–101.

Olani, Z., Solomon, S., Kaba, Z., Bikila, H., et al. (2023). A five-year (2016-2020) trend analysis of malaria surveillance data in oromia regional state, ethiopia. *BioMed Research International*, 2023.

Olaniyi, S. and Obabiyi, O. (2013). Mathematical model for malaria transmission dynamics in human and mosquito populations with nonlinear forces of infection. *International journal of pure and applied Mathematics*, 88(1):125–156.

Olaniyi, S., Okosun, K., Adesanya, S., and Lebelo, R. (2020). Modelling malaria dynamics with partial immunity and protected travellers: optimal control and cost-effectiveness analysis. *Journal of Biological Dynamics*, 14(1):90–115.

Omondi, E., Mbogo, R., and Luboobi, L. (2018). Mathematical modelling of the impact of testing, treatment and control of hiv transmission in kenya. *Cogent Mathematics & Statistics*, 5(1):1475590.

Orwa, T., Mbogo, R., and Luboobi, L. (2018). Mathematical model for the in-host malaria dynamics subject to malaria vaccines. *Letters in Biomathematics*, 5(1):222–251.

Orwa, T. O. (2020). *Mathematical models for Hepatocytic-Erythrocytic dynamics and therapeutic control of Malaria*. PhD thesis, Strathmore University.

Orwa, T. O., Mbogo, R. W., and Luboobi, L. S. (2019). Multiple-strain malaria infection and its impacts on plasmodium falciparum resistance to antimalarial therapy: A mathematical modelling perspective. *Computational and Mathematical Methods in Medicine*, 2019.

Orwa, T. O., Mbogo, R. W., and Luboobi, L. S. (2022). Optimal control analysis of hepatocytic-erythrocytic dynamics of plasmodium falciparum malaria. *Infectious Disease Modelling*, 7(1):82–108.

Osii, R. S., Otto, T. D., Garside, P., Ndungu, F. M., and Brewer, J. M. (2020). The impact of malaria parasites on dendritic cell–t cell interaction. *Frontiers in Immunology*, 11:1597.

Oxborough, R. M. (2016). Trends in us president's malaria initiative-funded indoor residual spray coverage and insecticide choice in sub-saharan africa (2008–2015): urgent need for affordable, long-lasting insecticides. *Malaria journal*, 15(1):146.

Pattaradilokrat, S., Sawaswong, V., Simpalipan, P., Kaewthamasorn, M., Siripoon, N., and Harnyuttanakorn, P. (2016). Genetic diversity of the merozoite surface protein-3 gene in plasmodium falciparum populations in thailand. *Malaria journal*, 15(1):1–15.

Perelson, A. S. and Ribeiro, R. M. (2013). Modeling the within-host dynamics of hiv infection. *BMC biology*, 11:1–10.

Perko, L. (2013). *Differential equations and dynamical systems*, volume 7. Springer Science & Business Media.

Pilyugin, S. S. and Antia, R. (2000). Modeling immune responses with handling time. *Bulletin of mathematical biology*, 62(5):869–890.

Pinheiro, L., Feitosa, L. M., SILVEIRA, F. F., and Boechat, N. (2018). Current antimalarial therapies and advances in the development of semi-synthetic artemisinin derivatives. *Anais da Academia Brasileira de Ciências*, 90:1251–1271.

Plowe, C. V., Alonso, P., and Hoffman, S. L. (2009). The potential role of vaccines in the elimination of falciparum malaria and the eventual eradication of malaria.

Pontryagin, L. S. (2018). *Mathematical theory of optimal processes*. Routledge.

Powell, D. R., Fair, J., LeClaire, R. J., Moore, L. M., and Thompson, D. (2005). Sensitivity analysis of an infectious disease model. In *Proceedings of the international system dynamics conference*.

Rihan, F., Sheek-Hussein, M., Tridane, A., and Yafia, R. (2017). Dynamics of hepatitis c virus infection: mathematical modeling and parameter estimation. *Mathematical Modelling of Natural Phenomena*, 12(5):33–47.

Risco-Castillo, V., Topçu, S., Marinach, C., Manzoni, G., Bigorgne, A. E., Briquet, S., Baudin, X., Lebrun, M., Dubremetz, J.-F., and Silvie, O. (2015). Malaria sporozoites traverse host cells within transient vacuoles. *Cell host & microbe*, 18(5):593–603.

RTS, S. C. T. P. (2011). First results of phase 3 trial of rts, s/as01 malaria vaccine in african children. *New England Journal of Medicine*, 365(20):1863–1875.

RTS, S. C. T. P. (2012). A phase 3 trial of rts, s/as01 malaria vaccine in african infants. *New England Journal of Medicine*, 367(24):2284–2295.

Sabatinelli, G. (2000). The malaria situation in the who european region. *Meditsinskaia Parazitologiia i Parazitarnye Bolezni*, (2):4–8.

Samba, E. (1997). The burden of malaria in africa. *Africa health*, 19(2):17.

Selemani, M. A., Luboobi, L. S., and Nkansah-Gyekye, Y. (2016). On stability of the in-human host and in-mosquito dynamics of malaria parasite. *Asian Journal of Mathematics and Applications*, 2016.

Selemani, M. A., Luboobi, L. S., and Nkansah-Gyekye, Y. (2017a). The in-human host and in-mosquito dynamics of malaria parasites with immune responses. *New Trends in Mathematical Sciences*, 5(3):182–207.

Selemani, M. A., Luboobi, L. S., and Nkansah-Gyekye, Y. (2017b). Modelling of the in-human host and in mosquito dynamics of parasite. *J. Math. Comput. Sci.*, 7(3):430–455.

Sherling, E. S. and van Ooij, C. (2016). Host cell remodeling by pathogens: the exomembrane system in plasmodium-infected erythrocytes. *FEMS microbiology reviews*, 40(5):701–721.

Song, T., Wang, C., and Tian, B. (2019). Mathematical models for within-host competition of malaria parasites. *Mathematical Biosciences and Engineering*, 16(6):6623–6653.

Sontakke, B. and Shaikh, A. (2015). Properties of caputo operator and its applications to linear fractional differential equations. *Int. J. Eng. Res. Appl*, 5(5):22–27.

Sreenivasamurthy, S. K., Dey, G., Ramu, M., Kumar, M., Gupta, M. K., Mohanty, A. K., Harsha, H., Sharma, P., Kumar, N., Pandey, A., et al. (2013). A compendium of molecules involved in vector-pathogen interactions pertaining to malaria. *Malaria journal*, 12(1):1–7.

Stauffer, W. and Fischer, P. R. (2003). Diagnosis and treatment of malaria in children. *Clinical infectious diseases*, 37(10):1340–1348.

Stevenson, M. M. and Riley, E. M. (2004). Innate immunity to malaria. *Nature Reviews Immunology*, 4(3):169–180.

Su, X.-z., Zhang, C., and Joy, D. A. (2020a). Host-malaria parasite interactions and impacts on mutual evolution. *Frontiers in Cellular and Infection Microbiology*, 10:587933.

Su, Y., Liu, S., Song, S., Li, X., and Ye, Y. (2020b). Stability analysis and clinic phenomenon simulation of a fractional-order hbv infection model. *Complexity*, 2020.

Sule, A. and Abdullah, F. A. (2015). A model for hiv/aids pandemic with optimal control. In *AIP conference proceedings*, volume 1660. AIP Publishing.

Tabo, Z., Luboobi, L. S., and Ssebuliba, J. (2017). Mathematical modelling of the in-host dynamics of malaria and the effects of treatment.

Tchoumi, S. Y., Chukwu, C., Diagne, M., Rwezaura, H., Juga, M., and Tchuenche, J. (2022). Optimal control of a two-group malaria transmission model with vaccination. *Network Modeling Analysis in Health Informatics and Bioinformatics*, 12(1):7.

Tewa, J.-J., Fokouop, R., Mewoli, B., and Bowong, S. (2012). Mathematical analysis of a general class of ordinary differential equations coming from within-hosts models of malaria with immune effectors. *Applied Mathematics and Computation*, 218(14):7347–7361.

Tumwiine, J., Luckhaus, S., Mugisha, J., and Luboobi, L. S. (2008a). An age-structured mathematical model for the within host dynamics of malaria and the immune system. *Journal of Mathematical Modelling and Algorithms*, 7:79–97.

Tumwiine, J., Mugisha, J., and Luboobi, L. (2008b). On global stability of the intra-host dynamics of malaria and the immune system. *Journal of Mathematical Analysis and Applications*, 341(2):855–869.

Ullah, R., Ellahi, R., Sait, S. M., and Mohyud-Din, S. (2020a). On the fractional-order model of hiv-1 infection of cd4+ t-cells under the influence of antiviral drug treatment. *Journal of Taibah University for Science*, 14(1):50–59.

Ullah, S., Khan, M. A., and Gómez-Aguilar, J. (2019). Mathematical formulation of hepatitis b virus with optimal control analysis. *Optimal Control Applications and Methods*, 40(3):529–544.

Ullah, S., Ullah, O., Khan, M. A., and Gul, T. (2020b). Optimal control analysis of tuberculosis (tb) with vaccination and treatment. *The European Physical Journal Plus*, 135:1–27.

Ullman, J. B. (2006). Structural equation modeling: Reviewing the basics and moving forward. *Journal of personality assessment*, 87(1):35–50.

Van den Driessche, P. and Watmough, J. (2002). Reproduction numbers and sub-threshold endemic equilibria for compartmental models of disease transmission. *Mathematical biosciences*, 180(1-2):29–48.

Vande Waa, J., Jensen, J., Akood, M., and Bayoumi, R. (1984). Longitudinal study on the in vitro immune response to plasmodium falciparum in sudan. *Infection and immunity*, 45(2):505–510.

Venkatesan, P. (2024). The 2023 who world malaria report. *The Lancet Microbe*.

Wells, W. (1995). Aerodynamics of droplet nuclei, airborne contagion, and air hygiene.

WHO (2016). *World malaria report 2015*. World Health Organization.

WHO et al. (2023). *World malaria report 2023*. World Health Organization.

Wu, Y., Sinden, R. E., Churcher, T. S., Tsuboi, T., and Yusibov, V. (2015). Development of malaria transmission-blocking vaccines: from concept to product. *Advances in parasitology*, 89:109–152.

Yang, H. M. (2014). The basic reproduction number obtained from jacobian and next generation matrices–a case study of dengue transmission modelling. *Biosystems*, 126:52–75.

Zada, I., Naeem Jan, M., Ali, N., Alrowail, D., Sooppy Nisar, K., and Zaman, G. (2021). Mathematical analysis of hepatitis b epidemic model with optimal control. *Advances in Difference Equations*, 2021(1):1–29.

Zhang, L., Huang, G., Liu, A., Fan, R., et al. (2015). Stability analysis for a fractional hiv infection model with nonlinear incidence. *Discrete Dynamics in Nature and Society*, 2015.

Zhang, X.-X., Jin, Y.-Z., Lu, Y.-H., Huang, L.-L., Wu, C.-X., Lv, S., Chen, Z., Xiang, H., and Zhou, X.-N. (2023). Infectious disease control: from health security strengthening to health systems improvement at global level. *Global Health Research and Policy*, 8(1):38.

Zheng, J., Pan, H., Gu, Y., Zuo, X., Ran, N., Yuan, Y., Zhang, C., and Wang, F. (2019). Prospects for malaria vaccines: Pre-erythrocytic stages, blood stages, and transmission-blocking stages. *BioMed research international*, 2019.

APPENDIX A

MATHEMATICAL PRELIMINARIES

In this Appendix, we present some important definitions and Theorems which are used in this dissertation as input from existing literature. The concepts related to stability analysis, optimal control problem, and fractional order derivative are included.

A.1 Dynamical system of differential equations

Dynamics is primarily the study of the time-evolutionary process and the corresponding system of equations is known as a dynamical system. Generally, a system of n first-order differential equations in the space R^n is called a dynamical system of dimension n which determines the time behavior of the evolutionary process. Evolutionary processes may possess the properties of determinacy/non-determinacy, finite/infinite dimensionality, and differentiability. A process is called deterministic if its entire future course and its entire past are uniquely determined by its state at present. Otherwise, the process is called nondeterministic Layek et al. (2015). The evolutionary process may describe, namely: a continuous time process and a discrete-time process. The continuous-time process is represented by differential equations, whereas the discrete-time process is by difference equations (or maps).

The dynamical system of ordinary differential equations can be expressed as:

$$\frac{dx}{dt} = f(t,x), \tag{A.1}$$

where $f(t,x)$ is a sufficiently smooth function defined on some subset $D \subset R^n \times R$, $x \in R^n$ Euclidean space and t is usually interpreted as time. The above equation together with an initial condition $x(t_0) = x_0 \in D \subset R^n$ is known as an initial value problem and given as:

$$\frac{dx}{dt} = f(t,x), \quad x(t_0) = x(0), \tag{A.2}$$

The equation (A.1) is called autonomous or time-invariant if $f(t,x)$ is explicitly time-independent. Otherwise, it is nonautonomous.

A.1.1 Existence and uniqueness Theorem

Definition A.1. Suppose $f(t,x)$ is satisfy the Lipsccitz condition or Lipschitz continuous in x with Lipschitz constant L if

$$||f(t,x) - f(t,y)|| \leq L||x-y||,$$

where $x, y \in D$.

Theorem A.1. ***(Existence and uniqueness theorem)****: Suppose $f(t,x)$ is continuous in D and Lipschitz continuous with respect to x. Then the initial value problem (A.2) has a unique solution if $|t-t_0| \leq min\left(a, \frac{d}{M}\right)$ with $M = \sup_D ||f||$, where a and d are positive constants.*

Definition A.2. (***Positively invariant region***): A region $\Omega \subseteq R^n$ is a positive invariant for the dynamical system (A.2) if all the initial condition $x_0 \in \Omega$, then all the solutions $x(t) \in \Omega$, for all $t \geq t_0$.

Theorem A.2. *Perko (2013). Let $f : R^n \to R^n$ is differentiable at x^0, then all the partial derivatives $\frac{\partial f_i}{\partial x_j}$, for $i, j = 1, 2, \ldots, n$ exist and for all $x \in R^n$,*

$$Df(x^0)x = \sum_{j=1}^{n} \frac{\partial f}{\partial x_j}(x^0)x_j$$

Thus, if f is a differentiable function, the derivative is given by the $m \times m$ Jacobian matrix

$$Df(x^0) = \left[\frac{\partial f_i}{\partial x_j}\right]$$

A.1.2 Equilibria and stability of autonomous systems

Definition A.3. **(Linearisation)**: In mathematics, linearisation refers to the process of finding a linear approximation to a function at a given point.

The concept of linearisation is very important in the study of dynamical systems. It enables us to assess the local stability of the equilibrium point(s) of a non-linear dynamical system. Consider the dynamical system (A.2) and it is linearisation is given by

$$\begin{pmatrix} x_1' \\ x_2' \\ x_3' \\ \vdots \\ x_n' \end{pmatrix} = \begin{pmatrix} \frac{\partial f_1}{\partial x_1} & \frac{\partial f_1}{\partial x_2} & \frac{\partial f_1}{\partial x_3} & \cdots & \frac{\partial f_1}{\partial x_n} \\ \frac{\partial f_2}{\partial x_1} & \frac{\partial f_2}{\partial x_2} & \frac{\partial f_2}{\partial x_3} & \cdots & \frac{\partial f_2}{\partial x_n} \\ \frac{\partial f_3}{\partial x_1} & \frac{\partial f_3}{\partial x_2} & \frac{\partial f_3}{\partial x_3} & \cdots & \frac{\partial f_3}{\partial x_n} \\ \vdots & \vdots & \vdots & \cdots & \vdots \\ \frac{\partial f_n}{\partial x_1} & \frac{\partial f_n}{\partial x_2} & \frac{\partial f_n}{\partial x_3} & \cdots & \frac{\partial f_n}{\partial x_n} \end{pmatrix} \begin{pmatrix} x_1 \\ x_2 \\ x_3 \\ \vdots \\ x_n \end{pmatrix} = \frac{dx}{dt} = Df(x^*)x,$$

where

$$\begin{pmatrix} \frac{\partial f_1}{\partial x_1} & \frac{\partial f_1}{\partial x_2} & \frac{\partial f_1}{\partial x_3} & \cdots & \frac{\partial f_1}{\partial x_n} \\ \frac{\partial f_2}{\partial x_1} & \frac{\partial f_2}{\partial x_2} & \frac{\partial f_2}{\partial x_3} & \cdots & \frac{\partial f_2}{\partial x_n} \\ \frac{\partial f_3}{\partial x_1} & \frac{\partial f_3}{\partial x_2} & \frac{\partial f_3}{\partial x_3} & \cdots & \frac{\partial f_3}{\partial x_n} \\ \vdots & \vdots & \vdots & \cdots & \vdots \\ \frac{\partial f_n}{\partial x_1} & \frac{\partial f_n}{\partial x_2} & \frac{\partial f_n}{\partial x_3} & \cdots & \frac{\partial f_n}{\partial x_n} \end{pmatrix} = D(f(x^*)) = J \tag{A.3}$$

is the Jacobian matrix of the dynamical system (A.2) evaluated at equilibrium point $x^* = (x_1^*, x_2^*, x_3^*, \ldots x_n^*)$. This is guaranteed by the *Hartman–Grobman theorem* and by the fact that zero is an asymptotically stable solution of a linear system with constant coefficients if and only if all eigenvalues have a negative real part.

Definition A.4. The equilibrium point x^* is said to be ***stable*** if all the eigenvalues of the Jacobian matrix (A.3) evaluated at x^*, have negative real parts. The equilibrium point is *unstable* if at least one of the eigenvalues of the Jacobian matrix (A.3) has a positive real part.

Definition A.5. The equilibrium point x^* of (A.2) is said to be hyperbolic if none of the eigenvalues for the Jacobian J evaluated at x^* have a zero real part. Otherwise, it is said to be nonhyperbolic.

The Routh-Hurwitz stability criterion is a method for determining whether a linear system is stable or not, by examining the location of the roots of the characteristic equation. The method determines only if there are roots that lie outside of the left half plane

Theorem A.3. *Consider the polynomial,*

$$P(\lambda) = \lambda^n + b_1\lambda^{n-1} + b_2\lambda^{n-2} + b_3\lambda^{n-3} + \cdot + b_{n-1}\lambda + b_0,$$

where the coefficients b_j are real constants, $j = 1,...,n$. All the roots of the characteristic polynomial $P(\lambda)$ are negative or have negative real part if and only if the following condition holds: (i) All the coefficients b_j, for $j = 1,2,3,\ldots,n$ are non-negative and (ii) The $det(H_k) > 0$, k=1,2,3,...,n. That is, for $n = 2$ the Routh-Huwirtz criteria satisfy if $b_1 > 0$, $b_2 > 0$, $det(H_1) = b_1 > 0$ and

$$det(H_2) = \begin{vmatrix} b_1 & 1 \\ 0 & b_2 \end{vmatrix} = b_1 b_2 > 0$$

For the characteristic polynomial equation of degree $n = 3,4$, and 5, we have the following Routh-Huwirtz stability criteria.
$n = 3 : b_1 > 0, b_3 > 0$ and $b_1 b_2 > b_3$.
$n = 4 : b_1 > 0, b_3 > 0, b_4 > 0$ and $b_1 b_2 b_3 > b_3^2 + b_1^2 b_4$
$n = 5 : b_i > 0, j = 1,2,3,\ldots,n$ and $b_1 b_2 > b_3$, $b_1 b_2 b_3 > b_3^2 + b_1^2 b_4$, and $b(_1 b_4 - b_5)(b_1 b_2 b_3 - b_3^2 - b_1^2 b_4) > b_5(b_1 b_2 b_3)^2 + b_1 b_5^2$.

Definition A.6. *(Descartes' Rule of signs)*: Given the polynomial

$$P(x) = a_n x^n + a_{n-1}x^{n-1} + a_{n-2}x^{n-2} + \ldots + a_1 x + a_0 = 0 \tag{A.4}$$

with $a_i, i = 1,2,3,\ldots,n$ the coefficients of polynomial. Then the number of positive roots of the polynomial equation (A.4) is either equal to the number of sign changes between consecutive

(nonzero) coefficients or is less than it by an even number. That is by Descartes' Rule of signs the polynomial equation (A.4) has at most k roots, which are real and positive, and further, that there are $k, k-2, k-4, \ldots,$ real positive roots.

Definition A.7. Suppose $D \subset R^n$ that contains the origin or $\boldsymbol{0}$. A function $V : D \to R$ is said to be

(a) a positive semi-definite in D if the following condition is satisfied. (i) $V(0) = 0$ and $0 \in D$, (ii) $V(x) \geq 0$, for all $x \in D$.

(b) positive definite in D if (i) $V(0) = 0$ and $0 \in D$ (ii) $V(x) > 0$, for all $x \in D \backslash \{0\}$.

(c) negative definite (semi-definite) in D if $-V(x)$ is positive definite.

Theorem A.4. ***(Lyapunov stability theorem)****: Suppose x^* be an equilibrium point of the dynamical system (A.2), where $f : D \to R^n$ is locally Lipschitz and $D \in R^n$ a domain that contains x^*. Suppose a function $V : D \to R$ is a continuously differentiable and positive definite function in D. Then if*

(i) $\dot{V}(x) = \nabla V(x).f(x) \leq 0$, then x^* is globally stable.

(ii) $\dot{V}(x) = \nabla V(x).f(x) < 0$, then x^* is globally asymptotically stable

Theorem A.5. ***(Lassalle's invariance principles)****: Let Ω be a compact set that is positive invariant of system (A.2). Let $V(x)$ be a continuously differentiable function on Ω such that $\dot{V}(x) \leq 0$ in Ω. Let $D \in \Omega$ be the set of all points in Ω such that $\dot{V}(x) = 0$ and M be the largest positive invariant set in E, then every solution starting in Ω approaches M as $t \to \infty$.*

A.1.3 The basic reproduction number

The basic reproduction number R_0, which represents the average number of secondary infections that occur when one infective is introduced into a completely susceptible host population (Nishiura, 2010). The basic reproduction number is an important non-dimensional quantity in epidemiology as it sets the threshold in the study of infectious diseases both for predicting its outbreak and for evaluating its control strategies. Basic reproduction can determine whether a disease becomes persistent or dies out in a community depending on the value of R_0 (Yang, 2014). Furthermore, the stability of equilibrium points can be analyzed using R_0. That is if $R_0 < 1$ it means that every infectious individual will cause less than one secondary infection and hence the disease will die out and if $R_0 > 1$, every infectious individual will cause more than one secondary infection and hence the disease will invade the populations. A large number of R_0 may indicate the possibility of a major epidemic. For the case of a model with a single infected class, R_0 is simply the product of the infection rate and the mean duration of the infection.

A.1.4 Next-generation matrix

In epidemiology, the next-generation matrix is used to derive the basic reproduction number, for a compartmental model of the spread of infectious diseases. The technique to determine the basic reproduction ratio using the next-generation matrix is given by (Diekmann et al., 1990) and (Van den Driessche and Watmough, 2002).

The basic reproduction number cannot be determined from the structure of the mathematical model alone, but depends on the definition of infected and uninfected compartments. Consider the the compartmental model (A.2). Suppose that the whole population is divided into n compartments in which there are $m < n$ infected compartments. Let $x \in R^n$ and $y \in R^m$ be the population in each of these compartments. Then, the model can be as follows:

$$\frac{dx}{dt} = \mathscr{F}_i(x,y) - \mathscr{V}_i(x,y), \;\; i = 1,2,3,\ldots,n$$
$$\frac{dy}{dt} = h_j(x,y), \;\; j = 1,2,3,\ldots,m,$$

where $\mathscr{F}_i$ is the rate of new appearance in the i^{th} compartment, and $\mathscr{V}_i$ is the rate of transfer from one compartment to other (progression, death, and recovery decrease) of the i^{th} compartments. Note that $\mathscr{V}_i = \mathscr{V}_i^- - \mathscr{V}_i^+$, where $\mathscr{V}_i^-$ indicates the rate of transfer of individuals into compartment i by all other means and $\mathscr{V}_i^+$ indicates the rate of transfer of individuals out of compartment i.

Suppose that the disease-free system $\frac{dy}{dt} = h(0,y)$ has a unique equilibrium E_0 that is locally asymptotically stable within the disease-free space. Then the non-negative matrix F and non-singular matrix V are obtained by differentiating the vectors $\mathscr{F}_i$ and $\mathscr{V}_i$ at disease-free equilibrium point as follows:

$$\mathscr{F} = \frac{\partial \mathscr{F}_i}{\partial x_j} \;\; and \;\; \mathscr{V} = \frac{\partial \mathscr{V}_i}{\partial x_j}, \;\; 1 \leq i, \; j \leq n.$$

To interpret the entries of $\mathscr{F}\mathscr{V}^{-1}$ and develop a meaningful definition of R_0, consider the rate of an infected individual introduced into compartment k of a disease-free population. The (j,k) entry of $\mathscr{V}^{-1}$ is the average length of time this individual spends in compartment j during its lifetime, assuming that the population remains near the disease-free equilibrium point and barring reinfection. The (i,j) entry of $\mathscr{F}$ is the rate at which the infected individuals in compartment j produce new infections in compartment i. Hence, the (i,k) entry of the product $\mathscr{F}\mathscr{V}^{-1}$ is the expected number of new infections in compartment i produced by the infected individual originally introduced into compartment k.

Then the next-generation matrix is $\mathscr{K} = \mathscr{F}\mathscr{V}^{-1}$, and the basic reproduction number R_0

can be defined as the dominant eigenvalue of $\mathscr{K}$, that is,

$$R_0 = \rho(\mathscr{F}\mathscr{V}^{-1})$$

The disease-free equilibrium point is locally asymptotically stable if $R_0 < 1$, i,e, the disease will die out from the community, and if $R_0 > 1$ the disease-free equilibrium point is unstable, endemic equilibrium is stable and disease persist in the community.

A.1.5 Bifurcation Analysis

Bifurcation theory refers to the study of qualitative changes to the state of a system as a parameter is varied. It can be applied to steady-state systems, or dynamical systems and can be understood best at the level of a mathematical model, although recent techniques allow the method to be applied to experiments with feedback control. Typically the theory is applied to a continuous model, but can also be used in discrete models and mathematics, difference equations. In recent years Castillo-Chavez and Song's bifurcation theorem is a technique used to evaluate the direction of the bifurcation at $R_0 = 1$. For the most part, in epidemic models, there are two distinct bifurcations at $R_0 = 1$ forward (supercritical) and backward (subcritical). A forward bifurcation happens when R_0 crosses unity from below; a small positive asymptotically stable equilibrium appears and the disease-free equilibrium loses its stability Castillo-Chavez and Song (2004). On the other hand, a backward bifurcation happens when R_0 is less than unity; a small positive unstable equilibrium appears while the disease-free equilibrium and a larger positive equilibrium are locally asymptotically stable. Epidemiologically, a backward bifurcation "says" that it is not enough to only reduce the basic reproductive number to less than one to eliminate disease and that when R_0 crosses unity, hysteresis takes place.

Center manifold theory has been used to decide the local stability of a nonhyperbolic equilibrium (linearization matrix has at least one eigenvalue with zero real part) Carr (1981); Wells (1995)

Theorem A.6. ***(Castillo-Chavez and Song)****: Consider a general system of ordinary differential equations with a parameter* ϕ

$$\frac{dx}{dt} = f(x,\phi), \quad f : R^n \times R \to R^n \ \ and \ \ f \in \mathbb{C}^2(R^n \times R), \tag{A.5}$$

where 0 is an equilibrium for System, that is $f(0,\phi) = 0$, for all values of the parameter ϕ. Assume

(A_1) $A = D_x f(0,0) = \left(\frac{\partial f_i}{\partial x_j}(0,0)\right)$ is the linearization matrix of system (A.5) around the equilibrium 0 with ϕ evaluated at 0. Zero is a simple eigenvalue of A, and other eigenvalues have negative real parts.

(A_2) Matrix A has a nonnegative right eigenvector w and left eigenvector v corresponding to the zero eigenvalue.
Let f_k be the k^{th} component of f and

$$\begin{aligned} a &= \sum_{k,i,j=1}^{n} v_k w_i w_j \frac{\partial^2 f_k}{\partial x_i \partial x_j}(0,0) \\ b &= \sum_{k,i=1}^{n} v_k w_i \frac{\partial^2 f_k}{\partial x_i \partial \phi}(0,0). \end{aligned} \tag{A.6}$$

The local dynamics of the system (A.5) around 0 is totally determined by the signs of the quantities a and b:

i. $a > 0$, $b > 0$. When $\phi < 0$, with $|\phi| \ll 1$, 0 is locally asymptotically stable, and there exists a positive unstable equilibrium; when $0 < \phi \ll 1$, 0 is unstable and there exists a negative and locally asymptotically stable equilibrium;

ii. $a < 0$, $b < 0$. When $\phi < 0$, with $|\phi| \ll 1$, 0 is unstable; when $0 < \phi \ll 1$, 0 locally asymptotically stable, and there exists a positive unstable equilibrium;

iii. $a > 0$, $b < 0$. When $\phi < 0$, with $|\phi| \ll 1$, 0 is unstable, and there exists a locally asymptotically stable negative equilibrium; when $0 < \phi \ll 1$, 0 is stable, and a positive unstable equilibrium appears;

iv. $a < 0$, $b > 0$. When ϕ changes from negative to positive, 0 changes its stability from stable to unstable. Correspondingly a negative unstable equilibrium becomes positive and locally asymptotically stable.
Particular, backward bifurcation occurs at $\phi = 0$ if $a > 0$ and $b > 0$, whereas forward occur $\phi = 0$ if $a < 0$ and $b > 0$.

A.1.6 Sensitivity Analysis

Sensitivity analysis is used to measure the major characteristics of the model that have a significant impact on the prevalence of infection. This will also enable us to determine which of the parameter (constant) controls leads to the greatest reduction in within-host reproduction number R_0, allowing us to identify the control strategy that is most effective at preventing within-the-host malaria infection. To do this, we compute the normalized forward sensitivity index of the reproduction number with respect to these parameters. This index measures the relative change in a variable concerning relative changes in its parameters Chitnis et al. (2008) and is defined as follows:

Definition A.8. The normalized forward sensitivity index of a variable, M, that depends differentiably on a parameter, ϑ, is defined as:

$$\Theta_{\vartheta}^{M} = \frac{\partial M}{\partial \vartheta} \times \frac{\vartheta}{M}$$

A.2 Fractional Calculus

Fractional calculus is a branch of mathematical analysis that studies the several different possibilities of defining real number powers or complex number powers of differentiation and integration. Fractional calculus (FC) has been extensively applied in many fields of engineering and science such as electromagnetics, viscoelasticity, fluid mechanics, electrochemistry, biological population models, optics, and signals processing (Dalir and Bashour, 2010). Currently, it's a warm research area, many mathematicians and applied researchers have tried to model real processes using fractional calculus. The major cause of use is that fractional differential equations are naturally related to systems with memory which exists in most biological systems (Arafa et al., 2014).
In this section, we introduce some basic definitions of fractional order differential operators, Theorems, and properties of fractional calculus that will be required in our study.

Definition A.1. Ullah et al. (2020a). The gamma function $\Gamma(x)$ is defined in terms of improper integral given as

$$\Gamma(x) = \int_0^{\infty} e^{-t} t^{x-1} dt, x > 0. \tag{A.7}$$

The gamma function that satisfies the condition $\Gamma(x+1) = x\Gamma(x), x > 0$. For any positive integer n, $\Gamma(n) = (n-1)!$

Definition A.2. Miao et al. (2017). The functional integral order $\alpha > 0$ of a function $f : R^{+} \to R$ is given by

$$I^{\alpha} f(x) = \frac{1}{\Gamma(\alpha)} \int_0^{x} (x-t)^{\alpha-1} f(t) dt, \tag{A.8}$$

where $\Gamma(\alpha)$ is gamma function.

Definition A.3. Sontakke and Shaikh (2015). The Riemann-Liouville fractional derivative or Riemann-Liouville fractional differential of function $f(t)$ with order $\alpha > 0$ is defined as

$$D^{\alpha} f(t) = \frac{1}{\Gamma(n-\alpha)} \frac{d^n}{dt^n} \int_a^{t} \frac{f(s)}{(t-s)^{\alpha-1+n}} ds, \quad n-1 < \alpha < n, t > a, \alpha, a, t \in R. \tag{A.9}$$

Definition A.4. Ullah et al. (2020a). Reimann-Liouville fractional integral of order α of function $f : (0, \infty) \to R^n$ is defined as

$$I_t^{\alpha} f(t) = \frac{1}{\Gamma(\alpha)} \int_0^{t} (t-s)^{\alpha-1} f(s) ds, \tag{A.10}$$

where $\Gamma(\alpha)$ is gamma function.

Definition A.5. Kazem (2013); Sontakke and Shaikh (2015). For $\alpha, \beta > 0$ and $z \in C$, Mittag-Leffler functions in one and two parameters defined as,

$$E_\alpha(z) = \sum_{m=0}^{\infty} \frac{z^m}{\Gamma(m\alpha+1)}, \tag{A.11}$$

$$E_{\alpha,\beta}(z) = \sum_{m=0}^{\infty} \frac{z^m}{\Gamma(m\alpha+\beta)}. \tag{A.12}$$

Definition A.6. Kazem (2013). The fractional-order derivative in Caputo sense for order $\alpha > 0$ is defined as:

$${}_a^C D_t^\alpha f(t) = \frac{1}{\Gamma(n-\alpha)} \int_a^t \frac{f^n(s)}{(t-s)^{\alpha-n+1}} ds \tag{A.13}$$

where $n-1 < \alpha \leq n$, $n \in N$, $f \in C^{n-1} \in [0,t]$.

Definition A.7. Aba Oud et al. (2021). The Caputo fractional integral with order $\alpha > 0$ is defined as

$$I_t^\alpha f(t) = \frac{1}{\Gamma(\alpha)} \int_0^t \frac{f(s)}{(t-s)^{1-\alpha}} ds, \;\; 0 < \alpha < 1, t > 0. \tag{A.14}$$

Definition A.8. Dehingia et al. (2022). The Atangana–Baleanu Caputo fractional derivative for a given function of order α is defined as

$${}_a^{ABC} D_t^\alpha f(t) = \frac{H(\alpha)}{1-\alpha} \int_a^t \frac{df}{ds}(s) E_\alpha \left[-\frac{\alpha}{1-\alpha}(t-s)^\alpha \right] ds, \tag{A.15}$$

where $H(\alpha) = (1-\alpha) + \frac{\alpha}{\Gamma(\alpha)}$, is a normalization function and $E_\alpha \left[-\frac{\alpha}{1-\alpha}(t-s)^\alpha \right]$ is the Mittag–Leffler function.

Definition A.9. Dehingia et al. (2022). The Atangana–Baleanu Caputo fractional integral of function $f \in C^{'}(a,b)$ is given by

$${}_a^{ABC} I_t^\alpha f(t) = \frac{1-\alpha}{H(\alpha)} f(t) + \frac{\alpha}{H(\alpha)\Gamma(\alpha)} \int_a^t f(s)(t-s)^{\alpha-1} ds \tag{A.16}$$

and the integral will be zero for a constant function $f(t)$.

Definition A.10. Al-Refai and Pal (2019); Nazir et al. (2020). Let $f \in H^1(a,b), a < b, 0 < \alpha < 1$, the Caputo-Fabrizio fractional derivative in the Caputo sense is defined by

$${}_a^{CFC} D_t^\alpha f(t) = \frac{\mathscr{N}(\alpha)}{1-\alpha} \int_a^t \frac{df(s)}{dt} e^{-\frac{\alpha}{1-\alpha}(t-s)} ds, \tag{A.17}$$

where $\mathscr{N}(\alpha)$ is a normalization function satisfying $\mathscr{N}(0) = \mathscr{N}(1) = 1$.

Definition A.11. Al-Refai and Pal (2019). Let $\alpha \in [0,1]$, then the Caputo-Fabrizo integral with order α of function f is defined as

$$ {}^{CFC}_{a}I^{\alpha}_{t} f(t) = \frac{1-\alpha}{\mathscr{N}(\alpha)} + \frac{\alpha}{\mathscr{N}(\alpha)} \int_a^t f(s)ds, \quad 0 < \alpha < 1. \tag{A.18} $$

Theorem A.1. *Su et al. (2020b). Let a nonlinear fractional-order system in the sense of Caputo derivative is*

$$ \begin{cases} {}^{C}_{a}D^{\alpha}_{t} x(t) = f(t, x(t)) \\ x(t_0) = x_0 \end{cases} \tag{A.19} $$

where $0 < \alpha < 1$. If a point x^{**} satisfies $f(x^{**}) = 0$, then x^{**} is called an equilibrium point of the system. The equilibrium x^{**} is said to be locally asymptotically stable if all eigenvalues λ_i of the Jacobian matrix $J = \frac{\partial f}{\partial x}$ evaluated at x^{**} satisfy the conditions $|arg(\lambda_i)| > \frac{\alpha\pi}{2}$.

Corollary A.2. *(Odibat and Shawagfeh, 2007) Suppose that $g(t) \in C[p,q]$ and ${}^{C}D^{\alpha}_{t} g(t) \in C[p,q]$, where $\alpha \in (0,1)$. Then if ${}^{C}D^{\alpha}_{t} g(t) \geq 0$, for all $t \in (p,q)$, then $g(t)$ is nondecreasing and if ${}^{C}D^{\alpha}_{t} g(t) \leq 0$, for all $t \in (p,q)$, then $g(t)$ is nonincreasing.*

Definition A.12. Let (X,d) be a metric space. Then a map $T : X \to X$ is called a contraction mapping on X if there exists $q \in [0,1)$ such that $(T(x), T(y)) \leq qd(x,y)$, for $x, y \in X$.

Theorem A.3. *(Banach fixed-point theorem). Let (X,d) be a non-empty complete metric space with a contraction mapping $T : X \to X$. Then T admits a unique fixed-point * in X (i.e. $T(c^* = x^*)$). Furthermore, x^* can be found as follows: start with an arbitrary element $x_0 \in X$ and define a sequence $(x_n)_n \in N$ by $x_n = T(x_{n-1})$ for $n \geq 1$. Then $\lim_{n\to\infty} x_n = x^*$.*

A.2.1 Fractional order Routh–Hurwitz conditions

Consider the system

$$ {}^{C}D^{\alpha}_{t} x(t) = f(x,y), \;\; {}^{C}D^{\alpha}_{t} y(t) = g(x,y), \;\; \alpha \in [0,1), \tag{A.20} $$

where the fractional derivative in (A.20) is in the sense of Caputo. The equilibrium solutions are defined by $f(x^*, y^*) = 0$, and it is locally asymptotically stable if all the eigenvalues λ of the Jacobian matrix

$$ J = \begin{bmatrix} \partial f/\partial x & \partial f/\partial y \\ \partial g/\partial x & \partial g/\partial y \end{bmatrix} $$

evaluated at the equilibrium point satisfies

$$|arg(\lambda)| > \frac{\alpha\pi}{2}. \tag{A.21}$$

The condition (A.21) poses an interesting question namely what are the conditions that all the roots of the polynomial equation

$$P(\lambda) = \lambda^n + a_1\lambda^{n-1} + a_2\lambda^{n-2} + a_3\lambda^{n-3} + \ldots + a_{n-1}\lambda + a_n \tag{A.22}$$

satisfy $|arg(\lambda)| > \frac{\alpha\pi}{2}$, where all the coefficients in A.22 are real. For $\alpha = 1$ the solution is Routh–Hurwitz conditions holds. For $\alpha \in (0,1)$ these conditions are sufficient but not necessary. Thus, the following proposition summarizes the condition:

Proposition A.4. *(Ahmed et al., 2006)(Fractional order Routh–Hurwitz conditions)*

i. For $n = 1$ the condition for A.21 is $a1 > 0$.

ii. For $n = 2$ the condition for A.21 is are either Routh–Hurwitz conditions or $a_1 < 0,\ 4a_2 > (a_1)^2,\ |\tan^{-1}\sqrt{4a_2 - a_1^2}/a_1| > \alpha\pi/2$.

iii. For $= 3$ if the discriminant of$p(\lambda)D(P)$ is positive then Routh–Hurwitz conditions are the necessary and sufficient conditions for (A.21), i.e., $a_2 > 0,\ a_3 > 0,\ a_1a_2 > a_2$ if $D(P) > 0$.

iv. If $D(P) < 0$,$a_1 \geq 0$, $a_2 \geq 0$, $a_3 > 0$, $\alpha < (2/3)$ then (A.21) is satisfied. Also if $D(p) < 0$, $a_1 < 0$, $a_2 < 0$, $\alpha > (2/3)$ then all roots of $p(\lambda) = 0$ satisfies $|arg(\lambda)| < \alpha\pi/2$.

A.3 Optimal control theory

Optimal control theory deals with finding a control for a dynamical system over a period of time such that an objective function $J(t,x(t),u(t))$ is optimized (maximize or minimize), where $x(t)$ is the state variable and $u(t)$ is the control. Here, we've used ideas from optimal control theory to explore the impacts of various governance strategies. An optimal control problem that seeks to optimize (or maximize/minimize) an objective function subject to a dynamical system equation (A.2) with the initial condition is given as:

$$\begin{aligned} J[x(.),u(.)] &= \int_{t_0}^{t_f} g(t,x(t),u(t))dt \rightarrow max \\ &\quad Subject\ \ to \\ \frac{dx}{dt} &= f(t,x(t),u(t)) \\ x(t_0) &= x_0,\ \ x(t_f)\ \ free\ \ and\ \ u \in PC,\ \ for\ all\ t \in [t_0,t_f]. \end{aligned} \tag{A.23}$$

We assume functions f and g to be continuously differentiable in all their three arguments. Thus, as the control(s) will always be piecewise continuous (PC), the associated states will always be piecewise differentiable.

A.3.1 Pontryagin's maximum principle (PMP)

To look into the most efficient management strategies, we examine optimal control theory via the perspective of Pontryagin's maximum principle (Pontryagin, 2018).

Theorem A.1. *(Lenhart and Workman, 2007) If x^* and u^* is optimal for the problem (A.23), then there exists a piecewise differentiable adjoint (co-state) variable $\lambda(t)$, such that the following conditions hold for all t in the interval $[t_0, t_f]$:*
(i) The optimality condition

$$\frac{\partial H}{\partial u} = (t, x(t), u(t), \lambda(t)) = 0.$$

(ii) The Hamiltonian system

$$\frac{\partial x}{\partial t} = \frac{\partial H}{\partial \lambda}(t, x(t), u(t), \lambda(t))$$
$$\frac{\partial \lambda}{\partial t} = -\frac{\partial H}{\partial x}(t, x(t), u(t), \lambda(t)).$$

(iii) The tranisversality condition

$$\lambda(t_f) = 0.$$

Where the Hamiltonian H is defined as

$$H(t, x(t), u(t), \lambda(t)) = g(t, x(t), u(t)) + \lambda(t).f(t, x(t), u(t)).$$

A.4 Numerical Schemes

In this appendix section, we present the numerical schemes that are used in this dissertation.

A.4.1 Runge-Kutta Fourth order Scheme

Consider the following system of ordinary differential equations (A.2), then the fourth order Runge-Kutta (RK4) method is a numerical approach used to solve ordinary differential equation and the optimality system is defined as

$$y_{i+1} = y_i + (b_1 k_1 + b_2 k_2 + b_3 k_3 + b_4 k_4)h, \tag{A.24}$$

where the value of $y = y_i$ at the point x_i , we can find the value of $y = y(i+1)$ at the point x_{i+1},

and $h = x_{i+1} - x_i$ is the step size. The first five terms of the Taylor's expansion of (A.24) is

$$y_{i+1} = y_i + f(x_i, y_i)h + \frac{1}{2!}f^{'}(x_i, y_i)h^2 + \frac{1}{3!}f^{''}(x_i, y_i)h^3 + \frac{1}{4!}f^{'''}(x_i, y_i)h^4 + O(h) \tag{A.25}$$

Now, from equation (A.25), we found that

$$y_{i+1} = y_i + \frac{1}{6}(k_1 + 2k_2 + 2k_3 + k_3),\ for\ i = 0, 1, 2, \ldots, n-1,$$

where

$$\begin{aligned} k_1 &= f(x_i, y_i), \\ k_2 &= f(x_i + \frac{h}{2}, y_i + \frac{h}{2}k_1), \\ k_3 &= f(x_i + \frac{h}{2}, y_i + \frac{h}{2}k_2), \\ k_4 &= f(x_i + h, y_i + hk_3) \end{aligned}$$

A.4.2 Generalized predictor-corrector of the Adams-Bashforth-Moulton method

Consider an initial value problem (IVP) fractional differential equation

$$\begin{cases} {}^{C}D_t^{\alpha}u(t) = f(t, u(t)) \\ u^k(0) = u_0^k, k = 0, 1, 2, \ldots, m-1 \end{cases} \tag{A.26}$$

with $\alpha > 0$, $m = \lceil \alpha \rceil - 1$ and u_0^k, $k = 0, 1, 2, \ldots$ are real numbers. A function $u(t)$ is continuous and it is a solution of the initial value problem of (A.26) if and only if it solves the following Volterra integral equation

$$u(t) = \sum_{k=0}^{\lceil \alpha \rceil - 1} u_0^k \frac{t^k}{k!} + \frac{1}{\Gamma(\alpha)} \int_0^t (t-s)^{\alpha-1} f(s, u(s))ds. \tag{A.27}$$

Next, a generalized form of the Adams-Moulton technique for fractional order (A.26) is presented. The uniform mash $h = \frac{t_n}{n}$, $n = 0, 1, 2, \ldots, N$, $N \in \mathbb{N}, h > 0$ is the step size. We first examine the approximations $u_h(t_i) \approx u(t_i), i = 1, 2, \ldots, n$, then computing the approximations $u_h(t_{n+1})$ using equation (A.27). The corrector product trapezoidal quadrature formula is improved to find the (A.27) with nodes, $t_i = 0, 1, 2, \ldots, n+1$. This then gives the fractional variant of the step-Adams-Moulton technique, which gives

$$u_h(t_{n+1}) = \sum_{k=0}^{\lceil \alpha \rceil - 1} \frac{t_{n+1}^k}{k!} u_0^k + \frac{h^{\alpha}}{\Gamma(\alpha+2)} f(t_{n+1}, u_h^p(t_{t+1})) + \frac{h^{\alpha}}{\Gamma(\alpha+2)} \sum_{i=1}^{n} c_{i,n+1} f(t_i, u_h(t_i)), \tag{A.28}$$

where

$$c_{i,n+1} = \begin{cases} 1, & if \;\; i = n+1 \\ (n-i+2)^{\alpha+1} - 2(n-i+1)^{\alpha+1}, & if \;\; 1 \le i \le n \\ n^{\alpha+1} - (n-\alpha)(n+1)^{\alpha}, & if \;\; i = 0. \end{cases} \tag{A.29}$$

However, for the determination of the predictor, a product of a rectangle is utilized. Thus, the predictor value is determined by the fractional Adams-Bashforth method is

$$u_h^p(t_{n+1}) = \sum_{k=0}^{\lceil \alpha \rceil - 1} \frac{t_{n+1}^k}{k!} u_0^k + \frac{1}{\Gamma(\alpha)} \sum_{i=0}^{n} d_{i,n+1} f(t_i, u_h(t_i)), \tag{A.30}$$

where

$$d_{i,n+1} = \frac{h^\alpha}{\alpha} \left((n+1-i)^\alpha - (n-i)^\alpha \right). \tag{A.31}$$

Combining these, two schemes (equations (A.28) and A.30) for the solution of fractional order equation (A.26) called generalized predictor-corrector of the Adams-Bashforth-Moulton method given as follows: (see detail (Diethelm et al., 2002)).

$$\begin{aligned} u_h(t_{n+1}) &= \sum_{k=0}^{\lceil \alpha \rceil - 1} \frac{t_{n+1}^k}{k!} u_0^k + \frac{h^\alpha}{\Gamma(\alpha+2)} f(t_{n+1}, u_h^p(t_{t+1})) + \frac{h^\alpha}{\Gamma(\alpha+2)} \sum_{i=1}^{n} c_{i,n+1} f(t_i, u_h(t_i)), \\ u_h^p(t_{n+1}) &= \sum_{k=0}^{\lceil \alpha \rceil - 1} \frac{t_{n+1}^k}{k!} u_0^k + \frac{1}{\Gamma(\alpha)} \sum_{i=0}^{n} d_{i,n+1} f(t_i, u_h(t_i)), \end{aligned} \tag{A.32}$$

APPENDIX B

MATLAB AND PYTHON CODE

B.1 Matlab codes

B.1.1 Matlab codes for simulation model (4.1)

Code Listing B.1: Matlab codes

```
% Numerical results of problem I
%Matbal code for the data semulations
function dxdt = Pr_I(~,x)
dxdt = zeros(6,1);
global beta b0 b1 b2 b3 c  delta mu_h nu mu_x mu_y mu_c mu_m
    mu_g alpha gamma theta xi c0 c1 eta pi_h pi_c pi_x  N
%X=x(1), Y=x(2), M=x(3), G=x(4), C=x(5), H=x(6),
%N = x(1)+x(2)+x(3)+x(4)+x(5); %Total population size
%System equation of within-host malaria parasite
dxdt(1) = pi_x-beta*x(1)*x(3)/(1+b0*x(6))-mu_x*x(1);
dxdt(2) = beta*x(1)*x(3)/(1+b0*x(6))-mu_y*x(2)-gamma*x(2)*x
   (5);
dxdt(3) = (1-nu)*N*mu_y*x(2)/(1+b1*x(5))-mu_m*x(3)-theta*x
   (3)*x(6);
dxdt(4) =nu*c*x(2)/(1+b2*x(6))-mu_g*x(4)-eta*x(4)*x(6);
dxdt(5) = pi_c+xi*x(2)*x(5)/(1+b3*x(2))-mu_c*x(5);
dxdt(6) = pi_h+alpha*x(3)*x(6)/(1+c0*x(3))+delta*x(4)*x(6)
   /(1+c1*x(4))-mu_h*x(6);
end
```

Code Listing B.2: The time evolution of the state variables

```
%Concentration infected red blood cells at time t
clear all;
close all;
global beta b0 b1 b2 b3 c delta mu_h mu_x mu_y  nu mu_c mu_m
    mu_g alpha gamma theta xi c0 c1 eta pi_h pi_c pi_x  N
%Parameters values
beta =0.08;
```

```
b0= 0.5;
b1= 0.00005;        b2 = 0.004;          b3 = 0.05;
mu_h = 0.05;        delta = 0.0005;      c = 0.02;
mu_x = 0.83;        mu_c = 0.05;         mu_y = 0.0003;
mu_g = 0.000625;    mu_m = 48;           alpha = 0.00005;
gamma = 0.0009;     theta = 0.3;         xi = 0.0005;
c0 = 0.000667;      c1 = 0.000667;       eta = 0.003;
pi_x = 2.5*10^6;    pi_c = 10;           pi_h = 30;
nu = 0.14;          N = 16;
% Time inteval
t0 = 0;
tf = 100;
tspan = [t0,tf];
%Initail conditions
x0 = [500000, 300,40000,20, 0.001, 0.001];
[t,x] = ode45 ('Pr_I',tspan,x0);
plot(t, x(:,2),'Linewidth', 2.5)
%plot(t, x(:,1),'Linewidth', 2.5)
%plot(t, x(:,3),'Linewidth', 2.5)
%plot(t, x(:,4),'Linewidth', 2.5)
%plot(t, x(:,5),'Linewidth', 2.5)
%plot(t, x(:,6),'Linewidth', 2.5)
%%plot(t ,x(:,1), t ,x(:,2), t,x(:,3) ,t,x(:,4),t, x(:,5), t
   , x(:,6), 'Linewidth', 2.25)
%%plot(t,x(:,3), 'b',t ,x(:,4),'--r','Linewidth', 2.5)
%%legend('X(t)','Y(t)','M(t)','G(t)','C(t)', 'H(t)')
 %%legend('Merozoite','Gametocyte')
xlabel('Time(days)')
ylabel('iRBCs')
%title('Blood cell populations')
box on
print(gcf,'XYl.png','-dpng','-r300')
```

Code Listing B.3: Impat of model parameters on the within-host dydnamics malaria parasite

```
% Efficacy of antibody-mediated immune response on
   erythrocytic invasion
clear all;
close all;
```

```
% Time inteval
%bb = [16 64 128 256];
%bb = [0 0.0009];
bb = [0.5 0.05 0.005 0.0005];
t0 = 0;
tf = 100;
tspan = [t0 tf];
for i=1:4
        b0=bb(i);
x0 = [500000, 100,40000,20, 0.001, 0.001];  %Initial
   conditions
[t,x] = ode45 ('Pr_I',tspan,x0);
 plot(t,x(:,1),'linewidth',2.5)
%title('Susceptible populations')
xlabel('Time(days)')
ylabel('Healthy RBCs')
%legend('\omega=0.09326','\omega=1.09326','\omega=2.0962','\
   omega=3.09326')
legend('b0=5\times 10^{-1}', 'b0=5\times 10^{-2}', 'b0=5\
   times 10^{-3}', 'b0=5\times 10^{-4}')
%legend('\delta=3\times 10^{-2}', '\delta=3\times 10^{-3}',
   '\delta=3\times 10^{-4}', '\delta=3\times 10^{-5}')
 hold on
end
print(gcf,'gams Gam wot.png','-dpng','-r300')

% Immune sinsitivity of the sexual replication of the
   malaria parasite
clear all;
close all;
 %eta = 0.003;
% Time inteval
%bb = [16 64 128 256];
%bb = [0 0.0009];
%bb = [0.5 0.05 0.005 0.0005];
bb = [0.001 0.004 0.007 0.009];
t0 = 0;
tf = 45;
```

```
tspan = [t0 tf];
for i=1:4
        eta=bb(i);
% x_0 = [326 36  4 3 5];
x0 = [500000, 100,40000,20, 0.001, 0.001];  %Initial
   conditions
%Plote the the dynamical system COVID-19 epivemic disease
[t,x] = ode45 ('Pr_I',tspan,x0);
 plot(t,x(:,4),'linewidth',2.5)
%title('Susceptible populations')
xlabel('Time(days)')
ylabel('Gametocytes')
%legend('\omega=0.09326','\omega=1.09326','\omega=2.0962','\
   omega=3.09326')
%legend('b2=4\times 10^{-1}', 'b2=4\times 10^{-2}', 'b2=4\
   times 10^{-3}', 'b2=6\times 10^{-4}')
%legend('without immune response \gamma=0', 'response
   againest iRBCs')
legend('\eta=3\times 10^{-2}', '\eta=3\times 10^{-3}', '\eta
   =3\times 10^{-4}', '\eta=3\times 10^{-5}')
 hold on
end
print(gcf,'gams Gam wot.png','-dpng','-r300')
```

B.1.2 Fractional order model

Code Listing B.4: Numerical solution of the fractional order model with order of detivative one

```
%Numerical solution of the fractional order model
FDEFUN = @(t,y)[r1-d1*y(1);r2-beta1*y(1)*y(2)/(1+b0*y(8))-d2
   *y(2);
    beta1*y(1)*y(2)/(1+b0*y(8))-delta*y(3)-k1*y(3)*y(8);
    r3-beta2*y(4)*y(6)/(1+b0*y(8))-d3*y(4);
    beta2*y(4)*y(6)/(1+b0*y(8))-gamma*y(5)-k2*y(5)*y(8);
   (delta*N*y(3)+gamma*Q*y(5))/(1+b1*y(8))-d4*y(6)-k3*y(6)*y
      (8);
   c*y(5)/(1+b1*y(8))-d5*y(7)-k4*y(7)*y(8);
   r4+(xi*y(3)/(1+a0*y(3))+nu*y(5)/(1+a0*y(5))+sigma*y(6)
```

```
      /(1+a0*y(6))+theta*y(7)/(1+a0*y(7)))*y(8)-d6*y(8)];
alpha = 1; t0 = 0; tfinal = 20;
y0 = [200;1000;100;500000;100;10000;10; 0.001];
% h =0.00005 ;
% Parameters
beta1=0.01; beta2=0.08; b0=0.005; b1=0.05; r1=20; r2
   =2.5*10^6; r3=2.5*10^5;
r4=10; d1=0.95; d2=0.029; d3=0.083; d4=48; d5=0.000625; d6
   =2;
k1=0.00000009; k2=0.000000009; k3=0.0000000009; k4
   =0.00000003; delta=0.095; gamma=0.05; N=1000;
Q=16;  c=0.04; xi=0.05; nu=0.003; sigama=0.00005; theta
   =0.0004; a0=0.06;
[t,y]=fde12(alpha,FDEFUN,t0,tfinal,y0,h);
figure(1)
 plot(t,y(2,:), 'g','Linewidth', 2.5) ;
```

Code Listing B.5: Impac of fractional order derivative on the evolutionary dynamics of parasite infection

```
%The evolutionary dynamics of the state variables with
   different fractional order derivative

FDEFUN = @(t,y)[r1-d1*y(1);r2-beta1*y(1)*y(2)/(1+b0*y(8))-d2
   *y(2);
    beta1*y(1)*y(2)/(1+b0*y(8))-delta*y(3)-k1*y(3)*y(8);
    r3-beta2*y(4)*y(6)/(1+b0*y(8))-d3*y(4);
    beta2*y(4)*y(6)/(1+b0*y(8))-gamma*y(5)-k2*y(5)*y(8);
   (delta*N*y(3)+gamma*Q*y(5))/(1+b1*y(8))-d4*y(6)-k3*y(6)*y
      (8);
   c*y(5)/(1+b1*y(8))-d5*y(7)-k4*y(7)*y(8);
   r4+(xi*y(3)/(1+a0*y(3))+nu*y(5)/(1+a0*y(5))+sigma*y(6)
      /(1+a0*y(6))+theta*y(7)/(1+a0*y(7)))*y(8)-d6*y(8)];
% alpha = 1;
t0=0; tfinal = 70;
tspan=[t0 tfinal];
y0 = [200;5000;100;55000;100;10000;10; 0.001]; h=0.0005;
% Parameters
beta1=0.001; beta2=0.008; b0=0.05; b1=0.005; r1=20; r2
```

```
   =2.5*10^6; r3=2.5*10^5;
r4=10; d1=0.95; d2=0.029; d3=0.00083; d4=48; d5=0.000625; d6
   =2;
k1=0.000009; k2=0.00009; k3=0.0009; k4=0.0003; delta=0.095;
   gamma=0.05; N=1000;
Q=16;  c=0.02; xi=0.00005; nu=0.0003; sigma=0.0005; theta
   =0.0004; a0=0.0006;
 %bb = [0.90 0.92 0.94 0.96 0.98 1];
 %bb = [0.92 0.94 0.96 0.979 0.9896 1];
%  bb = [0.85 0.89 0.93 0.97 0.96 1];
 bb = [0.80 0.84 0.88 0.92 0.96 1];
% bb = [0.85 0.88 0.91 0.94 0.97 1];
for i = 1:6
    alpha = bb(i);
[t,y]=fde12(alpha,FDEFUN,t0,tfinal,y0,h);
figure(1)
 plot(t,y(6,:),'Linewidth', 2.5);
 xlabel('Time (days)') ;
 ylabel('Merozoites') ;
%legend('y_1(t)','y_2(t)') ;
legend('\alpha=0.80' , '\alpha=0.84','\alpha=0.88', '\alpha
   =0.92', '\alpha=0.96', '\alpha=1')
%legend('\alpha=0.75' , '\alpha=0.80','\alpha=0.85', '\alpha
   =0.90', '\alpha=0.95', '\alpha=1')
grid on
print(gcf,'Mg12.png','-dpng','-r300')
 hold on
end
```

B.2 Python codes

Code Listing B.6: The healthy hepatocytes with administarions of all four control measutements

```
#Strategy seven
"""
Created on Thu Dec 21 20:34:44 2023
@author: jems
"""
```

```
"""
Created on Sun Jul 16 14:14:01 2023
@author: jems
"""
# Within-host malaria parasite Optimal Control Using GEKKO
import numpy as np
from gekko import GEKKO
import matplotlib.pyplot as plt
m = GEKKO(remote=False)
# constants
Lambda_h=2.5*10**8; Lambda_r=2.5*10**6;  Lambda_e=2
Lambda_p = 20;      N = 10000;           Q = 64
b0= 0.05;           b1=0.05;             b2=0.005
b3=0.005;           b4=0.004;            a0=0.004
a1=0.00667;         a2=0.00667;          a3=0.00667
beta1=0.001;        beta2=0.008;         delta=0.95
mu_h=0.029;         mu_m=48;             mu_g = 0.0000625
mu_r=0.0083;       vartheta_1=9*10**-11; vartheta_2=0.00009
vartheta_m=0.03;    vartheta_g=0.0003;   alpha=0.03
c= 0.02;            xi=0.00005;          nu=0.00005
theta=0.0005;       sigma=0.0005;        tau=2;
mu_e=2;             mu_p=1.2*10**-11
#Wieght constant
A1=1;              B1=2400               #B1=2400
A2=1;              B2=400                #B2=400
A3=1;              B3=500                #B3=500
A4=1;              B4=200                #B4=200
B1=2400
#define variables
H = m.Var(value=5000)
HI = m.Var(value=40)
R = m.Var(value=500000)
RI = m.Var(value=100)
M = m.Var(value=40000)
P = m.Var(value=20)
G = m.Var(value=30)
E = m.Var(value=0.001)
u1 = m.MV(value=0,lb=0,ub=0.85)
```

```
u2 = m.MV(value=0,lb=0,ub=0.75)
u3 = m.MV(value=0,lb=0,ub=0.85)
u4 = m.MV(value=0,lb=0,ub=0.85)
# Dynamical Sytem equatgion
m.Equation(H.dt()==Lambda_h-(1-u1)*beta1*H*P/(1+b0*E)-mu_h*H
   )
m.Equation(HI.dt()==(1-u1)*beta1*H*P/(1+b0*E)-delta*HI-
   vartheta_1*HI*E)
m.Equation(R.dt()==Lambda_r-(1-u2)*beta2*R*M/(1+b1*E)-mu_r*R
   )
m.Equation(RI.dt()==(1-u2)*beta2*R*M/(1+b1*E)-alpha*RI-
   vartheta_2*RI*E)
m.Equation(M.dt()==(1-u3)*N*delta*HI/(1+b2*E)+(1-u4)*Q*alpha
   *RI/(1+b3*E)-vartheta_m*M*E-beta2*R*M/(1+b1*E))
m.Equation(P.dt()== Lambda_p-mu_p*P-beta1*H*P/(1+b0*E))
m.Equation(G.dt()== c*RI/(1+b4*E)-(u4+mu_g)*G-vartheta_g*G*E
   )
m.Equation(E.dt()== tau*Lambda_e+E*(xi*HI/(1+a0*HI)+nu*RI
   /(1+a2*RI)+sigma*M/(1+a1*M)+theta*G/(1+a3*G)))
#Ttime point
T=80
nt =160; m.time = np.linspace(0,T,nt)
p = np.zeros(nt); p[-1] = 1.0
final = m.Param(value=p)
# initialize with simulation
m.options.IMODE=7
m.options.NODES=2
m.solve(disp=False)
# plot the prediction
plt.figure(figsize=(6,5))
plt.plot(m.time,   HI.value, color='red', lw=3, label='
   without control')
# optimize
m.options.IMODE=7
#i.UPPER = 0.02
u1.STATUS = 1
u1.DCOST=0
u2.STATUS = 1
```

```
u2.DCOST=0
u3.STATUS = 1
u3.DCOST=0
u4.STATUS = 1
u4.DCOST=0
m.options.SOLVER =3
m.options.TIME_SHIFT = 1
#State Variable value
H.value = G.value.value
HI.value = HI.value.value
R.value = R.value.value
RI.value = RI.value.value
M.value = M.value.value
P.value = P.value.value
G.value = G.value.value
E.value = E.value.value
#objective function
obj = m.integral(A1*HI+A2*RI+A3*M+A4*G+0.5*B1*u1**2 + 0.5*B2
   *u2**2+0.5*B3*u3**2+ 0.5*B4*u4**2)
m.Minimize(final*obj)
m.solve(disp=False)
plt.plot(m.time, HI.value, color='blue', lw=3,ls='--', label
   ='with control')
plt.ylabel('Hepatocytes')
plt.legend()
plt.xlim(0,80)
plt.ylim(0)
plt.xlabel('Time (days)')
#plt.ylim(0,45)
plt.tick_params(top=True, right=True, which='both')
#plt.xlabel('Time (weeks)')
plt.savefig('Mu2u3u4')
plt.show()
```